UNIVERSITÀ DEGLI STUDI DI PADOVA

Head Office: Università degli Studi di Padova

Department of Biology

Ph.D. COURSE IN BIOSCIENCES

CURRICULUM: Cell Biology and Physiology

SERIES XXXV

Unravelling novel players in astrocyte-mediated brain clearance

Coordinator : Prof. Ildikò Szabò

Supervisor : Dr. Laura Civiero

Ph.D. Student : Veronica Giusti

“The Brain is a world
consisting of a number of unexplored continents
and great stretches of unknown territory”

Santiago Ramon y Cajal

Table of contents

List of abbreviation

Adenosine triphosphate	ATP
Affinity purification	AP
Aldehyde dehydrogenase 1 L1	Aldh1L1
Alzheimer disease	AD
Annexin A2	ANXA2
Apolipoprotein E	APOE
Aquaporin 4	AQP4
Atypical chemokine receptor 3	Ackr3
ATP binding cassette subfamily A member 1	ABCA1
Basal Medium Eagle	BME
Blood Brain Barrier	BBB
Bovine serum albumin	BSA
Brain Derive Neurotrophic Factor	BDNF
Calcium	Ca^{2+}
Carboxy SNARF-1®	SNARF1
Catechol-o-metyltranspherase	COMT
Cathepsin B	CtsB
Central Nervous System	CNS
Complement component 3	C3
Complement component 1q	C1q
Complement receptor 3	CR3
Deep brain stimulation	DBS
Dulbecco's modified Eagle's medium	DMEM
Dulbecco's Phosphate Buffered Saline	DPBS
Enhanced Chemi Luminescence	ECL
Fetal Bovine Serum	FBS
Fold change	FC
Gamma-aminobutyric acid	GABA
Gene ontology	GO
Genome Wide Association Studies	GWAS
Glial fibrillar acidic protein	GFAP

Gliotransmitters	GT
Glutamate aspartate transporter 1	GLAST/EAAT1
Glutamate-transporter-1	GLT1/EAAT2
Glutamine synthetase	GS
Horseradish peroxidase	HRP
Horseradish peroxidase	HRP
Human Induced pluripotent stem cells derived astrocytes	iHAstrocytes
Huntington disease	HD
Idiopathic PD	iPD
Immunoprecipitation	IP
Induced pluripotent stem cells	iPSC
Inositol 1,4,5-triphos-phate receptor type 2	IP3R2
Inositol trisphosphate receptors	IP3R
Interleukin-33	IL-33
Ionized calcium-binding adapter molecule 1	Iba1
Kufor-Rakeb syndrome	KRS
Leucine rich repeat kinase 2	LRRK2
Leucine-rich repeat	LRR
Lewy bodies	LBs
Lewy neurites	LNs
Liquid chromatography mass spectrometry	MS
Luria-Bertani	LB
Lysosomal associated membrane protein	LAMP
Molecular function	MF
Multiple EGF-like domains 10	MEGF10
Myelin basic protein	MBP
Neurodegenerative diseases	NDs
Nitric oxide	NO
Non-amyloid component	NAC
Oxygen radical species	ROS
Paraformaldehyde	PFA
Parkinson’s disease	PD
Pearson's correlation coefficient	PCC
Penicillin-Streptomycin	Pen-Strep

Phagocytic index	PI
Phosphatidyl ethanolamine	PE
Phosphatidyl serine	PS
Poly-Acrylamide Gel Electrophoresis	SDS-PAGE
Polyethyleneimine	PEI
Polyvinylidene fluoride	PVDF
Postsynaptic density	PSD
Potassium	K^+
Pre-Formed Fibrils	PFFs
Presenilin 1	PS1
Protein Phosphatase 1	PP1
Protein-protein interaction	PPI
Proto-oncogene tyrosine-protein kinase MER	MERTK
Radio-Immunoprecipitation Buffer	RIPA
Ras of Complex	ROC
Reactive oxygen species	ROS
Ribonucleic acid	RNA
Room temperature	RT
Sample Buffer	SB
Small interfering RNA	siRNA
Sodium	Na+
Substantia nigra pars compacta	SNpc
Synaptic vesicles	SVs
Trans-Golgi network	TGN
Transforming growth factor β	TGFβ
Transmission Electron Microscopy	EM
Tris-Tween Buffered Saline buffer	TTBS
Tunneling nanotubes	TNTs
Vesicle associated membrane protein 2	VAMP2
α-amino-3-hydroxy-5methyl-4-isoxazolepropionic acid	AMPA
α-synuclein	α-syn
β-amyloid	Aβ

Abstract

Under certain conditions, astrocytes demonstrate phagocytic capability and cooperate with microglia as an ancillary clearance system to clear up the brain. Astrocyte processes are in close association with synapses and contribute to synaptic health at several levels. Noteworthy, astrocytes are efficient sensors of synaptic dysfunction or degeneration. Indeed, they intervene by eliminating neuronal terminals, engulfing debris and internalizing neuronal-released aggregated proteins. However, the molecular machinery recruited for the recognition of specific targets is only in part clarified.

The main aim of this PhD Project is to molecularly characterize astrocyte-mediated brain clearance both in health and disease, from different perspectives and through several approaches.

In the first part of this PhD project, we identified a novel molecular mechanism behind astrocyte-mediated synapse elimination. We used a high throughput system to study the role of 3000 genes in the internalization kinetic of astrocytes We validated the most promising modulator: the Atypical Chemokine Receptor 3 (Ackr3). For the first time we demonstrated that the absence of Ackr3 abolishes synaptosome internalization in primary astrocytes. By employing biochemical and imaging approaches we also confirmed a direct involvement of Ackr3 in neuronal terminal recognition and internalization and identified Cxcl12 as a possible novel "eat/find me" signal. Specifically, we detected that Cxcl12 is attached to the synaptosomal membrane and increased Cxcl12 enhance astrocyte clearance capacity. Of note, we revealed that Cxcl12 recognizes phosphatidylethanolamine at the plasma membrane, a lipid that increases its externalization in the early phase of neuronal death. Finally, we demonstrate the involvement of Ackr3 in synaptosomes internalization in human iPSC-derived astrocytes, suggesting conserved mechanisms across species. Although additional data are required, these results generate new fundamental knowledge on the molecular machinery involved in astrocyte-mediated synaptic elimination. Studies on Ackr3 dysfunction in astrocytes as possible contributor in human diseases, such as glioma, are now on-going.

In the second part of this PhD project, we described a novel mechanism by which astrocytes internalize the toxic form of α-syn, a protein that accumulates in many neurodegenerative diseases, including Parkinson's disease. In collaboration with the University of Uppsala, we showed an impaired α-syn clearance in primary astrocytes harboring th

G2019S pathogenic mutation in the leucine-rich repeat kinase 2 (LRRK2), a kinase involved in the pathogenesis of PD. This clearance deficit correlates with deleterious changes in the architecture of the endosomal/lysosomal organelles of astrocytes. We identified ANXA2 as a LRRK2 interactor and showed that decreased levels of Anxa2 in primary astrocytes are associated to an impairment of α-syn clearance. We also demonstrated that in the presence of the G2019S mutation, there is a decrease expression of AnxA2 both in cell culture and in human post-mortem brains of PD patients. Moreover, in the pathological background, Anxa2 fails to re-localize into puncta in close proximity to internalized α-syn particles. Notably, we proved that this phenotype could be completely reverted a selective LRRK2-inhibitor. Altogether, our results offer a better understanding of the molecular mechanisms behind impaired α-syn clearance in G2019S astrocytes, pointing to Anxa2 as a novel target for astrocytes' loss of function in neurodegenerative diseases.

In conclusion, we identified i) Ackr3 as a novel receptor involved in astrocyte-mediated synapses engulfment and ii) Anxa2 as a novel critical player in astrocyte-mediated α-syn clearance. Given the importance of astrocyte-mediated clearance to maintain brain homeostasis, these data offer the opportunity to investigate cell-targeted therapies as a novel approach in the context of neurological disorders.

Chapter 1

Astrocytes

1. Introduction

The central nervous system (CNS) consists of the brain and spinal cord and is separated from the rest of the body by the Blood-Brain Barrier (BBB), which regulates the molecule dispersion between the two tissues. (Bradbury et al., 1993; Engelhardt et al., 2003). The CNS derives from the neuroepithelium, which consists of stem-like progenitor cells that generate neurons and radial glia as well as basal progenitors. (Götz et al., 2005). Of note, radial glia cells produce other radial glia and immature neurons or basal progenitors through asymmetric cell divisions. Moreover, radial cells differentiate into mature glial cells known as macroglia and composed by oligodendrocytes, ependymal cells, and astrocytes (Miyata et al., 2001; Noctor et al., 2001; Shimojo et al., 2011). Instead, microglia are other glial cell subtypes which are not derived from neuroepithelial cells (Nayak et al 2014). Specifically, microglia colonize the CNS during development and are considered the macrophage of the brain (Kierdorf et al., 2013). Neurons provide the electrical transmission allowing both conscious and autonomic behaviors (Zoidl et al., 2002; Burdakov et al., 2004). Instead, glial cells have been considered as the structural "glue" to physically support neural networks rather than play active roles in the CNS (García-Marín et al., 2007). More recently, glial cells have gained more importance since numerous studies revealed their critical roles in many physiological and pathological processes (Barres et al., 2008).

Of note, astrocytes in cooperation with microglia have been recently found to be involved in the elimination of extracellular materials including unwanted synapses and neuronal-released proteinaceous aggregates (Jung and Chung, 2018; Lindström et al., 2017; Loria et al., 2017; Sacino et al., 2017). In the Chapter 1, I will provide an overview on astrocyte biology focusing on the physical and functional interaction of these cells with the neuronal synapses in health and disease. In the Chapter 2, I will summarize the known molecular mechanisms of astrocyte-mediated synapse elimination and the functional implication of this process. In the Chapter 3, I will describe the contribution of astrocytes in the clearance of toxic, fibrillar α-synuclein (α-syn) in the context of Parkinson's disease (PD), a common neurodegenerative disease.

1.1. Astrocyte classification and structure

In 1846, Virchow first described that nerve cells were inserted in a connective tissue that he called 'nervenkitt' or nerve glue. In 1909, Ramón y Cajal used silver-gold impregnation to

reveal the morphology of star-shaped cells called astrocytes (García-Marín et al., 2007). Astrocytes are distinguished in two main types according to their morphology and anatomical localization: protoplasmic and fibrous astrocytes. Specifically, protoplasmic astrocytes ensheath synapses and contact blood vessels in the grey matter, whereas fibrous astrocytes contact nodes of Ranvier and blood vessels in the white matter (Barres et al., 2008) (Figure 1.1). Moreover, an additional astrocytic subtype, named pial astrocytes (given their localization at the pial surface), has also been shown to present a different developmental origin, morphology, location and thus has been suggested to have a different function (García-Marqués et al., 2013).

Recent studies identify two other novel astrocytes subtypes, named varicose-projection astrocytes and interlaminar astrocytes, being specific to humans and chimpanzees' brain (Falcone et al., 2021; Falcone et al., 2022). Specifically, varicose-projection astrocytes are characterized by long varicosities-containing processes while interlaminar astrocytes possess long interlaminar processes that extend radially toward the cerebral cortex (Falcone et al., 2021; Falcone et al., 2022).

The number of astrocytes in relation to brain complexity is controversial. In literature, authors often refer to astrocytes as the most abundant cell type in the brain or that the number of astrocytes per neuron is drastically increased in high-order primates. However, a recent study showed that the astrocytes/neuron ratio differs consistently across brain regions in a variety of mammalian species such as: rodents, insectivores, non-human, and human primates (Herculano-Houzel et al., 2014). For instance, another study determined that astrocytes only represent approximately 20% of the total glial cells in the human neocortex (Pelvig et al., 2008). Thus, it appears that astrocyte complexity rather than number increases with brain size, especially in humans (Oberheim et al., 2009). Commonly, astrocytes constituting 20 – 50% of the cerebral volume (Filous et al., 2016), and they are found throughout the whole healthy CNS in a non-overlapping, highly well-organized manner (Bush et al., 1999). Indeed, astrocytes form a very heterogeneous population, not only morphologically but also because of their region specificity.

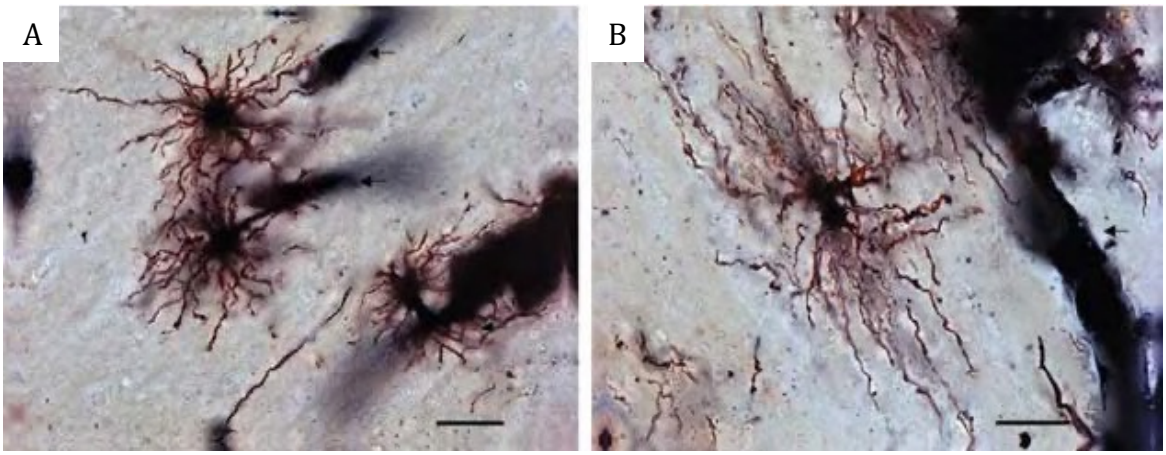

Figure 1.1 Types of astrocytes. **A** Protoplasmic astrocyte, much ramified, with uniformly distributed processes and **B** fibrous astrocytes, less ramified (Torres-Platas et al., 2011).

In the mouse brain, each astrocyte encompasses 300-600 neuronal dendrites (Halassa et al., 2007), 140 000 synapses (Bushong et al., 2002) and contact blood capillaries with their perivascular processes named end feet. Studies in the early 90s revealed that astrocytic processes ensheath the synapses and that, thanks to this proximity, they closely monitor the synaptic activity (Ventura et al., 1999). The bidirectional communication between astrocytes and neurons gave birth to the concept of the tripartite synapse in which astrocytes are active partners in synaptic activity (Araque et al., 1999; Perea et al., 2009) (Figure 1.2). Specifically, the tripartite synapse comprises of a presynaptic axonal bouton, a post synaptic dendritic spine and an astrocyte process where astrocyte processes show close contacts with dendritic spines sometimes forming an `O´ ring structure (Panatier et al., 2014).

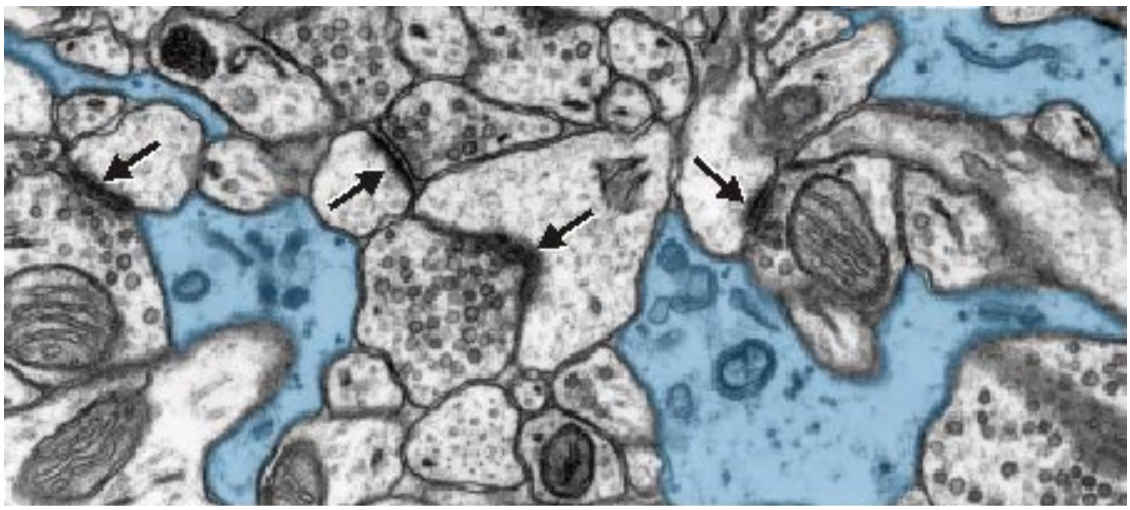

Figure 1.2 Astrocyte processes at the synapse. Electron microscopy image from rat hippocampus, showing astrocytes (blue) in close contact with synaptic terminals (arrows) (Kim et al., 2022)

The structure of the astrocyte cytoskeleton is supported by the network of intermediate filaments (Sonofroniew and Vinters., 2010). The fundamental component of these filaments is the glial fibrillary acidic protein (GFAP) that is upregulated in brain damage and degeneration (Middeldorp et al., 2011). GFAP was first isolated from multiple sclerosis patients' demyelinated plaques, where it was found in high concentrations (Lucas et al., 1980). Indeed, GFAP is the most widely used marker of reactive astrocytes, astrocytes that undergo morphological, molecular, and functional changes in response to pathological situations (Escartin et al., 2021). However, GFAP expression and astrocyte morphology are not the only features to qualify astrocytes as reactive. For instance, GFAP does not label all astrocytes in healthy CNS tissue or astrocytes distant from CNS injuries (Sonofroniew and Vinters, 2010). Nowadays, other markers have been used for immunohistochemical detection of homeostatic astrocytes such as glutamine synthetase and S100β, however, different to GFAP, they are also expressed in neural cells as neurons or oligodendrocytes (Norenberg, 1979; Goncalves et al., 2008). Transcriptomic analyses revealed some other proteins highly expressed in astrocytes (Lovatt et al., 2007; Cahoy et al., 2008) such as: aldehyde dehydrogenase 1 L1 (Aldh1L1), an enzyme that has been proposed by Cahoy and colleague as a more sensitive and reliable immunohistochemical astrocyte marker. Cahoy and colleagues have shown that Aldh1L1 is expressed specifically by astrocytes, and it is not being expressed in neurons, oligodendrocytes or in OPCs, and that it can label both astrocyte perikarya and processes throughout both grey and white matter unlike GFAP, which labels mainly thick main processes of astrocytes (Cahoy et al., 2008). In addition, all GFAP positive cells are also labelled with Adh1L1, whereas the latter one strongly labels many more astrocytes (Cahoy et al., 2008). Interestingly, dye-filling experiments reporter mice with fluorescent astrocytes, have allowed the visualization of the real morphology of these cells. In fact, astrocytes have a complex morphology, with highly ramified processes (Wilhelmsson et al., 2006). Therefore, the GFAP labeling only represents approximately 15% of the total volume occupied by an astrocyte (Bushong et al., 2002).

Astrocytes are found throughout the whole healthy CNS in a non-overlapping, highly well-organized manner (Bushong et al., 2002). More recently, Salmon and colleagues, using high-resolution serial electron microscopy datasets and computer vision, provides a systematic analysis of astrocytic nanoarchitecture of adult mouse neocortex, and presents quantitative evidence that astrocytes organize their morphology into purposeful, classifiable assemblies with unique structural and subcellular organelle adaptations related to their physiological functions (Salmon et al., 2021).

1.2 Astrocyte functions

During the last 20 years, a wide variety of functions have been attributed to these cells. Astrocytes primarily support neuronal activity and function by providing important growth factors or supporting neuronal metabolism through the conversion of glucose to ATP and glutamine to glutamate from the peripheral blood (Joe et al 2018). They directly participate in the tripartite synapse by harboring as many as two million synapses in humans (Oberheim et al., 2009). Moreover, they support the neuronal activity by controlling extracellular ion balance and neurotransmitter homeostasis. Also, they provide biochemical support of endothelial cells, nutrients to the nervous tissue, and regulation of neurogenesis and brain wiring (Vasile et al., 2017).

Astrocytes control water and ion homeostasis (Alvarez-Maubecin et al., 2000). Endfeet of perivascular astrocytes form the BBB along with the pericytes, the basal lamina and the endothelial cells allowing a selective communication between the peripheral blood flow and the brain. Specifically, water transport to the cerebral blood flow is mainly made through the water channel aquaporin 4 (AQP4), enriched at the astrocytic endfeet. Interestingly, in brain tumors, both AQP4 and Kir4.1 channels are redistributed at astrocyte endfeet, which participate in the BBB disruption (Bataveljić et al., 2012; Nwaobi et al., 2016). Astrocytes release angiogenic factors, such as vascular endothelial growth factor, involved in the formation and the maintenance of the BBB (Alvarez et al., 2013). Furthermore, astrocytes are organized as a network, coupled by gap-junction channels (Giaume et al., 2010). Gap-junction channels are formed by the apposition of two connexons, each resulting of the assembly of six connexins. The main astroglial connexins are the connexins 43 and 30, which are permeable to small molecules including ions, second messengers, inositol-3-phosphate, energy substrates and amino acids (Giaume et al., 2010; Escartin and Rouach, 2013).

Among the different factors that regulate synaptic plasticity, glial cells are key players in maintenance of synapse homeostasis (Eroglu and Barres, 2010). Gliotransmitters (GT) released by astrocytes modulate the synaptic activity through vescicular-dependent endocytosis, further activating intracellular calcium (Ca^{2+}) signals. Glutamate, gamma-aminobutyric acid (GABA) and ATP are the most studied gliotransmiters. Astrocytic membranes are enriched in glutamate and GABA transporters (GAT) that are differentially expressed throughout the adult brain. These transporters serve as an efficient mechanism for clearing these neurotransmitters (NTs) from the extracellular space after neuronal activity (Danbolt, 2001). Glutamate transporters,

concretely GLAST (EAAT1) and GLT1 (EAAT2) are responsible for removing 80% of glutamate released from the presynaptic neurons, being just 20% of glutamate taken up by post-synaptic glutamate transporters (Iovino et al., 2020). In astrocytes, glutamate can be metabolized to glutamine-by-glutamine synthetase (GS), then being released to the extracellular space to be taken up by neurons and used to resynthesize glutamate or GABA (Iovino et al., 2020). GLT-1 and GLAST deficient rats developed neurodegeneration and progressive paralysis (Iovino et al., 2020). Regarding to GABA transporters, GAT-3 is the most abundant GAT in astrocytes and is localized in astrocytic processes that are adjacent to synapses and cell bodies. Activation of GAT-3 results in a rise in Na^+ concentrations in hippocampal astrocytes and a consequent increase in intracellular Ca^{2+} through the action of Na^+/Ca^{2+} exchangers (Doengi et al., 2009). Thus, GABA-uptake by astrocytic GAT-3 can stimulate the release of ATP/adenosine that contributes to downregulation of the excitatory synaptic transmission and provides a mechanism for homeostatic regulation of synaptic activity (Boddum et al., 2016). Interestingly, alteration of GABA release is associated with various pathological conditions such as epilepsy (Pirttimaki et al., 2013), Alzheimer's disease (AD) (Jo et al 2014) and Huntington Disease (HD) (Wójtowicz et al., 2013). Astrocytes predominantly show potassium (K^+) conductance (Hertz et al 2013), which is mainly mediated by Kir4.1, aquaporin-4, chloride channels, or sodium (Na^+) -Ca^{2+} exchangers (Halnes et al., 2013). This allows the rapid uptake of K^+ from the synaptic cleft and redistribution of K^+ in the extracellular space during neuronal activity (Seifert et al., 2018). Furthermore, AQP4, that transports water, and Na^+-$Ca2^+$ exchangers are involved in the maintenance of a correct pH surrounding the synapse (Obara et al., 2008).

Astrocytic glycogen utilization can support neuronal activity in hypoglycemic conditions and through transient events where neuronal activity is increased (Brown et al., 2007; Won Suh et al., 2007). Moreover, while glycogen mobilization may also fulfill the astrocytes' own metabolic needs (Sickmann et al., 2009; Walls et al., 2009), glycogen breakdown typically results in lactate production and release in the extracellular space to provide neuronal energy needs (Dringe et al., 1993; Walls et al., 2009). Moreover, astrocytic glycogen mobilization is relevant in maintaining glutamatergic synaptic transmission (i.e., neurotransmitter release), as demonstrated in neuron-astrocyte co-culture models (Sickmann et al., 2009; Mozrymas et al., 2011). There is evidence suggesting that astrocytes have a greater metabolic plasticity than neurons. Astrocytes respond to nitric oxide (NO) with an increase in glucose metabolism through the glycolytic pathway, thereby limiting the fall in ATP levels and preventing apoptosis. In neurons, however, this response does not seem to be present, and a similar NO challenge

causes a massive ATP depletion, leading to apoptosis (Almeida et al., 2001). Furthermore, metabolic astrocyte-neuron interactions (in particular through lactate release by astrocytes) also influence higher brain functions, such as long-term memory formation (Suzuki et al 2011).

In addition to the release of trophic molecules, astrocytes play an important role in the antioxidant defense of the brain. Cellular respiration produces reactive oxygen species (ROS). The production of ROS is tightly regulated by antioxidant defense in the brain. Indeed, uncontrolled ROS production is deleterious for neurons and involved many pathological conditions (Vicente-Gutierrez et al., 2019). This feature makes astrocytes as cellular sentinels of neuronal energy metabolism (Dringen et al., 2000). Astrocytes secrete higher levels of various antioxidant molecules and ROS- detoxifying enzymes compared to neurons, including glutathione, ascorbic acid, heme-oxygenase 1, glutatione peroxidase, glutathione S transferase, catalase, and thioredoxin reductase (Dringen et al., 2000; Shih et al 2003; Bélanger and Magistretti, 2009).

In the last decade, many studies reported astrocytes as CNS phagocytes that clear dead cells and parts of live cells, such as synapses and axons (Jung and Chung 2018), as well as extracellular protein aggregates (Lindström et al., 2017; Loria et al 2017; Sacino et al 2017). Multiple pathways and receptors have been demonstrated to participate in this astrocytic mechanism (Cahoy et al., 2008). However, all the proteins and the mechanism behind this novel astrocytic function are not completely dissected.

1.2.1 Astrocytes cooperate with microglia to clear up the CNS

Appropriate clearance of potentially harmful material, such as dead cells, synapses or protein aggregates, is necessary for the development, maintenance, and regeneration of CNS. As mentioned above, microglia are historically considered the tissue-resident macrophages of the brain, and efficiently remove potentially harmful extracellular materials (Kabba et al., 2017, Colonna and Butovsky, 2017). However, many extracellular targets are mostly common between astrocytes and microglia, although astrocytes are considered less efficient in engulfing and degrading extracellular material (Lee J.K. et al., 2021). Astrocyte-mediated elimination of extracellular material was reported in the mammalian brain more than half a century ago (Colonnier, 1964; McMahan, 1967; Mugnaini and Walberg, 1967). In 2008, Cahoy and colleagues (Cahoy et al., 2008), by performing microarray analysis of isolated astrocytes, identified several receptors, including: AXL and MERTK, both of which are members of the

TYRO3/AXL/MERTK (TAM) family phagocytic receptors (Lemke, 2013), MEGF10, which is a mammalian homolog of Drosophila phagocytic receptor Draper (Freeman et al., 2003), αvβ5 integrin (Finnemann et al., 1997), and LRP1 (Gardai et al., 2005). Additionally, other cytosolic or transmembrane molecules as Crk1 (ced-2), Dock1 (ced-5) and Gulp1 (ced-6), which are homologous of phagocytic-related genes for apoptotic cells in *C. elegans*, point astrocytes as phagocytes in the context of gene expression profiles. (Figure 1.3)

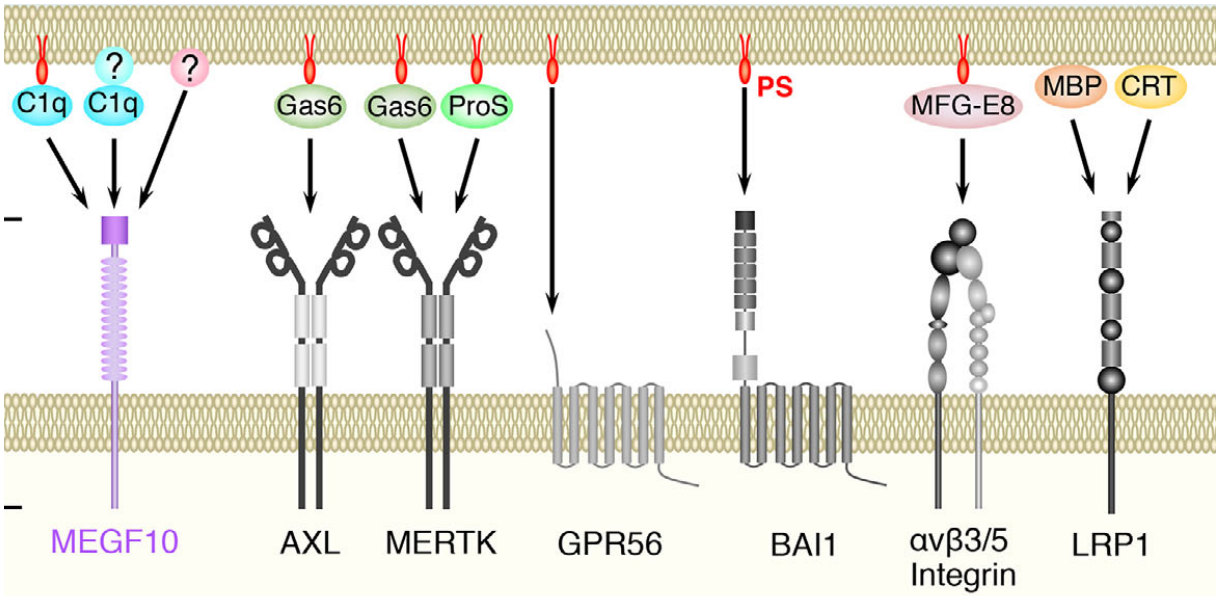

Figure 1.3 Receptors for the recognition of extracellular material by astrocytes. Astrocyte-specific receptors are shown in magenta and receptors commonly expressed by both astrocytes and microglial cells are shown in black and white. The ligands for each phagocytic receptor are also represented. (Adapted from Konishi et al., 2022)

In vivo studies have reported that astrocytes, rather than microglia, predominantly engulfed cell debris and dying or dead cells but with a smaller size (Damisah et al., 2020; Morizawa et al., 2017). Moreover, studies using cultured astrocytes indicated that kinetics of both uptake and digestion of cell debris are significantly lower in astrocytes compared to microglia (Lööv et al., 2015; Magnus et al., 2002). Thus, the astrocytic clearance of extracellular material is expected to be lower than in microglia. Recently, Damisah and colleagues demonstrate that astrocytes internalized the cell body of apoptotic neurons instead of microglia when microglia were pharmacologically depleted (Damisah et al., 2020). These findings suggest that astrocytes can offer a significant help in brain clearance activity and may compensate for impaired microglial phagocytosis (Konishi et al., 2020).

Nearly a decade ago, astrocytes emerged also as pivotal players in synaptic elimination in concert with microglia (Chung et al., 2013; Paolicelli et al., 2011; Tremblay et al., 2010; Sipe et al., 2016; Yang et al., 2016). Chung et al. revealed that the astrocytic MEGF10 and MERTK, both of which are receptors for dead cells, are also involved in synapse removal (Chung et al., 2013). Interestingly, studies have reported that synapses are preferentially phagocytosed by astrocytes at certain conditions. For instance, in the hippocampal CA1 region of normal adult mice, the number of internalized synapses is larger within astrocytes than microglia, indicating that astrocytic mechanism is predominant (Lee J. K. et al 2021). Astrocyte-mediated synapse elimination occurs both in physiological context such as in brain development and experience-dependent plasticity (Wolff and Missler, 1993; Kamiyama et al., 2006), and in pathological condition as an early feature of Neurodegenerative Diseases (NDs) (Henstridge et al., 2018). A more detailed dissection of astrocyte-mediated synapses elimination will be discussed in later section.

Furthermore, astrocytes have been showed to take up extracellular protein aggregates, such as β-amyloid (Aβ), Tau and α-syn (Koistinaho et al., 2014; Lee H. J. et al., 2008; Wakabayashi et al., 2000). Studies in cultured cells from rats or mice have reported the involvement of the scavenger receptor-A, low-density lipoprotein receptor-related protein 1 and integrin-associated protein in the internalization of Aβ both in astrocytes and microglia (Liu C.C. et al., 2017; Jones et al., 2013; Zhang et al., 2014). Additionally, integrin-associated protein has been shown to mediated astrocytes Tau PFFs internalization (Wang and Ye, 2021). The internalization of monomeric, oligomeric or fibrillar α-syn in astrocytes seems to be quite different depending on the molecular species, and the exact mechanism is still under investigation (Dilsizoglu Senol et al., 2021; Rostami et al., 2017). *In vitro* studies have reported that microglia displayed faster degradation rate compared to astrocytes which, conversely, appeared to store or release α-syn aggregates rather than degrade them (Rostami et al., 2021). However, astrocytes have been clearly reported as pivotal players in α-syn uptake and degradation (Rostami et al., 2021; Gustafsson et al., 2017; Rostami et al., 2017, Huang et al., 2022; Ihse et al., 2017). A more detailed digression of astrocyte-mediated α-syn uptake will be described in later section (Section 3.2.1).

Chapter 2

Astrocytes and synapses

2. Astrocyte-mediated synapse elimination

Synaptic connections are initially overbuilt during development, and phagocytic pruning of unnecessary synapses is essential for the establishment of proper neural networks (Chung et al., 2013; Paolicelli et al., 2011). Moreover, within the mature CNS, the refinement of neuronal networks is a dynamic activity-dependent process involving synapse elimination (Clarke and Barres, 2013). Synaptic formation and elimination also occur in adulthood in an experience-dependent manner (Trachtenberg et al., 2002). Those unwanted synapses need to be removed to obtain precise neuronal connection (Chung et al., 2013; Schafer et al., 2012). Synapses elimination continues in the adult nervous system, in the form of experience-dependent structural synaptic plasticity, although the frequency of elimination events might decline with aging. Remodeling of synapses network is crucial for the formation of the brain circuit, and it plays a crucial role in learning and memory. An abnormal elimination of synapses during development could lead to an increase or decrease of synapses density, which might cause schizophrenia or autism spectrum disorders (Penzes et al., 2011). Compelling evidence shows that synapse elimination by astrocytes and microglia is important in the activity-dependent wiring of the brain. (Schafer et al., 2012; Chung et al., 2013; Sipe et al., 2016; Yang et al., 2016). For instance, in the developing retino-thalamic system, a well-characterized model for experience-dependent synaptic refinement (Penzes et al., 2011) has been demonstrated that microglia are active players in experience-dependent remodeling of neural circuits (Tremblay et al., 2010; Schafer et al., 2012; Sipe et al., 2016). However, a sensory deprivation *i.e.* closure of one eye, during the visual critical period results in enhanced engulfment of synaptic terminals by astrocytes (Chung et al., 2013; Sipe et al., 2016).

Several pathways and receptors have been implicated in synapse elimination. Synapse elimination could occur *via* autonomous pathways within the damaged neuron, due to localized "eat-me" signals (Wishart et al., 2006; Ertürk et al., 2014) or *via* active non-cell-autonomous removal of synapses by surrounding glial cells (Hong et al., 2016; Paolicelli et al., 2017). After having identified astrocytic MEGF10 and MERTK as receptor for synapse elimination, Chung and colleagues reported the significance of MEGF10 in synaptic elimination in adult mice. Indeed, they demonstrated that astrocytes eliminate excitatory synapses through MEGF10 in the adult hippocampus to maintain circuit homeostasis or form memories (Lee J. K. et al 2021). Indeed, using an AAV-based phagocytic reporters that allow the detection of synapse engulfment by glial cells, Lee and colleagues showed that astrocytes are the major player in the elimination excitatory and inhibitory pre- and post-synapses in the hippocampal CA1 (Lee J. K.

et al 2021). Interestingly, it has been showed that activating the hippocampal CA1 region leads to an enhance astrocyte-mediated excitatory synapse elimination instead of microglia-mediated elimination. While the absence of astrocityc-Megf10 in adult hippocampus results in a rapid increase in the number of excitatory instead of inhibitory synapses that lead to a learning and memory formation deficits (Lee J. K. et al 2021). Furthermore, it has been shown that astrocytes contribute to synapse elimination in an inositol 1,4,5-triphos-phate receptor type 2 (IP3R2)-dependent manner via activation of purinergic signaling (Yang et al., 2016). In addition, astrocytic Ephrin-B1 was shown to mediate astrocyte-mediated elimination of EphB receptor-positive synapses, regulating long-term contextual memory (Koeppen et al., 2018) (Figure 1.3)

Extracellular material elimination, as well as synapses, seem to be triggered through the recognition of an "eat-me" signals exposed at the surface of target debris. Of note, phosphatidyl serine (PS) has been reported as one of the major “eat-me” signal exposed on the synaptic surface that cause glial-mediated synapses elimination in a similar manner as in apoptotic cells removal (Györffy et al., 2018; Li et al., 2020; Park et al., 2021; Scott-Hewitt et al., 2020). However, in some cases, bridging molecules which binds to "eat-me" signal, may be required. Lemke and colleagues, demonstrate that MERTK recognizes PS on the synaptic surface via Gas6 or ProS (Park et al., 2021). (Figure 2.1) Conversely, Chung et al. demonstrate that the complement component 1q (C1q), which is required for apoptotic cell removal, is not involved in MEGF10-dependent synapses elimination (Chung et al., 2013; Iram et al., 2016). In addition, recent studies identified an isoform of the adhesion G-protein coupled receptor GPR56 as a novel PS receptor (Chiou et al., 2021). GPR56 is highly expressed in astrocytes and a direct binding of GPR56 to the PS exposed at the synaptic surface, as in microglial cells, could triggers synapses elimination (Chiou et al., 2021) (Figure 1.3).

An interesting aspect is the crosstalk between microglia and astrocytes in synapse elimination. Collecting evidence indicates that microglia modulate astrocytic function as well as astrocytes can regulate microglial phenotypes (Jha et al., 2019). Astrocyte-microglia crosstalk will be discussed more in detail in Section 2.5.

While synapse elimination in the context of brain development and experience-dependent plasticity is a physiological process (Wolff and Missler, 1993; Kamiyama et al., 2006), its later and dysregulated occurrence is recognized as an early pathological feature of NDs (Henstrige et al., 2018) (Figure 2.2). Indeed, one of the earliest hallmarks of NDs is the loss

of presynaptic terminals and dendritic spines, which correlate with cognitive impairment (Scheff et al., 2014). Moreover, the majority of NDs are characterized by the accumulation of toxic protein aggregates (Soto and Pritzkow, 2018). In such diseases as PD and AD, pathological proteins often accumulate at the synapse (Henstridge et al., 2018), leading to synaptic dysfunction and increasing synapses vulnerability (Pieri et al., 2003; Shankar et al., 2007; Crimins et al., 2012). Yet, the causes and the molecular mechanisms leading to pathological synapse loss have not been fully elucidated (Henstridge et al., 2016).

Taken together all these findings confirmed that astrocytes take part to the clearance of synapses in physiological and, possibly, pathological processes. Interestingly, distinct receptors and/or "eat-me" signals might be recruited in the two contexts or even specific molecular machineries might be involved according to the function required.

2.1. Sleep-wake cycle

Various studies have shown that information gathered during wake periods significantly influences synapse activation, leading to a net increase in synaptic strength. In contrast, sleep causes a general weakening of synapses and restores synaptic homeostasis, both of which are necessary for the consolidation and integration of memories. Using two-photon microscopy or serial scanning electron microscopy, it has been revealed that the quantity and size of dendritic spines in the higher cortical regions of mice decreased during the sleep phase (de Vivo et al., 2017; Bushey et al., 2011). Additionally, it has been discovered that Homer1a- and mGluR1/5-dependent pathways cause the removal and dephosphorylation of AMPA receptors during sleep, which cause a consequent net weakening of synapses (Diering et al., 2017). Synapses weakening and depression could lead to structural elimination, thus, it might suggest a glial-mediated synapse clearance role in sleep-wake cycle. Numerous studies have demonstrated that sleep can enhance astrocytes phagocytosis ability in *Drosophila*. Indeed, sleep facilitates Draper/MEGF10-dependent glial elimination of degenerating axons and weak synapses in axotomized flies (Stanjope et al., 2020) (Figure 2.1). Even though the relevance of these findings in injured brain is unclear, it suggests the potential role of sleep-wake cycle as a regulator of astrocytes clearance in healthy mammalian brains. In contrast, data in a mouse model of acute sleep deprivation, demonstrate that astrocytic elimination of synapses, but not microglial phagocytosis, was promoted in the cerebral cortex (Bellesi et al., 2017). Although sleep deficits in rodents causes an increased expression of astrocytic Mertk and Gas6, no changes in synaptic

density or axonal spine number point that overexpression of does receptor not directly influence synapses elimination (Bellesi et al., 2017).

Future studies are required to clarify whether astrocytes can eliminate weak synapses during normal sleep, and the consequent general role of persistent sleep-dependent engulfment of synapses in the adult CNS.

2.2. Aging

Aging causes major changes in glial gene expression as well as synapse dynamics. Interestingly, C1q accumulates in aged brains approximately 300-folds more than that in younger brains (Boisvert et al., 2018; Pan et al., 2020; Stephan et al., 2013). It has been hypothesized that the significant accumulation of C1q protein makes the brain more susceptible to the hyperactivation of the complement cascade and the injury from unchecked microglial phagocytosis (Hong et al., 2016). Notably, an increase in C1q binding to unwanted synapses induce an excessive microglia-mediated synapses elimination. Whereas there is no evidence that an increased C1q-synapses binding affects astrocytes-mediated clearance. In *Drosophila Melanogaster* aged brains, it has been reported that a reduced translation of Draper and a consequent decrease in glial cells phagocytosis (Purice et al., 2016) (Figure 2.1). The restoration of Draper level improves glial cells' ability to remove weak synapse as well as damaged axonal debris in old brains, similar as in the young brains. These results suggest that a reduced translation of phagocytosis-related genes may result in an increase of senescent synapses and synaptic debris thus contributing to aging-related dysfunction such as synaptic homeostasis. In the context of aged-human brain, un unbalanced synaptic homeostasis might cause neuroinflammation and expose healthy synapses to damage.

Despite all of those finding, the exact role of astrocytes in regulating synapse loss in aged-brain and the mechanism behind this process need to be clarified in the future.

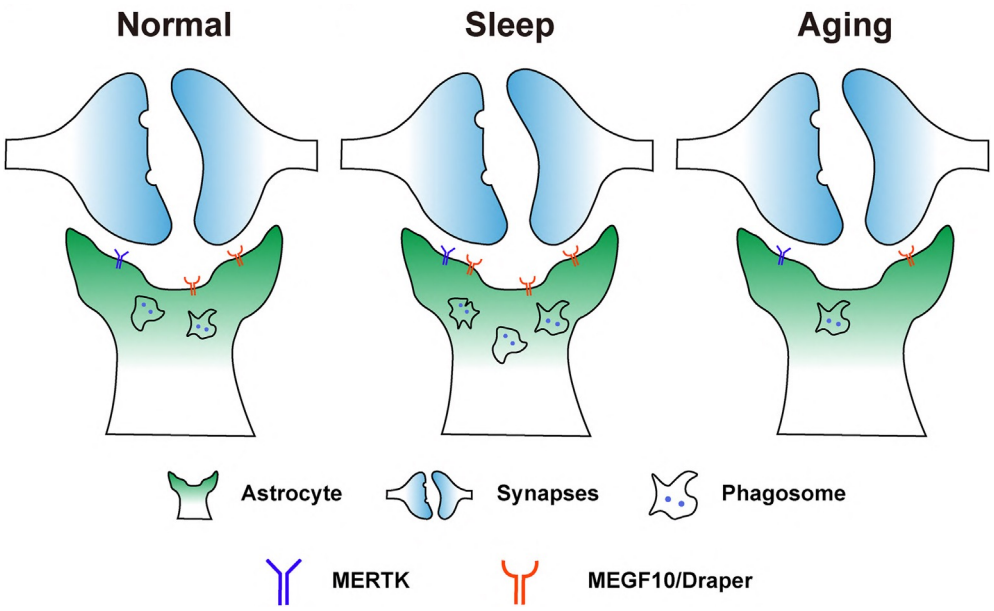

Figure 2.1 Potential changes in astrocyte-mediated synapse elimination during sleep and aging. Under physiological conditions, astrocytes (green) mediate synapse (light blue) elimination through MERTK (blue) and MEGF10/Draper (red) receptors. During sleep, MEGF10/Draper may be upregulated, leading to enhanced synapse phagocytosis. In normal aging, downregulation of MEGF10/Draper translation have been reported, decreasing synapse phagocytosis (adapted from Lee and Chung et al., 2021).

2.3. Neurodegenerative diseases and brain injury

In pathological conditions, it has been demonstrated that neuroinflammation induce astrocytes shift to reactive "A1 or A2 astrocytes". Although this classification is under debate, astrocytes have been distinguished in these two polarized states: the neurotoxic or pro-inflammatory phenotype (A1) and the neuroprotective or anti-inflammatory phenotype (A2). (Escartin et al., 2021). Although both subtypes commonly express certain reactive genes such as Gfap, Vimentin, Lcn2, and Cxcl10, A1 and A2 astrocytes specifically express distinct sets of genes. For instance, A1 astrocytes displayed a decrease capacity to eliminate synapses, which might be explained by the observed downregulation of MEGF10 and MERTK (Liddelow et al., 2017). A1 astrocytes have been identified in several NDs, as PD and AD. Thus, it has been suggested that they could contribute to the disease's progression because of their deficits in synaptic removal (Liddelow et al., 2017; Yun et al., 2018; Joshi et al., 2019). It has been suggested that in APOE4 knock-in mouse model of AD, astrocytes display a decreased phagocytic activity (Chung et al., 2016). Indeed, C1q accumulation has been observed in the

hippocampus of aged APOE4 knock-in mice, suggesting an increased amount of senescent and weak synapses (Chung et al., 2016). In contrast, APOE2, a well-known protective allele for AD, has been shown to enhances the synapses clearance capacity of astrocytes both *in vitro* and *in vivo*. Indeed, in APOE2 knock-in animals, it has been observed a significantly decreased of C1q protein suggesting fewer senescent synapses and consequent less vulnerability to astrocyte-mediated synapse elimination. Although, a reduced C1q accumulation might suggests less weak and/or senescent synapse, a decrease clearance capacity of astrocytes can lead to the accumulation of potentially harmful material as synapses debris, that could trigger AD progression. Astrocyte-mediated synapse elimination has been showed also in amyloid precursor protein (APP)/PS1 mice, a genetic model of AD. Using electron microscopy Gomez-Arboledas and colleagues showed that dystrophic vesicular glutamate transporter 1 (VGLUT1) positive terminals being cleared by astrocytic endfeet in the hippocampus of APP/PS1 mice. (Gomez-Arboledas et al., 2018). In PD, has been reported that striatal neural dynamics undergoes profound alteration. Indeed, striatal medium spiny neurons have been shown to be rapidly eliminated upon dopamine depletion (Graves and Sumeier, 2019). However, the exact role of astrocytes as well as microglia, in mediating synapse loss in PD need future studies. Recently, Shi and colleagues demonstrated that during the poststroke repair and remodeling stage, reactive astrocytes play a role in engulfing synapses through MEGF10- and MERTK-related pathways (Shi et al., 2021). Interestingly, mice lacking MEGF10 and MERTK receptors, they found that a decreased astrocyte-mediated synapse engulfment could help the recovery of ischemic stroke mice but not of hemorrhagic stroke mice. By comparing the transcriptomics of ischemic and hemorrhagic stroke mouse brains, they observed a downregulation of phagocytosis-related genes in astrocytes after a hemorrhagic stroke. Furthermore, Morizawa and colleagues showed that after transient ischemic injury, reactive astrocytes use ATP binding cassette subfamily A member 1 (ABCA1), to eliminate synapses (Morizawa et al., 2017).

All together, these findings suggest that astrocytes respond differentially to different pathological microenvironments and, paradoxically, that in some condition the inhibition of synapses engulfment could be beneficial for improving neurobehavioral outcomes (Shi et al., 2021).

2.4. Astrocytes-microglia crosstalk in synapses elimination

Recent research demonstrates that astrocytes not only eliminate synapses, but also facilitate microglia phagocytosis during development. In fact, during synapses maturation, astrocytes produce the cytokine interleukin-33 (IL-33) (Vainchtein et al., 2018). The IL-33 receptor gene Il1rl1 is expressed in microglial cells during development, according to RNA sequencing data. In mouse brains, Il33 or Il1rl1 deletion results in increased excitatory and inhibitory synapse density and decreased synaptic engulfment by microglia, which is reversed by IL-33 administration (Vainchtein et al., 2018). This suggests that the formation of neuronal circuits depends on the removal of microglial synapse by astrocytes. Moreover, transforming growth factor β (TGFβ) secretion by astrocytes can increase C1q expression and causes an excessive microglial-mediated synapses removal during development of the retinogeniculate system (Bialas and Stevens, 2013). C1q-mediated mechanism has been demonstrated as major pathway that allows microglia to engulf synapses. When C1q binds to synapses, it induces the shift of complement component 3 (C3) into C3b, which activates the microglial complement receptor 3 (CR3) and promotes synapses engulfment (Schafer et al.,2012; Stevens et al., 2007; Gunner et al., 2019). Interestingly, in aged murine brain astrocytes express C3, the ligand of microglial-CR3 receptor, pointing to astrocytes as possible active players in synapses removal through complement-dependent microglial phagocytosis in aging (Lian et al., 2016).

Furthermore, several studies suggested that the release of different pro-inflammatory molecules, such as IL-1α, TNF-α, and C1q, by microglia can induce astrocytes' shift to neurotoxic "A1 astrocytes". As mentioned above, A1 astrocytes display a decreased phagocytic activity (Liddelow et al., 2017), suggesting that microglia-derived pro-inflammatory molecules reduce clearance activity of astrocytes. Similarly, during development, microglial activation through TREM2-mediated signal, inhibits synapses elimination by astrocytes (Jay et al., 2019). Notably, astrocytes engulfed more synaptic elements in Trem2 knockout mice. Moreover, cultured astrocytes show a decreased synaptosomes uptake when they were incubated for 24 hours with microglial conditioned media derived from wild-type mice and not from the Trem2 knockout mice. These data suggesting that TREM2-mediated microglial activation stimulates secretion of some factor that inhibit astrocytic synapses elimination.

Although these data clearly confirm a pivotal role of astrocyte- and microglia-released molecules in synapse elimination, future research is required to reveal specific conditions that can trigger this process.

Chapter 3

Astrocytes and protein aggregates

3. Astrocyte-mediated clearance of protein aggregates

Proteinopathies of the CNS are characterized by the progressive accumulation of misfolded and aggregated proteins, finally resulting in neuronal dysfunction and death. These neurodegenerative processes start as a stochastic event, by virtue of which native proteins dismiss their original conformation and turn into insoluble fibrils (Soto and Pritzkow, 2018, Ross and Poirier, 2004). α-syn is one of prototypical examples of amyloidogenic proteins and similarities in their course of misfolding, aggregation and spreading, support the idea that common aberrant mechanisms may set off their pathological implication in synucleinopathies. (Bayer, 2015). Neurons can secrete fibrillar debris via unconventional exocytosis mechanisms as an extreme attempt of the cells to discard toxic proteins; alternatively, fibrils can be poured into the extracellular space upon membrane disruption (Lee H. J. et al., 2005; Wang et al., 2017; Jang et al., 2010; Emmanouilidou et al., 2010; Pérez et al., 2019). Irrespective of the mechanisms of release, protein aggregates are likely to accumulate and clutter the extracellular space, thus perturbing brain homeostasis and inducing neuronal dysfunction. Indeed, it has been shown that extracellular aggregates can alter neurotransmitters' signaling, impair synaptic transmission and long-term potentiation, and induce cellular toxicity (Diògenes et al., 2012; Gòmez-Ramos et al., 2006; Puzzo et al., 2017). Moreover, a correlation between the appearance of extracellular aggregates and the onset of NDs does exist (Medina and Avila et al., 2014; Volpicelli-Daley et al., 2011; Luk et al., 2012; Lee S. J. et al., 2010). Therefore, the proper removal of extracellular aggregates is crucial to preserve a viable microenvironment and prevent CNS damage.

However, the mechanisms and the key modulators responsible for fibrils recognition and internalization by astrocytes have not been identified yet.

3.1 Parkinson's disease

3.1.1 Epidemiology and classification

PD was first described as 'paralysis agitans' by James Parkinson in 1817. PD is the second most common neurodegenerative disorder after AD and has severe implication for patients and their families (Alves, 2008). PD is a chronic and progressive disorder without cure and affecting 1% of the population over 65 years. The prevalence of PD is higher in Europe, North America and South Africa compared to other countries (Kalia and Lang, 2015). Moreover, ethnicity and

gender are risk factors for the disease (Kalia and Lang, 2015). In USA, the incidence of PD is highest in Hispanic derived people, and, in most populations, PD is twice as common in men than in female (Van Den Eeden et al., 2003; Maruyama and Takedate, 1990). On one hand, some protective effect in woman sex hormones has been observed. On the other hand, gender specific differences associated to exposure to environmental risk factor can explain this gender prevalence (Schrang and Schott, 2006). Aging is also another risk factor for this disorder and, specifically, the prevalence and incidence increase with older age and peak after 80 years of age (Pringsheim et al., 2014). The contribution to PD development is also determined by environmental exposure to a variety of risk factors.

Pesticide exposure, rural living, agricultural occupation, prior head injury, beta-blockers' use and well-water drinking can increase the risk of developing PD. However, there are human behaviors associated with a decreased risk as tobacco smoking, coffee drinking, calcium channel blocker use, alcohol consumption and non-steroidal anti-inflammatory drug use (Noyce et al., 2012). The contribution of genetics in PD risk is well documented, about 900 genetic association studies link dozens of potential gene loci to PD (Nalls et al., 2015). Moreover, many studies have been contributed to the identification of several monogenic forms of this disorder and numerous genetic risk factors (Hely et al., 2008). In particular, the 15% of patients have a family history and between them the 5-10% suffer from a monogenic form of the disease with Mendelian transmission (Deng et al., 2018).

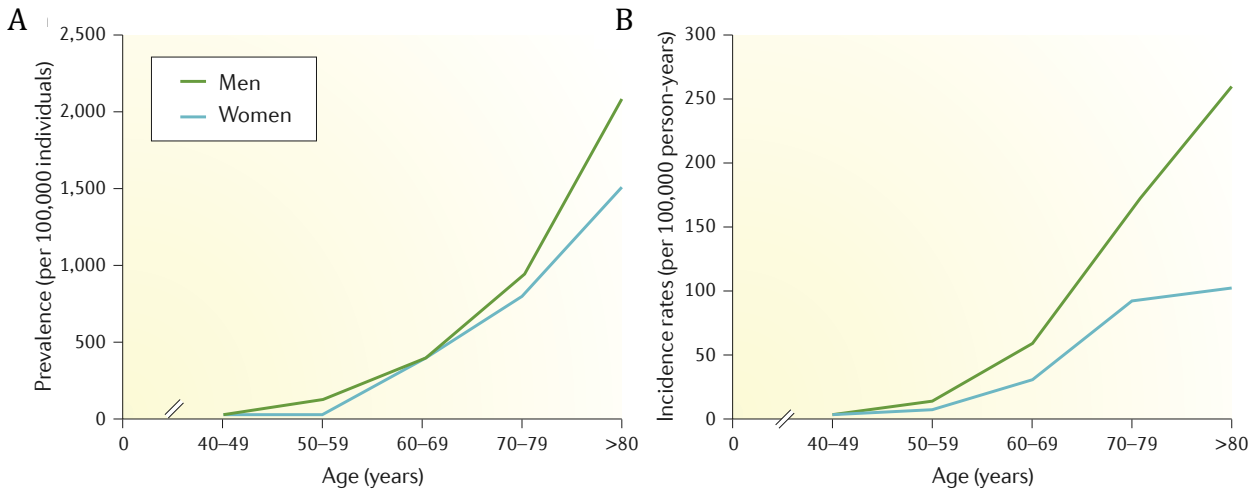

Figure 3.1 Epidemiology of Parkinson disease A. Prevalence of PD in men and women per 100,000 individuals; **B.** Incidence rate of PD per 100,000 person- years. Adapted from Poewe et al., 2017.

3.1.2 Clinical and neuropathological features

PD is a progressive neurological disorder defined by early notable death of dopaminergic neurons in the *substantia nigra pars compacta* (SNpc). SNpc constitutes part of the circuitry that intervenes in the modulation of voluntary movements, and it is located in the basal ganglia. The SNpc is the master regulator of the circuit, it mainly communicates using the chemical dopamine, but other chemical transmitters (glutamate and GABA) are also used to communicate between other areas of the basal ganglia (Dickson et al., 2012). The most profoundly affected area of SNpc is the ventrolateral, which contains neurons that project to the striatum, in particular to the putamen *i.e.* dopaminergic nigrostriatal pathway. Dopamine deficit within the basal ganglia leads to the classical resting tremor, which is the most well-known manifestation of PD and it is found in 70% of patients. Other motor symptoms are bradykynesia, muscle rigidity and postural and gait impairment. PD has a rapid progression and often characterized by other non-motor symptoms such as dementia and cognitive decline (Massano and Bhatia, 2012). Occasionally, in PD there are atypical features such as myoclonus and central hypoventilation (Polymeopoulos et al.,1996). Indeed, neurodegeneration progresses to other brain regions following a typical pattern according to the Braak's model (Braak et al., 1998). It has been shown that SNpc is affected later over the course of pathology compared with other brain regions. Neurodegeneration begins in the lower brainstem and the olfactory system and could be responsible for some of the earliest symptoms such as constipation and loss of smell. Then, it moves further up the brainstem, travelling to the area below the SN involved in pain, sleep and mood (Levy et al., 2009). In the third stage, neuronal loss has entered the SN and subsequently the pathology spreads to the limbic system involved in emotion, motivation and long-term memory stage. In the later stages of PD progression, neuronal degeneration reaches the mesocortex, the region between limbic system and cerebral cortex and, finally, it spreads in all directions into the structures of the temporal, parietal, and frontal lobes. At this stage, changes in the neocortex start to affect the memory and sensory areas in the brain (Levy et al., 2009). Motor and non-motor symptoms that affect PD patients are summarized in Table 1.

Motor symptoms of PD	Non-motor symptoms
Resting tremor	Constipation
Rigidity	Autonomic dysfunction
Bradykinesia	Impaired olfaction
Postural instability	Dementia
Festinating gait	Depression
Micrographia	Sleep disorders
Masked facies	Impulse control disorders
Retropulsion	Psychosis
Hypophonic speech	

Table 1. **Clinical syndrome of PD.** Motor and non-motor symptoms (Jakel and Stacy, 2014).

Another distinct pathological hallmark of PD is the accumulation of cytoplasmic proteinaceous inclusions known as Lewy bodies (LBs) and Lewy neurites (LNs). LBs and LNs are mainly composed by two proteins: aggregated α-syn and ubiquitin (Levy et al., 2009) (Figure 3.2).

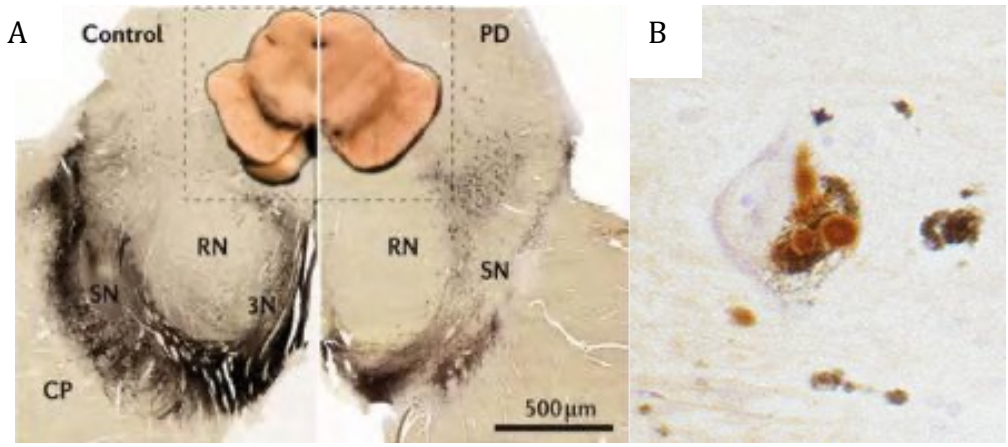

Figure 3.2 Pathological hallmarks of PD. A. Dopaminergic neuronal death in the SNpc and **B.** Cytoplasmic inclusions, LBs (Levy et al., 2009).

Compelling evidence suggests the possibility that α-syn is a prion-like protein and that PD is a prion-like disease. Autopsy studies of patients with advanced PD who received transplantation of fetal nigral mesencephalic cells demonstrated that typical Lewy pathology had developed within grafted neurons (Loria et al 2017). This suggests that α-syn had migrated from affected to unaffected cells. So far, laboratory studies confirm that aggregated α-syn can transfer from affected to unaffected neurons in vivo but also from neurons to glia cells (Loria et al 2017).

Extended neuroinflammation is another feature of PD pathology (Tansey and Goldberg, 2010). This state is probably caused by neuronal degeneration and the release of α-syn containing neurons as well as cellular debris. The presence of an active inflammatory response in the brain is mediated primarily by resident microglia. Activated microglia can release trophic factors, such as brain-derived neurotrophic factor and glial-derived neurotrophic factor, but also harmful reactive oxygen and nitrogen species and pro-inflammatory cytokines. Whether the balance of these actions is beneficial or harmful to neurons is not yet established (Tansey and Goldberg, 2010). Moreover, also astrocytes can intervene in neuroinflammation and their involvement in PD has been long recognized, but somewhat overlooked. Accordingly, both reactive astrocytes and microglia occur within brain areas affected by neurodegeneration in PD.

In PD, microglia and astrocytes are both involved in clearance of extracellular debris and protein aggregates, which might aid in the survival of neurons. Near the remaining nigral DA neurons, microglia display the characteristic morphology of phagocytic cells, similar to those seen in aging (Tremblay et al., 2019). The involvement of microglial phagocytosis in PD pathogenesis is further supported by the fact that microglia uptake and remove DA cell debris in vivo (Tremblay et al., 2019). Recent studies show that astrocytes actively participate in phagocytic processes, and they might intervene in PD. Specifically, both microglia and astrocytes can engulf and degrade aggregated α-syn (Tremblay et al., 2019). Considering the reported prion-like ability of aggregated α-syn released by degenerating neurons to propagate to other cells, it is important to consider whether glial-mediated phagocytosis contribute to the spreading process. To understand the molecular mechanism and the physio-pathological significance of glial phagocytosis in PD might provide novel opportunities for drug intervention.

Currently, all treatments for PD are palliative and not curative. Indeed, the therapy is dedicated to maximizing patients´ quality of life and minimize disability. Levodopa (L-dopa), the main dopamine precursor, is the most potent drug for controlling PD symptoms, particularly those related to bradikynesia. It alleviates the symptoms for approximately 5 years (Janković et al., 2006). After that time, the majority of the patients experience diverse adverse effects, predominantly motor fluctuations and dyskinesia (Jankovic, 2005). In addition to L-dopa, also dopamine agonists, catechol-o-metyltranspherase (COMT) inhibitors, or anticholinergic drugs may be used concomitantly depending on the clinical profile of the patient. Also, neurological surgery has become a therapeutic strategy to ameliorate the PD

symptoms. Currently, deep brain stimulation (DBS) of the basal ganglia is considered the best alternative for disabling PD relative symptoms (Jankovic and Aguilar, 2008). Finally, in the last couple of years, PD symptoms and tremor is reduced by using "High Intensitive Focused Ultrasound". This innovative technique is based on the inactivation of the subthalamic nucleus using high frequency ultrasound and is completely non-invasive and definitive (Bauer and Pllana, 2014). In the last decade, several groups-initiated cell therapy by fetal stem cells transplantation that ameliorated the symptoms after a short time evaluation but failed at longer time after the transplantation (Stoker et al., 2020).

3.1.3 Genetics

The vast majority of PD cases is likely caused by a combination of environmental factors and genetic background. About the 15% of patients show a family history and the 5-10% suffer from a monogenic, Mendelian form of the disease (Kalinderi et al., 2016). To date, 13 PARK genes identified within the PARK loci have been associated with familiar autosomic dominant or recessive inheritance (Figure 3.3).

The first genetic modification linked to PD was the guanine changed to adenine at position 209 (A53T in the protein product) in the gene that encode for α-syn (*SNCA)* (Polymeropoulos et al., 1997). Several other point mutations, together with duplications and triplications of the entire locus, were later added to the list of PD-linked alterations with a clear genomic dosage-related phenotype*, i.e.* a more severe phenotype and a higher penetrance in the case of multiplications as compared to the effect of single mutations (Singleton et al., 2003). *SNCA* is located within the PARK1 locus on the chromosome 4 and SNCA mutations cause autosomic dominant forms of PD (Polymeropoulos et al., 1997). Patients carrying mutations in SNCA usually manifest early-onset PD (<50yr). Mutations in SNCA are overall rare: three missense, duplication and triplication mutations so far have been reported (Polymeropoulos et al., 1997). As mentioned, SNCA gene encodes for an abundant protein, α-syn, and the disease-causing mutations render α-syn more prone to aggregate. One of the most intriguing aspects of the majority of neurodegenerative diseases, and one that applies to PD, is that, although displaying a large heterogeneity in terms of clinical manifestation. The molecular defects underlying the pathology can be grouped under a relatively small number of cellular pathways such as mitochondria quality control, oxidative stress and membrane trafficking. In 1998, mutations in PRKN/PARK2 were found to be the cause of severe, autosomal recessive juvenile parkinsonism. Recessively inherited parkinsonism is more frequently associated with early

onset PD (<40yr) (Paisàn-Ruìz et al., 2004). Within patients showing PD onset before 45 years of age, mutations on Parkin have been detected in up to 50% of familial cases (Paisàn-Ruìz et al., 2004).

Another *PARK* locus causing early-onset PD is *PARK7*, where DJ-1 is located. DJ-1 has been shown to buffer oxidative stress. Finally, PARK14/PLA2G6 enters the list of mitochondria-related genes. PLA2G6 is a Ca^{2+} independent phospholipase particularly important for the homeostasis of mitochondrial membrane. Mutations in CHCHD2/PARK22 and VPS13C/PARK23 have been associated with different parkinsonian manifestations, *i.e.* autosomal dominant, late onset PD and autosomal recessive, early onset parkinsonism, respectively (Singleton and Hardy, 2016). A substantial number of PARK genes are involved in membrane fusion and endo-lysosomal functions. Starting from the dominantly inherited forms, PARK17/VPS35 encodes for a component of the retromer, a complex protein machinery important for the recycling of transmembrane receptors from endosomes to the trans-Golgi network (TGN). Instead, loss-of-function mutations in ATP13A2/PARK9 have been associated with Kufor-Rakeb syndrome (KRS), an autosomal recessive form of juvenile-onset parkinsonism. ATP13A2 encodes for a transmembrane P-type ATPase involved in cargo-sorting at the endo-lysosomal level as well as lysosomal function (ATP13A2) (Ramirez et al., 2006). The exclusively neuronal protein auxilin and the phosphatase synaptojanin-1 codified respectively by DNAJC6/PARK19 and SYNJ1/PARK20 are instead involved in clathrin-mediated endocytosis of synaptic vesicles (SVs).

Finally, mutations in LRRK2/PARK8 are the most common cause of familiar PD and LRRK2-linked PD manifests autosomic dominant inheritance with incomplete penetrance. LRRK2 encodes for Leucine rich repeat kinase 2 (LRRK2) This gene might be considered a unifying element in the frame of PD, as it interacts at different levels with other PARK genes it is a risk factor for PD70 and LRRK2 mutations have been found also in sporadic form of PD (Bechinger et al., 1992). A separate paragraph will be dedicated to a comprehensive discussion about LRRK2 and its relevance to PD.

Concluding, the advent of genome-wide association studies (GWAS) has helped in the identification of around forty loci, including LRRK2, carrying common SNPs that mildly increase PD risk (Bechinger et al., 1992). Considering the picture that has emerged to date regarding the genetics of PD, the estimates suggest that only one tenth of the heritable

component has been unveiled (Bechinger et al., 1992). Thus, additional studies will help to disclose novel genetic links and to define those networks that are deregulated in PD.

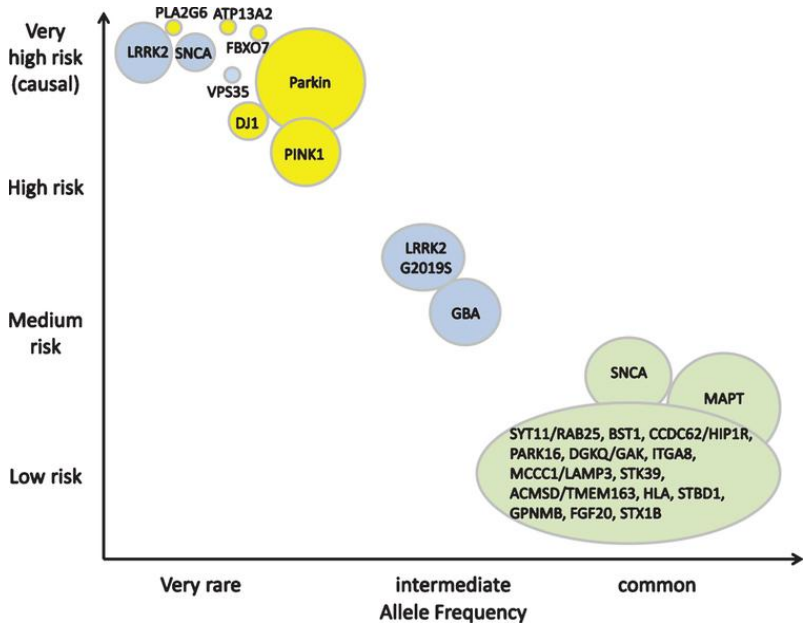

Figure 3.3. **Parkinson´s disease related mutated genes**. The most common mutations are usually associated with a lower risk of developing the disease, while the least common ones usually confer high risk of developing PD (Greggio et al., 2008).

3.2 α-synuclein

α-syn is a 14kDa protein composed of 140 amino acids and encoded by SNCA gene (Tamgüney and Korczyn, 2018). It is composed of three domains, an α-helical amino terminus, a non-amyloid component (NAC), and an unstructured carboxy terminus. These domains are essential for the pathogenic progress observed in PD and other synucleinopathies. The amino terminus of α-syn forms an α-helical structure that binds to protein interactors or lipid membranes (Lawand et al., 2015). α-syn is highly concentrated in presynaptic terminals (Renner and Melki, 2014) and its co-localization with the reserve pool of synaptic vesicles Lee S. J. et al., 2008) supporting the idea that α-syn may contribute to the cycling of synaptic vesicles. Suggested roles of α-syn are the modulation of vesicle pool size, mobilization or endocytosis (Vargas et al., 2014). Some studies suggest that α-syn is involved in the control of synaptic membrane processes (Bellucci et al., 2012) and participates in the control of neurotransmitter release via interactions with members of the SNARE family (Tsigelny et al., 2012). According to other studies, α-syn could also be transported in the nucleus (Hodara et

al., 2004) and modulate some mitochondrial transcription factors, thus negatively impacting on mitochondria homeostasis (Siddiqui et al., 2012; Desplats et al., 2009). Soluble α-syn is natively unstructured and monomeric. Emerging biophysical and biochemical studies demonstrated that the interaction between α-syn and lipids influences α-syn oligomerization and aggregation revealing the toxic function of the aggregates (Vaikath et al 2022). α-syn can turn into oligomeric and/or fibrillar conformations in particular pathological conditions, including gene mutations of SNCA, decreased rate of clearance, oxidative stress, iron concentration, or posttranslational modifications (Lawand et al., 2015; Sian-Hulsmann et al., 2015) (Figure 3.4). Posttranslational modifications of α-syn, such as phosphorylation (mostly in the serine residue S129J), ubiquitination, acetylation, sumoylation, and nitration, have been observed to alter α-syn structure and function, and are related to α-syn aggregation and neurotoxicity (Krieger et al., 1989). Moreover, the three most common PD-causing point mutations in SNCA (A30P, E46K and A53P) accelerate α-syn aggregation in vitro. This suggests that α-syn is heavily implicated in the pathogenesis of PD, both in familial and sporadic cases (Angot et al. 2012). As described by Spillantini and colleagues, α-syn is one of the main proteinaceous components of LB but the pathological role of α-syn in PD is still debated (Bengoa.Vergniory et al., 2017). More recent studies proposed that post-fibrillization of α-syn C-terminal truncation mediated by Calpains 1 and 2 plays critical roles in fibrillation, cell toxicity and LBs maturation (Mahul-Mellier et al., 2020). These results highlight the importance of developing more immunological tools to detect LBs in which α-syn is already truncated (most of the commercial antibodies are directed to the C-terminal) and encourage to develop therapeutic strategies based on targeting the C-terminus of α- syn.

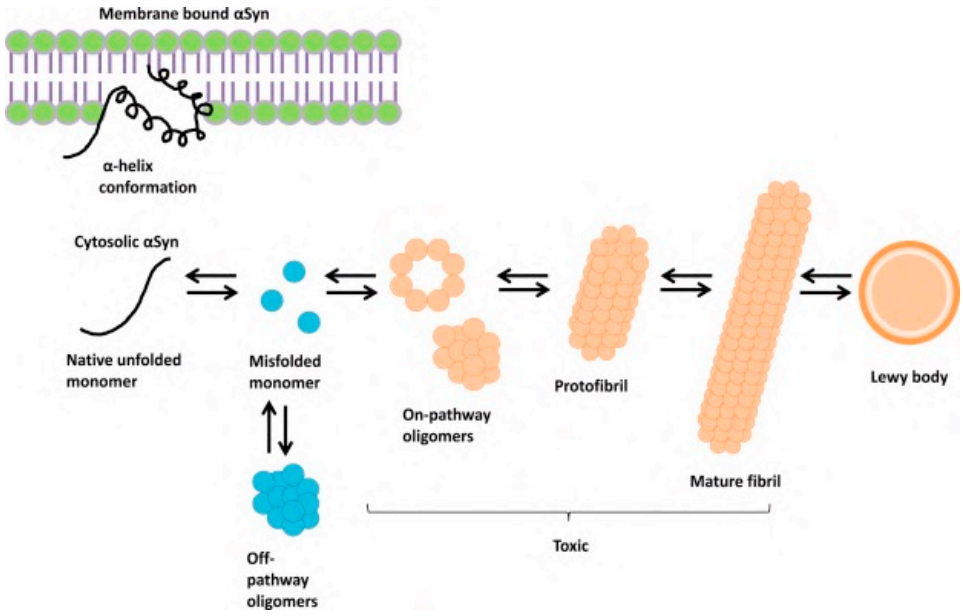

Figure 3.4. α-synuclein aggregation stages. Different stages of the aggregation of α-syn, from monomeric species to fibrils, through oligomers, the suspected toxic species (Mochizuki et al., 2018).

3.2.1 Astrocyte-mediated α-syn clearance

The role of astrocytes in NDs, specifically in synucleinopathies, is not well understood. Up to date, there is little evidence regarding the expression levels and the physiological role of α-syn in astrocytes (Castagnet et al., 2005). Of note, α-syn aggregates are found in different cell types as well as in different brain regions across the spectrum of α-synucleinopathies. Interestingly, clinical research identifies an increase of astrocytic α-syn positive inclusions in the Frontotemporal Dementia and advanced PD patients that may play a role in the symptomatic progression of these diseases and deserves further study to understand associated functional impairments (Braak et al., 2007). In some cases, astrocytes having α-syn inclusions are found so far from LB or dead neurons and sometimes even exceed LB-positive neurons (Braak et al., 2007).

The origin of α-syn accumulation in astrocytes remains unclear. Moreover, the process of α-syn internalization is thought to be different between cells in the brain, which suggests that this might potentially lead to formation of unique α-syn conformers within different cell types. Distinct α-syn aggregates formed in neurons are capable of templating normal soluble α-syn through a prion-like process (reviewed in Uchihara and Giasson, 2016). Resulting in a prion-like seeding process, pathological α-syn conformers can potentially be passage through inter-

neuronal or even neuro-astroglial contacts and result in astrocytic increase of pathologic α-syn (Männistö and Garcìa-Horsman, 2017). Interestingly, in the presence of α-syn aggregates, neurons and glial cells have been demonstrated to increase the formation of Tunneling nanotubes (TNTs) (Abounit et al., 2016; Rostami et al., 2017). TNTs were first discovered in 2004 as extensions of the cell cytoskeleton that enable distal and close contact among neighboring cells (Rustom et al., 2004). Furthermore, in vitro studies have reported the presence of TNTs that allow the transfer of α-syn between neurons and neuron-glia co-cultures (Abounit et al., 2016; Loria et al 2017; Dieriks et al., 2017; Rostami et al., 2017). In addition, α-syn released by neurons through an active process, such as exocytosis, or after cell death, can be taken up by astrocytes (Lee H. J. et al.,2010; Lindström et al., 2017; Rostami et al., 2017). In the early stage of PD and other α-synucleinopathies, astrocytes require TLR2, but not TLR4, as for microglia for α-syn engulfment (Fellner et al., 2013). Consistently, Fellner and colleagues demonstrated that TLR4 deficiency does not affect α-syn internalization by astrocytes (Fellner et al., 2013). However, despite the mechanisms underlying TLR2-mediated internalization of α-syn are not known, it has been suggested that aggregated α-syn fibrils could be a TLR2 ligand (Bèraud et al., 2011; Kim et al., 2013). Coherently, it has been shown that primary rat astrocytes expose to neuronal-derived α-syn, significantly increased TLR2 transcript levels and induces an inflammatory gene expression profile in vitro (Lee H. J. et al.,2010). More recently, several reports focus on proposed different mechanisms for the internalization of the fibrillar form of α-syn by astrocytes. Specifically, it has been explored whether primary murine and human iPSC-derived astrocytes were able to internalize α-syn Pre-Formed Fibrils (PFFs) in vitro. Interestingly, extracellular clusterin, a chaperone protein, interacts with α-syn PFFs (but not oligomers) by binding their exposed hydrophobic regions and that complexes can engulf astrocytes through the endocytic pathway. Of interest, clusterin KO astrocytes display a decreased endocytosis of PFFs, suggesting a direct role of this chaperone in the clearance of α-Syn. In support to this, the supplement of extracellular clusterin can rescue the effect of clusterin absence in astrocytes 33045109. Once internalized, α-syn can be subsequently transferred to the lysosomes (Lee H. J. et al.,2010; Lindström et al 2017). Luk and colleagues show that astrocytes can take up α-syn PFFs and direct them to lysosomes in organotypic slice cultures from wild type mice (Loria et al 2017). Moreover, it has been shown that upon extensive uptake of α-syn aggregates, astrocytic cells exhibit large intracellular deposits due to the overwhelming of endo-lysosomal machinery and to an incomplete digestion (Lindström et al 2017; Sacino et al 2017), indicating an impaired astrocytic phagocytic activity under pathological conditions.

In turn, the accumulation of α-syn in astrocytes impairs the astrocytic capability to support neuronal metabolism and synaptic function (Figure 3.5). Specific in vivo overexpression of mutant SNCA in astrocytes causes movement disorders and developed astrogliosis before the onset of symptoms (Gu et al., 2010). The affected astrocytes exhibited decreased expression of the glutamate transporters GLAST1 and GLT1 (Gu et al., 2010) and abnormal localization of the water channel AQP4 (Simard and Nedergaard, 2004). Moreover, α-syn accumulation in astrocytes can cause mitochondrial dysfunction. For example, in human primary astrocytes α-syn can accumulate into the mitochondria causing reduced oxygen consumption and ROS generation (Braidy et al., 2013). Consistent with this evidence, postmortem analyses showed loss of complex I activity and oxidative damage in the brain of sporadic PD patients (Keeney et al., 2006).

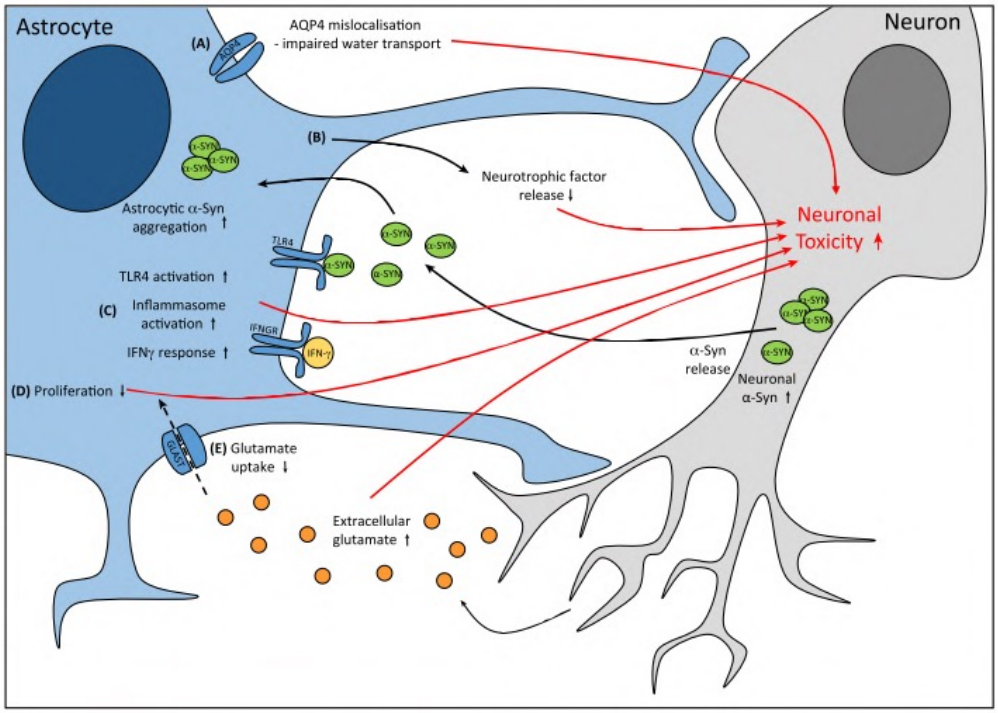

Figure 3.5. Dysfunctional astrocytes contribute to neuronal toxicity. Astrocyte dysfunction elicits neuronal toxicity via five main mechanisms; **A.** AQP4 water channels are mislocated away from the astrocyte end-feet, resulting in impaired water transport **B.** neurotrophic factor release is decreased, **C.** inflammatory signaling increases, **D.** astrocyte proliferation is impaired, and **E.** Glutamate uptake is reduced, potentially resulting in increased extracellular glutamate and, therefore, neuronal excitotoxicity (Booth et al., 2017).

Recent studies suggest that astrocytes contribute to the propagation of the disease by transferring undigested material to surrounding cells (Rostami et al., 2017) (Figure 3.5). It is hypothesized that misfolded α-syn can spread from affected to unaffected regions of the CNS, leading to neurodegeneration and the progression of PD pathology. Interestingly, the overexpression of α-syn in mouse astrocytes induces astrogliosis and disrupts normal astroglial function leading to neurodegeneration (Gu et al., 2010). When iPSC-derived astrocytes obtained from familial and sporadic PD patients were co-cultured with midbrain dopaminergic neurons, they induced morphological changes indicative of neuronal degeneration. This was attributed to the secretion and transfer of α-syn from astrocytes to neurons although release of additional toxic molecules that affect neuronal survival could not be ruled out (di Domenico et al., 2019). Nevertheless, α-syn transmission to astrocytes induces the production of multiple proinflammatory cytokines (IL-1α, IL-1β, IL-6, IL-18) and chemokines (CC-, CXC- and CXCL-type) as a response (Lee H. J. et al.,2010; Klegeris et al., 2006). As a result of the neuroinflammatory process, astrocytes become reactive as demonstrated in animal models and in SN and striatum of PD patients, increasing the expression level of IL-6 and TNF-α and increasing the risk of neuronal degeneration.

Despite these findings, future studies are necessaries to further clarify the molecular mechanisms involved in astrocytic clearance of α-syn, which may represent a future treatment for NDs as PD.

3.3 LRRK2

LRRK2 is also called dardarin, from the Basque word 'dardara' that means tremors. It is a large and complex protein that counts 2527 amino acids (286 kDa) and works as a dimer (Civiero et al., 2012). It consists of a dual catalytic core composed by the GTPase ROC followed by COR and kinase domain. It has been proposed that the kinase activity of LRRK2 is intimately linked to that of the ROC domain (Biosa et al., 2013). At the N-terminus, protein interaction domains are present including Armadillo, Ankyrin, and leucine-rich repeat domains, whereas the C-terminus includes a WD40 domain. LRRK2 is phosphorylated in the LRR region at a series of serine residues including S910, S935, S955 and S973. These phosphorylation sites are controlled by kinases of the IKK family and casein-kinases, and phosphatases like Protein Phosphatase 1 (PP1). All together, these sites are important for the binding of the chaperone

14-3-3s. 14-3-3s are seven conserved proteins that have many functions in the cell through the modulation of client protein interactome, localization, folding and activity. 14-3-3 proteins are of particular interest because of their multiple links with PD disease pathology (Biosa et al., 2013). LRRK2 is ubiquitously expressed through the body (Kang and Marto, 2017). LRRK2 mRNA and protein is found in different regions of the CNS including the olfactory bulb, striatum, cortex, hippocampus, midbrain, brainstem and cerebellum as well as in peripheral organs such as kidneys, lungs, spleen and immune cells (Kang and Marto, 2017). Within the human and murine brain, both neurons and glial cells express LRRK2. At the subcellular level, LRRK2 is predominantly located in the cytoplasm but it can be also associated with the mitochondrial external membrane or cellular structures involved in vesicular trafficking, such as endosomes and lysosomes (Roosen and Cookson, 2016).

The physiological role of LRRK2 is still not fully dissected but its association with membrane lipid rafts and the presence of a GTPase domain and a kinase domain in the protein suggest its implication in an intracellular signaling pathway (Roosen and Cookson, 2016) (Figure 3.6). LRRK2 is a well-established interactor of cytoskeletal components such as actin and tubulin (Roosen and Cookson, 2016). Many studies confirm the role of LRRK2 in the modulation of actin-linked cytoskeletal dynamics and microtubule polymerization in several cell types including neurons (Figure 3.6). Additional studies have been suggested the involvement of LRKK2 in the regulation of the autophagic process, in the vesicular trafficking and in the inflammatory process (Roosen and Cookson, 2016). Important evidence for a physiological role of LRRK2 came from knockout animals. Lrrk2-/- mice or rats show a normal dopaminergic system, with no alterations in the number of dopaminergic neurons or in the levels of striatal dopamine. However, Lrrk2-/- lungs and kidneys are and characterized by the accumulation of membranous organelles such as lamellar bodies and lysosomes, respectively (Baptista et al., 2013). Autophagic-lysosomal pathway is also dysregulated and apoptotic cell death and inflammatory responses are increased. It is now well established that LRRK2 has a regulatory action through a direct phosphorylation on a subset of Rab GTPase, including Rab3, Rab8, Rab10, Rab35, and Rab7L1, involved in the endocytosis and autophagy (Zerial and McBride, 2001). Rab proteins regulate membrane trafficking, vesicle formations and the movement along actin and tubulin networks. Moreover, Rab proteins are the master regulators of membrane fusion (Zerial and McBride, 2001). LRRK2 phosphorylates Thr72 residue in Rab8 and the structurally equivalent residues in other substrate Rab GTPases, and, importantly, the LRRK2-mediated phosphorylation is significantly enhanced by the PD-associated LRRK2

pathogenic mutations. It has been hypothesized that increased Rab phosphorylation promotes dissociation from the regulatory protein GDI in the cytosol with concomitant membrane insertion (Zerial and McBride, 2001). However, the function consequence, in both neuronal and glial cells, has not been elucidated.

Mutations in LRRK2 are the most common cause of familiar PD and account for around 10% of the total genetic PD. Moreover, LRRK2 polymorphisms are also associated with increased risk of sporadic PD (Healy et al., 2008). Pathological LRRK2 mutations mainly occur in the Roc, COR and kinase domains. Other PD liked mutations that fall outside the kinase region do not consistently cause increased kinase activity in vitro. However, it has been well established that many of them, *i.e.* R1441C, Y1699C and I2020T, induce enhanced LRRK2 autophosphorylation and phosphorylation of Rabs in cells and in mice. (Bonet-Ponce and Cookson, 2022). Importantly, an individual carrying a mutation does not necessarily develop PD, as the penetrance is age-dependent, incomplete and variable according to the mutation. Focusing on the G2019S mutation, the penetrance varies between 25% and 42.5% at 80 years of age, meaning that the probability of manifesting the disease for these subjects is relatively low compared to carriers of the R1441G mutation, whose penetrance reaches 95% in later life (Hernandez et al., 2016). This mutation is the most frequent pathogenic mutation in the overall LRRK2-PD population (Singleton et al., 2013) and occurs in 5-6% of the patients with autosomal dominant PD and 1-2% of the sporadic cases (Jaleel et al., 2007). G2019S occurs in the kinase domain of LRRK2, leading to an increase in kinase activity by 2-4-fold (West et al., 2007).

As mentioned above, LRRK2 is expressed in neurons, astrocytes, and microglia (Reyniers et al., 2014) and is associated with a large variety of functions, both in terms of its physiological and cellular roles (Wallings et al., 2015). This protein is involved in many different cell signaling pathways participating in mitochondrial functionality, cytoskeletal dynamics, response to ROS production or autophagy. It is implicated in the autophagy-lysosome pathway in many models, not only in neurons but also in astrocytes (Xing et al., 2013; Greggio et al., 2008) (Figure 3.6).

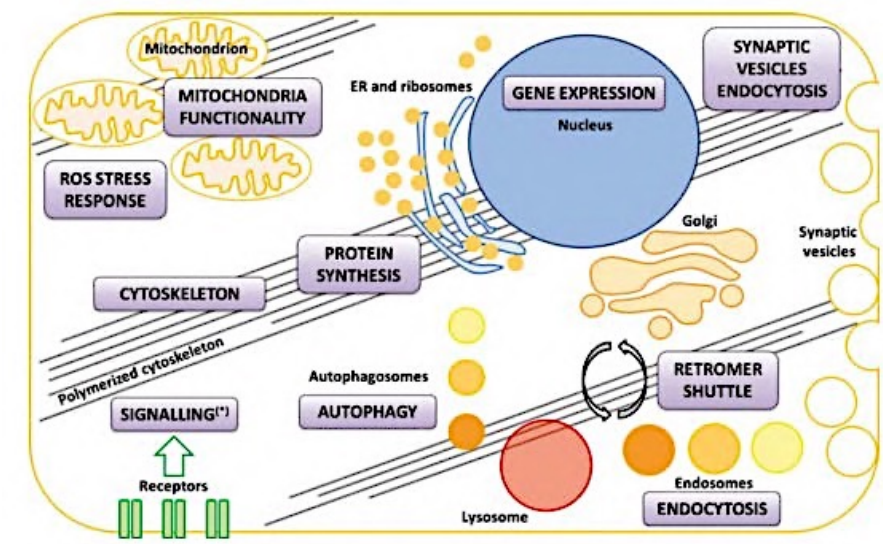

Figure 3.6 Cell processes associated with LRRK2. Representation of the cellular processes (boxes) that have been associated with LRRK2 function in physiology and/or disease (Walling et al., 2015).

3.3.2 LRRK2 function in astrocytes: does it contribute to Parkinson's disease?

Growing evidence highlights that LRRK2 controls multiple processes in glial cells, both microglia and astrocytes, and suggests that impaired LRRK2 activity in these cells, due to gene mutation, might be directly associated with pathological mechanisms underlying PD.

Astrocytic LRRK2 is involved in the autophagy-lysosome pathway (di Domenico et al., 2019; Henry et al., 2015). Manzoni and colleagues demonstrated that the inhibition of Lrrk2 kinase activity impacts autophagic-flux in primary astrocytes (Manzoni et al., 2013a; Manzoni et al., 2013b). Few years later, the same group reported that lacking LRRK2 kinase activity stimulate macro-autophagy through the activation of Benclin-1, a well-known protein involved in autophagy, suggesting a direct involvement of LRRK2 in autophagosome formation and maturation (Manzoni et al., 2016). Coherently, deficits in macroautophagy have been observed in iPSC-derived astrocytes harboring the G2019S mutation, causing a progressive α-syn accumulation (di Domenico et al., 2019).

LRRK2 has been implicated also in the regulation of lysosomal morphology and function in several models, including astrocytes. Indeed, LRRK2 has been detected in the lysosomal membrane in resting astrocytes. In mouse primary astrocytes, LRRK2 co-localizes with the

lysosomal markers, LAMP1 and LAMP2 (Henry et al., 2015). Recently, Herbst and colleagues reported, in microglia and macrophages, a recruitment of LRRK2 at damaged lysosomal membrane (Herbs et al., 2020). Authors proposed that LRRK2 moves to membrane of damaged lysosomes where it recruits and phosphorylates its substrates, as Rab8A, to repair the damage. Coherently, Bonet-ponce and colleagues observed the presence of LRRK2 on the surface of dysfunctional lysosomes in mouse primary astrocytes (Bonet-Ponce et al., 2020). Despite the beneficial role of LRRK2 at the lysosome, controversial literature is present regarding the role of LRRK2 kinase activity in the regulation of lysosomal structure and morphology. Of note, the expression of PD-linked LRRK2 mutants, such as R1441C, Y1699C and G2019S, in primary mouse astrocytes, has been reported to increase lysosomal size (Henry et al., 2015). Taken together, these data suggest a role of LRRK2 and PD-linked mutation in the regulation of the autophagy-lysosome pathway.

Although, LRRK2 has been demonstrated as a regulator of the phagocytic pathway via specific modulation of the actin-cytoskeletal regulator WAVE2, (Kim et al., 2018); the exact role of LRRK2 and its kinase activity in regulating clearance mechanisms is not completely resolved. The G2019S mutation in LRRK2 has been reported to induces a WAVE2-mediated enhancement of phagocytic response in macrophages and microglia from patients and mouse models (Kim et al., 2018). Thus, highlighting a LRRK2-dependent lysosomal dysfunction in astrocytes that might exacerbate the neurodegeneration process because of their inability to clear up extracellular material α-syn. Taken together these findings, point out that astrocytic LRRK2 mutations might be implicated in PD via dysregulating the autophagic-lysosomal pathway.

Despite the functions on LRRK2 in membrane trafficking, several reports highlighted a role of this protein and of the G2019S pathological mutation in other astrocytic function such as gliotransmission and metabolism. For instance, iPSC-derived astrocytes carrying the G2019S pathogenic mutation have been reported to exhibit a morphological atrophy which correlates with a decreased mitochondrial activity and ATP production along with an increase of glycolysis (Ramos-Gonzalez et al.,2021). Moreover, G2019S mutation, in primary astrocytes, has been shown to negatively impacts on GLT1 recycling at the plasma membrane, causing its intracellular re-localization and degradation. In agreement, a decreased level of the transported has been observed in LRRK2 G2019S human *post-mortem* caudate and putamen and in the striatum of PD mice model (Iovino et al., 2022). Furthermore, an increased kinase activity of LRRK2 has been demonstrated to interferes with ciliogenesis in astrocytes (Khan et al., 2021). Indeed, astrocytes carrying the G2019S mutation throughout the striatum showed a

ciliation impairment that correlates with a dysregulation of Hedgehog signaling, mechanism that has been shown to trigger neuroprotection.

Overall, emerging picture suggests that pathogenic LRRK2 can cause astrocytes' loss of beneficial roles or gain of toxic functions can contribute to neurodegenerative conditions. Thus, the study of the role of LRRK2 in this class of cells might unravel novel pathways involved in PD pathobiology.

Chapter 4

Aim of the Project

Aim of the project

The global aim of this PhD Project is to molecularly characterize astrocyte-mediated brain clearance both in health and disease, from different perspectives and through several approaches.

In the healthy brain, astrocytes maintain ion homeostasis of the microenvironment, provide structural and metabolic support, regulate synaptic transmission, water transport and blood flow (Reemst et al., 2016). However, some of the astrocyte functions are not completely understood and novel roles in the regulation of brain homeostasis have been recently conferred to this class of cells. Of note, astrocytes are considered phagocytes and can ingest cellular debris, aggregated protein, and other material such as synaptic elements (Morizawa et al., 2017; Wakida et al., 2018).

First, this thesis will be focused on astrocyte-mediated elimination of synaptic terminals. Synaptic pruning is the brain's way of removing neuronal connections that are no longer needed both during health and disease conditions (Sakai et al., 2020). Astrocytes have been shown to participate in the elimination of unwanted synapses as well as other extracellular materials in cooperation with microglia (Konishi et al., 2022). Specifically, astrocyte participates in developmental synaptic elimination and adult astrocytes engulf synaptic elements in healthy mice. Supporting this statement, transcriptome analysis identified MEGF10 and MERTK as genes involved in engulfment and phagocytosis of astrocytes (Chung et al., 2013). Although the MEGF10-MERTK is a confirmed phagocytic pathway in mediating synaptic elimination by astrocytes, a detailed dissection of the proteins involved in the recognition and degradation of such material is still missing. (Jung and Chung 2018). Here, we aimed to identify novel regulatory mechanism of astrocyte-mediated elimination of synaptic terminals.

The specific aims of the first part of the project are:

Objective 1 To provide a molecular characterization of the protein machineries involved in astrocytes-mediated synaptic pruning using a siRNA-based screening approach.

Objective 2 To validate the selected astroglial regulators *in vitro* both in murine primary astrocytes and in human iPSC-derived astrocytes.

The second part of the thesis will be dedicated to the study of the role of astrocytes in the elimination of extracellular, neuronal-released α-syn in PD. Indeed, astrocytes have been shown to participate in the clearance of toxic protein released by neurons. Recent data suggest that the internalization and accumulation of fibrillar α-syn in astrocytes may play an important role in PD progression and associated chronic neuroinflammation (Rostami et al., 2020; Rostami et al., 2017). Mutations in the leucine-rich repeat kinase 2 (LRRK2) gene represent one of the most common causes of familial PD and have been linked to impaired α-syn degradation in neurons (Schapansky et al., 2018; Paisàn-Riuz et al., 2013). LRRK2 is expressed in multiple cell types of the central nervous system, and it has been implicated in the regulation of lysosomal morphology and function in different cell types, including astrocytes and neurons (Herzig et al., 2011; Tong et al., 2012; Schapansky et al., 2018). LRRK2-linked impairment in the lysosomal pathway in neurons may cause cell death and consequent α-syn release. Hence, as microglia, astrocytes respond to pathological condition and switch into a phagocytic state to eliminate cell debris and aggregated proteins via the lysosomal pathway (Söllvander et al., 2016; Rostami et al., 2017; Tremblay et al., 2019). However, in which way pathogenic LRRK2 affects α-syn clearance by astrocytes remains unclear.

In this context, the specific aims of the second part of this project are:

Objective 1 To determine the effects of the Lrrk2 G2019S mutation in uptake and degradation of exogenous α-syn in primary cultures of astrocytes.

Objective 2 To unravel novel LRRK2 interactors in astrocytes and to elucidate their impacts on astrocytes both in health and disease.

Given the importance of astrocytes-mediated brain clearance in maintaining brain homeostasis, the outcomes of this PhD project will generate new fundamental knowledge in the astrocytes biology and open the possibility to target astrocyte-mediated brain clearance in human diseases.

Chapter 5

Materials & Methods

5. Materials and Methods PART I

5.1. Mouse primary astrocyte cultures

Mouse primary striatal astrocytes were obtained from animals between postnatal days 1 and 3. Brains were dissected from the skull and placed on a Petri dish containing cold Dulbecco's Phosphate Buffered Saline (DPBS, Biotest). Olfactory bulbs and cortices were removed under an optic microscope, and striata were transferred to a separate Petri dish containing cold DPBS. After the dissection, supplemented medium composed of Basal Medium Eagle (BME, Biowest) 10% fetal bovine serum (FBS, Corning), 100 U/ml penicillin and 100 µg/ml streptomycin, was added to the tissues. Striata were then sifted through a 70-µm cell strainer (Sarstedt), using a syringe plunger. The cell suspension was centrifuged (300×g, 15 min), and the pellet was washed twice with 25 ml of supplemented medium. Cells were seeded at a density of 5×10^6 cells/10 ml medium in cell culture flasks and maintained in supplemented medium at 37 °C and 5% CO_2 atmosphere. The culture medium was changed after 7 days and again after additional 3–4 days. When cell confluency reached about 80%, microglia were detached by shaking the flask (800 rpm) for 2 h at room temperature (RT). After shaking, the medium containing microglia was removed and replaced with fresh supplemented medium. Independent experiments were carried out using cells obtained from different pups.

5.2. pH-RODO synaptosome purification and conjugation

Synaptosomes were prepared as follows. Four Sucrose Tris-Percoll solutions (23-15-10-3%of Percoll, respectively) were prepared and stratified into a centrifuge tube. Whole Brain tissues were homogenized in a solution containing 10 mM Tris, 0.32M sucrose (pH 7.4) and protease inhibitors using a glass-Teflon tissue grinder (0.25 mm clearance). After centrifugation (1,000xg for 5 min at 4°C), the supernatant was added to the discontinuous density gradient solution. After a second centrifugation (33,500xg for 6 min at 4°C), the synaptosome fraction, located between the 23% and 15% density gradient solutions, was collected and the re-suspended in a physiological solution (140 mM NaCl; 3 mM KCl; 1.2 mM $MgSO_4$; 1.2 mM NaH_2PO_4; 10 mM HEPES; 10 mM glucose; dissolved in distilled water, pH 7.4). To obtain purified synaptosomes, a final centrifugation step at 20,000xg for 10 min at 4°C was performed and the pellet containing the synaptosomal fraction, was either conjugated or stored at -80°C in PBS containing 5% DMSO.

For conjugation, synaptosomes were incubated with pH-RODO™ Red, succinimidyl ester (Thermo Scientific) or 5-TAMRA (5-Carboxytetramethylrhodamine) (Thermo Scientific) in 0.1 M Na_2CO_3 (pH 9.0) at RT with gentle agitation. After 2h, unbounded pH-RODO was washed-out with DPBS by performing six rounds of centrifugations at 21,092xg. pH-RODO -conjugated synaptosomes were re-suspended with DPBS containing 5% DMSO for subsequent freezing. The fluorescence of conjugated synaptosomes was verified through Victor X3 Plate Reader (Perkin Elmer).

For chemokine binding assay, 10μg of synaptosomes were incubated with recombinant Cxl12 at a final concentration of 250nM for 1h at 37°C with gentle agitation. After 2h incubation, unbounded Cxcl12 was washed-out with DPBS by performing four rounds of centrifugations at 21,092xg.

5.3. Mass spectrometry

For mass spectrometry, 20μg of pure synaptosomes were sent to EMBL Core Facility. Protein samples were sent for analysis at EMBL Proteomics Core Facility in Heidelberg, Germany. There, samples were subjected to in-solution tryptic digestion using a modified version of the Single-Pot Solid-Phase-enhanced Sample Preparation (SP3). Methods are fully established and detailed in protocol (Walch et al.,2021; Selkrig et al., 2021; Määttä et al., 2020).

5.4. Sample preparation for Transmission Electron Microscopy (TEM) analysis

Pure synaptosomes were centrifuged at 21,092xg at RT, the medium was removed and Fixative buffer (glutaraldehyde 2.5% in 0.1M sodium cacodylate buffer) was added to the pellet for 1h at 4°C. Then, at the Microscopy Facility (Dept. of Biology, University of Padova), the samples were postfixed with 1% osmium tetroxide and 1% potassium ferrocyanide in 0.1M sodium cacodylate buffer for 1h at 4°C. After three washes with water, samples were dehydrated in a graded ethanol series and embedded with epoxy resin (Sigma-Aldrich). Ultrathin sections (60-70 nm) were obtained with an Ultrotome V (LKB) ultramicrotome, counterstained with uranyl acetate and lead citrate and viewed with a Tecnai G2 (FEI) transmission electron microscope operating at 100 kV. Images were captured with a 9800X, magnification using a Veleta (Olympus Soft Imaging System) digital camera.

5.5. Generation of human induced astrocytes (HiAastrocytes)

Human fibroblasts were obtained from two healthy donor from Coriel stem cell bank (Table 1).

Sample	Type	Code	Biopsy	Sex	Age	Kariotype
38530A	Healthy	Ctrl1	Skyn	M	55	Normal
291949	Healthy	Ctrl2	Skyn	M	66	Normal

Table 1. Summary of fibroblasts used for reprogramming and generation of astrocytes.

Human fibroblasts were grown in DMEM F12 (Gibco/ThermoFisher, Spain) and infected with the CytoTune iPS 2.0 Sendai Reprogramming Kit (Thermo- fisher, Spain). The commercial Sendai virus expressed the key genetic factors necessary for reprogramming somatic cells into iPSCs (Klf4/Oct3-4/Sox2-KOS, hc-Myc, Klf4). Infection efficiency was evaluated by co-infection with a EmGFP fluorescent reporter plasmid provided with the kit. Seven days later, transduced fibroblasts were seeded in Geltrex (ThermoFisher, Spain) in Essential 8 Flex medium (E8, Gibco/ThermoFisher, Spain). E8 medium was changed every day for 21 days until the formation of iPSC colonies was observed. Colonies were manually isolated using a 27G Braun Sterican Needle and replated in laminin-521 (LN521-Biolamina, Sundbyberg Sweden) with E8 medium supplemented with ROCK inhibitor (Y-27632; Millipore, Madrid, Spain). The day after, ROCK inhibitor was removed and replaced with fresh medium. Colonies were sequentially isolated and re-suspended as single cells. Embryoid bodies (EBs) were generated after re-suspending iPSC colonies in Essential 6 medium (E6, Gibco) for 2–4 days in Aggrewell™ 800 plates (StemCell, Grenoble, France). Half of the medium in the microwells was replaced daily with fresh medium. EBs were then seeded in LN521/LN211 mix (50% each) (Biolamina) and the differentiation to neural precursor cells (NPCs) as neural rosettes was promoted using the STEMdiff Neural Induction Medium (Stemcell). After 7 days, neural rosettes were selected and detached using the STEMdiff Neural Rosette Selection Reagent (Stemcell). Cells were incubated for 2 h with this reagent at 37°C with 5% CO_2, mechanically re-suspended at single cell level and seeded in LN211/LN111 (50% each) (Biolamina). Differentiation of NPCs to progenitor astrocytes was triggered using the astrocyte differentiation medium (STEMdiff astrocyte differentiation #100-0013, StemCell). To maintain the appropriate cell density (70% of confluence) cells were passed every week in the same coating mix for 21 days. Finally, astrocytes progenitor cells were maturated in Astrocyte Maturation Medium (STEMdiff

astrocyte maturation #100-0016, StemCell) for 60 to 75 days. During the whole protocol, the correct state of the cells in each step was evaluated using the EVOS FL microscope (Life Technologies, AME4300).

5.6. Cells transfection

For the High throughput screening, primary astrocytes were seeded in μClear 384-well (PerkinElmer) plates at a seeding density of 4 x 10^3 cells/well by taking advantages of Janus Liquid Handler (PerkinElmer) and transfected the following day. Cells were transfected with G-014675-E2 Mouse Druggable Subset Dharmacon siGENOME® SMARTpool® siRNA Library Lot.1400, Non-Targeting siRNA SMARTpool (Control), Megf10 siRNA SMARTPool, CtsB siRNA SMARTPool (Dharmacon) at a final concentration of 50nM, together with eGFP encoding plasmid using Lipofectamine 2000 (Thermo Scientific) following 1:3 siRNA-DNA/Lipofectamine ratio. DNA-siRNA and Lipofectamine were diluted in OPTIMEM (Gibco) and incubated for 20 min at RT to allow the formation of DNA-siRNA/PEI complexes. The mix was then added to the plates by taking advantage of the Precision XS pipetting system (Biotek). After 90 min the transfection medium was replaced with complete BME, and the experimental procedure was carried out at the appropriate time.

For the live-imaging experiments primary astrocytes were plated in μClear 96-well (Greiner) plates and transfected the day after the seeding. Cells were transfected with mouse Non-Targeting siRNA SMARTpool, Ackr3 siRNA SMARTPool, Megf10 siRNA SMARTPool, CtsB siRNA SMARTPool (Dharmacon), Human CXCR7-Tango (Plasmid #66265, Addgene) as described above.

For immunocytochemistry and western blot analyses, primary striatal astrocytes were seeded in 24-well plates at the seeding density of 0.025 × 10^6 cells/well. Cells were transfected with mouse Ackr3, Megf10, CtsB siRNA SMARTPool at a final concentration of 50nM (Dharmacon) using Lipofectamine 2000 (Thermo Scientific) following 1:3 siRNA to Lipofectamine ratio. After 72 h, the experimental procedure was carried out.

For live-imaging assay, iHAstrocytes were seeded in μClear 96-well (Greiner) plates coated with LN111/LN211 (Biolamina). The day after, cells were transfected with Non-Targeting siRNA SMARTpool, Ackr3 siRNA SMARTPool (Dharmacon) at a final concentration of 100nM, together with pmaxGFP™ (LONZA) using Lipofectamine Stem Transfection Reagent following 1:1 siRNA-DNA/Lipofectamine ratio.

5.7. Synaptosomes phagocytosis assay

For synaptosomes phagocytosis assay, the protocol established in Byun et al 2019 has been employed. Mouse primary astrocytes were seeded at 60% of confluency into μClear 384-well (PerkinElmer), μClear 96-well (Greiner) plates and after 24h cells were transfected as described above in Section 5.6. After one day upon transfection, cells were treated with 1ug/cm^2 of pH-RODO synaptosomes in OPTIMEM. After 90 min, cells were washed three times with pre-warmed DPBS and supplemented medium without Phenol red was added. Images were taken at different times after the pulse to follow pH-RODO synaptosomes internalization and acquired through High Content Imaging System Operetta (Perkin Elmer) using 10x NA and 20x WD magnification. Images were analyzed using Harmony Software (Perkin Elmer).
For immunocytochemistry analyses, primary striatal astrocytes and iHAstrocytes were seeded onto 24-well plates (10^5 cells/well) and treated with 1μg/cm^2 of TAMRA-synaptosomes diluted in OPTIMEM for 90 min at 37°C. After the pulse, cells were washed three times with pre-warmed DPBS, complete medium was added, and cells were fixed after 48h.

5.8. Immunocytochemistry and confocal microscopy analysis

Primary striatal astrocytes were cultured onto 12mm glass coverslips (Thermo-Scientific) in 24-well plates at 50% confluency. The coverslips had been previously sterilized in 70% v/v ethanol followed by 30 min exposure to UV light, then coated with Poly-L-Lysine (Sigma-Aldrich). Cells were plated at about half of the confluency and after transfection or synaptosome treatment fixed with an intermediate washing step in DPBS.
Fixation was performed with 4% w/v Paraformaldehyde (PFA), pH 7.4, for 20 min at RT. Cells were permeabilized with 0.1% v/v Triton® X-100 in DPBS for 20 min and successively incubated for 60 min with blocking solution (5% v/v FBS in DPBS) to saturate non-specific sites for primary antibodies. Primary antibodies diluted in blocking solution were then added to the permeabilized cells overnight (O/N) at 4°C in a humidity chamber. Primary antibodies were diluted in blocking solution as follows: rabbit anti-GFAP (Abcam #ab4674, 1:400), rat anti-Lamp-1 (clone 1D4B) (Abcam #ab25245, 1:100), rabbit anti-Lamp2A (Abcam #ab18528, 1:200), rabbit anti-Iba1 (Wako #019-19741 1:200), rabbit anti-Cxcr7 (Ackr3) (Thermo Fisher, # PA3-069 1:500). The next day, cells were washed three times with DPSB and stained for 1h at RT with secondary antibodies diluted with blocking solution 1:200. Secondary antibody incubation was carried out using Alexa Fluor 647 (Invitrogen #A21449 Alexa Fluor 488

(Invitrogen #A11034), and Alexa Fluor 568 (Invitrogen #A11004) fluorophores, antibodies were diluted 1:200 in Blocking Buffer. Cells were washed 3 times with DPBS. Cover glasses were mounted on a microscope slide (Thermo Scientific) using Mowiol (Calbiochem) supplied with DAPI. Images were acquired through Leica SP5 confocal microscope using a 40x objective in oil. iHAstrocytes were cultured onto 12mm glass coverslips (Thermo-Scientific) in 24-well plates. The day after, cells were fixed in 4% PFA (Merck/Sigma) for 8 min, permeabilized with 0.1% Triton (Sigma) and non-specific epitopes were blocked with 5% bovine serum albumin (BSA) in DPBS for 45 min at RT. Primary antibodies were incubated O/N at 4°C and then washed three times with 0.1% Triton in PBS. Secondary antibodies Alexa 488, Alexa 568 and Alexa 647 (Invitrogen, 1:500), were incubated for 1h in the dark at RT. After three washes with 0.1% Triton in PBS, cell nuclei were counter-stained for 1 min with DAPI (ThermoFisher). Finally, coverslips were mounted with Glycergel (Dako, Barcelona, Spain) and analyzed using the confocal microscope Leica TCS STED CW SP8.

5.9. Fluorescence Microscopy and Image Analysis

For live imaging studies with primary striatal astrocytes, images were acquired at 32-bit intensity resolution over 1024 × 1024 pixels, through the Operetta High Content Imaging System (Perkin Elmer), using a 10x long working distance dry objective. Four independent cultures were used. For each culture, four independent fields were evaluated and reported. eGFP-positive and pH-RODO positive area total were assessed using Harmony Software (Perkin Elmer). Phagocytic Index was calculated as total pH-RODO positive area normalized by Total eGFP positive area.

For post-fixation imaging of primary striatal astrocytes, images were acquired at 8-bit intensity resolution over 1024 × 1024 pixels, through Leica SP5 confocal microscope using a HC PL FLUOTAR ×40/0.70 oil objective. After setting the threshold, the JACoP plugin (ImageJ, https://imagej.nih.gov/ij/plugins/track/jacop2.html) was applied for the quantification of co-localization between Ackr3 signal and the Lamp1 and TAMRA-positive structures, graphically displayed as the Pearson's Correlation Coefficient. For the evaluation, four independent cell cultures were used. For each culture, four independent fields per experiment were evaluated and reported. All quantifications were normalized to the number of living cells identified by nuclei staining.

For live imaging studies of iHAstrocytes, images were acquired at 32-bit intensity resolution over 1024 × 1024 pixels, through Carl Zeiss ApoTome2, using a 20x dry objective. For the

evaluation two independent cell cultures were used. Phagocytic Index, area and number of Ph-RODO positive puncta were assessed manually using ImageJ. After setting the scale, ROIs were identified as the area of eGFP positive cells (green) and pH-RODO positive area (red) were calculated for each ROI. For the calculation of the phagocytic index, the total area of pH-RODO positive area per well was normalized by the total area of eGFP positive cells per well.
For post-fixation imaging of iHAstrocytes, images were acquired at 32-bit intensity resolution over 1024 × 1024 pixels, through confocal microscope Leica TCS STED CW SP8, using HC PL FLUOTAR ×40/0.70 oil objective. After setting the threshold, the JACoP plugin (ImageJ) was applied for the quantification of co-localization between Ackr3 signal and the Lamp1 and TAMRA-positive structures, graphically displayed as the Pearson's Correlation Coefficient. For the evaluation two independent cell cultures were used. For each culture, four independent fields per experiment were evaluated and reported. All quantifications were normalized to the number of living cells identified by nuclei staining.

5.10. Western Blot Analysis

Synaptosomes, murine cultures and iHAstrocytes were lysed in an appropriate volume of RIPA buffer (20 mM Tris-HCl pH 7.5, 150 mM NaCl, 1 mM EDTA, 0.5 mM sodium pyrophosphate ($Na_4P_2O_7$), 1 mM β-glycerophosphate ($C_3H_7Na_2O_6P$), 1 mM sodium orthovanadate (Na_3VO_4) containing 1% protease inhibitor cocktail (Sigma-Aldrich). Protein concentration was determined through the Pierce BCA Protein Assay Kit following the manufacturer's instructions (Thermo Scientific) and 25μg of each sample was prepared for SDS-PAGE with the addition of sample buffer 4x. Electrophoresis was performed using ExpressPlus PAGE precast gels 4-20% (GeneScript). After electrophoresis, protein samples were transferred to PVDF membranes (Bio-Rad) through a Trans-Blot TurboTM Transfer System (Bio-Rad) in semi-dry conditions, with the 1x transfer buffer (Bio-Rad) at 25 V for 20 min. Membranes were incubated with 5% milk (blocking buffer) diluted in DPBS at RT for 1 h. Proteins were identified by the appropriate primary antibodies against mouse anti-PSD95 (Abcam #ab2723, 1:1000) , mouse anti-β-actin (Sigma Aldrich #A3853, 1:10000), ATP5A (Abcam #ab14748, 1:1000), GFAP (Dako #Z0334, 1:10000), rabbit anti-Synaptophysin (EMD Millipore MAB258, 1:10000), rabbit anti-MBP (Abcam #ab40390; 1:1000), mouse anti-Vamp2 (homemade gently provided by Ornella Rossetto, 1:2000), rabbit anti-Megf10 (Sigma-Aldrich #ABC10 1:1000), CtsB (Abcam [CA10] #ab58802, 1:2000), rabbit anti-Cxcr7 (Ackr3) (Thermo Fisher, # PA3-069 1:2000), rabbit anti-SDF-1/Cxcl12 (Cell Signaling #3740, 1:1000) mouse anti-GAPDH (Cusabio #CSB-MA000195

1:5000), Flag M2-peroxidase (Sigma-Aldrich #A8592, 1:5000) and then incubated for 1h at RT with appropriate horseradish peroxidase (HRP)-conjugated secondary antibodies (Invitrogen). The visualization of the signal was conducted using Immobilon Forte Western HRP substrate (Millipore) and the VWR Imager Chemi Premium. Images were acquired in .tiff format and processed with the ImageJ software to quantify the total intensity of each single band.

For Dot-Blot assay, synaptosomes were lysed in an appropriate volume of RIPA buffer containing 1% protease inhibitor cocktail (Sigma-Aldrich). Protein concentration was determined through the Pierce BCA Protein Assay Kit following the manufacturer's instructions (Thermo Scientific). 10-20-30μg of sample was spotted onto nitrocellulose membranes (Bio-Rad) and allowed to dry. Briefly, membranes were incubated with blocking buffer at RT for 1h. Then, recombinant chemokine was added at 0.1 μg/ml in blocking buffer and incubated for 1h at RT. Proteins were identified by the appropriate primary antibodies against SDF-1 and then incubated for 1h at RT with appropriate horseradish peroxidase (HRP)–conjugated secondary antibodies (Invitrogen). The visualization of the signal was conducted using Immobilon Forte Western HRP substrate (Millipore) and the VWR Imager Chemi Premium. Images were acquired in .tiff format and processed with the ImageJ software to quantify the total intensity of each single band.

5.11. Ackr3 immunoprecipitation and pull-down Assay

Human CXCR7-Tango (Plasmid #66265, Addgene) purification was performed as follows. Briefly, transfected Hek293FT cells were solubilized in an appropriate volume of radioimmunoprecipitation assay buffer, RIPA buffer (20 mM Tris-HCl pH 7.5, 150 mM NaCl, 1 mM EDTA, 2.5 mM sodium pyrophosphate ($Na_4P_2O_7$), 1 mM β-glycerophosphate ($C_3H_7Na_2O_6P$), 1 mM sodium orthovanadate (Na_3VO_4) containing 1% protease inhibitor cocktail (Sigma-Aldrich). Lysates were centrifuged for 30 min at 14,000×g. Afterwards, lysates containing 3xFlag-tagged protein were incubated with anti-Flag M2 agarose beads O/N at 4 °C on a rotator. Proteins were then resolved by SDS-PAGE and Western Blot.

For the pull-down assay, 40μg of pure synaptosomes were incubated O/N at 4°C on a rotator with anti-Flag beads deriving from the immunoprecipitation. The following day anti-Flag beads were centrifuged for 1 min at 9000xg and the flow through was collected. Then the beads were washed several times with lysis buffer and protein were then resolved by SDS-PAGE and Western Blot.

5.12. Pip Strips

The lipid-binding specificity of recombinant murine SDF-1α-CXCL12 (Peprotech) was determined using PIP Strips (Thermo Scientific). These strips are spotted with 100 pmol of 15 different lipids found in cell membranes. First, strips were incubated with blocking buffer (1X Tris-buffered saline [TBS], 0.1% Tween-20, 3% BSA) for 1h at RT. Then, recombinant chemokine was added at 0.1 μg/ml in blocking buffer and incubated for 1h at RT. Strips were washed with TBS-T (TBS, 0.1% Tween-20), and bound protein was detected with specific rabbit anti-chemokine antibodies (Peprotech) followed by an HRP-conjugated anti-rabbit antibody (Abcam, Cambridge, Massachusetts, USA). Strips were developed with Immobilon Forte Western HRP substrate (Millipore) and the VWR Imager Chemi Premium.

5.13. Chemokines array

Mouse chemokines in astrocytes culture medium upon synaptosomes treatment or untreated astrocytes were measured using the microarray data and confirmed using a mouse cytokine antibody array (RayBiotech) according to the manufacturer's instructions. The kit consists of a nitrocellulose membrane containing 24 different anti-chemokine antibodies spotted in duplicate. The 24 chemokines included CCL1, CCL11, CCL12, CCL17, CCL19, CCL2, CCL20, CCL21, CCL22, CCL24, CCL25, CCL27, CCL3, CCL5, CCL9, CX3CL1, CXCL1, CXCL11, CXCL12, CXCL13, CXCL16, CXCL2, CXCL5, CXCL9. Briefly, membranes were incubated with blocking buffer at RT for 1h. Cell supernatants (0.5 ml) were incubated with an array membrane O/N at 4°C. The arrays were then washed three times for 10 min and then a cocktail of biotinylated detection antibodies incubated at RT for 1h, and then each was incubated with a membrane O/N at 4°C. The arrays were then washed three times for 10 min and subsequently incubated with horseradish peroxidase-conjugated streptavidin for 30 min at RT The visualization of the signal was conducted using Immobilon Forte Western HRP substrate (Millipore) and the VWR Imager Chemi Premium. The data were expressed as the change in expression of chemokines of synaptosomes treated astrocytes relative to that of the corresponding chemokines of untreated astrocytes.

5.14. Gene Ontology enrichment analysis

Molecular function enrichment analysis was provided through the use of Gene Ontology (GO), (Ashburner et al., 2019) categories. The list of genes that abolish the ability of astrocytes to

internalize synaptosome (red hits) and those that elicited the opposite (green hits) were analyzed testing the enrichment analysis of MF GO terms by using the ClusterProfiler R package (Wu et al., 2021.; Yu et al., 2012). MF GO terms with an adjusted p-values lower than 0.05 were considered for data interpretation and the top 10 ranked terms with the lowest p-value were represented in figures. Figures were generated with dotplot and cnetplot functions. All the analyses have been performed with R version 4.1.2 and Bioconductor version 3.14 (Huber et al., 2015).

5.15. Statistical Analysis

Experiments were performed using cell cultures obtained from at least three different groups of pups. iHAstrocytes were used at the same maturation day for the two independent experiments. Results are expressed as mean ± standard error of the mean (SEM) or median with interquartile range, depending on whether data followed a Gaussian distribution or not. Gaussian distribution was assessed by D'Agostino-Pearson omnibus and Shapiro-Wilk normality tests. Data including more than two groups were analyzed by one-way ANOVA (Gaussian distribution) or Kruskal-Wallis test (non-Gaussian distribution) respectively followed by Tukey's multiple comparisons test or Dunn's multiple comparisons test. Levels of significance were defined as $p \leq 0.05$, $p \leq 0.01$, $p \leq 0.001$. Statistical analysis was performed with Prism 6 (GraphPad).

PART II

5.16. Large scale isolation of plasmid DNA

The pCHMWS-3xflag-LRRK2 plasmid was used for mammalian expression of 3xFlag LRRK2 as published in Civiero et al. 2012. Competent Stbl3 cells were transformed with plasmidic DNA. After incubation on ice, 100 µl Super Optimal broth with catabolite repression (SOC) medium was added to the *E.coli*-DNA mixture and the cells were incubated at 37°C for 30 minutes in agitation. Cells were plated on an agarose-plate containing 100µg/ml of ampicillin and incubated at 37°C O/N. The day after, colonies were picked with a pipet tip and left O/Nat 37°C in 10 ml Luria-bertani (LB) medium with 100 ng/ml ampicillin. The DNA plasmid preparation was performed by means of a miniprep following the NucleoSpin® Plasmid EasyPure protocol (Macherey-Nagel). To assess quality of the DNA preparation, a small aliquot of the plasmid was digested with EcoRI, separated using agarose gel electrophoresis on a 1% agarose gel and

visualised using VWR® Imager Chemi Premium. Colonies with the expected DNA pattern were selected and inoculated into 250 ml of LB medium with 100 µg/ml ampicillin O/Nat 37°C in agitation. The day after, DNA was purified following the Nucleobond Xtra Midi Plus protocol.

5.17. Recombinant α-syn purification and Pre-Formed Fibrils (PFFs) preparation

To produce recombinant human α-syn from bacterial sources, the pET-αSyn plasmid was used as reported in Russo et al, 2015. An O/N culture of *E.coli* BL21 (DE3) endotoxin free transformed with pET- α Syn140 plasmid, was diluted to a final OD600nm of 0.08 in 1 liter of LB fresh medium supplemented with 25 µg/ml kanamycin and 25 µg/ml chloramphenicol. The bacterial culture was grown in agitation at 37°C. When OD600 reached 0.4-0.6, α-syn expression was induced using 100 µl IPTG and further incubated for 4h. Cells were harvested by centrifugation at 6000xg for 5 mins at RT. The cell pellet was kindly resuspended in 100 ml Osmotic Shock Buffer (Tris 30mM, EDTA 2mM, 40% sucrose pH 7.2) and incubated for 10 min at RT. After centrifugation at 12000xg for 20 min at 4°C, the pellet was resuspended with 90 ml cold water supplemented with 37.5 µl of saturated $MgCl_2$ and kept on ice for 3 min. Another centrifugation was performed and the supernatant, containing periplasmatic proteins, was collected and buffered with Tris-HCl pH 8.0. Subsequently, the sample was boiled for 10 min. The sample was centrifuged and the supernatant was subjected to $(NH_4)_2SO_4$ precipitation: a first step at 35% of saturation and then a second one until 55% of saturation. These steps eliminate some contaminants and concentrate α-syn. Finally, the protein was resuspended in 5-10 ml of Tris buffer. The solution containing the protein was dialyzed against water, and the centrifuged sample was loaded into a Resource Q 6 ml column pre-equilibrated in 20 mM Tris pH 8.0 and eluted using linear 0-500 mM NaCl gradient. The fraction containing α-syn was again dialyzed extensively against water and lyophilized. The sample was resuspended in DPBS and quantified using a spectrophotometer at 276 nm.

The volume was adjusted by adding DBPS until the desired concentration was reached. The solution containing purified α-syn at 250µM was aliquoted in 1,5 ml tubes and the fibrillation was performed following Pivato et al 2012. Briefly, the solution was kept for 7 days in a ThermoMixer (Eppendorf) at 800 rpm with a temperature set at 37°C. α-syn fibrils formation and quality was checked by transmission electron microscopy (EM). Then the protein was sonicated as described in literarure, with an Ultrasonicator (Covaris) in order to obtain fibrils with homogeneous dimension. The success of the treatment was checked again by EM analysis; PFFs finally resulted to be 100-200 nm long. For SNARF-PFFs preparation: α-syn monomers

were conjugated with a commercial fluorescent pH sensitive dye (Carboxy SNARF-1®, Setareh Biotech), following the protocol described in Kim et al 2012. Fibrils samples were then prepared as described above.

5.18. Human H4 cell line maintenance

Human H4 neuroglioma cells were kindly provided by Prof. Patrick A. Lewis (The Royal Veterinary College, London, UK). H4 cells were cultured in DMEM (Biowest) supplemented with 10% FBS (Corning), 100 U/ml penicillin, and 100 µg/ml streptomycin at 37 °C and 5% CO_2. Cells were plated on 100 mm Petri dishes (Corning) at a density of 5×10^6 cells/10 ml medium for purification procedure or on 12 mm glass coverslips (Thermo Scientific) at a density of 10^5 cells for immunocytochemistry analyses.

5.19. α-syn PFFs exposure

Cells were exposed to sonicated SNARF-1-labeled, or unlabeled α-syn PFFs at a concentration of 0.5 µM for 24h. To inhibit LRKK2 kinase activity, MLi-2 at a concentration of 200 nM (Tocris Bioscience) was applied 90 min before α-syn PFFs treatment and maintained for the entire PFFs exposure. Cells were then rinsed twice with culture medium to remove any excess α-syn PFFs. Subsequently, cells were either processed for immunocytochemistry, western blot, or live imaging assay (24h time point).

5.20. Cell transfection

For immortalized cell lines, transfection was made as follows. Once reached 80% of confluency in 100 mm Petri dishes, H4 cells were transiently transfected with 10 µg of pCHMWS- 3xflag-LRRK2 plasmids encoding for human LRRK2 and 5 µg of pEGFP-N3-AnxA2-GFP encoding for human annexin A2 (Addgene, #107196), using linear polyethylenimine (PEI, Polysciences) and following 1:2 DNA to PEI ratio. On 12-mm Ø glass coverslips, H4 cells were transiently transfected with 2 µg of pEGFP-N3- AnxA2-GFP at 60% of confluency. DNA and PEI were diluted in OPTIMEM (Gibco) and incubated for 20 min at RT to allow the formation of DNA/PEI complexes. The mix was added to cells and the experimental procedure was carried out after 48h.

Primary striatal astrocytes were seeded in 24-well plates at the seeding density of 2.5×10^4 cells/well. Cells were transfected with mouse AnxA2 siRNA SMARTPool as described in Section 5.6. After 72h, the experimental procedure was carried out.

5.21. Western Blot

Western Blot was performed as described in Section 5.10. Proteins were identified with the following primary antibodies: rabbit anti-LRRK2 (Abcam #ab133474, 1:300), mouse anti-β-actin (Sigma-Aldrich #A1978, 1:10000), rabbit anti-annexin II (GeneTex International #GTX101902, 1:1000), rabbit anti-alpha-synuclein (Abcam #ab138501, 1:10000), Flag M2-peroxidase (Sigma-Aldrich #A8592, 1:10000)

5.22. LRRK2 immunoprecipitation

3xFlag-LRRK2 purification was performed as follows. Briefly, transfected H4 cells were solubilized in an appropriate volume of radioimmunoprecipitation assay buffer, RIPA buffer containing 1% protease inhibitor cocktail (Sigma-Aldrich). Lysates were centrifuged for 30 min at 14,000×g. Afterwards, lysates containing 3xFlag- tagged protein were incubated with anti-Flag M2 agarose beads for 2h at 4 °C on a rotator. After extensive washing, proteins were eluted with 150 ng/ml of 3xFlag peptide by shaking for 30–40 min at 4 °C. Proteins were then resolved by SDS-PAGE and stained for 2 h with Colloidal Coomassie Brilliant Blue (0.1% w/v Brilliant Blue G-250, 25% v/v methanol, 5% v/v acetic acid and milli-Q water) for 1h. Then, destained with a colloidal destaining (7.5% v/v acetic acid, 5% v/v methanol and milli-Q water). Finally, the appropriate gel band was excised and assessed by mass spec (Section 5.23).

5.23. Mass Spectrometry Analysis

Gel slices were cut into small pieces and subjected to reduction with dithiothreitol (DTT 10 mM in 50 mM NH_4HCO_3, for 1 h at 56 °C), alkylation with iodoacetamide (55 mM in 50 mM NH_4HCO_3, for 45 min at RT and in the dark), and finally in-gel digestion with sequencing grade modified trypsin (12.5 ng/μL in 50 mM NH_4HCO_3, Promega). Samples were analyzed using a LTQ Orbitrap XL mass spectrometer (Thermo Fisher Scientific) coupled to a HPLC UltiMate 3000 (Dionex–Thermo Fisher Scientific) through a nanospray (NSI). Peptides were separated at a flow rate of 250 nL/min using an 11-cm-long capillary column (PicoFrit, 75-μm ID, 15-μm tip, New Objective) packed in house with C18 material (Aeris Peptide 3.6 μm XB C18;

Phenomenex). A linear gradient of acetonitrile/0.1% formic acid from 3 to 40% was used for peptide separation and the instrument operated in a data dependent acquisition mode with a Top4 method (one full MS scan at 60,000 resolution in the Orbitrap, followed by the acquisition in the linear ion trap of the MS/MS spectra of the four most intense ions). Raw data files were analyzed using Proteome Discoverer 1.4 (Thermo Fisher Scientific) connected to a Mascot local server (version 2.2.4, Matrix Science) and searched against the human section of the UniProt database (version July 2018, 95057 entries) using the following parameters: trypsin was selected as digesting enzyme with up to one missed cleavage allowed, precursor and fragment tolerance was set to 10 ppm and 0.6 Da respectively, carbamidomethylation of cysteine residues was set as a fixed modification and methionine oxidation as a variable modification. The precursor area ion detector node of Proteome Discoverer was used to integrate the area of precursor ions. A search against a randomized database and the algorithm Percolator were used to assess the false discovery rate (FDR), and data were filtered to keep into account only proteins identified with at least two unique peptides and an FDR ≤ 0.01 both at peptide and protein levels. Proteins were grouped into protein families according to the principle of maximum parsimony.

5.24. Immunocitochemistry

Immunocytochemistry was performed as described in Section 5.9. Primary antibody incubation was performed using rabbit anti-GFAP (Abcam #ab4674, 1:400), rat anti-Lamp-1 (clone 1D4B) (Abcam #ab25245, 1:100), rabbit anti-Lamp2A (Abcam #ab18528, 1:200), mouse anti-α-synuclein (BD Laboratories #610787, 1:400), rabbit anti-annexin II (GeneTex International #GTX101902, 1:200). Secondary antibody incubation was carried out using Alexa Fluor 647 (Invitrogen #A21449, 1:200), Alexa Fluor 488 (Invitrogen #A11034, 1:200), and Alexa Fluor 568 (Invitrogen #A11004, 1:200) fluorophores. In some experiments, cells were stained using Phalloidin-iFluor 647 Reagent (Abcam #ab176759, 1:1000). Cover glasses were mounted on a microscope slide (Thermo Scientific) using Mowiol (Calbiochem) supplied with DAPI. Images were acquired through Leica SP5 confocal microscope using a 40x objective in oil.

5.25. Fluorescence Microscopy and Image Analysis

For primary striatal astrocytes – live imaging studies, images were acquired at 8-bit intensity resolution over 1024 × 1024 pixels, through Leica SP5 confocal microscope, using a HC PL FLUOTAR ×20/0.50 dry objective. The number of independent cell cultures used was as

follows: Lrrk2 WT, n = 4; Lrrk2 KO, n = 4; and Lrrk2 GS, n = 4. Pictures were acquired at the two relevant ranges of the emission spectrum (channel1: 530–550 nm and channel2: 610–630 nm). For each culture, six to eight independent fields were evaluated and reported. SNARF-1-positive α-syn inclusions were analyzed using ImageJ. SNARF-1-labeled α-syn PFFs were assessed using an ImageJ macro including the following steps: set scale, convert to 8-bit, subtract background, set threshold, et measurements, and analyze particles. The ratio of the single-particle integrated density (area × mean intensity) between channel1 and channel2 and the number of particles per ROI were measured. ROIs were first identified in channel1 and then transferred to channel2.

For primary striatal astrocytes–post-fixation imaging, images were acquired at 8-bit intensity resolution over 1024 × 1024 pixels, through Leica SP5 confocal microscope using a HC PL FLUOTAR ×40/0.70 dry objective. Lamp2A-positive puncta were counted using the Analyze Particles plug-in in ImageJ. Fluorescent puncta were assessed by area and particle count. The number of independent cell cultures used for the evaluation of Lamp2A-positive puncta in Lrrk2 WT versus Lrrk2 KO versus Lrrk2 GS astrocytes was as follows: Lrrk2 WT, n = 3; Lrrk2 KO, n = 3; and Lrrk2 GS, n = 3. For each culture, eight independent fields per experiment were evaluated and reported. Proximity analysis for AnxA2 and unlabeled α-syn PFFs dots was performed using ComDet plug-in in ImageJ (https://imagej.net/Spots_colocalization_(ComDet)), using the following parameters: max colocalization distance (0.9 pixels) and particles dimension (AnxA2: 3 pixels and α-syn: 4 pixels). The number of AnxA2 dots and the number of α-syn puncta were assessed by "puncta count" output and the proximity between AnxA2 dots and engulfed α-syn as "co-localization" output. All quantifications were normalized to the number of living cells identified by nuclei staining. The number of independent cell cultures used in AnxA2 downregulation experiments was LRRK2 WT n = 3. For each culture, four independent fields per experiment were evaluated and reported. The number of independent cell cultures used for the evaluation of AnxA2 function in Lrrk2 WT versus Lrrk2 GS astrocytes was as follows: Lrrk2 WT, n = 3; Lrrk2 GS, n = 3. For each culture, eight independent fields per experiment were evaluated and reported.

5.26. Transmission Electron Microscopy and images analysis

Primary striatal astrocytes were seeded onto 24-well plates (10^5 cells) and fixed at 80% confluency. The medium was removed, and fixative buffer (glutaraldehyde 2.5% in 0.1 M

sodium cacodylate buffer) was added to the cells for 1h at 4 °C. Samples were processed as described in Section 5.4. We identified lysosomal-like structures using the following ultrastructural features: 0.05–0.5 μm in diameter and granular, electron dense appearance in electron micrographs. Lysosomal-like structures were counted, and their areas were determined using the oval selection tool of the ROI Manager tool (ImageJ). Lysosomal-like structure numbers were normalized to the field area. The number of independent cell cultures used was as follows: Lrrk2 WT, n = 4; Lrrk2 KO, n = 4; and Lrrk2 GS, n = 4. For each cell culture, fifty independent fields were analyzed for quantification.

5.27. Measurement of Lysosomal pH

Cells were plated in lumox 96 multiwell (4×10^4 cells) (Sarstedt) and treated with α-syn PFFs (0.5 μM, 24 h) once reached 95% of confluency with or without the autophagy inhibitor bafilomycin (50 nM, 1 h). Cells were then rinsed once and treated with the ratiometric dye, 2-(4-pyridyl)-5-((4-(2-dimethylaminoethylaminocarbamoyl) methoxy) phenyl) oxazole (RatioWorks PDMPO, AAT Bioquest) at a final concentration of 2 μM in OPTIMEM for 5 min. After the incubation, cells were rinsed three times in OPTIMEM and fluorescence was measured at 37 °C using a multi-plate reader (EnVision, Perkin Helmer). Specifically, the emitted fluorescence at 535 nm was acquired upon excitation at 340 nm and 380 nm. The ratio of the light excited at two wavelengths (340/380 nm) is proportional to lysosomal pH. For each sample, a replicate of two wells was used to determine the ratio.

5.28. Neutral Red Staining

Cells were plated in 24-well plates (105 cells) and treated with α-syn PFFs (0.5 μM, 24h) once reached 80% of confluency with or without bafilomycin (50 nM, 1h); at the end of the treatment, the cell culture medium was removed and OPTIMEM with a solution of 3-amino-7-dimethylamino-2-methyl-phenazine hydrochloride (neutral red, Sigma- Aldrich) with a final concentration of 40 ng/ml was added to the cells for 3–4h. Cells were washed twice with DPBS and dissolved in a destaining solution composed of 50% ethanol, 49% deionized water, and 1% glacial acetic acid, and the absorbance was recorded by the use of a multiwell plate reader at the wavelength of 540 nm (Victor, Perkin Helmer). For each sample, treated and untreated, a replicate of two wells was used to determine protein concentration (BCA assay). Data were expressed as absorbance at 540 nm normalized to the absorbance recorded for the BCA assay,

and the results in the graph were expressed as neutral red staining absorbance in comparison with untreated controls.

5.29. Statistical Analysis

Experiments were performed using cell cultures obtained from at least three different groups of pups. H4 cells were used at the same in vitro passage number for the two independent experiments. Results are expressed as mean ± standard error of the mean (SEM) or median with interquartile range; depending on whether data followed a Gaussian distribution or not. Gaussian distribution was assessed by D'Agostino-Pearson omnibus and Shapiro-Wilk normality tests. For Gaussian distribution, the statistical analysis between two groups was performed by unpaired Student's t test. Data including more than two groups were analyzed by one-way ANOVA (Gaussian distribution) or Kruskal-Wallis test (non-Gaussian distribution) respectively followed by Tukey's multiple comparisons test or Dunn's multiple comparisons test. Levels of significance were defined as $p \leq 0.05$, $p \leq 0.01$, $p \leq 0.001$. Statistical analysis was performed in Prism 6 (GraphPad).

Chapter 6

Results PART I

6. Results PART I

6.1 Primary astrocytes efficiently internalize synaptosomes

To visualize synaptosome internalization within the phagocytic pathway of the astrocytes, we conjugated them with a pH-sensitive fluorescence dye named pH-RODO dye as described in Byun et al 2019 (Materials and Methods Section 5.7). Then, we tested the ability of pH-RODO conjugated synaptosomes to emit fluorescence in live cells as established in Byun et al., 2019. To this purpose we employed primary striatal astrocytes that are routinely produced in the lab. Specifically, primary striatal astrocytes were treated with 1μg/cm^2 of pH-RODO synaptosomes. We monitored synaptosomes internalization over time by using time-lapse fluorescence microscopy. We observed that no fluorescence is detected after 1h upon treatment. However, the internalized materials start to emit bright fluorescence after 12h (data not shown). We therefore implemented the phagocytic readout by transfecting astrocytes with a plasmid encoding eGFP as optimized in (Streubel-Gallasch et al., 2021). Specifically, primary astrocytes were transfected with eGFP encoding plasmid and the day after cells were treated with 1μg/cm^2 of pH-RODO synaptosomes for 90 minutes. For each image acquired, we calculated the area of the pH-RODO positive puncta (red area) within the ROI designed by eGFP expressing cells and the area of the eGFP transfected cells (green area) using the Harmony software. Then, we calculated the PI (phagocytic index) as red area divided by green area. As shown in Figure 6.1.1, with this method we can follow synaptosomes engulfment. As already reported in literature the phagocytic kinetics of primary astrocytes display a peak at 48h (Byun et al., 2019).

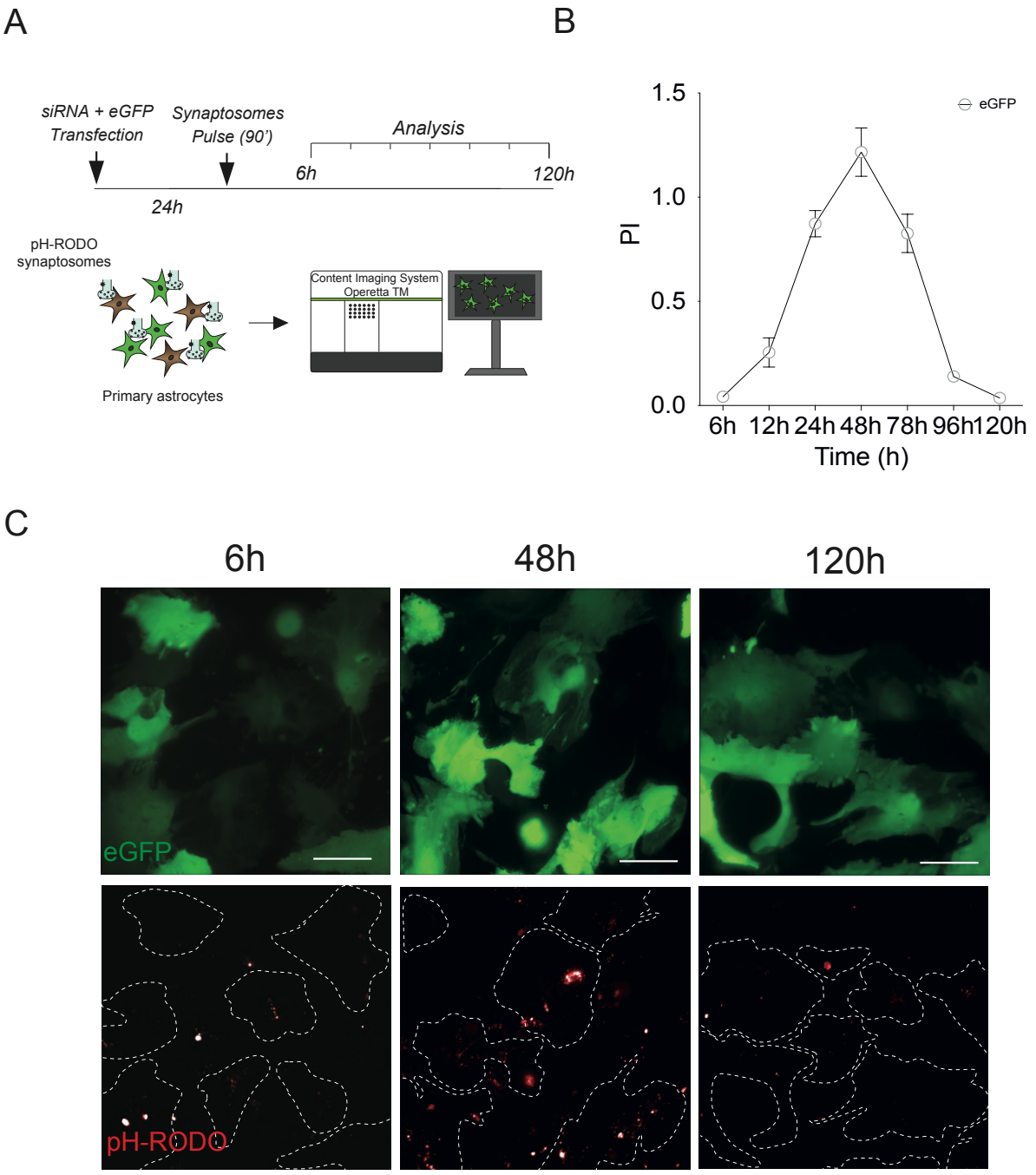

Figure 6.1.1. Synaptosome internalization kinetics in astrocytes. A. Schematic outline of the experimental setup. Cells were co-transfected using with an eGFP-encoding plasmid. 24h post transfection cells were treated with pH-RODO-labeled synaptosomes and imaged using High Content System Operetta; **B.** Representative graph showing the PI of primary astrocytes transfected with an eGFP-encoding plasmid at 6h, 12h, 24h, 48h, 78h and 120h upon synaptosomes treatment. Thirty field per conditions were analyzed, quantification of PI was performed using Harmony Software; n=3 biological replicates; **C.** Representative fluorescence images of primary astrocytes transfected with an eGFP-encoding plasmid at 6h, 48h and 120h upon synaptosomes treatment. Scale bar 50 μm.

Finally, we confirmed the internalization of the synaptic terminals and their destination within the cell using specific endo-lysosomal markers. Primary striatal astrocytes were treated with 1μg/cm^2 of synaptosomes conjugated with a dye suitable for immunocytochemistry named TAMRA. After 48h of treatment, primary astrocytes are fixed and stained for endogenous Lysosomal associated membrane protein 2 (Lamp2). Consistently with our previous results, we observed that engulfed TAMRA-labelled synaptosomes colocalized with Lamp2 (Figure 6.1.2).

Overall, these results confirmed that astrocytes can internalize purified neuronal terminals and direct them to acidic, endo-lysosomal compartments possibly for degradation.

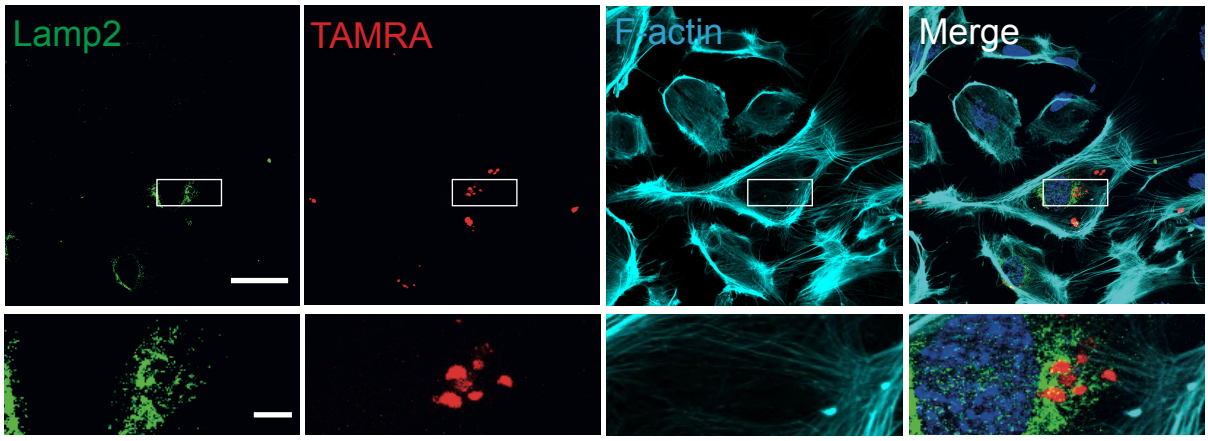

Figure 6.1.2. Synaptosome internalization in astrocytes. Representative z-stack confocal images of primary striatal astrocytes treated with TAMRA-synaptosomes (red). Cells were stained with anti-LAMP2 (green) antibody and F-actin (cyano). Insets show TAMRA and Lamp2 colocalization. Scale bar 20 μm; insets 5 μm.

6.2 Primary microglia cells do not interfere with astrocyte-mediated synaptosome internalization

Primary striatal astrocytes, routinely produced in the lab, are pure at the 95% (Streubel-Gallasch et al., 2021). The remaining 5% of our culture is constituted by microglia. To assess weather microglia can interfere with our analysis, we characterized the identity of the eGFP-transfected cell population by immunofluorescence staining. After 48h upon transfection, cells were fixed and stained for GFAP, a specific astroglia marker and for Iba1 for microglial cells, separately (Figure 6.2.1). We then evaluated the number of the cells GFAP+/eGFP+, GFAP-

/eGFP+, GFAP+/eGFP- and GFAP-/eGFP- in Fig 6.2.1 A and the fraction of Iba1+/eGFP+, Iba1-/eGFP+, Iba1+/eGFP- and Iba1-/eGFP- populations in Figure 6.2.1 B. Overall, we showed that all the eGFP+ cells are GFAP+. Consistently, no Iba1+/eGFP+ have been detected.

To further evaluate weather microglial cells could affect synaptosomes internalization mediated by astrocytes, we eliminated microglia from astrocytes cultures. To this purpose, primary astrocytes culture was exposed to 100µM of liposomal clodronate for 12h and liposomes without clodronate as a control. Liposomal clodronate has been demonstrated to eliminates microglia from astrocytic cultures without affecting astrocytes viability (Kumamaru et al., 2012). Then, astrocytes were transfected using eGFP encoding plasmid and 24h after expression cells were exposed to 1µg/cm^2 of pH-RODO synaptosomes for 90 minutes. Synaptosomes internalization was followed at three time points, 1h and 48h, using High Content System Operetta. As shown in Figure 6.2.2 we did not detect any statistical differences in the PI of all the conditions (Two-way ANOVA with Tukey's multiple comparison test, $p>0.05$). With this experiment, we evaluated that control astrocytes and clodronate treated astrocytes display the same PI, confirming that microglia cells do not affects astrocytes-mediated purified synaptic terminals internalization.

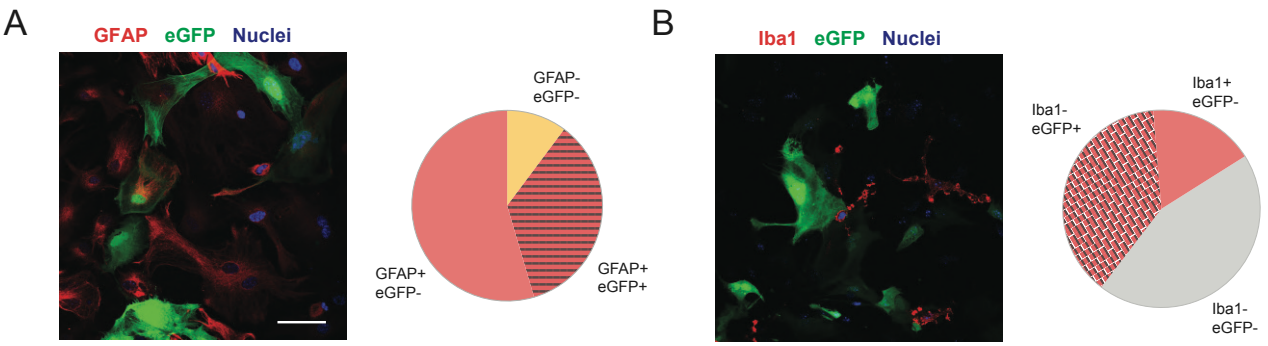

Figure 6.2.1 Characterization of the eGFP-transfected cell population. A. Representative fluorescence microscopy images and relative quantification. Cells were transfected with eGFP-encoding plasmid (green) and stained for GFAP (red); scale bar 50 µm; **B.** Representative fluorescence microscopy images and relative quantification for transfection efficiency. Cells were transfected with GFP-encoding plasmid (green) and stained for Iba1 (red). Scale bar 50 µm.

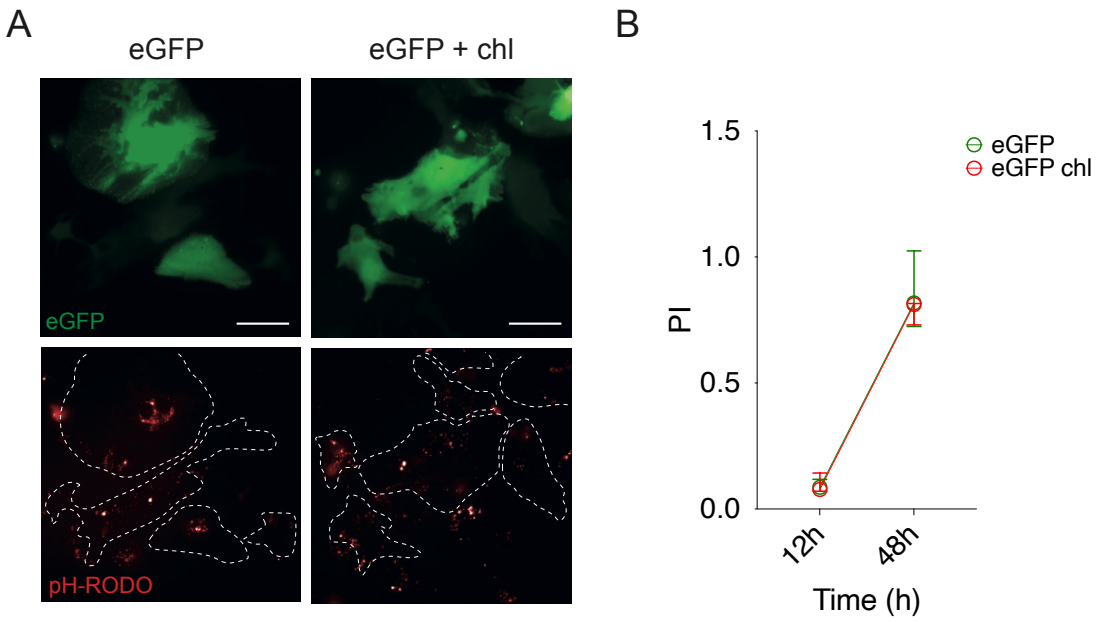

Figure 6.2.2 Effects of microglia depletion. **A.** Representative fluorescence images of primary astrocytes treated with liposomal clodronate (chl) and control liposome transfected with an eGFP-encoding plasmid at 48h upon synaptosomes treatment. Scale bar 50 μm; **B.** Representative graph showing the PI of primary astrocytes transfected with eGFP-encoding plasmid under basal and Liposomal Clodronate-treated condition at 12h and 48h upon pH-RODO synaptosomes treatment. Microglia-free culture does not show any PI differences at the three time points. Thirty field per conditions were analyzed, quantification of PI was performed using Harmony Software.

6.3 Downregulation of Megf10 and Cathepsin-B affects astrocyte phagocytic activity

To manipulate the phagocytic process, we downregulated Megf10, a receptor known to act on synaptosome internalization (Chung et al., 2013) and CtsB, an enzyme that affect lysosomal degradative capacity. Primary striatal astrocytes were efficiently transfected using Lipofectamine 2000 with a final concentration of 50nM siRNA for 72h as published by us in (Streubel-Gallasch et al., 2021). Thus, we assessed the downregulation of the target proteins using western blot and immunofluorescence analysis. Cells were transfected with siRNA against Megf10 and Ctsb and compared to a non-targeting siRNA (Control) as a control. Cells were lysated and the expression of the gene were assessed by western blot analysis in the overall cell population. As shown in Figure 6.3.1 A-D, the downregulation of Megf10 and CtsB reached the 50% of the total expression compared to the control sample transfected with scramble siRNA.

To functionally measure the effect of Megf10 and CtsB downregulation on synaptosomes internalization, we performed a live-imaging analysis using High Content System Operetta as previously set. To this purpose, the phagocytic kinetics of primary astrocytes was calculated at 12h and 48h upon pH-RODO synaptosomes treatment. As reported in Figure 6.3.1 E-F, we showed that Megf10 downregulation markedly reduces the PI of astrocytes compared to the control astrocytes. Whereas the absence of CtsB causes an accumulation of synaptosomes overtime, suggesting a lack in the degradation of synaptosomes.

Concluding, these two experimental conditions are suitable as additional controls in the siRNA screening.

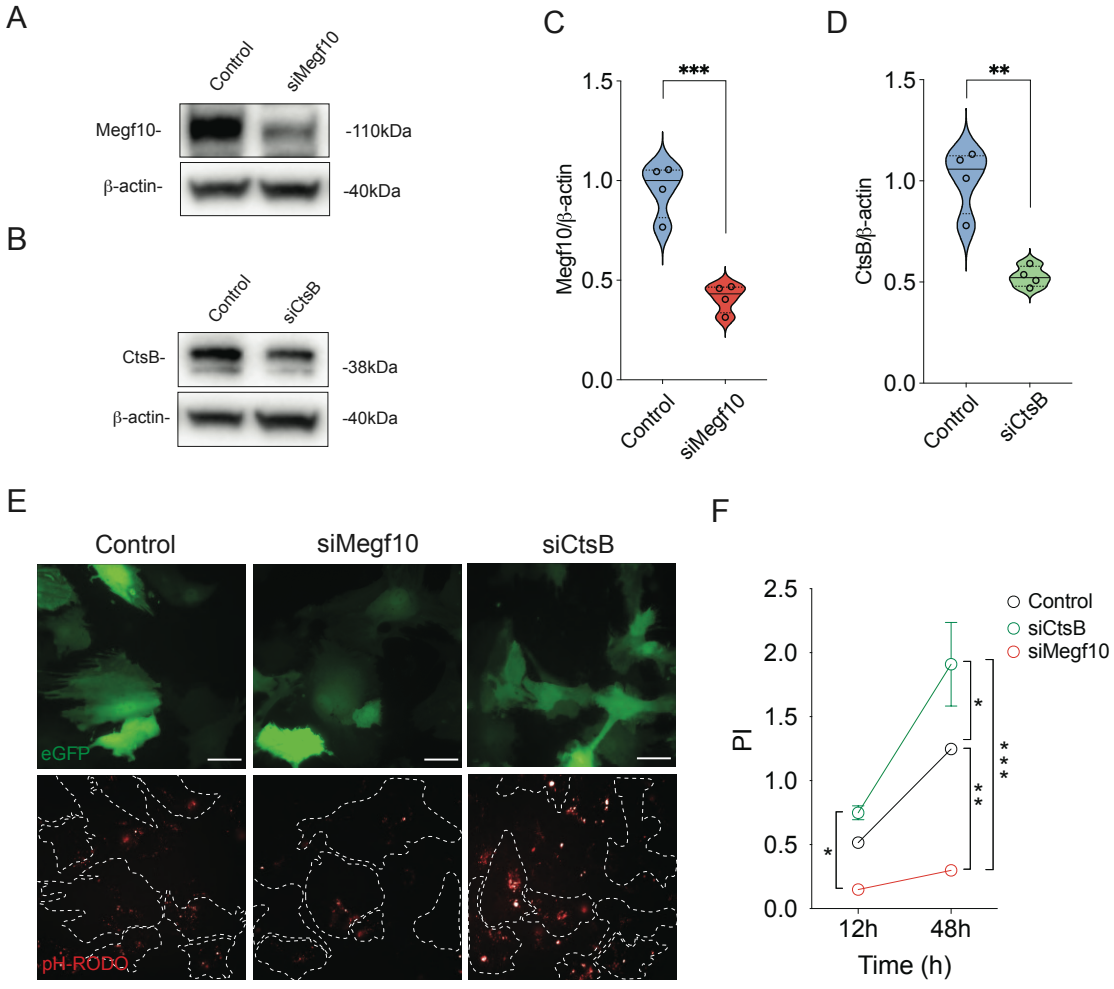

Figure 6.3.1 Biochemical and functional evaluation of Megf10 and CtsB downregulation. A. Western blot analysis and relative quantification in **C.** of primary astrocytes lysates transfected with Control and Megf10 siRNA; **B.** Western blot analysis and relative quantification in **D.** of primary astrocytes lysates transfected with Control and CtsB siRNA; **C, D.** Quantification of band intensity was

performed using ImageJ and normalized by β-actin. Differences between the two conditions have been evaluated using Student's t-test (significance ***p<0.001), n=4 biological replicates; **E.** Representative images of primary astrocytes transfected with Control, Megf10 or CtsB siRNA together with a GFP-encoding plasmid at 48h after synaptosome treatment. Scale bar 50 μm. Cells were transfected using siRNA and eGFP-encoding plasmid. 24h post transfection cells were treated with pH-RODO-labeled synaptosomes for 90 minutes and imaged using High Content System Operetta at 12h and 48h after the pulse**; F.** Representative graph showing the PI of primary astrocytes transfected with Control, Megf10 or CtsB siRNA. Megf10 downregulation decreased the PI at 12h and 48h while CtsB downregulation displayed a high PI at both time points. Forty field per conditions were analyzed, quantification of PI was performed using Harmony Software; Statistical analysis was performed using Two-Way ANOVA with Tukey's multiple comparison test (significance ***p<0.001; **p<0.01, *p<0.05).

6.4 Screening for novel regulators of astrocyte-mediated synaptosome engulfment

To identify novel potential modulators of synapse internalization, we leveraged on a siGENOME Mouse Druggable siRNA Library composed by near three thousand hits, which are sub-divided in eleven 384-well plates containing 280 genes. Primary murine astrocytes were seeded, and each well were co-transfected with eGFP-encoding plasmid and a single siRNA following the established protocol. In each plate, we reserved 7 wells for each control: Megf10 (red), CtsB (green) and Control (black) siRNA as represented in Figure 6.4.1 A 24h upon transfection cells were exposed to pH-RODO conjugated synaptosomes. Then, we acquired the whole well for each condition at 12h and 48h, using the High Content System Operetta. To overview the screening output, we first plotted the internal controls of each plate (Figure 6.4.1 B). Although a certain grade of variability has been detected at 48h in the CtsB downregulated wells, we concluded that the overall setting is adequate to screen novel modulators of synaptosome engulfment.

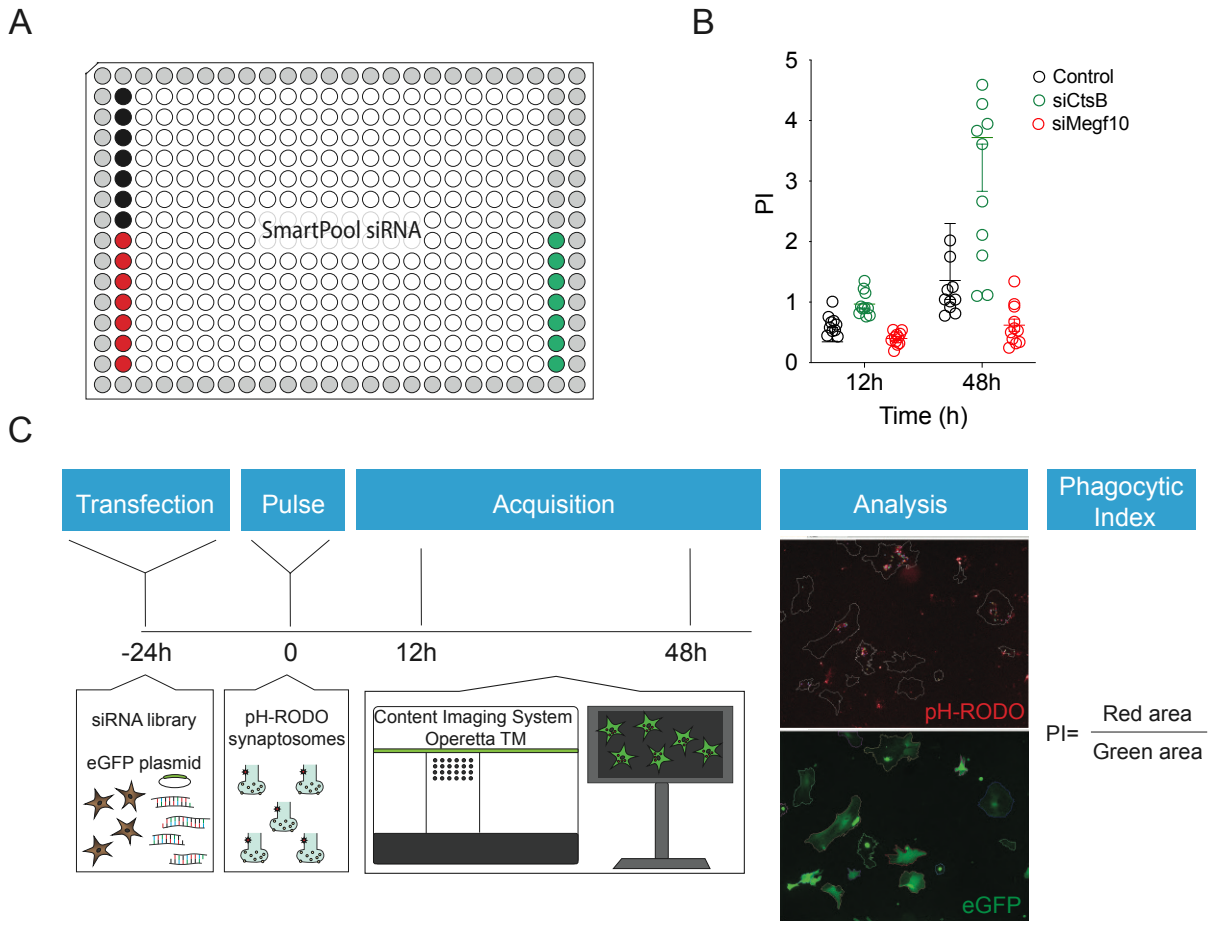

Figure 6.4.1. Experimental design. **A.** Experimental plate layout in 384-well format. Each plate contain: 7 wells of control siRNA (black well), 7 wells of Megf10 siRNA (red well), and 7 wells of CtsB siRNA (green well), 76 empty wells (grey) and 280 SmartPool siRNA of the Druggable Library; **B.** Representative graph showing the PI of primary astrocytes transfected with Control, Megf10 or CtsB siRNA. Megf10 downregulation decreased the PI at 12h and 48h while CtsB downregulation displayed a high PI at both time points. Five fields per conditions were analyze, quantification was performed using Harmony Software; **C.** Primary astrocytes were transfected with an eGFP-encoding plasmid together with siRNA library. The day after, cells were exposed to pH-RODO synaptosomes and the phagocytic kinetics was measured through long-term fluorescence live imaging using High Content System Operetta imaging system at 12h and 48h. Note that before live-images were taken, unbound synaptosomes were washed away after the incubation. To quantify phagocytosis, the area (μm^2) of red fluorescence signal is normalized to the eGFP positive area (μm^2) (Phagocytic Index, PI).

Therefore, we plotted the PI values at 12h vs 48h of the around 3000 hits as shown in Figure 6.4.2. The PI mean value +/- SD of the siRNA Control (0.6 +/- 0.05; 1.19 +/- 0.6), siMegf10 (0.4 +/-0.032; 0.60 +/- 0.1) and siCtsB (0.9 +/- 0.05; 2.59 +/- 0.4) are also reported in Figure 6.4.2. It is clearly visible that the disruption of several genes impacts synaptosome internalization and accumulation. As shown in Figure 6.4.2, a conspicuous number of hits clustered around the negative control identified as siRNA control. A second group (~ 100) that possess a PI at 12h lower than the PI mean value +/- SD of siMegf10 at 12h and 48h, have been categorized as genes that negatively regulate synapse internalization and are colored in red. Another group of genes (~ 200) have been identified as potential hits that impact on degradation (hits in green), with a PI higher than the PI mean value +/- SD of CtsB at the two time points. However, we cannot exclude that the genes underling in green are enhancing internalization.

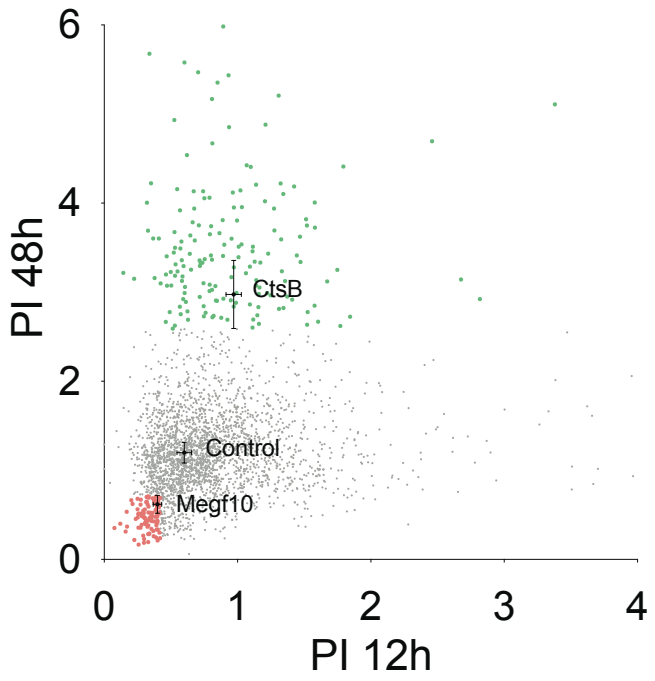

Figure 6.4.2 Phagocytic Index of the screening hits at 12h and 48h. Representative graph showing the comparison of PI at 12h versus 48h of downregulated primary astrocytes with siRNA against 3000 druggable genes upon synaptosomes pulse (grey) versus controls siRNA. Genes that abolish the ability of astrocytes to internalize synaptosome were highlighted in red; while genes that exerts an opposite effect were highlighted in green. Five fields per conditions were analyze, quantification was performed using Harmony Software.

To further investigate among the hits that impact astrocyte phagocytosis, we performed a gene ontology (GO) analysis in which we associated genes to their molecular function (in collaboration with Dr Enrica Calura). Figure 6.4.3 shows the top 10 significantly enriched GO terms. Molecular function (MF) analysis for the genes that abolish the ability of astrocytes to internalize synaptosome (red hits) shows enrichment in G protein-coupled receptor activity, peptide receptor activity and C-C chemokine receptor activity (Figure 6.4.3 A – dot plot). Specifically, G protein-coupled receptor and chemokine receptor are the top represented categories. As shown in Figure 6.4.3 B, genes that are mainly represented in the top categories are 8 chemokines receptors: Cxcr5, Ackr3, Cxcr2, Cxcr3, Ccr1, Ccr2, Ccr4 and Ackr2 (Figure 6.4.3 B – gene networkplot). Instead, MF analysis for the green hits identified protein kinase activity, protein serine/threonine kinase activity and identical protein binding activity as top categories (Figure 6.4.4 A – dot plot). Specifically, genes that mainly represented those categories are Acvr1, Cdk4, Tgfbr3, Stk19, Ttn, Akt3, Pim2, Ripk2 and Mapk7 (Figure 6.4.4 B – gene network plot). Overall, most of the genes in red hits possess receptor activity whereas genes in green hits are more related to intracellular signaling pathways.

Notably, the screening coupled with the gene set analyses identified eight chemokine receptors whose disruption impact on synaptosomes internalization (Figure 6.4.5 B). Among them, the Ackr3 receptor has been selected for validation based on its high expression in murine and human astrocytes (Figure 6.4.5 A-B).

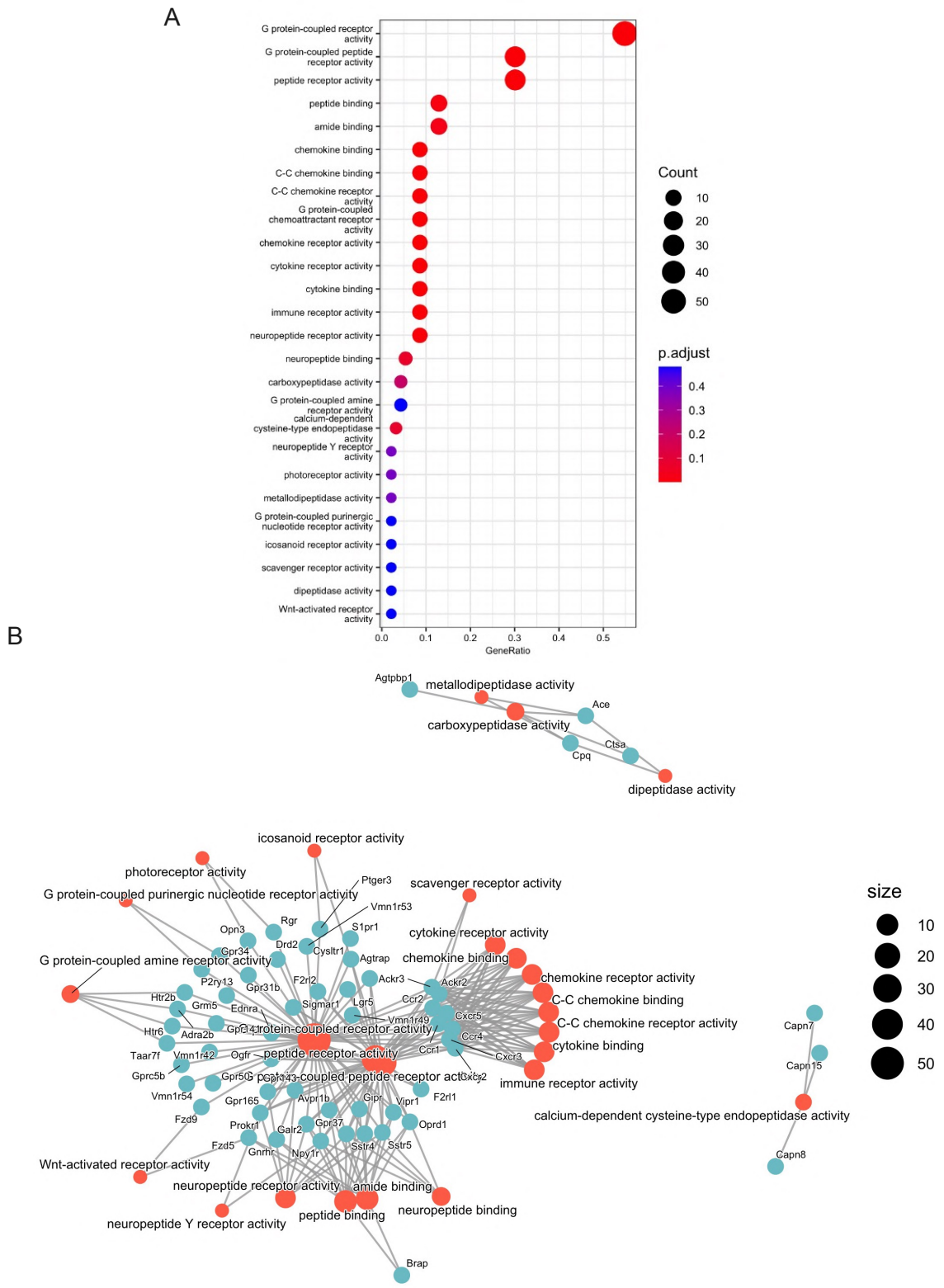

Figure 6.4.3 Molecular Functional enrichment analysis of red hits. A. Dotplot of red hits. Genes are plotted with a qvalue <0.5. Bubble plots highlight p.adjusted values of the GO categories (color scale) and the number of hits falling in the GO categories (size scale). Gene ratio defines the percentage of the enriched hits in the given GO term; **B.** Cnetplot of red hits showing the pathway-gene network. The linkages of genes (cyano) and biological categories (orange) are represented as a network.

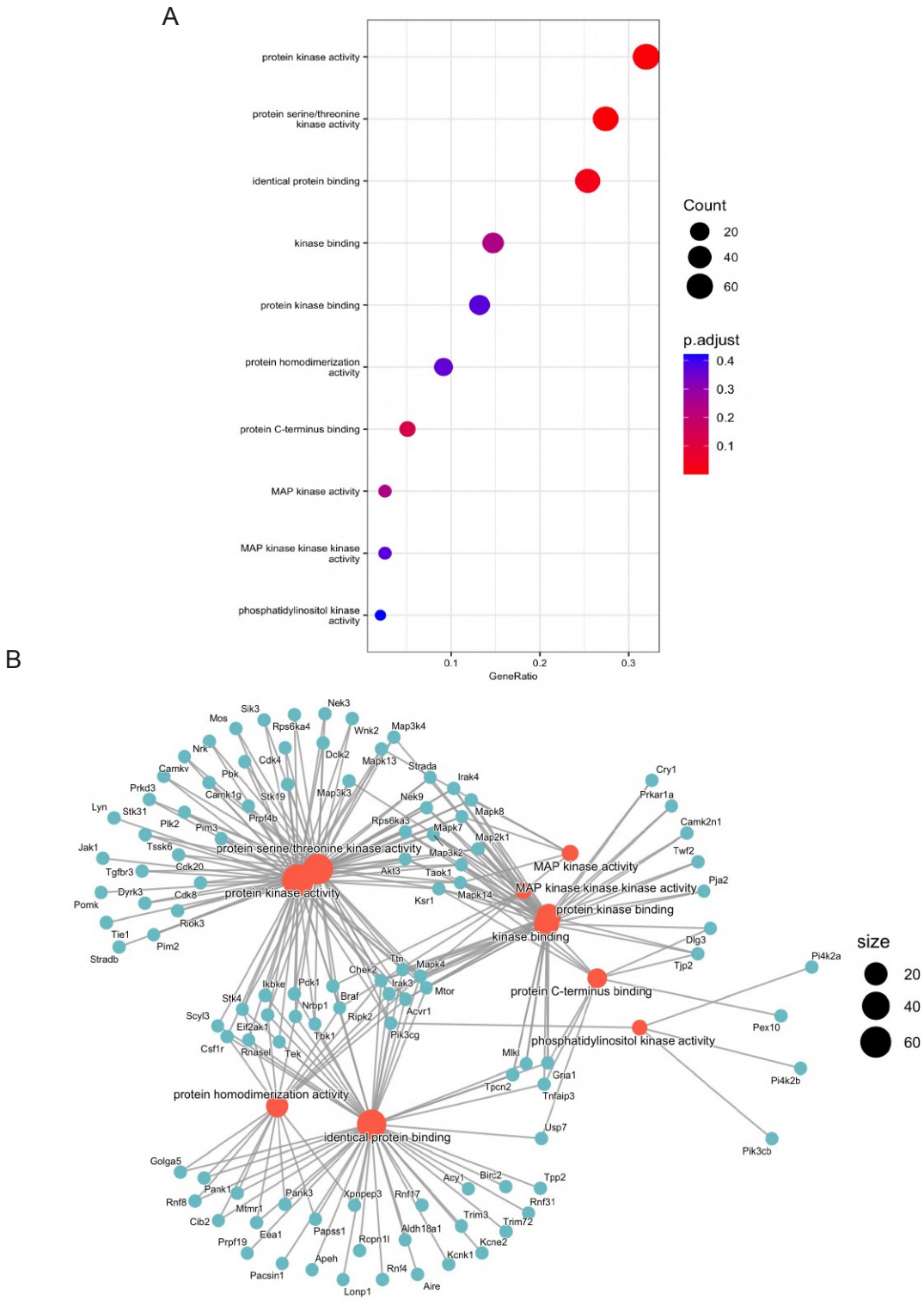

Figure 6.4.4 Molecular Functional enrichment analysis of green hits. A. Dotplot of green hits. Genes are plotted with a qvalue <0.5. Bubble plots highlight p.adjusted values of the GO categories (color scale) and the number of hits falling in the GO categories (size scale). Gene ratio defines the percentage of the enriched hits in the given GO term; **B.** Cnetplot of green hits showing the pathway-gene network. The linkages of genes (cyano) and biological categories (orange) are represented as a network.

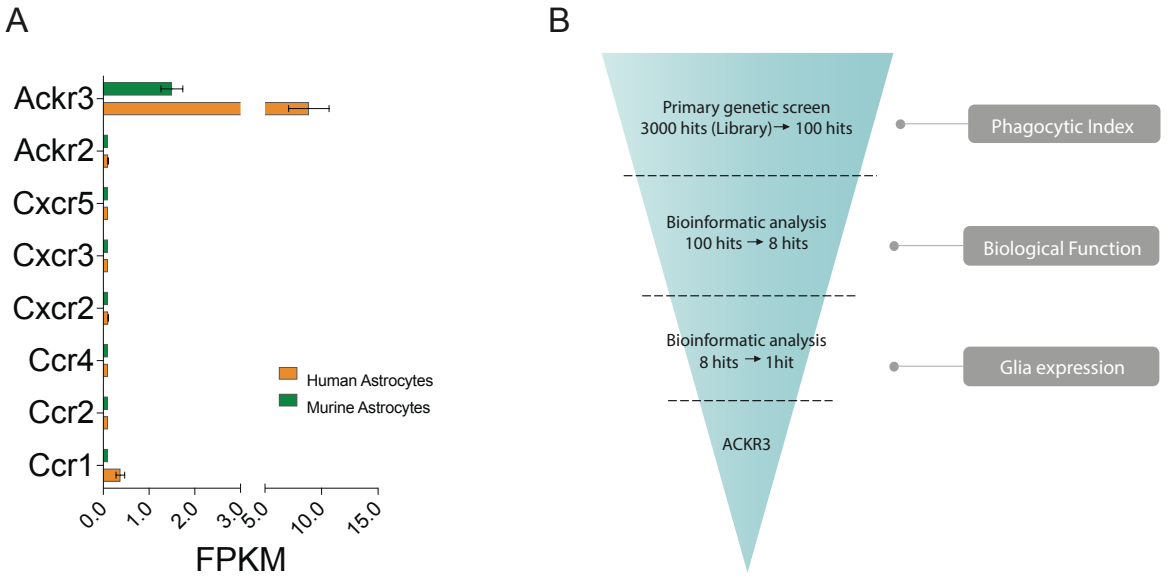

Figure 6.4.5 Chemokine receptors impact astrocytes-mediated synaptosomes engulfment. A. Transcriptomic data showing the differential expression of chemokine receptors identified by the high-throughput screening in murine and human astrocytes. Note that Ackr3 is highly enriched in both murine and human astrocytes compared to the other selected hits. Abbreviation: FPKM, fragments per kilobase of transcript per million mapped reads; **B.** Schematic representation of the approach followed in defining the possible modulators of astrocytes-mediated synapses elimination. First, primary genetic screen selected around 100 hits that abolish synaptosome internalization. Secondly, gene ontology analysis highlighted 8 chemokine receptors. Finally, genes were clustered relying on the glial expression, and Ackr3 was selected for validation.

6.4.1 Ackr3 impacts synaptosome internalizations

Ackr3 is a receptor belonging to the CXC chemokine receptor family that binds to CXCL11 and CXCL12 (Koch and Engele, 2020). Ackr3 is expressed in various tissues such as the heart, kidney, and brain, and more interestingly, is found in neurons, astrocytes, and vascular cells but not microglia However, the molecular mechanism behind Ackr3-mediated synaptic pruning is totally unknown. First, we validated the endogenous expression of Ackr3 in primary striatal astrocytes by western blot and its downregulation using the same set up applied in the screening. As evidenced by the quantification, the downregulation was up to 50-60% compared to the control astrocytes (Fig. 6.4.6 A-B). Moreover, the downregulation was assessed at single-cell level in astrocytes co-transfected with siRNA against Ackr3 and eGFP-encoding plasmid. As shown in Figure 6.4.6 C, the receptor is distributed in patchy areas in control astrocytes,

possibly clustered in the plasma membrane and/or in vesicular structures. Upon transfection with siRNA against Ackr3, we observed a pronounced decreased of the Ackr3 staining.

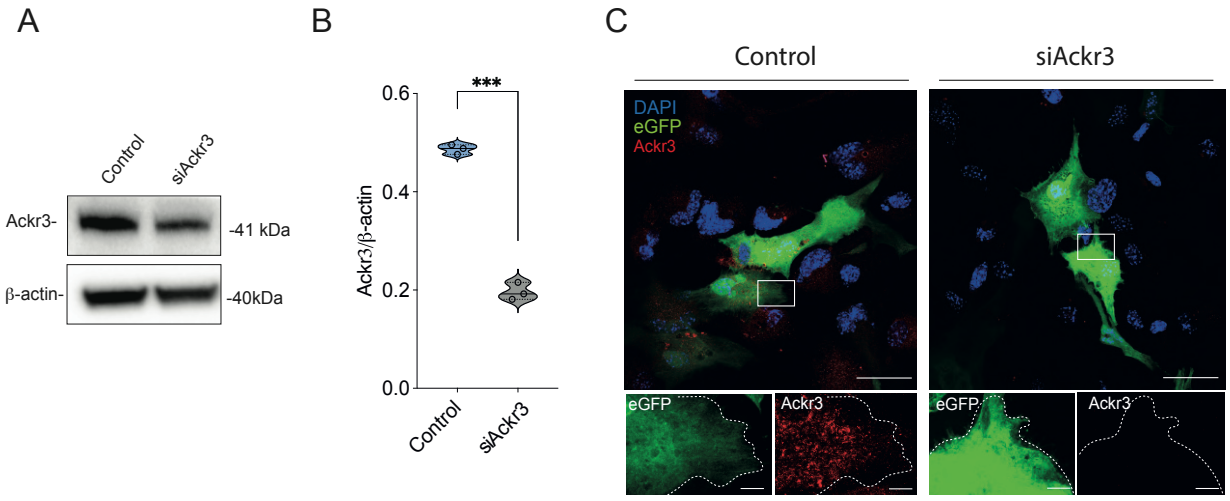

Figure 6.4.6 Primary striatal astrocytes express endogenous Ackr3. A. Western blot analysis and relative quantification in **B.** of primary astrocytes lysates transfected with Control and Ackr3 siRNA. Quantification of band intensity was performed using ImageJ and normalized by β-actin. Differences between the two conditions have been evaluated using Student's t-test (significance ***p<0.001), n=4 biological replicates; **C.** Representative images of primary astrocytes transfected with Control and Ackr3 siRNA together with an eGFP-encoding plasmid. Insets show Ackr3 staining inside eGFP positive cells. Scale bar 50 μm; Insets 20 μm.

To validate the role of Ackr3 in astrocytes-mediated synaptosomes internalization, we performed longitudinal live imaging assay following the same set up of the siRNA-based screening. pH-RODO labeled synaptosome internalization was followed over time at different time points: 6h, 12h, 24h, 48h, 78h, 96h, 120h (Figure 6.4.7 A) We confirmed a statistically significant decreased of the PI at 24h, 48h and 78h in Ackr3-downregulated astrocytes compare to control astrocytes (Figure 6.4.7 B-C).

To corroborate the involvement of Ackr3 in synaptosome internalization, we overexpressed Ackr3 in astrocytes. To this end, we transfected primary astrocytes with Flag-tagged Ackr3 together with an eGFP-encoding plasmid. After 24h upon transfection astrocytes were treated with 1μg/cm^2 of pH-RODO synaptosomes for 90 minutes and we then imaged using High content imaging system. We acquired two time points: 12h and 48h. PI calculation confirmed that in Ackr3-overexpressing astrocytes the PI is significantly higher compared to control astrocytes. Moreover, we transfected siRNA against Ackr3 in astrocytes overexpressing

the receptor to assess whether it could decrease the PI. Specifically, astrocytes were transfected with 50nM of siRNA 12 hours after Flag-Tagged Ackr3 overexpression. 24h after the siRNA transfection, astrocytes were treated with 1μg/cm^2 of pH-RODO synaptosomes. We followed synaptosomes internalization at 12h and 48h (Figure 6.4.8 A). As shown in Figure 6.4.8 B-C the downregulation with siRNA in Ackr3-overexpressing astrocytes partially revert the phenotype and thus decreasing the PI.

Together, these data again confirmed that the receptor modulates the internalization of synaptosomes in primary astrocytes.

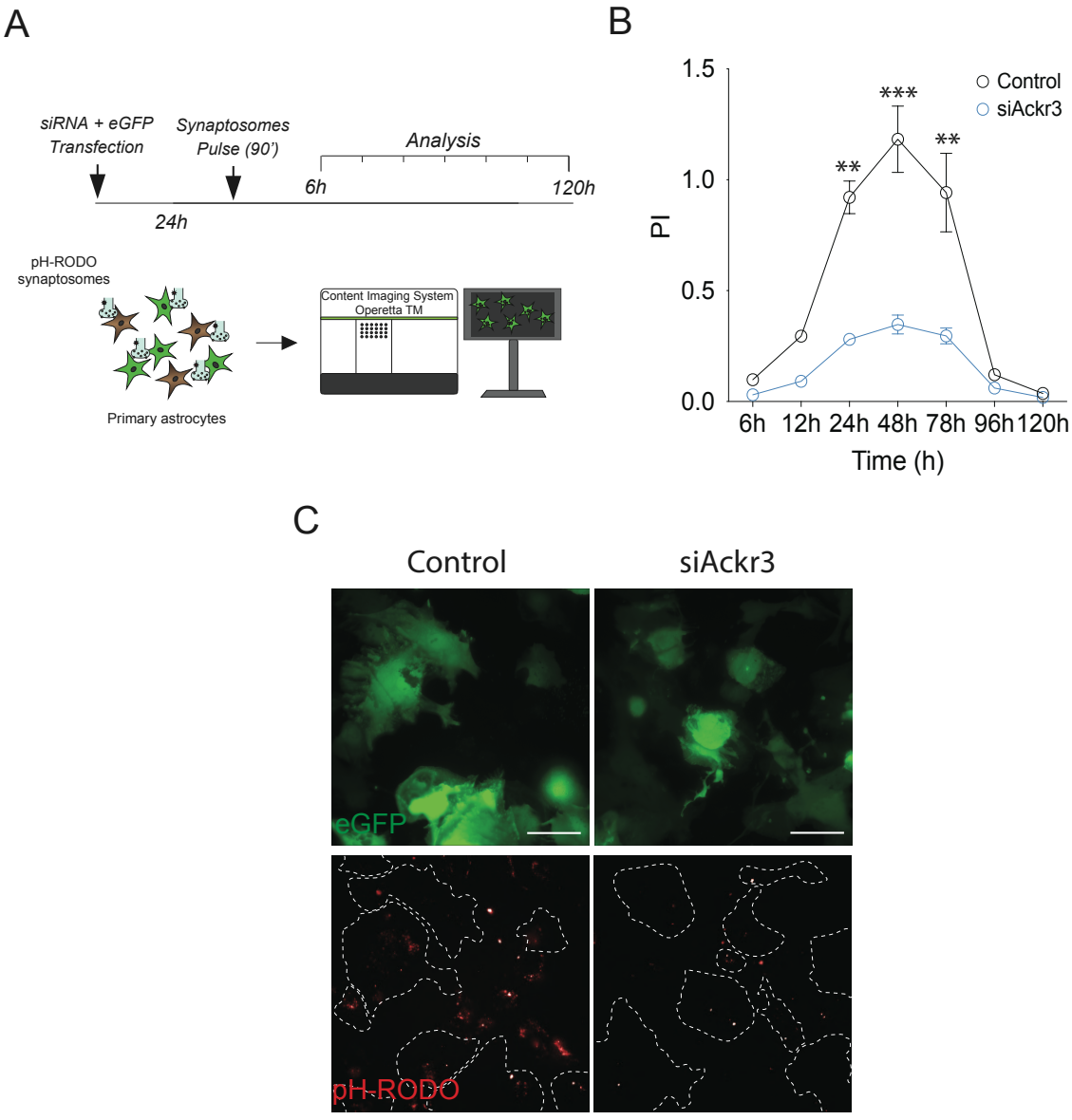

Figure 6.4.7 Ackr3 downregulation abolishes synaptosome internalization. A. Schematic outline of the experimental setup. Cells were co-transfected using Control and Ackr3 siRNA and eGFP-

encoding plasmid. 24h post transfection cells were treated with pH-RODO-labeled synaptosomes and imaged using High Content System Operetta; **B.** Representative graph showing the PI of primary astrocytes transfected with Control and Ackr3 siRNA at 6h, 12h, 24h, 48h, 78h, 96h and 120h upon synaptosomes treatment. Ackr3 downregulation decreased the PI at all the time points. Thirty field per conditions were analyzed, quantification of PI was performed using Harmony Software; Statistical analysis was performed using TWO-WAY ANOVA with Tukey's multiple comparison test (significance ***p<0.001; **p<0.01), n=3 biological replicates; **C.** Representative images of primary astrocytes transfected with control and Ackr3 siRNA together with an eGFP-encoding plasmid at 48h upon synaptosome treatment. Scale bar 50μm

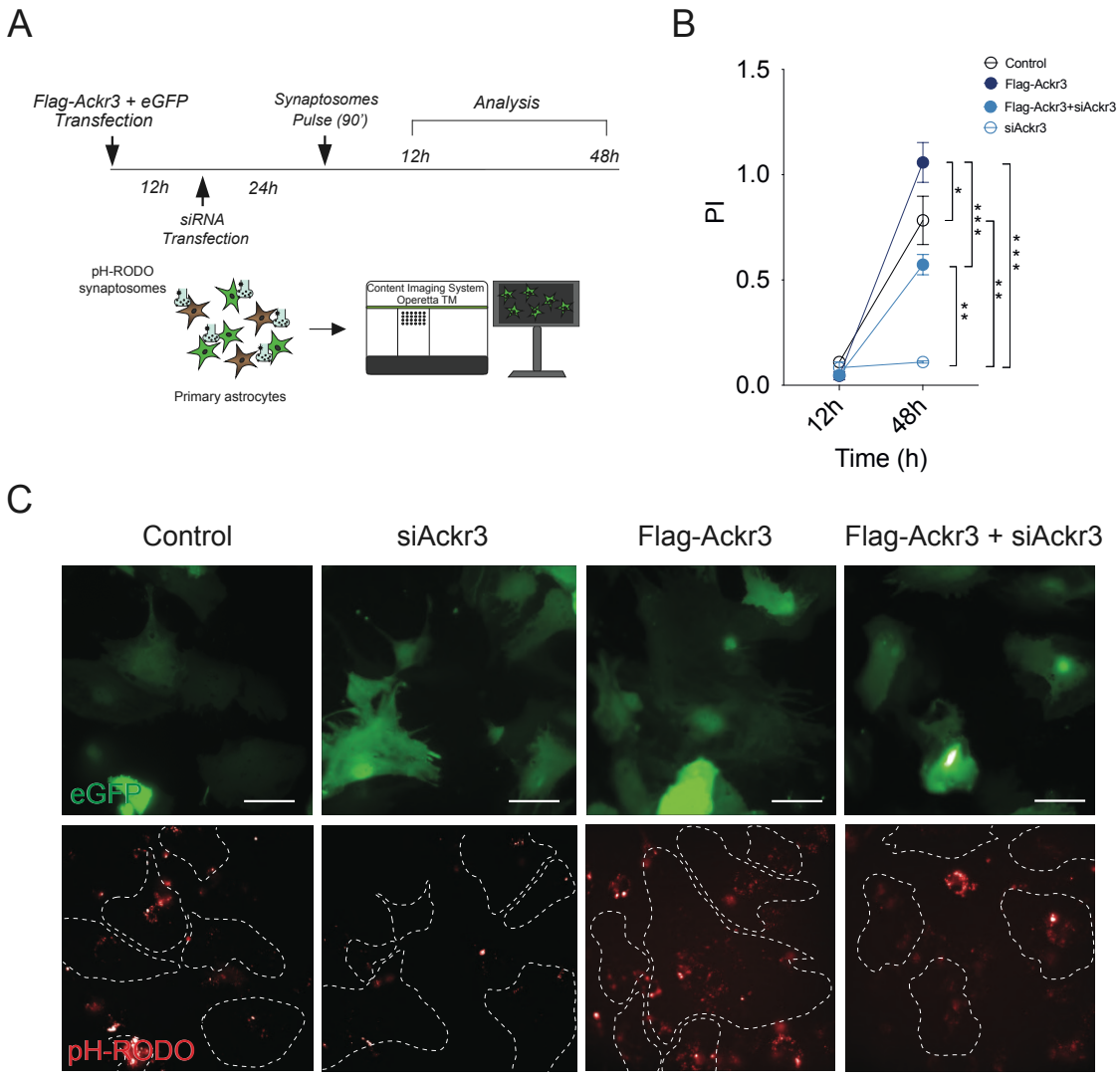

Figure 6.4.8 Ackr3 overexpression increases synaptosome internalization A. Schematic outline of the experimental setup. Cells were co-transfected using with Control, Ackr3 siRNA, Flag-Ackr3 or co-transfected with Flag-Ackr3 and Ackr3 siRNA together with a GFP-encoding plasmid. 24h post transfection cells were treated with pH-RODO-labeled synaptosomes and imaged using High Content

System Operetta; **B.** Representative graph showing the PI of primary astrocytes transfected with Control, Ackr3 siRNA, Flag-Ackr3 or co-transfected with Flag-Ackr3 and Ackr3 siRNA together with a GFP-encoding plasmid at 12h and 48h upon synaptosomes treatment. Thirty field per conditions were analyzed, quantification of PI was performed using Harmony Software; Differences between the two conditions have been evaluated using Student's t-test (significance ***$p<0.001$), n=3 biological replicates; **C.** Representative fluorescence images of primary astrocytes transfected with Control, Ackr3 siRNA, Flag-Ackr3 or co-transfected with Flag-Ackr3 and Ackr3 siRNA together with a GFP-encoding plasmid at 48h upon synaptosomes treatment. Scale bar 50 μm.

6.4.2 Ackr3 is directly involved in astrocyte-mediated synapses internalization

To further characterize the role of Ackr3 in synaptosome internalization, we investigated its localization by immunofluorescence both in basal condition and upon synaptosomes treatment in primary murine astrocytes. Primary astrocytes were treated with TAMRA-synaptosomes, and after 48h, astrocytes were fixed and stained with a primary antibody against endogenous Ackr3. In addition, lysosomal associated membrane protein 1 (Lamp1) was used as an intracellular marker for the endo-lysosomal pathway. As already shown in Figure 6.4.6 C and confirmed in Figure 6.4.9 A, Ackr3 is clustered in vesicular structures in the cytoplasm as well as along the cell perimeter and only partially co-localizes with Lamp1 in control astrocytes. Instead, endogenous Ackr3 re-localizes into Lamp1-positive vesicular structures as well as TAMRA-conjugated synaptosomes upon the treatment. We confirmed the co-localization with the Pearson's correlation coefficient (PCC). As shown in Figure 6.4.9 B, endogenous Ackr3 co-localize with and TAMRA-conjugated synaptosomes with a mean $r=0.4$ compared to the control, suggesting an internalization of the receptor together with synaptosomes ($p<0.001$). We then quantified the co-localization between TAMRA-synaptosomes and Lamp1-positive vesicles (Figure 6.4.9 C) ($p<0.001$). Quantification shows a high co-localization, confirming that internalized synaptosomes are directed to the lysosomal compartment. Then, to determine whether Ackr3 is directed to the lysosomal compartment as well as internalized synaptosomes, we quantified the co-localization between Ackr3 and Lamp1-positive vesicles. Interestingly, we observed a significant amount of Ackr3 co-localizing with Lamp1. Specifically, the co-localization increases 2-fold upon synaptosomes treatment with a $r=0.15$. While in control astrocytes the receptor only partially co-localizes with the

lysosomal compartment with a r=0.25 (p<0.001). Overall, our results suggest that Acrk3 interacts with synaptosomes, and this complex is directed to the lysosome upon engulfment.

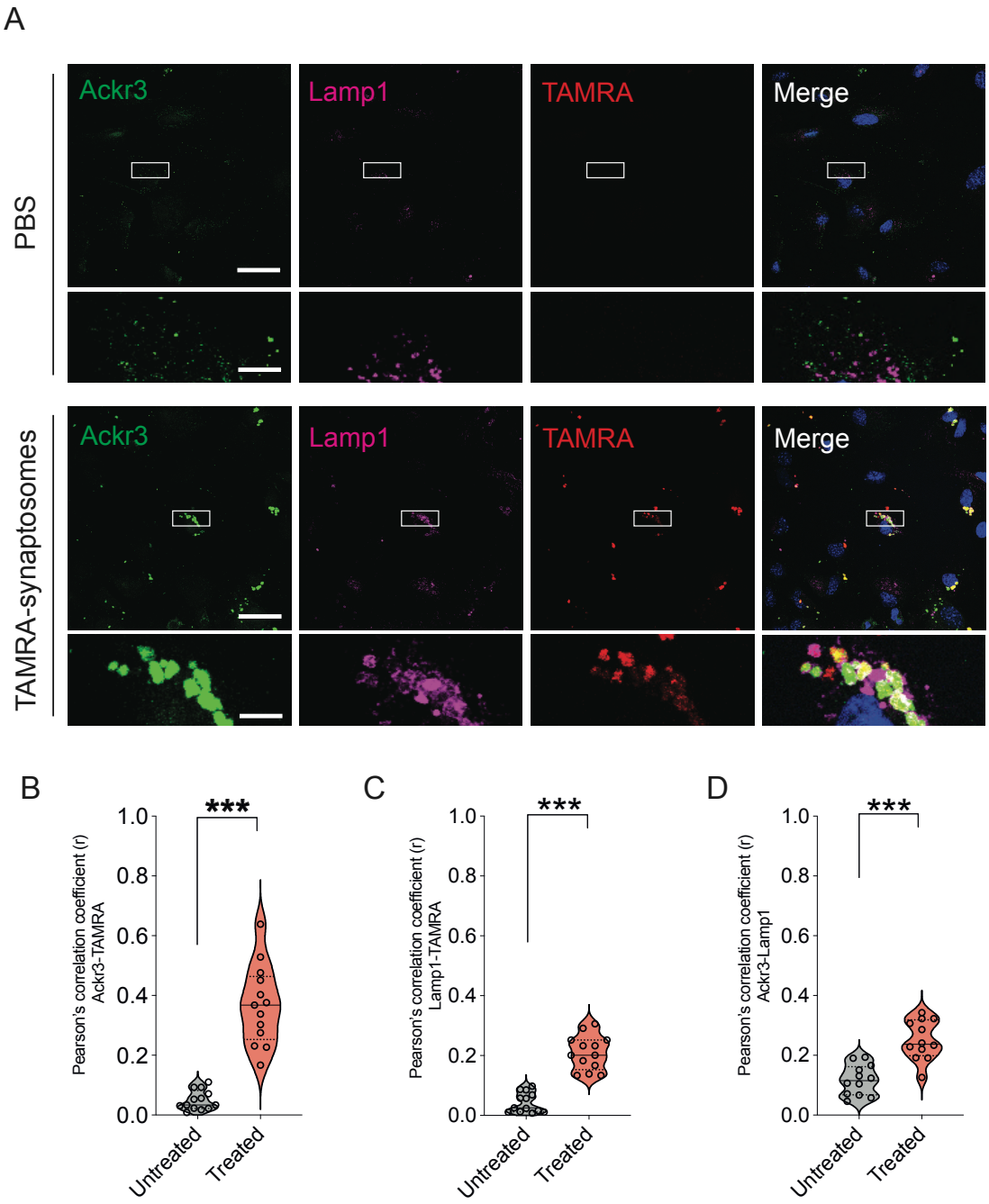

Figure 6.4.9 Ackr3-synaptome complex relocates to the endo-lysosomal pathway. A. Representative z-stack confocal images of primary striatal astrocytes in basal or TAMRA-synaptosomes (red) treatment conditions. Cells were stained with anti-Ackr3 (green) and anti-Lamp1 (purple) antibodies. Insets show Ackr3, TAMRA and Lamp1-positve area and Ackr3 re-localization in Lamp1-positive area upon synaptosomes treatment. Scale bar 20 µm; insets 5 µm; **B.** Pearson's correlation coefficient of Ackr3 co-localizing with TAMRA-positive fluorescent spots (n=12 images for conditions); **C.** Pearson's correlation coefficient of TAMRA co-localizing with Lamp1-positive compartment (n=12 images for conditions); **D.** Pearson's correlation coefficient of Ackr3 co-localizing

with Lamp1-positive compartment (n=12 images for conditions); Differences between the two conditions have been evaluated using Student's t-test (significance ***p<0.001), n=3 biological replicates.

6.4.3 Synaptosome treatment does not stimulate Cxcl11-12 production

Considering that Ackr3 is a chemokine receptor, we investigated the role of Cxcl11/Cxcl12 in the phagocytic process. Firstly, we checked whether astrocytes release chemokines including Cxcl11/Cxcl12 upon synaptosomes treatment. To test this possibility, we performed a chemokine array using media derived from astrocytes treated with synaptosomes and untreated as a control. After the pulse, the media were centrifuged to remove unbound synaptosomes and added to the cells. After 48h upon the treatment, media were collected and incubated with chemokines arrays where 24 different chemokines are spotted (Figure 6.4.10 A). As shown in Figure 6.4.10 B, we calculated the fold change (FC) of chemokine-related dot intensity between synaptosomes-treated over untreated conditioned cells media. Of note, we did not detect any statistical significance (Two-way ANOVA with Tukey's multiple comparison test, p>0.05). Thus, we can conclude that Cxcl11 and Cxcl12 are not released by astrocytes (or other contaminant cells) upon synaptosomes treatment.

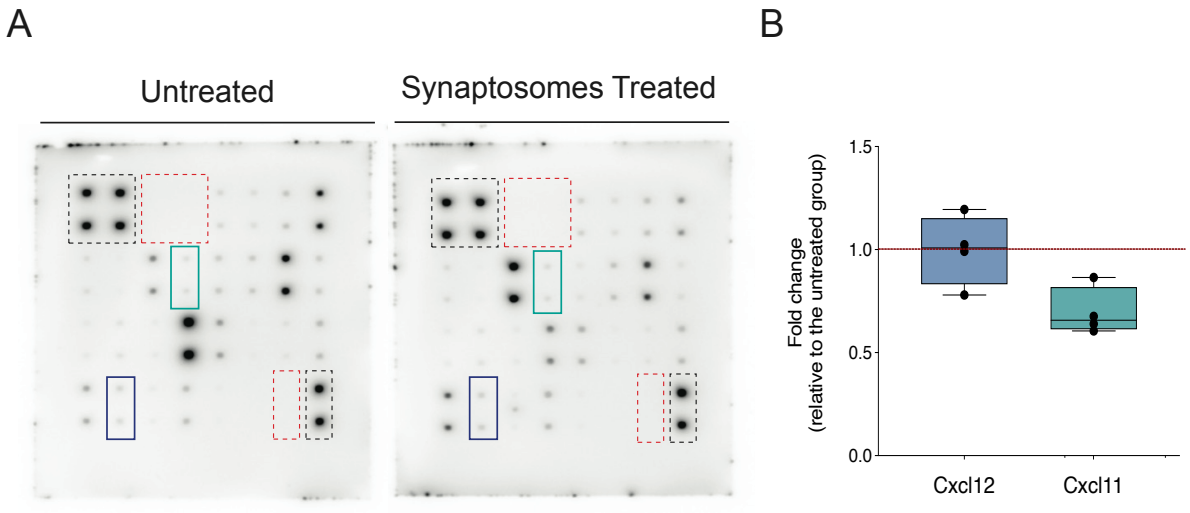

Figure 6.4.10 Cxcl11/Cxcl12 are not released by astrocytes. A. Collective analysis of 24 chemokines in the culture supernatant from synaptosomes treated and untreated astrocytes; Boxes show: Positive (black dotted) and Negative (red dotted) controls, Cxcl12 (blue) and Cxcl11 (green) expression; **B.** The relative fold change of Cxcl12 and Cxcl11 expression. The quantitative analysis of the pixel intensity data did not provide p-values to demonstrate significance levels. n=2 biological replicates, n=4 technical replicates.

6.4.4 Ackr3 interacts with purified synaptosomes *via* Cxcl12

We next hypothesized a direct interaction between Ackr3 and the synaptosomes. We therefore investigated the possible binding *in vitro* by performing a pull-down assay. To this purpose, we purified Flag-tagged Ackr3 from HEK293FT cells and we incubated the anti-Flag resin with non-transfected cell as a negative control. Thus, we incubated the Ackr3-bound resin and the control one with 10μg of purified synaptosomes for the pull-down assay. After extensive washes, we validated Ackr3-synaptosomes interaction by using Vamp2 as a marker for purified neuronal terminals. As shown in Figure 6.4.11 A-B, Vamp2 is retained only by the Ackr3-bound resin. Consistently, the signal of Vamp2 completely lack in the pull-down from the resin incubated with control cells only, confirming the specificity of synaptosomes binding to Flag-Ackr3.

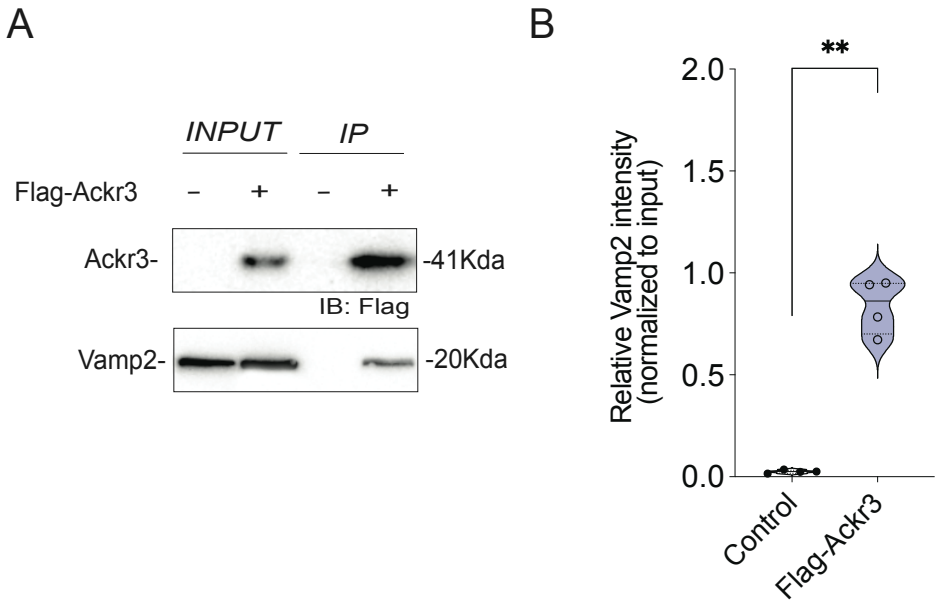

Figure 6.4.11. Ackr3 binds to synaptosomes. A. Western blot analysis of pull-down assay purified of Flag-Ackr3 and Vamp2; **B.** Relative quantification in of Vamp2 band intensity and compared to the input. Quantification of band intensity was performed using ImageJ. Statistical analysis was performed using Student's t-test (significance **p<0.001,), n=4 biological replicates.

Then, we examined the chemokine content in our preparation. Considering that Cxcl12 is the chemokine with the major affinity for Ackr3, we measured Cxcl12 amount in the synaptosomal preparation using western blot (Figure 6.4.12 A). To investigate the ability of synaptic terminal to bind additional chemokines, we incubated synaptosomes with 250nM of

recombinant Cxcl12. Interestingly, we detected a strong signal of Cxcl12 in synaptosomes preparation and we showed that synaptosome membranes can sequester more recombinant Cxcl12 upon incubation. (Figure 6.4.12 A-B)

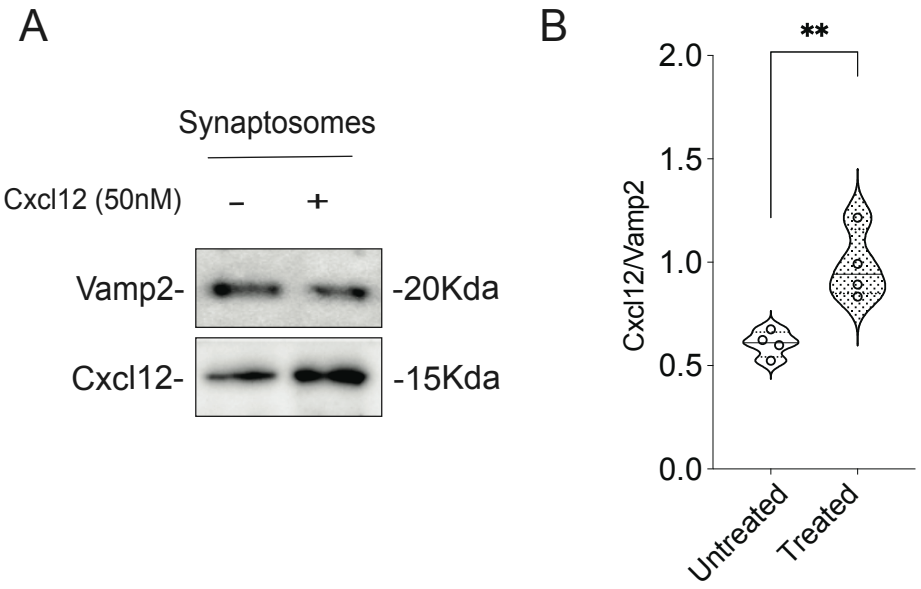

Figure 6.4.12 Synaptosomes possess and bind Cxcl12. A. Western blot analysis of synaptosomes untreated and treated with recombinant Cxcl12; **B.** Relative quantification in of Cxcl12 band intensity and compared to Vamp2. Quantification of band intensity was performed using ImageJ. Differences between the two conditions have been evaluated using Student's t-test (significance **p<0.01), n=4 biological replicates.

We also performed an overlay assay to validate Cxcl12/synaptosome binding. Increasing concentration of synaptosomes (5, 10, 25, 50µg) were spotted onto a nitrocellulose membrane. Then, membrane was saturated and subsequently incubated with 0.1µg/ml of recombinant Cxcl12 overnight at 4°C to allow the binding. The day after, Cxcl12 binding was detected using a specific primary antibody against the chemokine. As shown in Figure 6.4.13, the levels of Cxl12 bound increase proportionally with the increase of spotted synaptosomes, with a complete lack of signal in the control spot (Ripa buffer) confirming the specificity of Cxcl12 binding to synaptosomes.

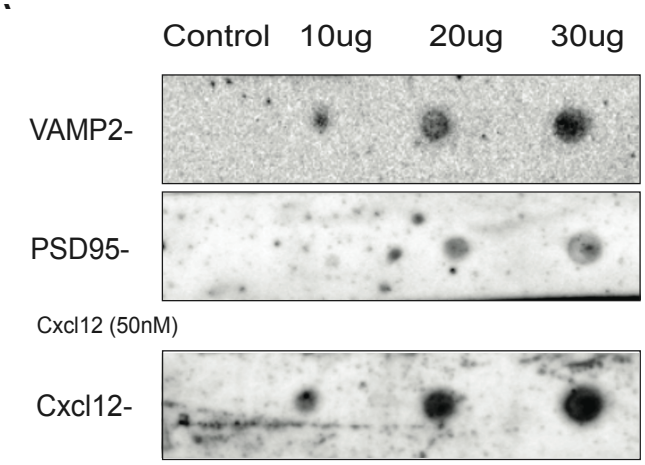

Figure 6.4.13 Biochemical evaluation of Cxcl12-synaptosomes binding. Immuno-dot blot analysis of increasing concentration of synaptosomes spotted onto a nitrocellulose membrane. Synaptosomes were detected using anti-VAMP2 and Anti-PSD95. Recombinant Cxcl12 were incubated with the membrane and bound was detected with anti-Cxcl12.

To assess whether the amount of Cxcl12 bound to synaptosomes can modulate the internalization, we compared the PI of astrocytes in contact with naive synaptosomes and Cxcl12-covered synaptosomes. To this end, we incubated pH-RODO synaptosomes with 250nM Cxcl12 and we performed a live imaging assay using High content technology as before. Astrocytes were co-transfected with Control siRNA, Ackr3 siRNA together with an eGFP-encoding plasmid. After 24h post transfection, astrocytes were treated with Cxcl12-covered pH-RODO synaptosomes and 0.5μg of naïve pH-RODO synaptosomes were used as a control. We followed synaptosomes internalization at 12h and 48h and we calculated the PI. As shown in Figure 6.4.14 A-B, astrocytes treated with Cxcl12-synaptosomes show an increased PI compared to astrocytes treated with control synaptosomes. Consistently with our previous results, we abolished the internalization in Ackr3-downregulated astrocytes in the two conditions, confirming once again that this receptor is critically involved in astrocyte-mediated phagocytosis.

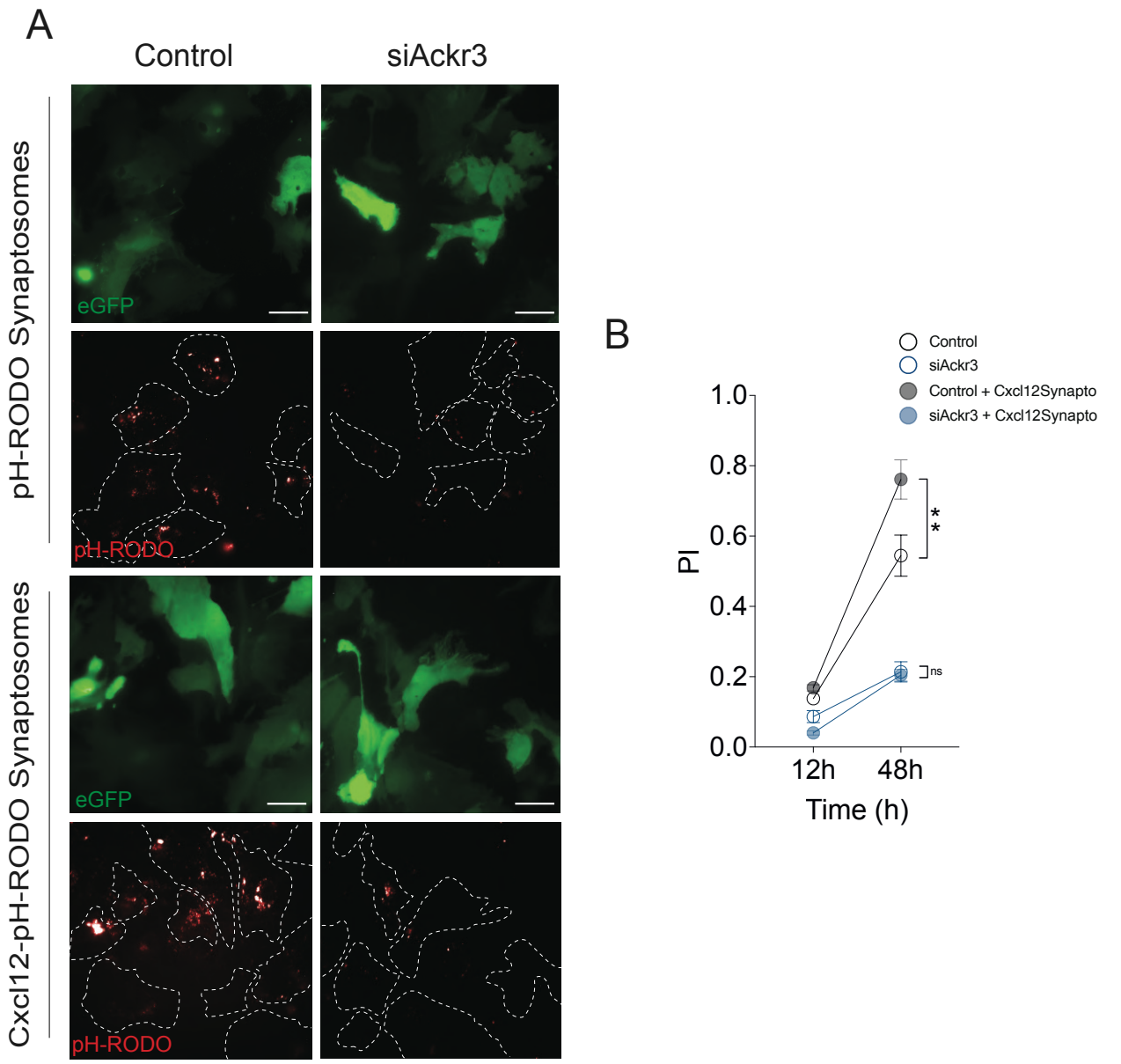

Figure 6.4.14 Cxcl12 increase synaptosomes engulfment. A. Representative fluorescence images of primary astrocytes transfected with Control, Ackr3 siRNA together with an eGFP-encoding plasmid at 48h upon Cxcl12-covered pH-RODO-synaptosomes and naïve pH-RODO Synaptosomes treatment. Scale bar 50 μm; **B.** Representative graph showing the PI of primary astrocytes transfected with Control, Ackr3 siRNA together with a GFP-encoding plasmid at 12h and 48h upon synaptosomes treatment. Thirty field per conditions were analyzed, quantification of PI was performed using Harmony Software. Statistical analysis was performed using Two-Way ANOVA with Tukey's multiple comparison test (significance **p<0.01), n=3 biological replicates.

6.4.5 Cxcl12 recognizes phosphatidylethanolamine at the plasma membrane

Pontejo and Murphy showed that chemokines display a high affinity binding for phosphatidylserine (PS) and for other anionic phospholipids (Pontejo et al., 2021). This characteristic is a general property of many but not all chemokines. Indeed, PS-binding has been tested for a group of 10 chemokines and not for Cxcl12. Of note, PS has been demonstrated as eat-me signal involved in synapses pruning (Faris et al., 2021).

We therefore hypothesized that Cxcl12 might bind phospholipids at the synaptosome surface. We conducted a simple screen using arrays containing 15 different phospholipids that compose biological membranes. Specifically, we incubate Pip Strips with recombinant Cxcl12 chemokines at 0.1µg/ml for 1h at room temperature. Notably, we revealed that Cxcl12 specifically recognizes phosphatidylethanolamine (PE) but not PS (Figure 5.4.15). PE is a lipid that together with PS increase its externalization into the outer leaflet of plasma membrane in the early phase of neuronal death (Faris et al., 2021). Although this data is still preliminary (n=1 independent experiment), it suggests that Cxcl12-PE interaction might be important for driving purified synaptic terminals elimination mediated by astrocytes and promoting their phagocytic activity.

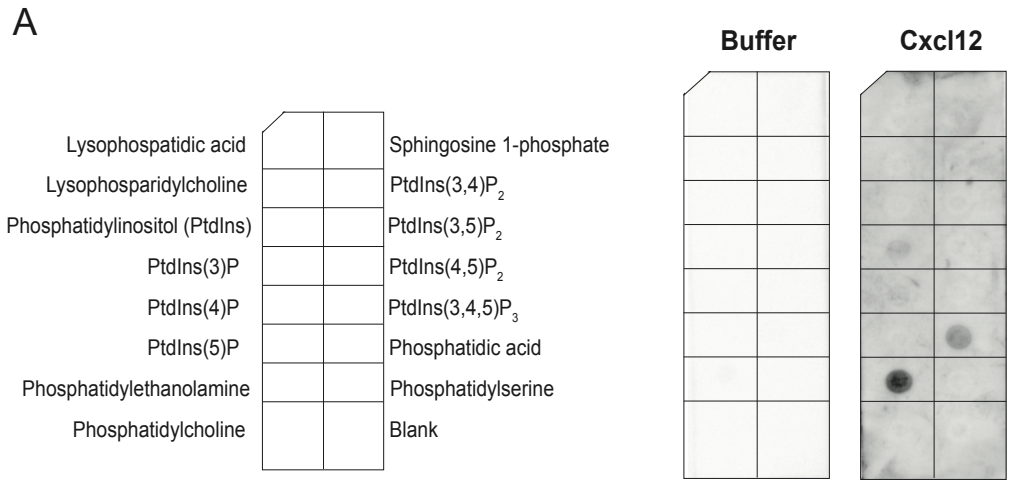

Figure 6.4.15. Cxcl12 interacts with PE. Arrays spotted with 15 different phospholipids (left panel) were incubated with buffer or 0.1µg/ml of recombinant Cxcl12. Bound chemokine was detected with specific antibody anti-Cxcl12.

6.5 Human astrocytic-ACKR3 impacts synaptosomes engulfment

To investigate the role of ACKR3 in a human background, we relied on human iPSC-derived astrocytes (iHAstrocytes), in collaboration with Fabio Cavaliere (Achucarro Basque Centre for Neuroscience). We first assessed the ability of human astrocytes to recognize and internalize (mouse) synaptosomes. To this purpose, we treated iHAstrocytes with 1μg/cm^2 of TAMRA-conjugated synaptosomes for 90 minutes. Astrocytes have been fixed and stained for endogenous Lamp1. As shown in Figure 6.5.1 A, human astrocytes efficiently internalized purified synaptic terminal.

After 48h from the pulse, astrocytes were fixed and stained for endogenous Ackr3 and Lamp1. We quantified the co-localization between endogenous Ackr3 and TAMRA-conjugated synaptosomes. As shown in Figure 6.5.1 B, the co-localization between Ackr3 and synaptosomes displays a mean r=0.55 compared to the control astrocytes. We then quantified the co-localization between Lamp1-positive vesicles and TAMRA-conjugated synaptosomes. Quantification shows a high co-localization, confirming that synaptosomes are efficiently internalized by iHastrocytes ($p<0.01$) (Figure 6.5.1 C). Then, to determine whether Ackr3 is directly involved in synaptosomes internalization and directed to the lysosomal compartment as in murine astrocytes, we quantified the co-localization between Ackr3 and Lamp1-positive vesicles. Interestingly, we observed that Ackr3-Lamp1 co-localize in basal condition with a mean r=0.3 and this co-localization increase after synaptosomal pulse ($p<0.01$) (Fig. 6.5.1 D). In accordance with our previous results obtained in murine astrocytes, endogenous human ACKR3 re-localizes into the Lamp1-positive vesicles together with the internalized synaptosomes, suggesting a pivotal role of this receptor in this astrocytic mechanism. Moreover, similarly to what we observed in murine astrocytes, Ackr3 is clustered in vesicular structures in the cytoplasm as well as along the cell perimeter and partially co-localizes with Lamp1 in control astrocytes.

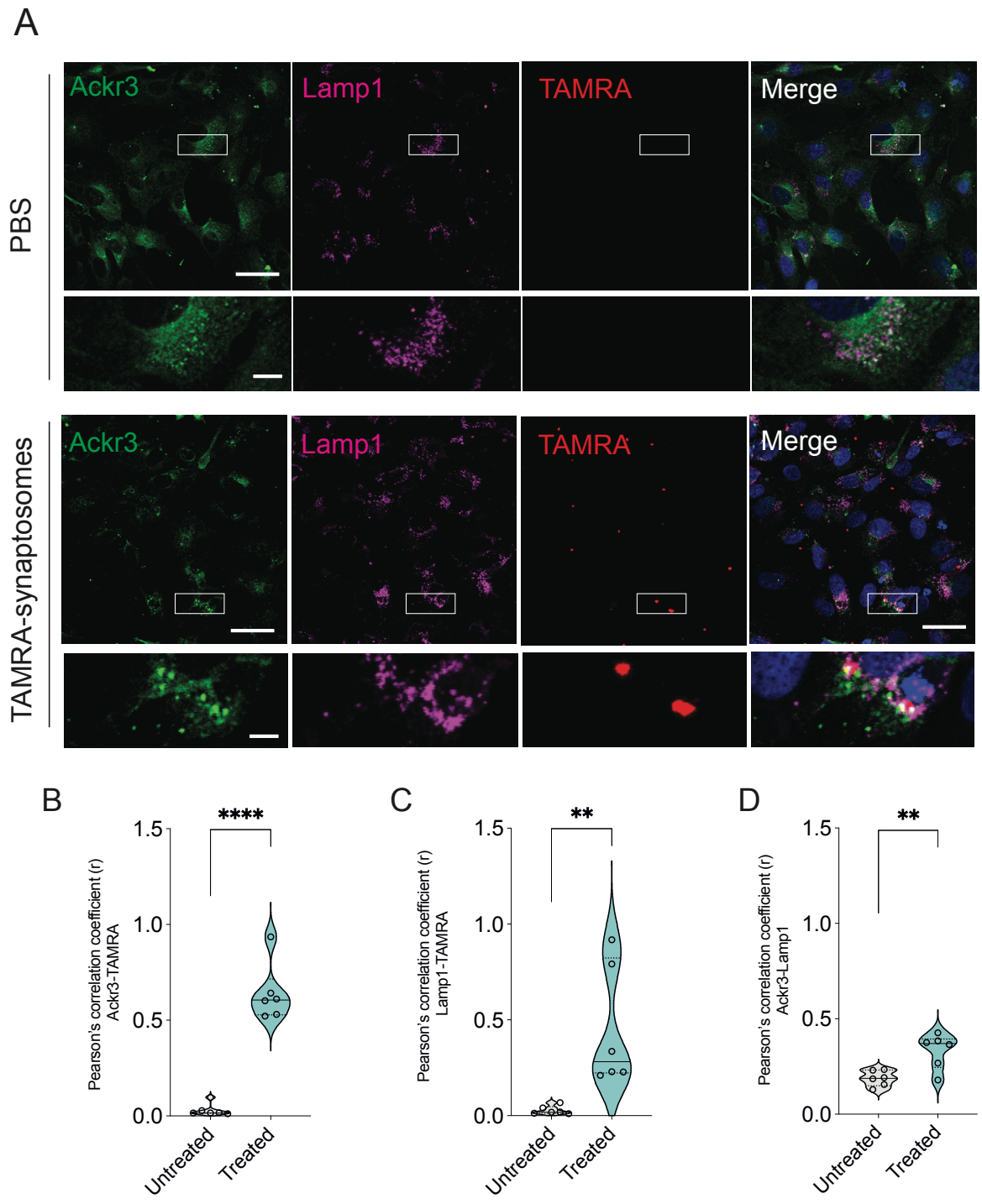

Figure 6.5.1 Human ACKR3 perfectly behaves as murine Ackr3. A. Representative z-stack confocal images of human mature astrocytes in basal or TAMRA-synaptosomes (red) treatment conditions. Cells were stained with anti-Ackr3 (green) and anti-Lamp1 (purple) antibodies. Insets show Ackr3, TAMRA and Lamp1-positve area and Ackr3 re-localization in Lamp1-positive area upon synaptosomes treatment. Scale bar 20 µm; insets 5 µm; **B.** Pearson's correlation coefficient of Ackr3 co-localizing with TAMRA-positive fluorescent spots (n=6 images for conditions); **C.** Pearson's correlation coefficient of TAMRA co-localizing with Lamp1-positive compartment (n=6 images for conditions); **D.** Pearson's correlation coefficient of Ackr3 co-localizing with Lamp1-positive compartment (n=6 images for

conditions); Statistical analysis was performed using Student's t-test (significance ***p<0.001; **p<0.01,), n=3 biological replicates.

Having validated the phagocytic ability of iHAstrocytes and the re-localization of Ackr3 upon synaptosomes treatment, we assessed the impact of Ackr3 depletion in synaptosomes internalization through a live imaging-assay. We firstly quantified the expression and the downregulation of the receptor in iHAstrocytes. To do so, iHAstrocytes were transfected with Smart Pool siRNA against Ackr3 at a final concentration of 50nM using Stem Cells Lipofectamine. After 72h upon transfection, cells were lysate and protein level were checked through western blot. Our western blot analysis revealed that the levels of endogenous Ackr3 is diminish up to 60% compared to control sample. Moreover, since we observe that iHastrocytes efficiently internalize synaptosomes, we validate the presence of Megf10 in this model. As show in Figure 6.5.2, we observed that Megf10 is expressed in human astrocytes and that the downregulation of Ackr3 does not impact on its expression.

Subsequently, iHAstrocytes were transfected with Ackr3 siRNA and with scramble siRNA as a control together with an eGFP-encoding plasmid. After 24h from the transfection, astrocytes were treated with 1μg/cm^2 of pH-RODO synaptosomes and then visualized at 12 and48 h using ApoTome2 microscopy. Then, the total area of eGFP-positive cells and pH-RODO positive puncta inside transfected cells were calculated manually using ImageJ. Briefly, we define the ROIs in the green channel around transfected cells, then, the same ROIs were transferred in the red channel and pH-RODO-positive puncta were identified using wand tool. Consistently with our hypothesis, the PI of astrocytes downregulated for Ackr3 is significantly lower compared to control astrocytes (Figure 6.5.3).

Together our results showed that human Ack3 is directly involved in purified neuronal terminals internalization and the lack of the receptor causes an impairment in synaptosomes engulfment.

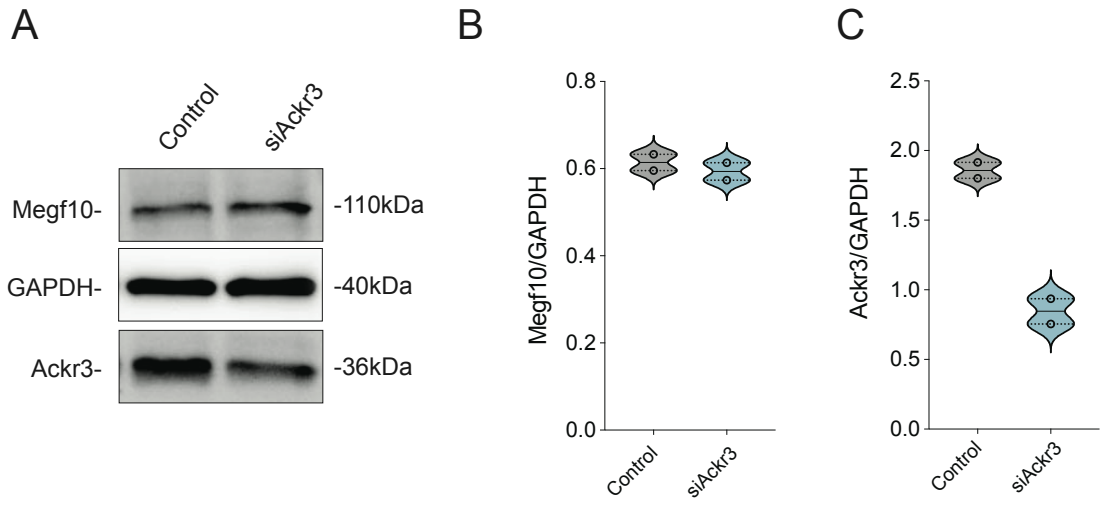

Figure 6.5.2 Biochemical evaluation of Ackr3 and Megf10 expression in human astrocytes A. Western blot analysis and relative quantification in **B.** of human mature astrocytes lysates transfected with Control and Ackr3 siRNA. Quantification of band intensity was performed using ImageJ and normalized by GAPDH. n=2 biological replicates.

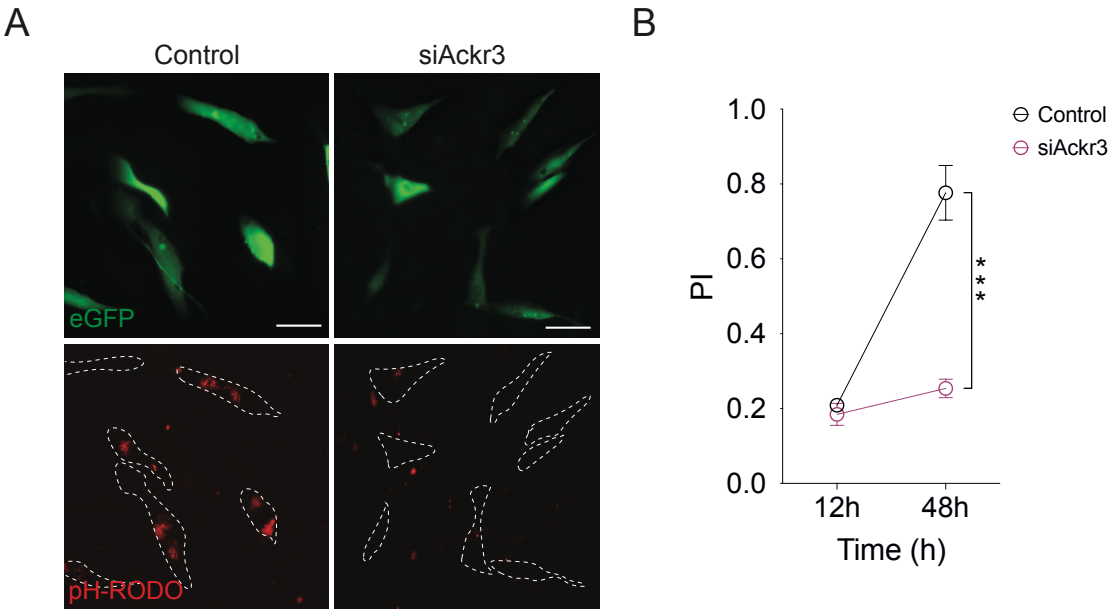

Figure 6.5.3 ACKR3 depletion decreases synaptosome internalization. A. Representative image of primary astrocytes transfected with Control and Ackr3 siRNA together with an eGFP-encoding plasmid at 48h upon synaptosome treatment. Scale bar 50 µm; **B.** Representative graph showing the PI of primary astrocytes transfected with Control and Ackr3 siRNA at 12h and 48h upon synaptosomes treatment. Ackr3 downregulation decreased the PI at all the time points. Fifty field per conditions were analyzed, quantification of PI was performed using ImageJ. Statistical analysis was performed using Two-Way ANOVA with Tukey's multiple comparison test (significance ***p<0.001), n=3 biological replicates.

Results PART II

7. Results PART II

The following section is published in Streubel-Gallasch et al., 2021.

7.1. G2019S Lrrk2 astrocytes display impaired exogenous α-syn handling

To study how LRRK2 affects exogenous fibrillar α-syn clearance in astrocytes in total absence of microglia, we examined the uptake and degradation capacities of cortical stem cell-derived astrocytes, in collaboration with Anna Erlandsson at the University of Uppsala (Sweden). We took advantage of two different genetic backgrounds: Lrrk2 knock out (-/-) mice, knock in Lrrk2-G2019S mice (GS/GS) and compare the results with wild- type (+/+) littermates as control. Astrocytes were exposed to 0.5 μM α-syn PFFs for 24 h, thoroughly rinsed and then processed for analysis or incubated for additional 6 days in α-syn-free medium. Our results show that intracellular Cy3 α-syn deposits localized around the nucleus of astrocytes. Moreover, we observed different types of Cy3 α-syn inclusions: small dot-like and larger, cottony deposits inclusions (Supplementary Figure 1 C-D-E). An ImageJ analysis macro was used to quantify area, number and integrated density of small and larger Cy3 α-syn deposits separately. Examining the small deposits, we observed that astrocytes carrying the G2019S pathological mutation displayed lower values of α-syn inclusions at 24h time point for all the parameters compared to wild-type. Moreover, we detected that Lrrk2 GS/GS astrocytes displayed lower Cy3 α-syn amounts compared to Lrrk2−/− in terms of particle count and integrated density. While we did not detect any differences for the area measurement (Supplementary Figure 2 A). On the other hand, the analysis of larger Cy3 α-syn inclusions did not reveal any statistically significant differences between the LRRK2 genotypes (Supplementary Figure 2 B). Next, we analyze the area, number and integrated density of Cy3 α-syn deposits at 24h + 6 days. As shown in Supplementary Figure 2, our quantification shows a statistically significant difference for the integrated density of small particles between Lrrk2 GS/GS and Lrrk2 −/− astrocytes. Considering the two time points, we observed that the integrated density increases 1.5 to 2-fold for both small and large Cy3 α-syn deposits. While the small particles number count shows a 1.2-fold increase only in the pathological background. These results suggest that astrocytes store rather than degrade protein aggregates, as already suggested in literature (Söllvander et al., 2016).

Overall, our data indicate that the amount of α-syn present inside Lrrk2GS/GS astrocytes is reduced compared to wild-type or Lrrk2−/− astrocytes. The effect is normalized over time,

suggesting that the pathogenic mutation influences the uptake rather than the degradation of α-syn.

7.2. G2019S striatal astrocytes show reduced engulfed α-syn *in vitro*

Astrocytes that populate the striatum are relevant to PD pathology since they are in close proximity to dopaminergic terminals of the SNpc. Moreover, it is unknown how striatal astrocytes respond to neuronal-released α-syn. Considering this and on our previous results, we investigated how Lrrk2 impacts on uptake and degradation of exogenous α-syn in primary striatal astrocytes.

As already discussed, we routinely isolate primary striatal astrocytes, and the culture purity is assessed by immunofluorescence as published in (Streubel-Gallasch et al., 2021). To quantify the effects of LRRK2 on α-syn PFFs clearance in primary astrocytes, we conjugated monomeric α-syn with a pH-sensitive dye named SNARF-1 followed by fibrillization and sonication. SNARF is particularly suitable to sense pH that ranges between 6 and 9 (Supplementary Figure 3) allowing us to monitor α-syn PFFs trafficking through the endo-lysosomal pathway. As shown by EM analysis, SNARF conjugation did not affect α-syn PFFs aggregation process (Figure 7.2 A). Relevant to the experimental set-up, we ruled out that the chemico-physical properties of the dye are changed upon conjugation and fibrillation process (Supplementary Figure 3). Indeed, the inflection point of free and conjugated SNARF curves are 7.826 (R = 0.9956) and 7.606 (R = 0.9918), respectively (Supplementary Figure 3). Astrocytes were treated with 0.5 μM SNARF-labeled α-syn PFFs and imaged after 24 h using live confocal microscopy at the two relevant emission ranges (Figure 7.2 B-C). As shown in Figure 7.1 D the three genotypes display a similar cumulative distribution of the 550/630 ratio at the single-particle level. Therefore, in the three genotypes, SNARF-labeled α-syn PFFs are distributed in overlapping organelle environments, excluding the possibility that LRRK2 can interfere with the flux of extracellular α-syn once internalized as well as with the global pH of the organelles. In agreement with previous data, the total particle number (Figure 7.2 D) and the number of particles per ROI were significantly reduced in the GS astrocytes (Figure 7.2 E).

Taken together, these results further support the idea that the G2019S pathological mutation in Lrrk2 modifies the ability of striatal astrocytes to accumulate exogenous α-syn, although it does not affect the distribution of engulfed α-syn.

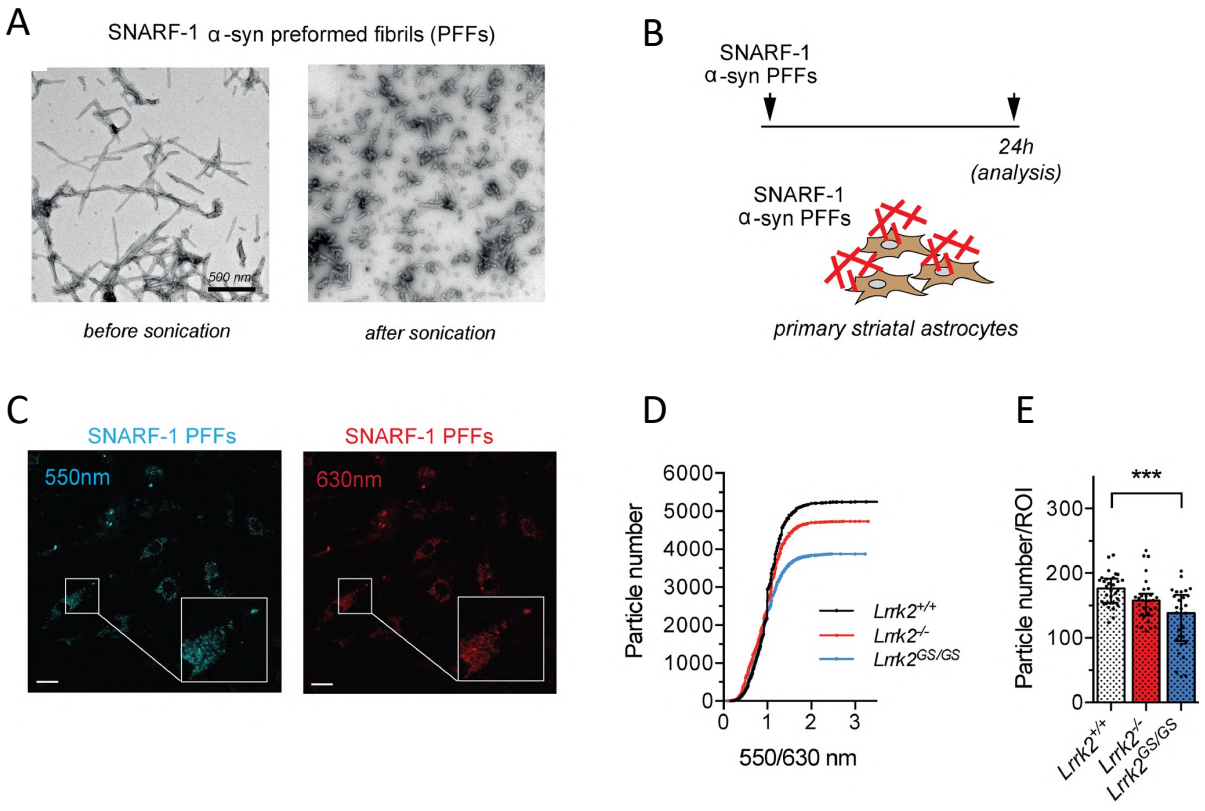

Figure 7.2 Internalization of aggregated α-syn in striatal astrocytes A. EM images of SNARF-1 α-syn PFFs pre- and post-sonication; **B.** Schematic outline of the experimental setup. Cells were exposed to 0.5 μM sonicated SNARF-1 α-syn PFFs for 24 h and imaged using live confocal laser scanning microscopy. **C** Representative images of primary Lrrk2 WT striatal astrocytes treated with SNARF-1 α-syn PFFs were acquired at 530–550 and 610–630 nm. Scale bar 50 μm; **D, E.** Eight images per cell culture were analyzed. For each image, ROIs were traced and quantification of α-syn single-particle 550/630 ratio (IntDen) and of particle number were performed using ImageJ. The cumulative distribution of the single-particle ratio; **D.** and particle number per ROI; **E.** were graphed for each genotype**.** Statistical analysis in **E** was performed using Kruskal-Wallis test followed by Dunn's multiple comparisons test. ***$p \leq 0.001$, n = 4 biological replicates.

7.3. Lrrk2 impacts on the endo-lysosomal morphology and functionality in striatal astrocytes

Considering that the pathogenic mutation in Lrrk2 GS astrocytes impairs their ability to store aggregated α-syn, we next investigated how it can affect the morphology and functionality of the endo-lysosomal pathway.

First, we studied whether Lrrk2 has an impact on the number and dimension of endo-lysosomal structures in mouse striatal astrocytes. Cultured primary striatal astrocytes were imaged by EM and the number and area of lysosomal-like structures were measured using ImageJ (Figure 7.3 A). As shown in Figure 7.3 B-C both Lrrk2 ablation and the G2019S pathological mutation caused a significant decrease in the number of lysosomal-like structures in astrocytic cells. In line with this, EM images on the intact striatum show the same trend (Supplementary Image 4). Moreover, the absence of Lrrk2 showed enlarged structures, compared to control astrocytes and to GS astrocytes (Figure 7.3 C). In addition, we evaluated the overall volume occupied by lysosomal structures calculated as lysosomal number × mean lysosome volume. Interestingly, we noticed a similar lysosomal volume in Lrrk2-/- and Lrrk2 +/+ astrocytes, which is respectively 1.7 $\mu m^3/mm^2$ and 2.0 $\mu m^3/mm^2$. However, Lrrk2 GS/GS astrocytes showed half of the lysosomal global volume (1.0 $\mu m^3/mm^2$) compared to the other two genotypes. To confirm our data, we analyzed the astrocytic endo-lysosomal compartment by immunofluorescence using Lamp2A as a marker of late endosomes/lysosomes. We revealed a significant reduction of the organelle number in KO and GS astrocytes, associated with organelle enlargement in the KO cells, confirming our previous results (Figure 7.3 D-E-F).

Next, we investigated whether lysosomal morphology is associated with a change in lysosomal pH. We labelled primary astrocytes from the three genetic backgrounds with the ratiometric probe RatioWork PDMPO (for further details see Materials & Methods Section 6.27). RatioWork PDMPO labels acidic organelles and is independent from the endo-lysosomal content. Astrocytes were cultured in 96-well plates and exposed to 0.5μM of α-syn PFFs. After 24h from the PFFs treatment, cells were treated with RatioWork PDMPO at a final concentration of 2μM for 5 min. We also used astrocytes treated with Bafilomycin, a well-known inhibitor of autophagy, as a control. As shown in Figure 7.3 G quantification does not underline any differences between the three genotypes in the absence or in the presence of α-syn PFFs. Instead, Bafilomycin, which dissipates endo-lysosomal pH, causes a significant increase of the fluorescence ratio in all the conditions tested.

Based on the previous results, indicating that GS astrocytes display impaired lysosomal-like structures, we wondered whether the pathological mutation could impact on the activation of the endo-lysosomal pathway. We performed the neutral red assay; neutral red is a non-ratiometric dye that is specifically retained by acidic vesicles, and it is frequently used as a reliable indicator of phagocytic activity (Repetto et al., 2008). We compared α-syn PFFs-treated striatal astrocytes, untreated astrocytes and astrocytes treated with Bafilomycin as a control. As expected, Bafilomycin treatment markedly decreases neutral red accumulation in all experimental conditions (Figure 7.3 G). As shown in Figure 7.3 H, we did not report any statistical difference between the three genotypes in the absence of α-syn PFFs. Instead, treatment with α-syn PFFs induced an increase of neutral red staining in astrocytes compared to untreated astrocytes. However, the difference between basal condition and upon PFFs treatment was not statistically significant in Lrrk2 GS/GS astrocytes, indicating that phagocytosis occurs efficiently in Lrrk2-/- and Lrrk2 +/+astrocytes but not in Lrrk2 GS/GS astrocytes.

Collectively, these results suggest that the G2019S mutation influences the morphology and number of endo-lysosomal vesicles but not their pH. However, the overall lysosomal degradation capacity appeared to be reduced in the presence of the G2019S pathological mutation.

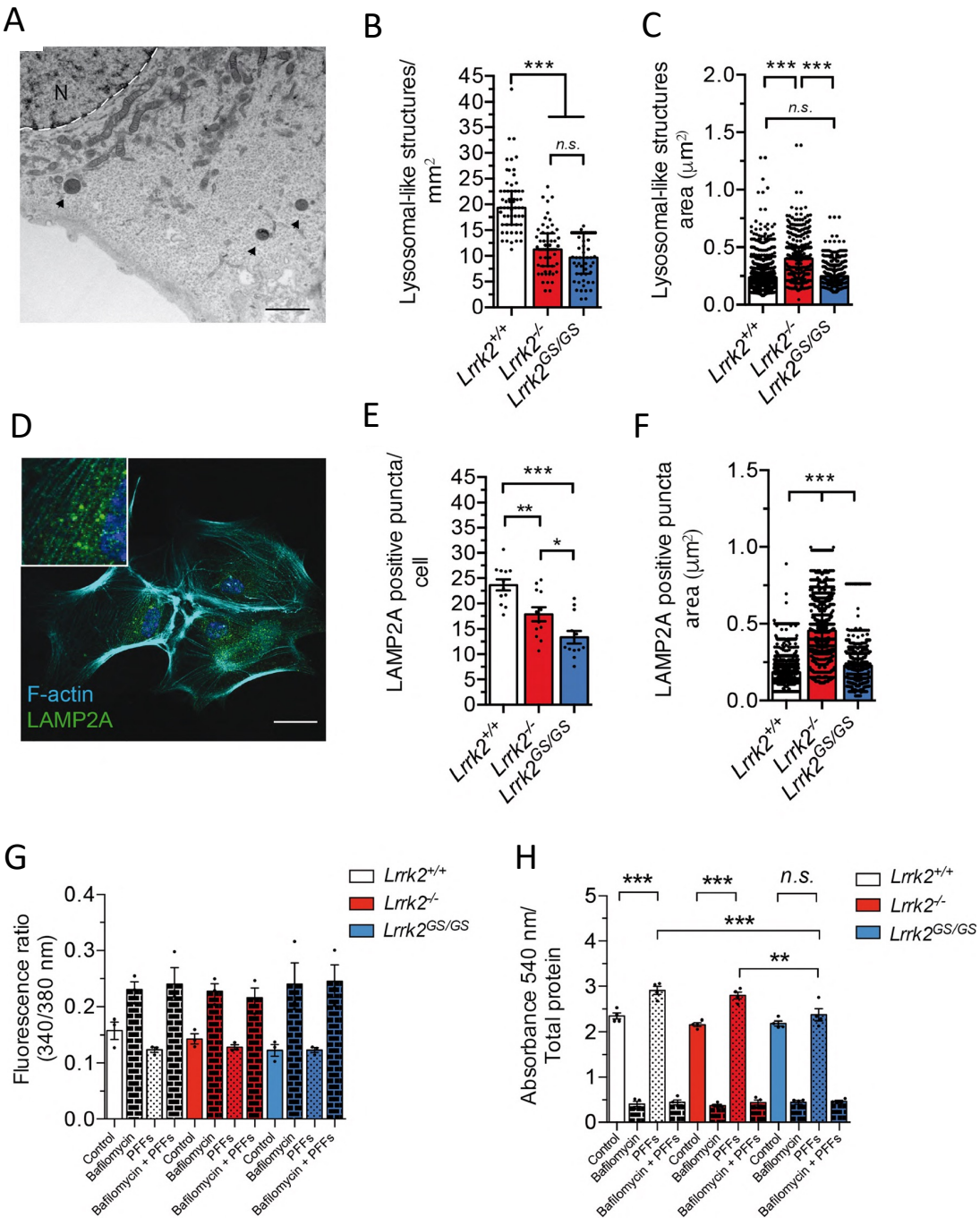

Figure 7.3 Description of the endo-lysosomal pathway in Lrrk2 striatal astrocytes. A. Representative EM image of primary striatal astrocyte section containing electron-dense lysosomal-like structures (arrows). Scale bar 2 µm; **B, C**. Forty EM images were acquired (n= 4 per genotype). Each cell was imaged by covering the entire cytoplasm and lysosomal-like structure number and area was measured using ImageJ; **D.** Representative image of the staining using Lamp2A (green) as a marker for the endo-lysosomal pathway, DAPI (blue) for the nuclei, and F-actin (cyano) to define cells. Scale bar 20 µm. Inset shows a close-up of Lamp2A-positive structures; **E, F.** Quantifications of Lamp2A-positive structure number and area were performed using ImageJ. Four images per cell culture were analyzed (n = 3 per genotype); **G.** Measurement of lysosomal pH was done in primary striatal astrocytes from the

three genotypes upon unlabeled α-syn PPF treatment (n = 3 per genotype). Bafilomycin has been applied as negative control. Fluorescence ratio of light acquired at 535 nm upon excitation at 340 and 380 nm is provided; **H.** Neutral red assay was performed in primary striatal astrocytes from the three genotypes upon unlabeled α-syn PPF treatment (n = 4 per genotype). Bafilomycin has been applied as negative control. Absorbance at 540 nm measured upon cell lysates was normalized by total protein content. Statistical analyses in **B, C**, and **F.** were performed with Kruskal-Wallis test followed by Dunn's multiple comparisons test. Statistical analyses in **E, G,** and **H.** were performed with one-way ANOVA followed by Tukey's multiple comparisons test. *p ≤ 0.05, **p ≤ 0.01, ***p ≤ 0.001

7.4. LRRK2 interacts with ANXA2

We next used an unbiased approach to identify LRRK2-specific effectors of astrocyte-mediated α-Syn PFFs clearance. Specifically, we performed a high-throughput screening of candidate protein-protein interaction (PPI) partners via affinity purification (AP) coupled with tandem mass spectrometry. We analyzed LRRK2-immunoprecipitated binders by LC-MS. Cells obtained from a human astroglial cell line (H4 cells) were transiently transfected with Flag-tagged LRRK2. 0.5uM of α-syn PFFs or an equal volume of vehicle (PBS) (unstimulated) has been applied to H4 cells for 24h. After lysis, samples were incubated with the appropriate amount of anti-Flag agarose beads resin overnight to perform the immunoprecipitation. Samples were then eluted from the resin to exclude contaminants with high affinity for the resin. Eluates were loaded onto SDS-PAGE and subsequently analyzed via LC-MS (in collaboration with Prof Giorgio Arrigoni, Department of Biomedical Sciences, University of Padova). We performed two independent rounds of experiments and crosschecked our data manually. We first cleaned the list of interactors by removing contaminants represented by common environmental keratins or undesirable sticky peptides that we found both in PFFs treated and untreated cells (Figure 7.4 A-B). As show in Figure 7.4 C, we identified a list of proteins reported as the ratio of the amount detected, *i.e.* peptide area, in treated versus non-treated conditions and then normalized by the immunoprecipitated LRRK2 level. Specifically, scores >1 indicate an increased interaction with LRRK2 upon treatment whereas scores <1 indicate a decreased affinity with LRRK2 in treated cells. The value was normalized by the peak area of immunoprecipitated LRRK2 in the two experimental conditions (Figure 7.4 C). To select possible players in LRRK2-mediated α-syn PFFs clearance, we followed three main criteria: (i) hits that are recruited selectively by LRRK2 upon treatment, (ii) functional relevance, and (iii) expression in glial cells. Among the top hits, we observed a large variety of proteins known as

main components of epidermal desmosomes and linked to cytoskeleton. Since the functional significance of desmosomes in brain astrocytes are not well recognized and are not related to any NDs, we decided to not consider this group of hits.

Of note, annexin A2 (human ANXA2) displayed increased affinity for LRRK2 upon α-syn PFFs treatment. ANXA2 is a Ca^{2+} regulated phospholipid-binding protein and it is implicated in the dynamic organization of membrane microdomains and the formation of membrane-cytoskeleton and membrane-membrane contacts (Gabel et al., 2020; Zhang et al., 2020). Intriguingly, ANXA2 intervenes in phagocytic processes at multiple levels (Stukes et al., 2016). Indeed, upon stimulation of phagocytic processes, ANXA2 is recruited to endosomal membranes where it has been proposed to stabilize the organelle (Yim W. W. et al., 2022). Moreover, ANXA2 deficits are linked to a decreased endocytosis and particle internalization (Stukes et al., 2016). Of note, ANXA2 interacts with the AD-linked protein, Presenilin 1 (PS1), and intervenes in PS1 degradation by directing and facilitating autophagosome-lysosome fusion (Bustos et al., 2017; Bustos et al., 2021) Importantly, ANXA2 is almost exclusively expressed in glial cells in the brain (Zhang et al., 2016).

We first validated the role of ANXA2 in regulating exogenous PFFs α-syn internalization. To this purpose, H4 astrocytic cells were transiently transfected with GFP-tagged ANXA2. Cells were treated with α-syn PFFs and fixed after 24h from the pulse. As shown in Supplementary Figure 5, GFP-ANXA2 shows a diffuse cytoplasmic distribution in cells, and it re-localizes around α-syn exogenous fibrils upon internalization.

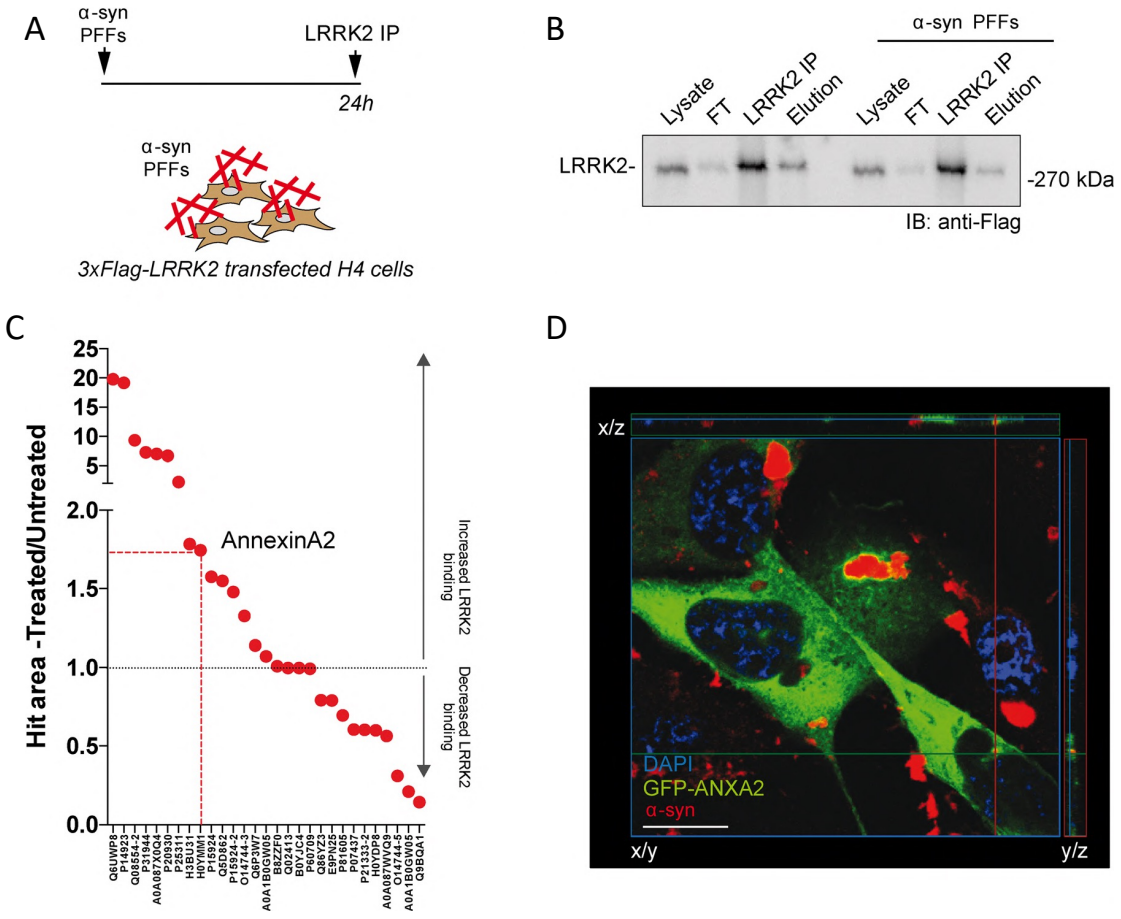

Figure 7.4 Characterization of LRRK2 interactoma in stimulated condition. A. Schematic outline of the experimental setup. H4 cells were transfected using 3xFlag-LRRK2 encoding plasmid and, after 48 h post transfection, cells were treated with 0.5 μM sonicated unlabeled α-syn PFFs for 24 h. LRRK2 was subsequently immunopurified using anti-Flag agarose beads (IP); **B.** Western blot analysis showing LRRK2 expression (lysate), immunopurification (LRRK2 IP), and Elution in H4 cells in treated and basal conditions and unbound LRRK2 (FT); **C.** Relative quantification of LRRK2 interactome under treated and untreated conditions. The area of the precursor ions identified by LC-MS/MS analysis was used as a quantitative measure of the protein content. The ratio between the area of the precursor ions of untreated and treated samples (normalized by the content of LRRK2) was then considered to highlight proteins showing a different affinity for LRRK2 in the two conditions (n = 2 biological replicate); **D.** H4 cells transfected with GFP- ANXA2 in α-syn PFFs-treated condition show the proximity of internalized α-syn fibrils and AnxA2. AnxA2-GFP (green), α-syn (red), DAPI (blue). Scale bar 30 μm.

7.5. Anxa2 affects murine astrocytes-mediated α-Syn clearance

The results we obtained from the MS analysis and in H4 cells support a role for ANXA2 in a-syn clearance. To gain more insights into the involvement of Anxa2 in these processes and to confirm its role in mouse astrocytes, we applied a siRNA approach.

Firstly, we checked the localization of endogenous mouse astrocytic AnxA2 through immunofluorescence analysis. To do so, astrocytes were treated with α-syn PFFs for 24h and then stained for endogenous Anxa2. As shown in Figure 7.5 A, Anxa2 localizes into subcellular puncta in the near proximity of internalized PFFs particles, suggesting an involvement of this protein in this mechanism. Next, we transfected primary astrocytes with a siRNA against Anxa2 or with a non-targeting siRNA as a control. After 72h from the transfection around 60% of AnxA2 downregulation was achieved compared to controls astrocytes (Figure 7.5 E). Of note, AnxA2 downregulation did not significantly affect LRRK2 protein levels in transfected astrocytes.

To establish the involvement of endogenous AnxA2 in astrocyte-mediated phagocytic clearance, we treated Anxa2-downregulated astrocytes with α-syn PFFs and imaged them after 24h (Figure 7.5 A). As discussed in the first part of this dissertation, to image siRNA recipient cells we co-transfected primary striatal astrocytes with AnxA2 siRNA and a GFP-encoding plasmid. As represented in Figure 7.5 C-D, we acquired images after 24h of PFFs treatment and we quantified α-syn-positive puncta using an ImageJ plug in. Quantification of internalized α-syn-positive puncta in GFP-positive cells revealed that AnxA2 down-regulation decreases the amount of intracellular α-syn PFFs deposits per cell compared to scramble transfected controls (Figure 7.5 D). Moreover, as an additional control for AnxA2 downregulation at single-cell resolution, we stained transfected GFP-positive astrocytes for the endogenous protein. Consistently with our previous results, the quantification shows a significantly decrease of AnxA2 puncta upon PFFs treatment in AnxA2 siRNA-astrocytes versus control (Supplementary Figure 6). To validate our findings, we also evaluated intracellular α-syn PFFs by western blot analysis upon AnxA2 downregulation (Figure 7.5 E-H). Again, AnxA2 downregulation was successfully achieved after PFFs treatment. A slight but significant decrease of AnxA2 was also revealed upon PFFs exposure in astrocytes treated with the scramble siRNA. However, our results showed that the amount of accumulated α-syn significantly decreased by comparing lysates obtained from AnxA2-downregulated astrocytes versus control.

Overall, our results confirmed that AnxA2 deficits influence the astrocytic ability to store α-syn aggregates, pointing to this protein a possible modulator of astrocytes-mediated PFFs engulfment.

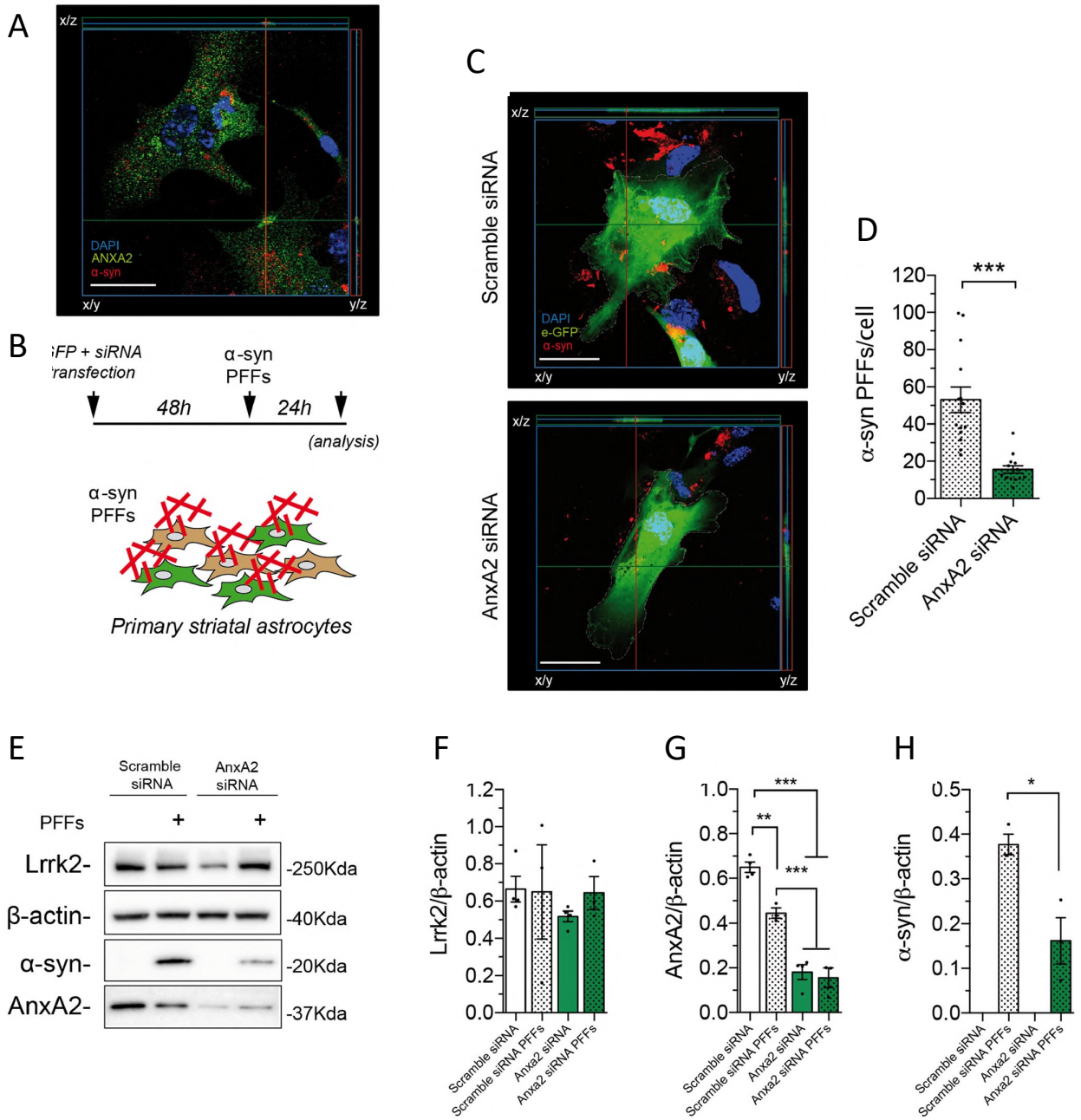

Figure 7.5 Investigation of AnxA2 function in astrocyte-mediated α-syn phagocytic clearance A. Unlabeled α-syn PFFs have been applied to primary astrocytes for 24 h. Projections verify the proximity of the internalized α-syn fibrils and endogenous AnxA2. Cell cytoskeleton (F-actin, cyano), α-syn (red), AnxA2 (green), DAPI (blue). Scale bar 20 μm; **B.** Schematic outline of the experimental setup. Cells were transfected using 3xFlag-GFP-encoding plasmid together with scramble or AnxA2 siRNA. 48 h post

transfection cells were treated with 0.5μM sonicated α-syn PFFs for 24 h and imaged using confocal microscopy; **C.** Representative images of primary striatal astrocytes transfected with scramble or Anxa2 siRNA together with a GFP-encoding plasmid in α-syn PFFs-treated condition. Projections verify the proximity of the internalized α-syn fibrils; GFP (green), α-syn (red), DAPI (blue). Scale bar 30μm; **D.** Four images per cell culture were analyzed. Quantifications of α-syn PFFs fluorescent-positive puncta were performed using ImageJ (ComDet plug-in). Statistical analysis was made by Kruskal-Wallis test followed by Dunn's multiple comparisons test. n=3 biological replicates; **E.** Western blot analysis of primary striatal astrocyte lysates transfected with scramble and AnxA2 siRNA under basal and PFFs-treated conditions. Anti-Lrrk2, anti-α-syn, and anti-AnxA2 antibodies have been employed. Quantification of band intensity shown in **E** was performed using ImageJ and normalized by β-actin. Statistical analysis in **F, G,** and **H.** was performed with an unpaired t-test or one-way ANOVA followed by Tukey's multiple comparisons test. (significance *$p \leq 0.05$, **$p \leq 0.01$, ***$p \leq 0.001$) n=3 biological replicates.

7.6. G2019S Lrrk2 striatal astrocytes display AnxA2 deficits

To determine whether Lrrk2 affects α-syn PFFs clearance through AnxA2, we measured AnxA2 protein content in primary astrocytes in basal conditions and upon α-syn PFFs treatment. In light of the results described, we decided to compare Lrrk2 GS/GS and Lrrk2 +/+ genotypes. Cell lysates from cultured striatal astrocytes were analyzed by western blot and AnxA2 endogenous expression was assayed. As shown in Figure 7.6 A-D, AnxA2 level is significantly decreased in Lrrk2 GS/GS astrocytes both under basal conditions and upon α-syn PFFs treatment compared to Lrrk2 +/+ astrocytes. Moreover, in agreement with what described earlier, AnxA2 downregulation in GS astrocytes is associated with a significant decrease in intracellular α-syn deposits compared to Lrrk2 +/+ astrocytes. We then evaluated AnxA2 localization and quantified ANXA2 fluorescent puncta in control and α-syn PFFs–exposed astrocytes in both genotypes. Primary striatal astrocytes were treated with 0.5 μM of α-syn PFFs for 24h, fixed and stained for endogenous AnxA2 (Figure 7.6 E). Interestingly, as already reported in literature (Negro et al., 2018) and as we have shown here for H4 astrocytic cells Supplementary Figure 5, AnxA2 is homogenously distributed within the cytoplasm under basal conditions but accumulates into discrete puncta upon α-syn PFFs treatment. Our results show that ANXA2 re-localization takes place in both Lrrk2 +/+ and Lrrk2 GS/GS astrocytes upon PFFs internalization, but it appears significantly decreased in cells harboring the pathogenic mutation (Figure 7.6 F-G). To assess whether this is due to the enhanced kinase activity of G2019S LRRK2, we treated Lrrk2 GS/GS primary astrocytes with MLi-2, a highly

specific and selective LRRK2 inhibitor (Fell et al., 2015). After 90 min of MLi-2 treatment, astrocytes were exposed to α-syn PFFs for 24h. As shown in Figure 7.6 F-G, statistical significance is also detected between GS primary astrocytes treated with PFFs in the presence and in the absence of MLi-2. We then quantified α-syn deposits associated with ANXA2 puncta within each cell by measuring particle proximity using ImageJ. We observed less α-syn intracellular inclusions in close proximity to ANXA2 in GS striatal astrocytes compared to controls astrocytes (Figure 7.6 F-G). Interestingly, the addition of MLi-2 inhibitor in astrocytes harboring the pathological mutation reverts the observed phenotype.

Finally, to investigate the relevance of these findings in PD pathology, we examined the expression of the ANXA2 in the basal ganglia of LRRK2 G2019S and idiopathic (iPD) PD patients and compared to age-matched healthy controls by western blot. Our data revealed that the level of ANXA2 is decreased in LRRK2 G2019S patients compared to healthy control and iPD patients (Figure 7.6.1). Although just preliminary, this observation points that ANXA2 deficiency in LRRK2-linked patients might have a role in α-syn clearance and it might exacerbate the progression of the pathology.

Overall, our results show that the ANXA2 level is diminished in murine astrocytes harboring the G2019S mutation and this phenomenon is associated with fewer intracellular α-syn deposits. Importantly, pharmacological inhibition of Lrrk2 kinase activity fully reverts the mutant phenotype. Moreover, our results indicate that pathogenic G2019S mutation interferes with the physiology of ANXA2, pointing astrocytic LRRK2 as an important target in PD.

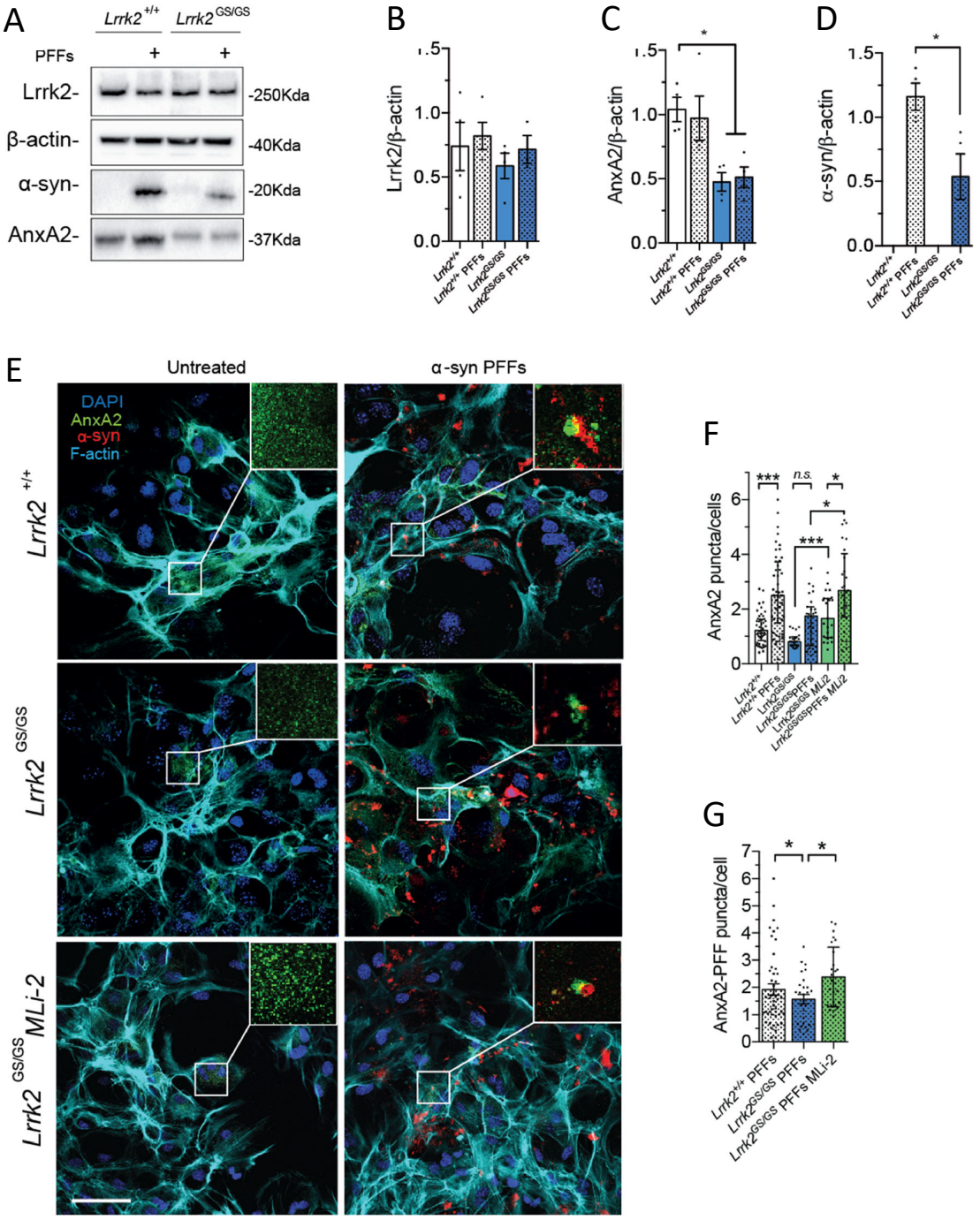

Figure 7.6 Analysis of AnxA2 function in G2019S primary striatal astrocytes at endogenous level. **A.** Western blot analysis of primary striatal astrocyte lysates under PFFs-treated and basal conditions using anti-Lrrk2, anti-α-syn, and anti-AnxA2 antibodies; **B, C, D.** Quantification of band intensity was performed using ImageJ and normalized by β-actin. Statistical analysis in **B, C** and **D.** was performed with unpaired t-test or one-way ANOVA followed by Tukey's multiple comparisons test. *p ≤ 0.05, **p ≤ 0.01, ***p ≤ 0.001; **E.** Representative images of Lrrk2 WT and Lrrk2 GS astrocytes treated or not with α-syn PFFs and stained with anti-AnxA2 (green), anti-α-syn (red), F-actin (cyano), and cell nuclei with

DAPI (blue). MLi-2-treated Lrrk2 GS astrocytes are shown in the bottom panels. Scale bar 20 µm. n=4 biological replicates. Insets show a close-up of α-syn inclusions and re-localized AnxA2. **F, G.** Eight images per cell culture were analyzed. Quantifications of Anxa2 puncta and AnxA2-α-syn PFFs proximity were performed using ImageJ. Statistical analysis in **F** and **G.** was made by Kruskal-Wallis test followed by Dunn's multiple comparisons test. n=3 biological replicates.

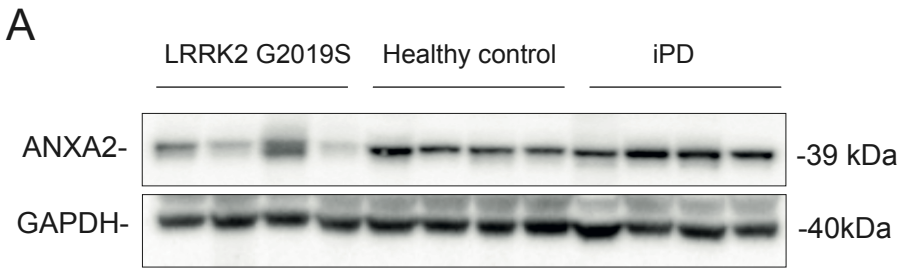

Figure 7.6.1 Anxa2 expression in PD patients A Western blot analysis of human caudate and putamen lysates of LRRK2 G2019S, iPD and healthy controls using anti-Anxa2, anti-GAPDH; n=4 age-matched healthy control, n=4 iPD, n=4 LRRK2 G2019S caudate and putamen samples.

SUPPLEMENTARY FIGURE 1

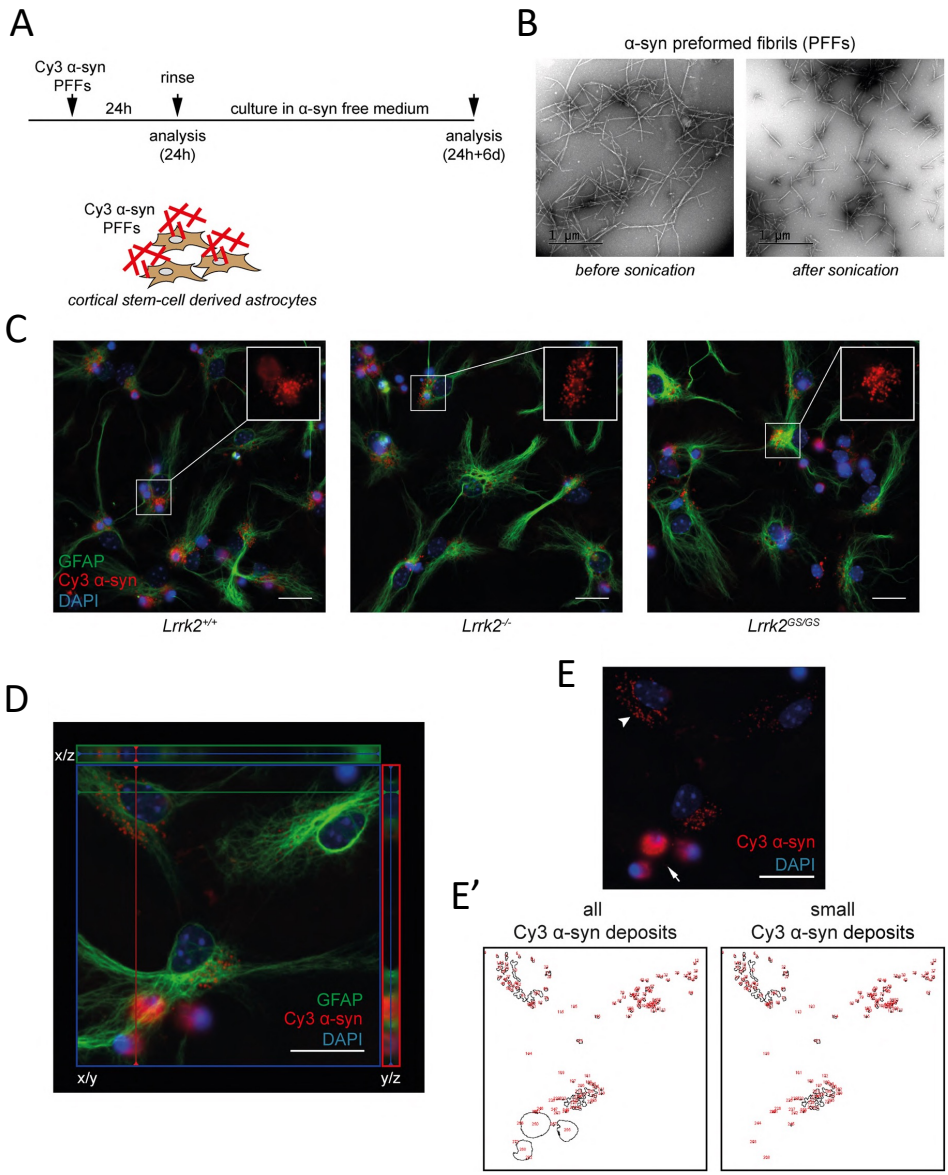

Supplementary figure 1 Accumulation of aggregated α-syn in Lrrk2 astrocytes A. Schematic outline of the experimental setup. Cells were exposed to 0.5µM sonicated Cy3 α-syn PFFs for 24h; **B.** EM images of α-syn PFFs pre- and post-sonication. Scale bars 1µm; **C** Representative fluorescence microscopy images of Lrrk2 WT, Lrrk2 KO, and Lrrk2 GS astrocytes (GFAP, green) at 24h; cell nuclei stained with DAPI (blue) and α- syn labeled with Cy3 (red). Insets show a close-up of Cy3 α-syn inclusions; **D.** Orthogonal projections of z-stack images taken with a fluorescence microscope: main view (x/y), top (x/z), and right (y/z). Projections were made along the lines depicted in the main image. Astrocytes (GFAP, green), Cy3 labeled α-syn (red), DAPI (blue); **E.** Fluorescence microscopy image showing the differently sized Cy3 α- syn inclusions observed: small dot-like inclusions (arrowhead) and larger, cottony deposits (arrow); **E'.** Display of the particle count obtained from the ImageJ analysis when including either all Cy3 α-syn deposits or only the small Cy3 α-syn inclusions. Scale bars = 20 µm (**C, D**, and **E**)

SUPPLEMENTARY FIGURE 2

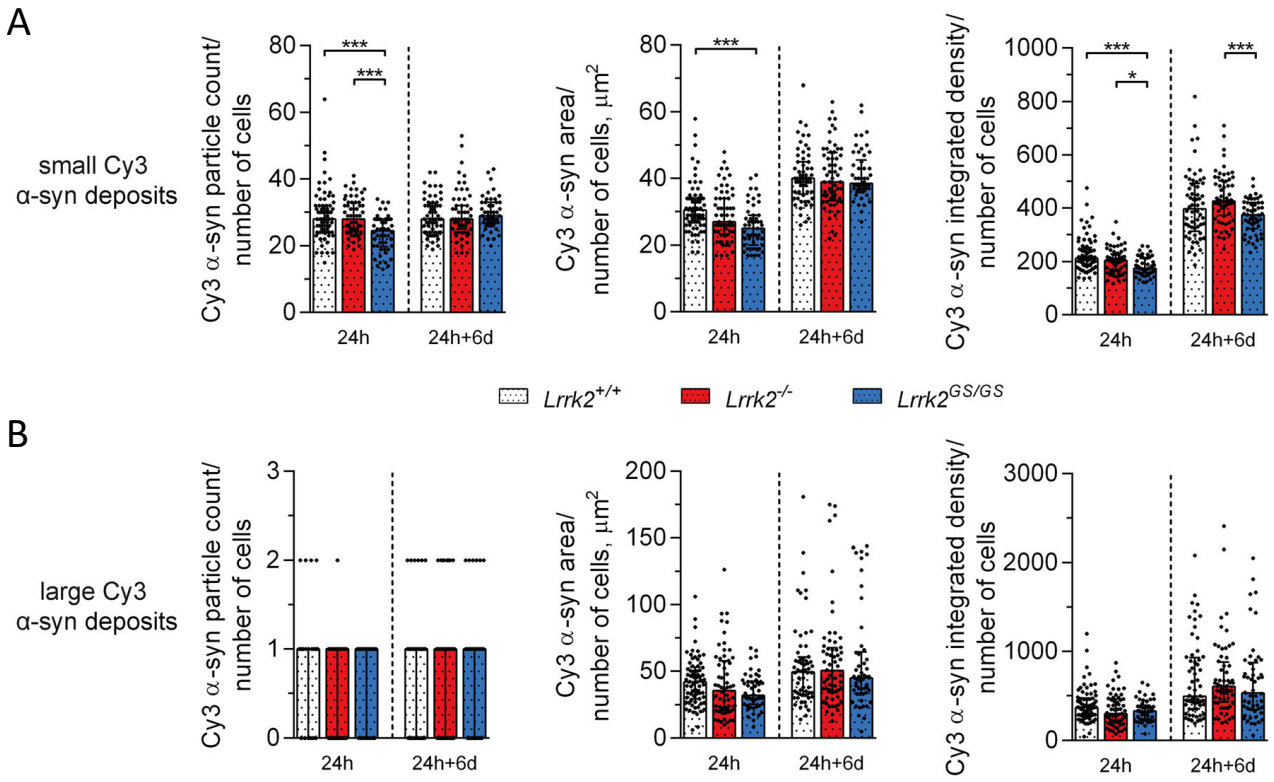

Supplementary Figure 2 Analysis of the differently sized α-syn inclusions in Lrrk2 astrocytes. A, B. Analysis of small and large Cy3 α-syn inclusions, respectively. Quantifications of Cy3 α-syn particle count, total area, and integrated density were performed using ImageJ. For both time points, ten images per independent cell culture (24 h: Lrrk2 +/+, n = 7; Lrrk2 -/-, n = 6; and Lrrk2 GS/GS, n=5;24h+6d:Lrrk2 +/+, n=6;Lrrk2 -/-,n=6;and Lrrk2 GS/GS, n = 5) were analyzed and reported. For each time point, the statistical analysis was performed with the Kruskal-Wallis test followed by Dunn's multiple comparisons test, since the data did not follow Gaussian distribution for all groups. *p ≤ 0.05, **p ≤ 0.01, ***p ≤ 0.001

SUPPLEMENTARY FIGURE 3

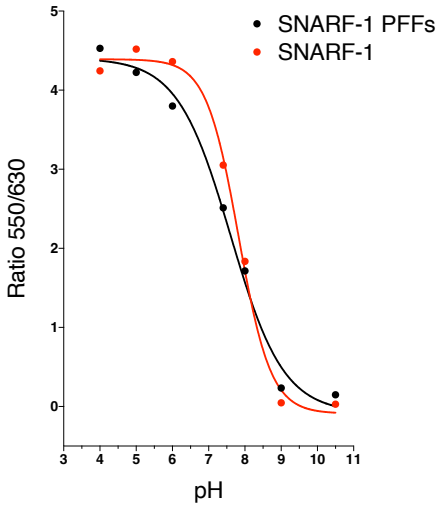

Supplementary Figure 3 SNARF-1 calibration Free SNARF and sonicated SNARF-labeled α-syn PFFs were resuspended using buffers at different pH and the emission spectra were acquired within 520-660 nm range upon laser excitation at 488 nm using a fluorimeter device. The value ratio 550/630 nm is reported in the graph.

SUPPLEMENTARY FIGURE 4

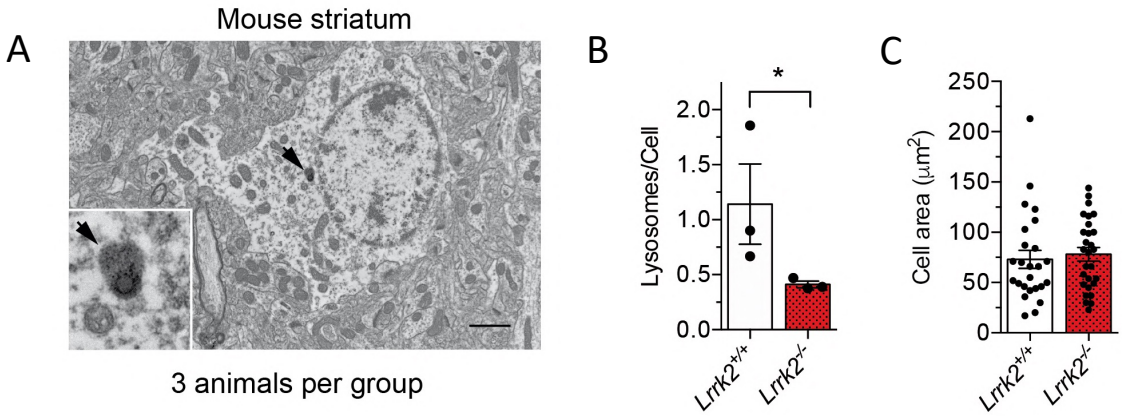

Supplementary Figure 4 Lrrk2-/- astrocytes display less lysosomal-like structures in mouse striatal slices. A. Representative image of a *Lrrk2* wild-type astrocyte containing a lysosome; **B.** Quantification of lysosomes in Lrrk2 wild-type and *Lrrk2-/-* astrocytic cell bodies (*Lrrk2 WT+*, n=3, 20 to 30 cells per animal; *Lrrk2 -/-*, n=3, 15 to 20 cells per animal); $p < 0.01$, unpaired t-test); **C.** Quantification of astrocyte area; $p > 0.05$, unpaired t-test). Scale bar = 10 μm.

SUPPLEMENTARY FIGURE 5

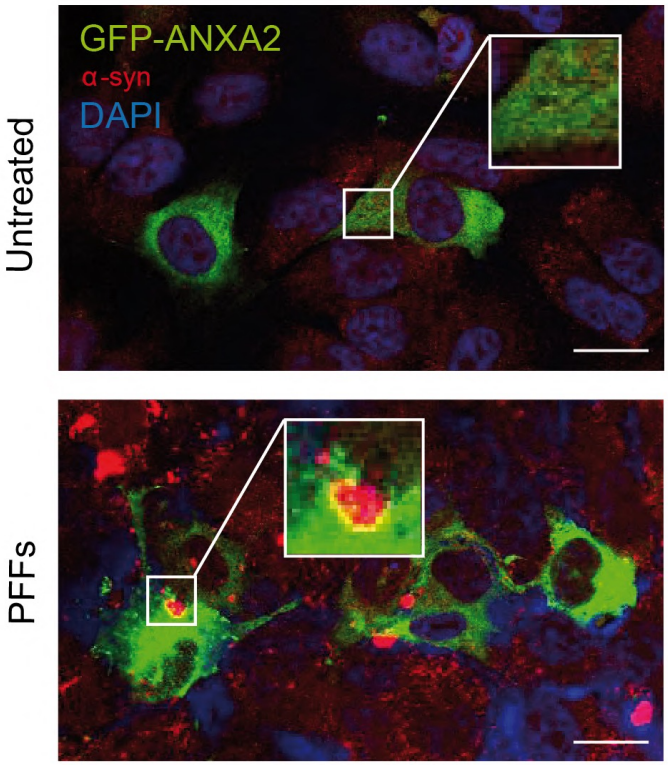

Supplementary Figure 5 ANXA2 distribution in H4 cells. Representative images of H4 cells transfected with GFP-ANXA2 in PFF-treated and basal condition (GFP, green; DAPI, blue; α syn, red). Scale bars 20 μm.

SUPPLEMENTARY FIGURE 6

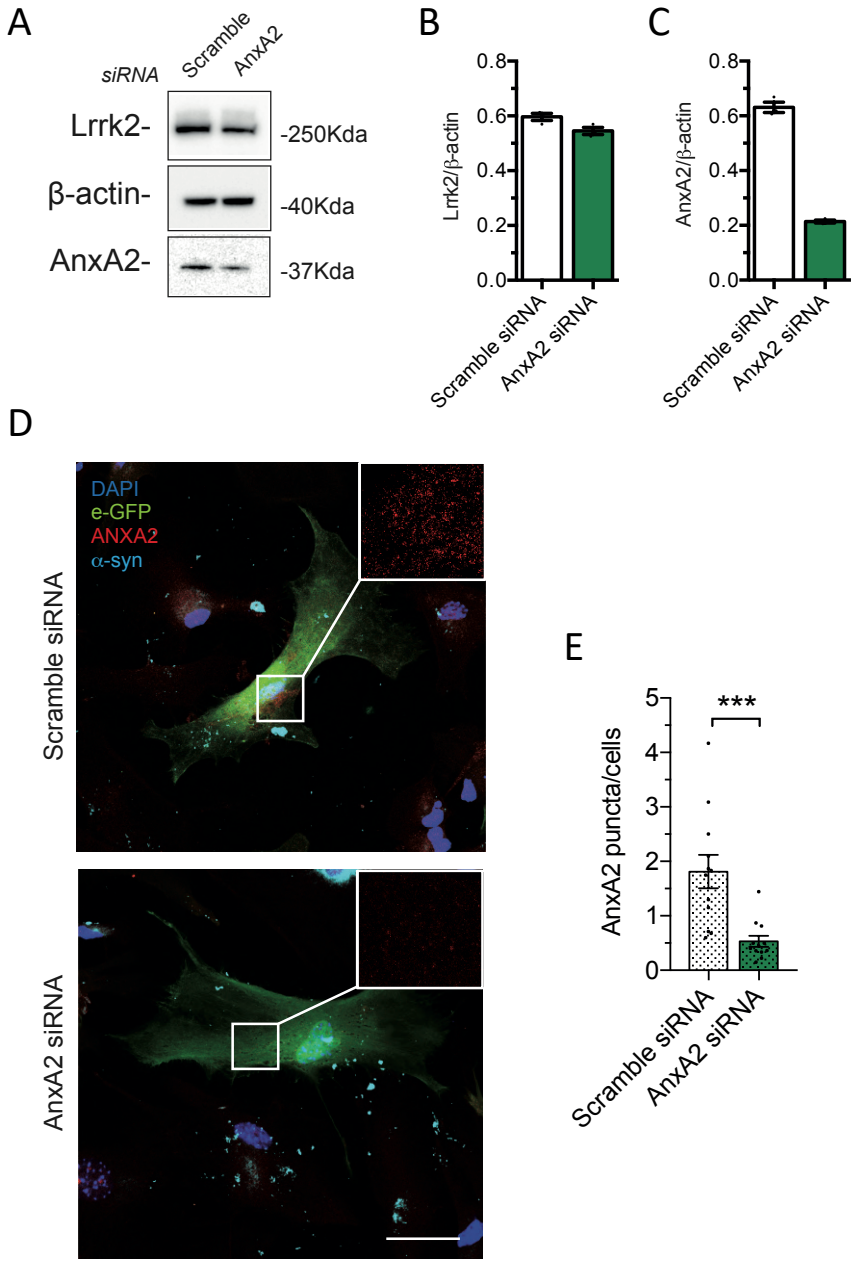

Supplementary Figure 6. Setting of AnxA2 downregulation in primary astrocytes. A. Western blot analysis of primary striatal astrocyte lysates transfected with scramble siRNA and AnxA2 siRNA using anti-Lrrk2, anti-β-actin and anti-AnxA2 antibodies; **B.** and **C.** Quantification of band intensity was performed using ImageJ and normalized by β-actin (n=3); **D.** Immunocytochemistry of AnxA2 endogenous expression in scramble siRNA and AnxA2 siRNA transfected cells using anti-AnxA2 antibody**.** Recipient cells are visualized by GFP expression; **E.** Eight images were analyzed (n=2 independent cultures). Quantification of Anxa2 puncta was performed using ImageJ. Statistical analysis in **E.** was made by Unpaired T-test * $p \leq 0.05$ ** $p \leq 0.01$ *** $p \leq 0.001$. Scale bar = 30 µm

Chapter 7

Discussion and Conclusion PART I

8.1 Discussion and Conclusion PART I

In the first section of thesis project, we optimized an efficient live-imaging assay to identify possible modulators of astrocyte-mediated synapse elimination and we validated Ackr3 as the most promising one.

We conjugated in vitro purified brain murine synapses with pH indicator-conjugated synaptosomes and we first validated primary astrocyte-mediated internalization kinetic. Coherently to previous studied, our data show that primary astrocytes possess a long engulfment kinetics, with a peak at 48h (Chung et al., 2013). Our study begins with a genetic screening, by which we identified several genes that impacts synaptosome internalization. We found several clusters of genes with differential effects on astrocyte-mediated synaptosome engulfment. GO analysis identified G protein-coupled receptor and C-C chemokine receptor as top GO terms involved in synaptosome uptake. Additionally, we identified other categories related to the intracellular signaling pathway that cause accumulation of internalized synaptosomes. Since the pH-sensitive dye bights only at later stages of the phagocytic in the intracellular signaling are enhancing internalization or blocking the degradation.

Among the hits that impact synaptosome internalization, we were particularly intrigued by chemokines receptor family members. Specifically, the screening yield eight chemokines receptor: Cxcr5, Ackr3, Cxcr2, Cxcr3, Ccr1, Ccr2, Ccr4 and Ackr2. Thus, we checked the expression of the eight chemokine receptors in acutely isolated astroglial cells. We showed that Ackr3 is highly expressed both in murine and human astrocytes compare to the other selected hits. In the brain, Ackr3 is also found in neurons and vascular cells but not in microglia (Schönemeier et al.,2008). Ackr3 is known to serve as a scavenger and/or decoy receptor for its ligands: Cxcl11 and Cxcl12. Ackr3 play different role both in physiology and pathology; for example, it has been shown that Ackr3 participates in migration of interneurons during cortical development (Sànchez-Alcañiz et al., 2011). Moreover, active Ackr3-dependent cell signaling seems to occur in tumor cells promoting tumor cell growth, adhesion, and invasion (Liu et al., 2014). Ackr3 is classified as a non-classical G-protein-coupled receptor that apparently fails to activate bound G proteins, but instead can signal through beta-arrestin-2 (Levoye et al., 2009; Zabel et al., 2009). Moreover, Ma and colleagues reported that the activation of Ackr3 increased the uptake of bacterial in human macrophages (van der Vorst et al., 2019). However, the molecular mechanism behind Ackr3-mediated synaptic elimination is totally unknown.

Our results show that Ackr3-deficient murine astrocytes display an impaired capacity in synaptosomes engulfment. In accordance with our previous results, the overexpression of human-ACKR3 receptor in murine astrocytes significantly increase synaptosomes engulfment.

We also observed that endogenous Ackr3 re-localizes into Lamp1-positive structures together with internalized synaptosomes. This finding suggested a direct involvement of Ackr3 in the recognition and the internalization of synaptic terminals rather than a parallel, stimulating signaling converging on *i.e.* Megf10. However, whether Megf10 and Ackr3 modulate astrocyte-mediated synapses engulfment through a parallel or a separate pathway need to be further investigated.

Considering that Ackr3 is a chemokine receptor, we investigated the role of Cxcl11/Cxcl12 in the phagocytic process. To date, an increased synapses elimination has been clearly reported when cultured astrocytes are exposed to astrocytes-conditioned medium which contains secreted factors. Astrocyte-released cytokines and chemokines are reported to assists microglial phagocytosis by acting as a chemoattractant to a specific site, although only one study showed that Cxcl12 is chemotactic for mouse astrocytes (Choi et al., 2014; Odemis et al., 2002). Our data excluded that Cxcl11/Cxcl12 are released by astrocytes upon synaptosome treatment. Instead, we confirmed that Flag-tagged Ackr3 interacts with purified synaptic terminals *in vitro*, suggesting the presence of a target molecule *i.e.* Cxcl12 on synaptosome membrane. Accordingly, Cxcl12 is present in our synaptosomal preparation and synaptosome membranes can bind additional recombinant Cxcl12 upon incubation.

The common feature for synapses engulfment by glial cells is the presence of an “eat-me” signal exposed in the outer leaflet of the plasma membrane. Of note, altered distribution of PS is associated with neuronal death and externalized membrane PS act as an “eat-me” signal for apoptotic cells or synapses elimination (Mellèn et al., 2009; Scott-Hewitt et al., 2020). However, the presence of synaptic tags other than PS or bridging molecules involved in astrocytes-mediated clearance in general are currently under debate. For instance, MEGF10-mediated apoptotic cells elimination requires C1q as an adaptor for PS (Iram, Ramirez-Ortiz, et al., 2016). Conversely, a study denied the involvement of C1q for Megf10-mediated synapses recognition (Chung et al., 2013).

Here, we demonstrated that Cxcl12-covered synaptosomes significantly increase the PI of astrocytes compared to the naïve suggesting that the chemokine function as eat me signal and

might be recognized by receptor at the neuronal cell membrane, Supporting our data, a recent paper showed that a subset of chemokines bind exposed PS and act as a signal for macrophage-mediated phagocytosis (Pontejo and Murphy et al., 2021), We reported that Cxcl12 is not released by astrocytes upon synaptosome contact and it already present in the synaptosome preparation. However, we cannot define the source of the chemokine that we detected in the preparation since Cxcl12 is expressed by neurons but also by other cells in the brain.

Considering Cxcl12 as a bridging molecule, by screening a pool of lipids, we revealed that this chemokine specifically recognizes PE. Of note, PE is a lipid that together with PS increases its externalization into the outer leaflet of plasma membrane in the early phase of neuronal death (Faris et al., 2021). Even though the molecular mechanism underlying PS and PE externalization at synapses remains elusive, few reports demonstrate that phospholipid-flippase regulate phospholipid asymmetry at the plasma membrane (Li et al., 2021; Mioka et al., 2018) Interestingly, the lack of phospholipid-flippase chaperone CDC50A, also known as TREM30A, increased PS and PE translocation to the cell surface (Kato et al., 2013; Li et al., 2021). Using pSIVA as a fluorescent tag for PS (Ruggiero er al., 2012), we confirmed an increased PS exposure in primary cultured neurons downregulating for TREM30A (data not shown). In line with this, we now validating the exposure of PE by using fluorescent-tagged Duramycin, a lantibiotic peptide derived from *Streptoverticillium cinnamoneus* which binds PE with high affinity and specificity (Faris et al., 2021). However, the mechanism by which PE and Cxcl12 might act as synaptic tag, such as PS and C1q, allowing astrocyte-mediated synapse elimination in the brain need to be further investigate and confirmed *in vivo*.

Along this line, we are now studying the role of Ackr3 in astrocyte-mediated synapse elimination using *in vivo* model in collaboration with Dr. Won-Suk Chung in Korea. Specifically, we are measuring the synaptic density changes in mice Ackr3 is overexpressed and downregulated specifically in brain astrocytes. Moreover, we are employing Duramycin, to corroborate the role of Cxcl12 as a bridging molecule between PE and astrocytic-Ackr3. Our preliminary data showed that Duramycin injection does not affects the synaptic density; meanwhile it caused a decrease in the expression of Ackr3 and GFAP (data not shown).

Ackr3 is conserved and expressed in human astrocytes. Moreover, an increase in astrocytic Ackr3 expression have been detected in many human brain pathologies such as in infarcted human cerebral cortex, in the hippocampus of AD patients as well as glioblastoma multiforme (GBM) (Puchert et al., 2017). Thus, humanized models represent the appropriated

tool to study ACKR3 biology both in physiological and pathological conditions. Clearance activity of iHAstrocytes has not been fully characterized. Lin et al demonstrated that iHAstrocytes can engulf a large amount of Aβ but there is no literature regarding their involvement in synapses internalization. Here, we confirm for the first time that iHAstrocytes can internalized neuronal terminals. Of note, we observed that the lack Ackr3 disrupts synaptosomes elimination ability of astrocytes also in the human background. In accordance with our previous results on murine astrocytes, we observed a re-localization of the receptor into the lysosomal vesicles together with internalized synaptosomes, suggesting a conserved mechanism of astrocyte-mediated synaptic terminal removal across species. Moreover, we observed that Megf10 is expressed in iHAstrocytes and its endogenous level is not affected by Ackr3 downregulation. On this line, we are employing STED microscopy to further investigate whether Ackr3-Megf10 cooperate or acts on a parallel pathway in regulating astrocyte-mediated synaptic terminal engulfment.

Related to GBM, high expression of Ackr3 correlates with poor prognosis and potential treatment resistance, making this receptor and its pathway an attractive therapeutic target (Smit et al., 2021, Salazar et al., 2018). However, the molecular mechanisms by which the Cxcl11/12-Ackr3 axis contributes to the progression of GBM are not fully understood. Our preliminary results indicated that Ackr3 is expressed in tumor-associated astrocytes (TAAs) positive for Galectin-3, a marker of phagocytic cells (Figure 8.1). Thus, TAAs could intervene in the elimination of live neurons and synapses in GBM and contribute to the tumor progression. My current studies are focused on the dissection of Ackr3-mediated synaptic elimination in GBM murine and human models as well as in patient biofluids.

Concluding, we identified Ackr3 as a novel modulator of astrocyte-mediated synapse engulfment. Although additional mechanistic investigations are needed, we propose that PE-Cxcl12 binding acts as a possible novel “find/eat-me” signal for synapses elimination in the brain. In a broader context, our work revealed that astrocytic-Ackr3 is a novel receptor for synaptic terminals removal both in murine and human background, opening the possibility to better target astrocyte-mediated clearance dysfunction in human diseases.

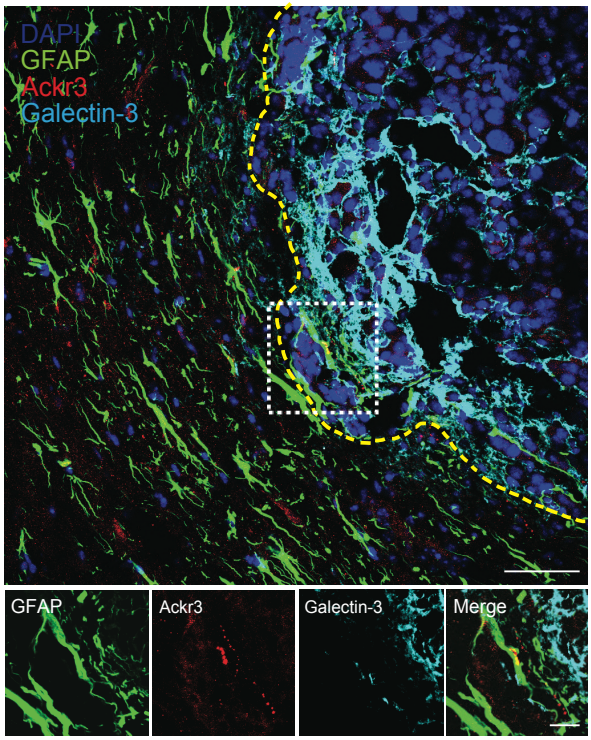

Figure 8.1 Ackr3 expression in TAAs astrocytes. Representative z-stack confocal images for Ackr3 (red), GFAP (green) and Galectin-3 (cyan) in GBM mouse model; Insets show the co-localization of the three astrocytic markers. Scale bar 20 μm, insets 5 μm.

Discussion and Conclusion PART II

8.2 Discussion and Conclusion PART II

In the second part of the thesis project, we revealed that the most common pathogenic mutation in LRRK2, G2019S, negatively regulates the amount of engulfed fibrillar α-syn in astrocytes. Moreover, we reported that Anxa2 deficit in astrocyte impacts on α-syn clearance.

Protein aggregates internalization by astrocytes has been clearly reported in the last decade (Rostami et al., 2021; Gustafsson et al., 2017; Rostami et al., 2017, Huang et al., 2022). Astrocytes have been shown to ingest particularly large amounts of aggregated α-syn that are then intracellularly stored, rather than degraded. Moreover, G2019S PD-related LRRK2 mutation in astrocytes has been reported to disrupt structure and function of lysosomes (Henry et al., 2015). However, how G2019S mutation impacts on astrocyte-mediated α-syn clearance was not fully dissected. Our data, in collaboration with the University of Uppsala, demonstrated that the pathological mutation negatively regulated uptake of small α-syn particles by cortical stem cell-derived astrocytes. In agreement with this result, it has been proposed that increasing LRRK2 kinase activity block micropinocytosis in phagocytes (Liu et al., 2020). Moreover, looking at α-syn inclusion after 6 days after the exposure to PFFs, we observed an increase both in the amount and area of α-syn deposits. The larger area measurements in combination with an unchanged particle count indicates the formation of bigger aggregates over time. In fact, α-syn particles previously below the detection limit, may have clustered and thus become detectable at a later time point. Interestingly, we noticed this increase not only in the presence of the pathological mutation but also in wild-type astrocytes as well as in absence of LRRK2. This α-syn accumulation, without distinction among the three genotypes, suggest a mechanism completely unrelated with LRRK2 kinase activity. Instead, the reason for this increase could be explained as a failure of astrocytes in degrading engulfed material which was consequently stored in the cells. Therefore, this astrocytic α-syn accumulation in specific PD-linked brain region, as striatum, might speed up the progression of the pathology.

Astrocytes that populate the striatum are relevant to PD pathology since they are in close proximity to dopaminergic terminals of the SNpc. Furthermore, it is unknown how they respond to neuronal-released α-syn. In line with our data on cortical stem cell-derived astrocytes, we confirmed that PD-linked mutation in Lrrk2 negatively impacts on striatal astrocyte-mediated α-syn clearance. Indeed, we demonstrated that astrocytes carrying the G2019S mutation displayed a reduced amount of internalized α-syn.

An impairment in the lysosomal architecture has been also in G2019S PD patient–specific human neuroepithelial stem cells and in primary cortical neurons from Lrrk2GS/GS mice settings (Schapansky et al., 2018; Walter et al., 2019). In contrast, Henry et al. indicated enlarged lysosomes in cultured cortical astrocytes overexpressing G2019S human LRRK2 compared to wild-type astrocytes, without discriminating between the contribution of the pathogenic mutation and the LRRK2 level (Henry et al., 2015). However, our data reported that G2019S pathogenic mutation cause a decrease in the number and area of lysosomal-like structures in primary striatal astrocytes. Whereas we observed that the genetic ablation of Lrrk2 caused an enlargement of the lysosomal structures. Change in lysosomal size that was however compensated by an overall decrease in the number of lysosomal structures, as also shown for astrocytes in Lrrk2 -/- striatum brain sections. Despite all these differences in the size and number of lysosomal structures, we did not report any differences in the pH of astrocytes. However, we observed an increase in the acidic compartments upon α-syn treatment both in wild-type and in absence of LRRK2, suggesting an activation of the endo-lysosomal system. Meanwhile, in the presence of the pathological mutation we did not detect any increase in the acidic compartments, suggesting a deficit in the endo-lysosomal system activation. Taken together these results confirmed that striatal astrocytes harboring the G2019S mutation displayed both a structural and functional deficit in the endo-lysosomal system, resulting in an impaired uptake of α-syn aggregates.

Using and unbiased approach, we dissect a novel mechanism through which LRRK2 affects astrocyte-mediated α-syn clearance. For the first time, our study identifies ANXA2 as a novel player in α-syn clearance in astrocytic cells. ANXA2 is an actin binding protein that modulates many intracellular trafficking events, via the regulation of actin polymerization dynamics. Specifically, ANXA2 is recruited to the plasma membrane, during the formation of the phagocytic cup, and assists endosomes upon particle internalization by preventing destabilization (Law et al., 2009; Scharf et al., 2012). Moreover, Anxa2 has been recruited to lysosomal membrane in case of lysosomal leakage (Yim et al, 2022). With the high involvement in dynamic events of membrane events, ANXA2 plays a crucial role in mediating autophagy (Varyukhina et al 2022; Zhang et al., 2021). Indeed, ANXA2 ablation leads to a defect in the phagophore membrane initiation and a deficiency in the autophagic pathway (Morozova et al., 2015). In line with these findings, we demonstrated that endogenous AnxA2 downregulation negatively impacts on α-syn clearance in primary striatal astrocytes. Our MS analysis pointed that ANXA2 enhanced its affinity for LRRK2 upon α-syn treatment suggesting a functional

interaction between the two proteins. We demonstrated that Lrrk2 GS/GS astrocytes displayed an evident phenotype characterized by a significant downregulation of AnxA2 protein level. Moreover, we validate that a decreased expression of AnxA2 in G2019S astrocytes correlate with an impaired ability of the protein to re-localize into puncta in close proximity to α-syn particles. Deficits that were completely reverted by the application of Lrrk2 kinase inhibitors Mli-2. Taken together, our findings suggest an AnxA2 deficit in the presence of the pathological mutation that could explain the impaired astrocytic α-syn clearance. However, how LRRK2 kinase activity regulates the ANXA2 level in astrocytes needs to be explored in the future.

Of note, we observed a decrease in ANXA2 protein level in *post-mortem* caudate and putamen from PD patients carrying the LRRK2 G2019S mutation, which recapitulate what we validated in primary astrocytes. Interestingly, an increased in ANXA2 expression has been observed at the cell periphery in reactive astrocytes positioned in close proximity to senile plaques and degenerating neurons of AD human *post-mortem* brains. 8080046 These observations suggest an ANXA2-dependent mechanism(s) in brain disease, specifically in aggregated protein-related pathologies. As discussed above, ANXA2 modulates many intracellular trafficking events via the regulation of actin polymerization that might impacts on autophagy-mediated fibrils uptake. Compelling evidence showed that starvation induced an increase in ANXA2 expression level correlated with an increase in the autophagic pathway (Moreau et al., 2015). Of note, is emerging that diet habits might have important implications for brain health, and for several brain disorders as PD. Preclinical and clinical studies on low-fat diet showed that it has beneficial effects on motor and non-motor symptoms of PD patients (Phillips et al., 2018). Therefore, these observations suggest that modulation of ANXA2 level through diet might have beneficial effects on protein aggregates uptake, reducing PD progression. However, the role of astrocytic-ANXA2 in protein fibrils clearance, specifically in human, need to be further investigate.

On this regard, future studies in the lab will be addressed to dissect the molecular mechanism of protein aggregates handling mediated by ANXA2. Our data clearly reported an ANXA2-mediated mechanism for α-syn clearance, however, ANXA2 might impacts on the uptake of other protein fibrils. Notably, physical interaction between ANXA2 and the extreme N-terminal of Tau has been reported (Gauthier-Kemper et al., 2018). Our preliminary data demonstrated that Tau deposits decrease upon ANXA2 downregulation in astrocytes (Figure 8.2 A), similarly to what we observed in α-syn clearance. This data suggest that astrocyte-mediated internalization of Tau PFFs depends on ANXA2 level. However, the molecular

mechanism that regulate ANXA2-mediated α-syn and Tau fibrils uptake is fully unknown. On this line, to identify the protein complexes that regulate the recognition and internalization of protein fibrils through ANXA2 we will employ an unbiased MS proteomic analysis using purified astrocytic phagosomes. Specifically, we will purify early, and mature phagosomes form astrocytes treated with latex/polystyrene beads coated with α-syn or Tau PFFs. (Figure 8.2 B). Data analysis will discriminate among the biological process and the functional interactions in which hits are involved at the different stages of fibrils uptake. A deeper investigation of ANXA2-mediated aggregate removal will open new windows for pharmacological intervention in different pathologies.

In conclusion, we reported a novel molecular mechanism behind impaired α-syn clearance in G2019S astrocytes highlighting ANXA2-mediated aggregate uptake as a valuable target in PD as well as other proteinopathies.

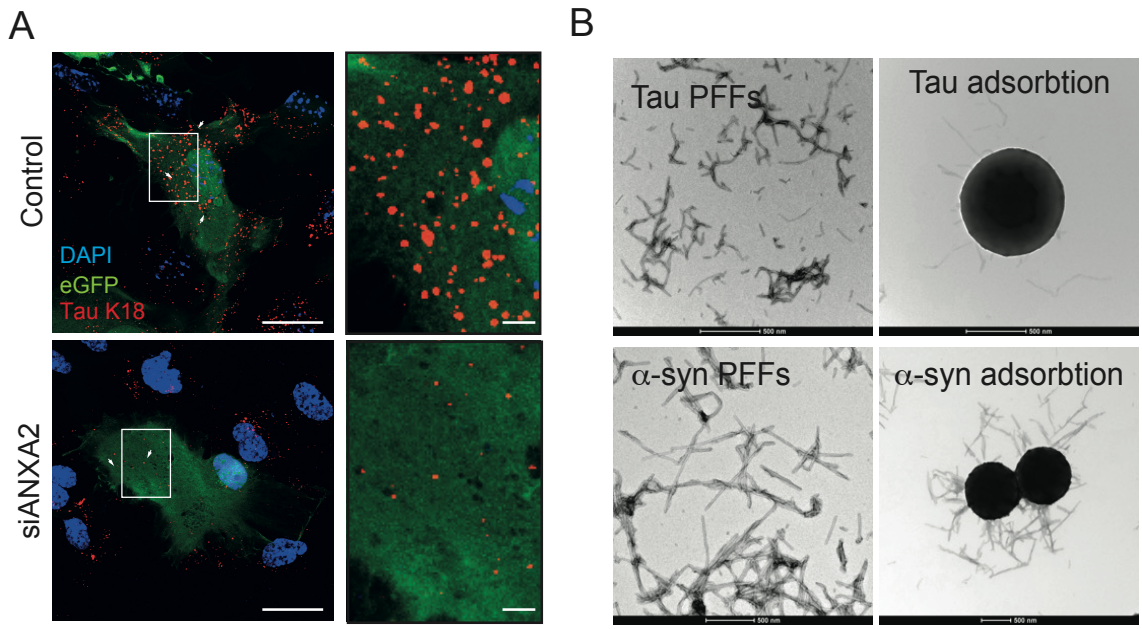

Figure 8.2 Preliminary data. A. Primary mouse astrocytes transfected with an eGFP encoding plasmid (green) together with a control or AnxA2 siRNA, treated with Tau PFFs (red). Scale bar 50μm, insets scale bar 20μm; **B.** EM images of in-house prepared Tau and α-syn fibrils (left) and latex beads passively adsorbed with PFFs (right). Scale bar 500nm.

BIBLIOGRAPHY

Abounit, S., Bousset, L., Loria, F., Zhu, S., de Chaumont, F., Pieri, L., Olivo-Marin, J. C., Melki, R., & Zurzolo, C. (2016). Tunneling nanotubes spread fibrillar α-synuclein by intercellular trafficking of lysosomes. The EMBO journal, 35(19), 2120–2138. https://doi.org/10.15252/embj.201593411

Almeida, A., Almeida, J., Bolaños, J. P., & Moncada, S. (2001). Different responses of astrocytes and neurons to nitric oxide: the role of glycolytically generated ATP in astrocyte protection. Proceedings of the National Academy of Sciences of the United States of America, 98(26), 15294–15299.

Alvarez-Maubecin, V., Garcia-Hernandez, F., Williams, J. T., & Van Bockstaele, E. J. (2000). Functional coupling between neurons and glia. The Journal of neuroscience : the official journal of the Society for Neuroscience, 20(11), 4091–4098. https://doi.org/10.1523/JNEUROSCI.20-11-04091.2000

Alvarez, J. I., Katayama, T., & Prat, A. (2013). Glial influence on the blood brain barrier. Glia, 61(12), 1939–1958. https://doi.org/10.1002/glia.22575

Angot, E., Steiner, J. A., Lema Tomé, C. M., Ekström, P., Mattsson, B., Björklund, A., & Brundin, P. (2012). Alpha-synuclein cell-to-cell transfer and seeding in grafted dopaminergic neurons in vivo. PloS one, 7(6), e39465. https://doi.org/10.1371/journal.pone.0039465

Araque, A., Parpura, V., Sanzgiri, R. P., & Haydon, P. G. (1999). Tripartite synapses: glia, the unacknowledged partner. Trends in neurosciences, 22(5), 208–215. https://doi.org/10.1016/s0166-2236(98)01349-6

Ashburner, M., Ball, C. A., Blake, J. A., Botstein, D., Butler, H., Cherry, J. M., Davis, A. P., Dolinski, K., Dwight, S. S., Eppig, J. T., Harris, M. A., Hill, D. P., Issel-Tarver, L., Kasarskis, A., Lewis, S., Matese, J. C., Richardson, J. E., Ringwald, M., Rubin, G. M., & Sherlock, G. (2000). Gene ontology: tool for the unification of biology. The Gene Ontology Consortium. Nature genetics, 25(1), 25–29. https://doi.org/10.1038/75556

Baptista, M. A., Dave, K. D., Frasier, M. A., Sherer, T. B., Greeley, M., Beck, M. J., Varsho, J. S., Parker, G. A., Moore, C., Churchill, M. J., Meshul, C. K., & Fiske, B. K. (2013). Loss of leucine-rich repeat kinase 2 (LRRK2) in rats leads to progressive abnormal phenotypes in peripheral organs. PloS one, 8(11), e80705. https://doi.org/10.1371/journal.pone.0080705

Barres B. A. (2008). The mystery and magic of glia: a perspective on their roles in health and disease. Neuron, 60(3), 430–440. https://doi.org/10.1016/j.neuron.2008.10.013

Bataveljić, D., Nikolić, L., Milosević, M., Todorović, N., & Andjus, P. R. (2012). Changes in the astrocytic aquaporin-4 and inwardly rectifying potassium channel expression in the brain of the amyotrophic lateral sclerosis SOD1(G93A) rat model. Glia, 60(12), 1991–2003. https://doi.org/10.1002/glia.22414

Bauer, H., & Pllana, A. (2014). EEG-based local brain activity feedback training-tomographic neurofeedback. Frontiers in human neuroscience, 8, 1005. https://doi.org/10.3389/fnhum.2014.01005

Bayer T. A. (2015). Proteinopathies, a core concept for understanding and ultimately treating degenerative disorders?. European neuropsychopharmacology : the journal of the European College of Neuropsychopharmacology, 25(5), 713–724. https://doi.org/10.1016/j.euroneuro.2013.03.007

Bechinger, B., Zasloff, M., & Opella, S. J. (1992). Structure and interactions of magainin antibiotic peptides in lipid bilayers: a solid-state nuclear magnetic resonance investigation. Biophysical journal, 62(1), 12–14. https://doi.org/10.1016/S0006-3495(92)81763-0

Bélanger, M., & Magistretti, P. J. (2009). The role of astroglia in neuroprotection. Dialogues in clinical neuroscience, 11(3), 281–295. https://doi.org/10.31887/DCNS.2009.11.3/mbelanger

Bellesi, M., de Vivo, L., Chini, M., Gilli, F., Tononi, G., & Cirelli, C. (2017). Sleep Loss Promotes Astrocytic Phagocytosis and Microglial Activation in Mouse Cerebral Cortex. The Journal of neuroscience : the official journal of the Society for Neuroscience, 37(21), 5263–5273. https://doi.org/10.1523/JNEUROSCI.3981-16.2017

Bellucci, A., Zaltieri, M., Navarria, L., Grigoletto, J., Missale, C., & Spano, P. (2012). From α-synuclein to synaptic dysfunctions: new insights into the pathophysiology of Parkinson's disease. Brain research, 1476, 183–202. https://doi.org/10.1016/j.brainres.2012.04.014

Bengoa-Vergniory, N., Roberts, R. F., Wade-Martins, R., & Alegre-Abarrategui, J. (2017). Alpha-synuclein oligomers: a new hope. Acta neuropathologica, 134(6), 819–838. https://doi.org/10.1007/s00401-017-1755-1

Béraud, D., Twomey, M., Bloom, B., Mittereder, A., Ton, V., Neitzke, K., Chasovskikh, S., Mhyre, T. R., & Maguire-Zeiss, K. A. (2011). α-Synuclein Alters Toll-Like Receptor Expression. Frontiers in neuroscience, 5, 80. https://doi.org/10.3389/fnins.2011.00080

Bialas, A. R., & Stevens, B. (2013). TGF-β signaling regulates neuronal C1q expression and developmental synaptic refinement. Nature neuroscience, 16(12), 1773–1782. https://doi.org/10.1038/nn.3560 (Retraction published Nat Neurosci. 2022 Feb;25(2):265)

Boddum, K., Jensen, T. P., Magloire, V., Kristiansen, U., Rusakov, D. A., Pavlov, I., & Walker, M. C. (2016). Astrocytic GABA transporter activity modulates excitatory neurotransmission. Nature communications, 7, 13572. https://doi.org/10.1038/ncomms13572

Boisvert, M. M., Erikson, G. A., Shokhirev, M. N., & Allen, N. J. (2018). The Aging Astrocyte Transcriptome from Multiple Regions of the Mouse Brain. Cell reports, 22(1), 269–285. https://doi.org/10.1016/j.celrep.2017.12.039

Bonet-Ponce, L., & Cookson, M. R. (2022). LRRK2 recruitment, activity, and function in organelles. The FEBS journal, 289(22), 6871–6890. https://doi.org/10.1111/febs.16099

Bonet-Ponce, L., Beilina, A., Williamson, C. D., Lindberg, E., Kluss, J. H., Saez-Atienzar, S., Landeck, N., Kumaran, R., Mamais, A., Bleck, C. K. E., Li, Y., & Cookson, M. R. (2020). LRRK2 mediates tubulation and vesicle sorting from lysosomes. Science advances, 6(46), eabb2454. https://doi.org/10.1126/sciadv.abb2454

Booth, H. D. E., Hirst, W. D., & Wade-Martins, R. (2017). The Role of Astrocyte Dysfunction in Parkinson's Disease Pathogenesis. Trends in neurosciences, 40(6), 358–370. https://doi.org/10.1016/j.tins.2017.04.001

Braak, H., de Vos, R. A., Jansen, E. N., Bratzke, H., & Braak, E. (1998). Neuropathological hallmarks of Alzheimer's and Parkinson's diseases. Progress in brain research, 117, 267–285. https://doi.org/10.1016/s0079-6123(08)64021-2

Braak, H., Sastre, M., & Del Tredici, K. (2007). Development of alpha-synuclein immunoreactive astrocytes in the forebrain parallels stages of intraneuronal pathology in sporadic Parkinson's disease. Acta neuropathologica, 114(3), 231–241. https://doi.org/10.1007/s00401-007-0244-3

Bradbury M. W. (1993). The blood-brain barrier. Experimental physiology, 78(4), 453–472. https://doi.org/10.1113/expphysiol.1993.sp003698

Braidy, N., Gai, W. P., Xu, Y. H., Sachdev, P., Guillemin, G. J., Jiang, X. M., Ballard, J. W., Horan, M. P., Fang, Z. M., Chong, B. H., & Chan, D. K. (2013). Uptake and mitochondrial dysfunction of alpha-synuclein in human astrocytes, cortical neurons and fibroblasts. Translational neurodegeneration, 2(1), 20. https://doi.org/10.1186/2047-9158-2-20

Brown, A. M., & Ransom, B. R. (2007). Astrocyte glycogen and brain energy metabolism. Glia, 55(12), 1263–1271. https://doi.org/10.1002/glia.20557

Burdakov D. (2004). Electrical signaling in central orexin/hypocretin circuits: tuning arousal and appetite to fit the environment. The Neuroscientist : a review journal bringing neurobiology, neurology and psychiatry, 10(4), 286–291. https://doi.org/10.1177/1073858404263597

Bushey, D., Tononi, G., & Cirelli, C. (2011). Sleep and synaptic homeostasis: structural evidence in Drosophila. Science (New York, N.Y.), 332(6037), 1576–1581. https://doi.org/10.1126/science.1202839

Bushong, E. A., Martone, M. E., Jones, Y. Z., & Ellisman, M. H. (2002). Protoplasmic astrocytes in CA1 stratum radiatum occupy separate anatomical domains. The Journal of neuroscience : the official journal of the Society for Neuroscience, 22(1), 183–192. https://doi.org/10.1523/JNEUROSCI.22-01-00183.2002

Bustos, V., Pulina, M. V., & Ledo, J. (2021). Amyloidogenic and anti-amyloidogenic properties of presenilin 1. Advances in pharmacology (San Diego, Calif.), 90, 239–251. https://doi.org/10.1016/bs.apha.2020.09.010

Bustos, V., Pulina, M. V., Bispo, A., Lam, A., Flajolet, M., Gorelick, F. S., & Greengard, P. (2017). Phosphorylated Presenilin 1 decreases β-amyloid by facilitating autophagosome-lysosome fusion. Proceedings of the National Academy of Sciences of the United States of America, 114(27), 7148–7153. https://doi.org/10.1073/pnas.1705240114

Buzsáki, G., & Chrobak, J. J. (2005). Synaptic plasticity and self-organization in the hippocampus. Nature neuroscience, 8(11), 1418.

Byun, Y. G., & Chung, W. S. (2019). In Vitro Engulfment Assay to Measure Phagocytic Activity of Astrocytes Using Synaptosomes. Methods in molecular biology (Clifton, N.J.), 1938, 155–168. https://doi.org/10.1007/978-1-4939-9068-9_11

Cahoy, J. D., Emery, B., Kaushal, A., Foo, L. C., Zamanian, J. L., Christopherson, K. S., Xing, Y., Lubischer, J. L., Krieg, P. A., Krupenko, S. A., Thompson, W. J., & Barres, B. A. (2008). A transcriptome database for astrocytes, neurons, and oligodendrocytes: a new resource for understanding brain development and function. The Journal of neuroscience : the official journal of the Society for Neuroscience, 28(1), 264–278. https://doi.org/10.1523/JNEUROSCI.4178-07.2008

Castagnet, P. I., Golovko, M. Y., Barceló-Coblijn, G. C., Nussbaum, R. L., & Murphy, E. J. (2005). Fatty acid incorporation is decreased in astrocytes cultured from alpha-synuclein gene-ablated mice. Journal of neurochemistry, 94(3), 839–849. https://doi.org/10.1111/j.1471-4159.2005.03247.x

Chiou, B., Gao, C., Giera, S., Folts, C. J., Kishore, P., Yu, D., Oak, H. C., Jiang, R., & Piao, X. (2021). Cell type-specific evaluation of ADGRG1/GPR56 function in developmental central nervous system myelination. Glia, 69(2), 413–423. https://doi.org/10.1002/glia.23906

Choi, S. S., Lee, H. J., Lim, I., Satoh, J., & Kim, S. U. (2014). Human astrocytes: secretome profiles of cytokines and chemokines. PloS one, 9(4), e92325. https://doi.org/10.1371/journal.pone.0092325

Chung, W. S., Clarke, L. E., Wang, G. X., Stafford, B. K., Sher, A., Chakraborty, C., Joung, J., Foo, L. C., Thompson, A., Chen, C., Smith, S. J., & Barres, B. A. (2013). Astrocytes mediate synapse elimination through MEGF10 and MERTK pathways. Nature, 504(7480), 394–400. https://doi.org/10.1038/nature12776

Chung, W. S., Verghese, P. B., Chakraborty, C., Joung, J., Hyman, B. T., Ulrich, J. D., Holtzman, D. M., & Barres, B. A. (2016). Novel allele-dependent role for APOE in controlling the rate of synapse pruning by astrocytes. Proceedings of the National Academy of Sciences of the United States of America, 113(36), 10186–10191. https://doi.org/10.1073/pnas.1609896113

Civiero, L., Vancraenenbroeck, R., Belluzzi, E., Beilina, A., Lobbestael, E., Reyniers, L., Gao, F., Micetic, I., De Maeyer, M., Bubacco, L., Baekelandt, V., Cookson, M. R., Greggio, E., & Taymans, J. M. (2012). Biochemical characterization of highly purified leucine-rich repeat kinases 1 and 2 demonstrates formation of homodimers. PloS one, 7(8), e43472. https://doi.org/10.1371/journal.pone.0043472

Clarke, L. E., & Barres, B. A. (2013). Emerging roles of astrocytes in neural circuit development. Nature reviews. Neuroscience, 14(5), 311–321. https://doi.org/10.1038/nrn3484

Colonna, M., & Butovsky, O. (2017). Microglia Function in the Central Nervous System During Health and Neurodegeneration. Annual review of immunology, 35, 441–468. https://doi.org/10.1146/annurev-immunol-051116-052358

Colonnier M. (1964). Experimental degeneration in the cerebral cortex. Journal of anatomy, 98(pt 1), 47–53.

Crimins, J. L., Rocher, A. B., & Luebke, J. I. (2012). Electrophysiological changes precede morphological changes to frontal cortical pyramidal neurons in the rTg4510 mouse model of

progressive tauopathy. Acta neuropathologica, 124(6), 777–795. https://doi.org/10.1007/s00401-012-1038-9

Damisah, E. C., Hill, R. A., Rai, A., Chen, F., Rothlin, C. V., Ghosh, S., & Grutzendler, J. (2020). Astrocytes and microglia play orchestrated roles and respect phagocytic territories during neuronal corpse removal in vivo. Science advances, 6(26), eaba3239. https://doi.org/10.1126/sciadv.aba3239

Danbolt N. C. (2001). Glutamate uptake. Progress in neurobiology, 65(1), 1–105. https://doi.org/10.1016/s0301-0082(00)00067-8

de Vivo, L., Bellesi, M., Marshall, W., Bushong, E. A., Ellisman, M. H., Tononi, G., & Cirelli, C. (2017). Ultrastructural evidence for synaptic scaling across the wake/sleep cycle. Science (New York, N.Y.), 355(6324), 507–510. https://doi.org/10.1126/science.aah5982

Deng, H., Wang, P., & Jankovic, J. (2018). The genetics of Parkinson disease. Ageing research reviews, 42, 72–85. https://doi.org/10.1016/j.arr.2017.12.007

Desplats, P., Lee, H. J., Bae, E. J., Patrick, C., Rockenstein, E., Crews, L., Spencer, B., Masliah, E., & Lee, S. J. (2009). Inclusion formation and neuronal cell death through neuron-to-neuron transmission of alpha-synuclein. Proceedings of the National Academy of Sciences of the United States of America, 106(31), 13010–13015. https://doi.org/10.1073/pnas.0903691106

Dickson D. W. (2012). Parkinson's disease and parkinsonism: neuropathology. Cold Spring Harbor perspectives in medicine, 2(8), a009258. https://doi.org/10.1101/cshperspect.a009258

Dieriks, B. V., Park, T. I., Fourie, C., Faull, R. L., Dragunow, M., & Curtis, M. A. (2017). α-synuclein transfer through tunneling nanotubes occurs in SH-SY5Y cells and primary brain pericytes from Parkinson's disease patients. Scientific reports, 7, 42984. https://doi.org/10.1038/srep42984

Diering, G. H., Nirujogi, R. S., Roth, R. H., Worley, P. F., Pandey, A., & Huganir, R. L. (2017). Homer1a drives homeostatic scaling-down of excitatory synapses during sleep. Science (New York, N.Y.), 355(6324), 511–515. https://doi.org/10.1126/science.aai8355

Dilsizoglu Senol, A., Samarani, M., Syan, S., Guardia, C. M., Nonaka, T., Liv, N., Latour-Lambert, P., Hasegawa, M., Klumperman, J., Bonifacino, J. S., & Zurzolo, C. (2021). α-Synuclein fibrils subvert lysosome structure and function for the propagation of protein misfolding between cells through tunneling nanotubes. PLoS biology, 19(7), e3001287. https://doi.org/10.1371/journal.pbio.3001287

Diógenes, M. J., Dias, R. B., Rombo, D. M., Vicente Miranda, H., Maiolino, F., Guerreiro, P., Näsström, T., Franquelim, H. G., Oliveira, L. M., Castanho, M. A., Lannfelt, L., Bergström, J., Ingelsson, M., Quintas, A., Sebastião, A. M., Lopes, L. V., & Outeiro, T. F. (2012). Extracellular alpha-synuclein oligomers modulate synaptic transmission and impair LTP via NMDA-receptor activation. The Journal of neuroscience : the official journal of the Society for Neuroscience, 32(34), 11750–11762. https://doi.org/10.1523/JNEUROSCI.0234-12.2012

Doengi, M., Hirnet, D., Coulon, P., Pape, H. C., Deitmer, J. W., & Lohr, C. (2009). GABA uptake-dependent Ca(2+) signaling in developing olfactory bulb astrocytes. Proceedings of the National Academy of Sciences of the United States of America, 106(41), 17570–17575. https://doi.org/10.1073/pnas.0809513106

Dringen R. (2000). Metabolism and functions of glutathione in brain. Progress in neurobiology, 62(6), 649–671. https://doi.org/10.1016/s0301-0082(99)00060-x

Dringen, R., Gebhardt, R., & Hamprecht, B. (1993). Glycogen in astrocytes: possible function as lactate supply for neighboring cells. Brain research, 623(2), 208–214. https://doi.org/10.1016/0006-8993(93)91429-v

Emmanouilidou, E., Melachroinou, K., Roumeliotis, T., Garbis, S. D., Ntzouni, M., Margaritis, L. H., Stefanis, L., & Vekrellis, K. (2010). Cell-produced alpha-synuclein is secreted in a calcium-dependent manner by exosomes and impacts neuronal survival. The Journal of neuroscience : the official journal of the Society for Neuroscience, 30(20), 6838–6851. https://doi.org/10.1523/JNEUROSCI.5699-09.2010

Engelhardt B. (2003). Development of the blood-brain barrier. Cell and tissue research, 314(1), 119–129. https://doi.org/10.1007/s00441-003-0751-z

Eroglu, C., & Barres, B. A. (2010). Regulation of synaptic connectivity by glia. Nature, 468(7321), 223.

Ertürk, A., Wang, Y., & Sheng, M. (2014). Local pruning of dendrites and spines by caspase-3-dependent and proteasome-limited mechanisms. The Journal of neuroscience : the official journal of the Society for Neuroscience, 34(5), 1672–1688. https://doi.org/10.1523/JNEUROSCI.3121-13.2014

Escartin, C., & Rouach, N. (2013). Astroglial networking contributes to neurometabolic coupling. Frontiers in neuroenergetics, 5, 4. https://doi.org/10.3389/fnene.2013.00004

Escartin, C., Galea, E., Lakatos, A., O'Callaghan, J. P., Petzold, G. C., Serrano-Pozo, A., Steinhäuser, C., Volterra, A., Carmignoto, G., Agarwal, A., Allen, N. J., Araque, A., Barbeito, L., Barzilai, A., Bergles, D. E., Bonvento, G., Butt, A. M., Chen, W. T., Cohen-Salmon, M., Cunningham, C., … Verkhratsky, A. (2021). Reactive astrocyte nomenclature, definitions, and future directions. Nature neuroscience, 24(3), 312–325. https://doi.org/10.1038/s41593-020-00783-4

Falcone, C., Penna, E., Hong, T., Tarantal, A. F., Hof, P. R., Hopkins, W. D., Sherwood, C. C., Noctor, S. C., & Martínez-Cerdeño, V. (2021). Cortical Interlaminar Astrocytes Are Generated Prenatally, Mature Postnatally, and Express Unique Markers in Human and Nonhuman Primates. Cerebral cortex (New York, N.Y. : 1991), 31(1), 379–395. https://doi.org/10.1093/cercor/bhaa231

Falcone, C., McBride, E. L., Hopkins, W. D., Hof, P. R., Manger, P. R., Sherwood, C. C., Noctor, S. C., & Martínez-Cerdeño, V. (2022). Redefining varicose projection astrocytes in primates. Glia, 70(1), 145–154. https://doi.org/10.1002/glia.24093

Faris, H., Almasieh, M., & Levin, L. A. (2021). Axonal degeneration induces distinct patterns of phosphatidylserine and phosphatidylethanolamine externalization. Cell death discovery, 7(1), 247. https://doi.org/10.1038/s41420-021-00641-7

Fell, M. J., Mirescu, C., Basu, K., Cheewatrakoolpong, B., DeMong, D. E., Ellis, J. M., Hyde, L. A., Lin, Y., Markgraf, C. G., Mei, H., Miller, M., Poulet, F. M., Scott, J. D., Smith, M. D., Yin, Z., Zhou, X., Parker, E. M., Kennedy, M. E., & Morrow, J. A. (2015). MLi-2, a Potent, Selective, and Centrally Active Compound for Exploring the Therapeutic Potential and Safety of LRRK2 Kinase Inhibition. The Journal of pharmacology and experimental therapeutics, 355(3), 397–409. https://doi.org/10.1124/jpet.115.227587

Fellner, L., Irschick, R., Schanda, K., Reindl, M., Klimaschewski, L., Poewe, W., Wenning, G. K., & Stefanova, N. (2013). Toll-like receptor 4 is required for α-synuclein dependent activation of microglia and astroglia. Glia, 61(3), 349–360. https://doi.org/10.1002/glia.22437

Filous, A. R., & Silver, J. (2016). "Targeting astrocytes in CNS injury and disease: A translational research approach". Progress in neurobiology, 144, 173–187. https://doi.org/10.1016/j.pneurobio.2016.03.009

Finnemann, S. C., Bonilha, V. L., Marmorstein, A. D., & Rodriguez-Boulan, E. (1997). Phagocytosis of rod outer segments by retinal pigment epithelial cells requires alpha(v)beta5 integrin for binding but not for internalization. Proceedings of the National Academy of Sciences of the United States of America, 94(24), 12932–12937. https://doi.org/10.1073/pnas.94.24.12932

Freeman, M. R., Delrow, J., Kim, J., Johnson, E., & Doe, C. Q. (2003). Unwrapping glial biology: Gcm target genes regulating glial development, diversification, and function. Neuron, 38(4), 567–580. https://doi.org/10.1016/s0896-6273(03)00289-7

Gabel, M., Royer, C., Thahouly, T., Calco, V., Gasman, S., Bader, M. F., Vitale, N., & Chasserot-Golaz, S. (2020). Annexin A2 Egress during Calcium-Regulated Exocytosis in Neuroendocrine Cells. Cells, 9(9), 2059. https://doi.org/10.3390/cells9092059

García-Marín, V., García-López, P., & Freire, M. (2007). Cajal's contributions to glia research. Trends in neurosciences, 30(9), 479–487. https://doi.org/10.1016/j.tins.2007.06.008

García-Marqués, J., & López-Mascaraque, L. (2013). Clonal identity determines astrocyte cortical heterogeneity. Cerebral cortex (New York, N.Y. : 1991), 23(6), 1463–1472. https://doi.org/10.1093/cercor/bhs134

Gardai, S. J., McPhillips, K. A., Frasch, S. C., Janssen, W. J., Starefeldt, A., Murphy-Ullrich, J. E., Bratton, D. L., Oldenborg, P. A., Michalak, M., & Henson, P. M. (2005). Cell-surface calreticulin initiates clearance of viable or apoptotic cells through trans-activation of LRP on the phagocyte. Cell, 123(2), 321–334. https://doi.org/10.1016/j.cell.2005.08.032

Gauthier-Kemper, A., Suárez Alonso, M., Sündermann, F., Niewidok, B., Fernandez, M. P., Bakota, L., Heinisch, J. J., & Brandt, R. (2018). Annexins A2 and A6 interact with the extreme N terminus of tau and thereby contribute to tau's axonal localization. The Journal of biological chemistry, 293(21), 8065–8076. https://doi.org/10.1074/jbc.RA117.000490

Giaume C. (2010). Astroglial Wiring is Adding Complexity to Neuroglial Networking. Frontiers in neuroenergetics, 2, 129. https://doi.org/10.3389/fnene.2010.00129

Gomez-Arboledas, A., Davila, J. C., Sanchez-Mejias, E., Navarro, V., Nuñez-Diaz, C., Sanchez-Varo, R., Sanchez-Mico, M. V., Trujillo-Estrada, L., Fernandez-Valenzuela, J. J., Vizuete, M., Comella, J. X., Galea, E., Vitorica, J., & Gutierrez, A. (2018). Phagocytic clearance of presynaptic dystrophies by reactive astrocytes in Alzheimer's disease. Glia, 66(3), 637–653. https://doi.org/10.1002/glia.23270

Gómez-Ramos, A., Díaz-Hernández, M., Cuadros, R., Hernández, F., & Avila, J. (2006). Extracellular tau is toxic to neuronal cells. FEBS letters, 580(20), 4842–4850. https://doi.org/10.1016/j.febslet.2006.07.078

Gonçalves, C. A., Leite, M. C., & Nardin, P. (2008). Biological and methodological features of the measurement of S100B, a putative marker of brain injury. Clinical biochemistry, 41(10-11), 755–763. https://doi.org/10.1016/j.clinbiochem.2008.04.003

Götz, M., & Huttner, W. B. (2005). The cell biology of neurogenesis. Nature reviews. Molecular cell biology, 6(10), 777–788. https://doi.org/10.1038/nrm1739

Graves, S. M., & Surmeier, D. J. (2019). Delayed Spine Pruning of Direct Pathway Spiny Projection Neurons in a Mouse Model of Parkinson's Disease. Frontiers in cellular neuroscience, 13, 32. https://doi.org/10.3389/fncel.2019.00032

Greggio, E., Zambrano, I., Kaganovich, A., Beilina, A., Taymans, J. M., Daniëls, V., Lewis, P., Jain, S., Ding, J., Syed, A., Thomas, K. J., Baekelandt, V., & Cookson, M. R. (2008). The Parkinson disease-associated leucine-rich repeat kinase 2 (LRRK2) is a dimer that undergoes intramolecular autophosphorylation. The Journal of biological chemistry, 283(24), 16906–16914. https://doi.org/10.1074/jbc.M708718200

Gu, X. L., Long, C. X., Sun, L., Xie, C., Lin, X., & Cai, H. (2010). Astrocytic expression of Parkinson's disease-related A53T alpha-synuclein causes neurodegeneration in mice. Molecular brain, 3, 12. https://doi.org/10.1186/1756-6606-3-12

Gunner, G., Cheadle, L., Johnson, K. M., Ayata, P., Badimon, A., Mondo, E., Nagy, M. A., Liu, L., Bemiller, S. M., Kim, K. W., Lira, S. A., Lamb, B. T., Tapper, A. R., Ransohoff, R. M., Greenberg, M. E., Schaefer, A., & Schafer, D. P. (2019). Sensory lesioning induces microglial synapse elimination via ADAM10 and fractalkine signaling. Nature neuroscience, 22(7), 1075–1088. https://doi.org/10.1038/s41593-019-0419-y

Gustafsson, G., Lindström, V., Rostami, J., Nordström, E., Lannfelt, L., Bergström, J., Ingelsson, M., & Erlandsson, A. (2017). Alpha-synuclein oligomer-selective antibodies reduce intracellular accumulation and mitochondrial impairment in alpha-synuclein exposed astrocytes. Journal of neuroinflammation, 14(1), 241. https://doi.org/10.1186/s12974-017-1018-z

Györffy, B. A., Kun, J., Török, G., Bulyáki, É., Borhegyi, Z., Gulyássy, P., Kis, V., Szocsics, P., Micsonai, A., Matkó, J., Drahos, L., Juhász, G., Kékesi, K. A., & Kardos, J. (2018). Local apoptotic-like mechanisms underlie complement-mediated synaptic pruning. Proceedings of the National Academy of Sciences of the United States of America, 115(24), 6303–6308. https://doi.org/10.1073/pnas.1722613115

Halassa, M. M., Fellin, T., & Haydon, P. G. (2007). The tripartite synapse: roles for gliotransmission in health and disease. Trends in molecular medicine, 13(2), 54–63. https://doi.org/10.1016/j.molmed.2006.12.005

Halnes, G., Ostby, I., Pettersen, K. H., Omholt, S. W., & Einevoll, G. T. (2013). Electrodiffusive model for astrocytic and neuronal ion concentration dynamics. PLoS computational biology, 9(12), e1003386. https://doi.org/10.1371/journal.pcbi.1003386

Healy, D. G., Falchi, M., O'Sullivan, S. S., Bonifati, V., Durr, A., Bressman, S., Brice, A., Aasly, J., Zabetian, C. P., Goldwurm, S., Ferreira, J. J., Tolosa, E., Kay, D. M., Klein, C., Williams, D. R., Marras, C., Lang, A. E., Wszolek, Z. K., Berciano, J., Schapira, A. H., … International LRRK2 Consortium (2008). Phenotype, genotype, and worldwide genetic penetrance of LRRK2-associated Parkinson's disease: a case-control study. The Lancet. Neurology, 7(7), 583–590. https://doi.org/10.1016/S1474-4422(08)70117-0

Hely, M. A., Reid, W. G., Adena, M. A., Halliday, G. M., & Morris, J. G. (2008). The Sydney multicenter study of Parkinson's disease: the inevitability of dementia at 20 years. Movement disorders: official journal of the Movement Disorder Society, 23(6), 837–844. https://doi.org/10.1002/mds.21956

Henstridge, C. M., Pickett, E., & Spires-Jones, T. L. (2016). Synaptic pathology: A shared mechanism in neurological disease. Ageing research reviews, 28, 72–84. https://doi.org/10.1016/j.arr.2016.04.005

Henstridge, C. M., Sideris, D. I., Carroll, E., Rotariu, S., Salomonsson, S., Tzioras, M., McKenzie, C. A., Smith, C., von Arnim, C. A. F., Ludolph, A. C., Lulé, D., Leighton, D., Warner, J., Cleary, E., Newton, J., Swingler, R., Chandran, S., Gillingwater, T. H., Abrahams, S., & Spires-Jones, T. L. (2018). Synapse loss in the prefrontal cortex is associated with cognitive decline in amyotrophic lateral sclerosis. Acta neuropathologica, 135(2), 213–226. https://doi.org/10.1007/s00401-017-1797-4

Herbst, S., Campbell, P., Harvey, J., Bernard, E. M., Papayannopoulos, V., Wood, N. W., Morris, H. R., & Gutierrez, M. G. (2020). LRRK2 activation controls the repair of damaged endomembranes in macrophages. The EMBO journal, 39(18), e104494. https://doi.org/10.15252/embj.2020104494ù

Herculano-Houzel S. (2014). The glia/neuron ratio: how it varies uniformly across brain structures and species and what that means for brain physiology and evolution. Glia, 62(9), 1377–1391. https://doi.org/10.1002/glia.22683

Hertz, L., Xu, J., Song, D., Yan, E., Gu, L., & Peng, L. (2013). Astrocytic and neuronal accumulation of elevated extracellular K(+) with a 2/3 K(+)/Na(+) flux ratio-consequences for energy metabolism, osmolarity and higher brain function. Frontiers in computational neuroscience, 7, 114. https://doi.org/10.3389/fncom.2013.00114

Hodara, R., Norris, E. H., Giasson, B. I., Mishizen-Eberz, A. J., Lynch, D. R., Lee, V. M., & Ischiropoulos, H. (2004). Functional consequences of alpha-synuclein tyrosine nitration: diminished binding to lipid vesicles and increased fibril formation. The Journal of biological chemistry, 279(46), 47746–47753. https://doi.org/10.1074/jbc.M408906200

Hong, S., Beja-Glasser, V. F., Nfonoyim, B. M., Frouin, A., Li, S., Ramakrishnan, S., Merry, K. M., Shi, Q., Rosenthal, A., Barres, B. A., Lemere, C. A., Selkoe, D. J., & Stevens, B. (2016). Complement and microglia mediate early synapse loss in Alzheimer mouse models. Science (New York, N.Y.), 352(6286), 712–716. https://doi.org/10.1126/science.aad8373

Huang, J., Ding, J., Wang, X., Gu, C., He, Y., Li, Y., Fan, H., Xie, Q., Qi, X., Wang, Z., & Qiu, P. (2022). Transfer of neuron-derived α-synuclein to astrocytes induces neuroinflammation and blood-brain barrier damage after methamphetamine exposure: Involving the regulation of nuclear receptor-associated protein 1. Brain, behavior, and immunity, 106, 247–261. https://doi.org/10.1016/j.bbi.2022.09.002

Huber, W., Carey, V. J., Gentleman, R., Anders, S., Carlson, M., Carvalho, B. S., Bravo, H. C., Davis, S., Gatto, L., Girke, T., Gottardo, R., Hahne, F., Hansen, K. D., Irizarry, R. A., Lawrence, M., Love, M. I., MacDonald, J., Obenchain, V., Oleś, A. K., Pagès, H., … Morgan, M. (2015). Orchestrating high-throughput genomic analysis with Bioconductor. Nature methods, 12(2), 115–121. https://doi.org/10.1038/nmeth.3252

Ihse, E., Yamakado, H., van Wijk, X. M., Lawrence, R., Esko, J. D., & Masliah, E. (2017). Cellular internalization of alpha-synuclein aggregates by cell surface heparan sulfate depends on aggregate conformation and cell type. Scientific reports, 7(1), 9008. https://doi.org/10.1038/s41598-017-08720-5

Iovino, L., Giusti, V., Pischedda, F., Giusto, E., Plotegher, N., Marte, A., Battisti, I., Di Iacovo, A., Marku, A., Piccoli, G., Bandopadhyay, R., Perego, C., Bonifacino, T., Bonanno, G., Roseti, C., Bossi, E., Arrigoni, G., Bubacco, L., Greggio, E., Hilfiker, S., … Civiero, L. (2022). Trafficking of the glutamate transporter is impaired in LRRK2-related Parkinson's disease. Acta neuropathologica, 144(1), 81–106. https://doi.org/10.1007/s00401-022-02437-0

Iovino, L., Tremblay, M. E., & Civiero, L. (2020). Glutamate-induced excitotoxicity in Parkinson's disease: The role of glial cells. Journal of pharmacological sciences, 144(3), 151–164. https://doi.org/10.1016/j.jphs.2020.07.011

Iram, T., Ramirez-Ortiz, Z., Byrne, M. H., Coleman, U. A., Kingery, N. D., Means, T. K., Frenkel, D., & El Khoury, J. (2016). Megf10 Is a Receptor for C1Q That Mediates Clearance of Apoptotic Cells by Astrocytes. The Journal of neuroscience : the official journal of the Society for Neuroscience, 36(19), 5185–5192. https://doi.org/10.1523/JNEUROSCI.3850-15.2016

Jakel, R. J., & Stacy, M. (2014). Parkinson's disease psychosis. J Parkinsonism Restless Legs Syndrome, 4, 41-51.

Jaleel, M., Nichols, R. J., Deak, M., Campbell, D. G., Gillardon, F., Knebel, A., & Alessi, D. R. (2007). LRRK2 phosphorylates moesin at threonine-558: characterization of how Parkinson's disease mutants affect kinase activity. The Biochemical journal, 405(2), 307–317. https://doi.org/10.1042/BJ20070209

Jang, A., Lee, H. J., Suk, J. E., Jung, J. W., Kim, K. P., & Lee, S. J. (2010). Non-classical exocytosis of alpha-synuclein is sensitive to folding states and promoted under stress conditions. Journal of neurochemistry, 113(5), 1263–1274. https://doi.org/10.1111/j.1471-4159.2010.06695.x

Jankovic J. (2005). Motor fluctuations and dyskinesias in Parkinson's disease: clinical manifestations. Movement disorders : official journal of the Movement Disorder Society, 20 Suppl 11, S11–S16. https://doi.org/10.1002/mds.20458

Jankovic, J., & Aguilar, L. G. (2008). Current approaches to the treatment of Parkinson's disease. Neuropsychiatric disease and treatment, 4(4), 743–757. https://doi.org/10.2147/ndt.s2006

Janković, S. M., Sokić, D. V., Vojvodić, N. M., & Ristić, A. J. (2006). Srpski arhiv za celokupno lekarstvo, 134(9-10), 466–469. https://doi.org/10.2298/sarh0610466j

Jay, T. R., von Saucken, V. E., Muñoz, B., Codocedo, J. F., Atwood, B. K., Lamb, B. T., & Landreth, G. E. (2019). TREM2 is required for microglial instruction of astrocytic synaptic engulfment in neurodevelopment. Glia, 67(10), 1873–1892. https://doi.org/10.1002/glia.23664

Jha, M. K., Jo, M., Kim, J. H., & Suk, K. (2019). Microglia-Astrocyte Crosstalk: An Intimate Molecular Conversation. The Neuroscientist : a review journal bringing neurob

Jha, M. K., Jo, M., Kim, J. H., and Suk, K. (2018). Microglia- astrocyte crosstalk: an intimate molecular conversation. Neuroscientist doi: 10.1177/1073858418783959 [Epub ahead of print].

Jo, S., Yarishkin, O., Hwang, Y. J., Chun, Y. E., Park, M., Woo, D. H., Bae, J. Y., Kim, T., Lee, J., Chun, H., Park, H. J., Lee, D. Y., Hong, J., Kim, H. Y., Oh, S. J., Park, S. J., Lee, H., Yoon, B. E., Kim, Y., Jeong, Y., … Lee, C. J. (2014). GABA from reactive astrocytes impairs memory in mouse models of Alzheimer's disease. Nature medicine, 20(8), 886–896. https://doi.org/10.1038/nm.3639

Joe, E. H., Choi, D. J., An, J., Eun, J. H., Jou, I., & Park, S. (2018). Astrocytes, Microglia, and Parkinson's Disease. Experimental neurobiology, 27(2), 77–87. https://doi.org/10.5607/en.2018.27.2.77

Jones, R. S., Minogue, A. M., Connor, T. J., & Lynch, M. A. (2013). Amyloid-β-induced astrocytic phagocytosis is mediated by CD36, CD47 and RAGE. Journal of neuroimmune pharmacology : the official journal of the Society on NeuroImmune Pharmacology, 8(1), 301–311. https://doi.org/10.1007/s11481-012-9427-3

Joshi, A. U., Minhas, P. S., Liddelow, S. A., Haileselassie, B., Andreasson, K. I., Dorn, G. W., 2nd, & Mochly-Rosen, D. (2019). Fragmented mitochondria released from microglia trigger A1 astrocytic response and propagate inflammatory neurodegeneration. Nature neuroscience, 22(10), 1635–1648. https://doi.org/10.1038/s41593-019-0486-0

Jung, Y. J., & Chung, W. S. (2018). Phagocytic Roles of Glial Cells in Healthy and Diseased Brains. Biomolecules & therapeutics, 26(4), 350–357. https://doi.org/10.4062/biomolther.2017.133

Kabba, J. A., Xu, Y., Christian, H., Ruan, W., Chenai, K., Xiang, Y., Zhang, L., Saavedra, J. M., & Pang, T. (2018). Microglia: Housekeeper of the Central Nervous System. Cellular and molecular neurobiology, 38(1), 53–71. https://doi.org/10.1007/s10571-017-0504-2

Kalia, L. V., & Lang, A. E. (2015). Parkinson's disease. Lancet (London, England), 386(9996), 896–912. https://doi.org/10.1016/S0140-6736(14)61393-3

Kalinderi, K., Bostantjopoulou, S., & Fidani, L. (2016). The genetic background of Parkinson's disease: current progress and future prospects. Acta neurologica Scandinavica, 134(5), 314–326. https://doi.org/10.1111/ane.12563

Kamiyama, T., Yoshioka, N., & Sakurai, M. (2006). Synapse elimination in the corticospinal projection during the early postnatal period. Journal of neurophysiology, 95(4), 2304–2313. https://doi.org/10.1152/jn.00295.2005

Kato, U., Inadome, H., Yamamoto, M., Emoto, K., Kobayashi, T., & Umeda, M. (2013). Role for phospholipid flippase complex of ATP8A1 and CDC50A proteins in cell migration. The Journal of biological chemistry, 288(7), 4922–4934. https://doi.org/10.1074/jbc.M112.402701

Keeney, P. M., Xie, J., Capaldi, R. A., & Bennett, J. P., Jr (2006). Parkinson's disease brain mitochondrial complex I has oxidatively damaged subunits and is functionally impaired and misassembled. The Journal of neuroscience : the official journal of the Society for Neuroscience, 26(19), 5256–5264. https://doi.org/10.1523/JNEUROSCI.0984-06.2006

Khan, S. S., Sobu, Y., Dhekne, H. S., Tonelli, F., Berndsen, K., Alessi, D. R., & Pfeffer, S. R. (2021). Pathogenic LRRK2 control of primary cilia and Hedgehog signaling in neurons and astrocytes of mouse brain. eLife, 10, e67900. https://doi.org/10.7554/eLife.67900

Kierdorf, K., Erny, D., Goldmann, T., Sander, V., Schulz, C., Perdiguero, E. G., Wieghofer, P., Heinrich, A., Riemke, P., Hölscher, C., Müller, D. N., Luckow, B., Brocker, T., Debowski, K., Fritz,

G., Opdenakker, G., Diefenbach, A., Biber, K., Heikenwalder, M., Geissmann, F., … Prinz, M. (2013). Microglia emerge from erythromyeloid precursors via Pu.1- and Irf8-dependent pathways. Nature neuroscience, 16(3), 273–280. https://doi.org/10.1038/nn.3318

Kim, C., Ho, D. H., Suk, J. E., You, S., Michael, S., Kang, J., Joong Lee, S., Masliah, E., Hwang, D., Lee, H. J., & Lee, S. J. (2013). Neuron-released oligomeric α-synuclein is an endogenous agonist of TLR2 for paracrine activation of microglia. Nature communications, 4, 1562. https://doi.org/10.1038/ncomms2534

Kim, K. S., Marcogliese, P. C., Yang, J., Callaghan, S. M., Resende, V., Abdel-Messih, E., Marras, C., Visanji, N. P., Huang, J., Schlossmacher, M. G., Trinkle-Mulcahy, L., Slack, R. S., Lang, A. E., Canadian Lrrk2 in Inflammation Team (CLINT), & Park, D. S. (2018). Regulation of myeloid cell phagocytosis by LRRK2 via WAVE2 complex stabilization is altered in Parkinson's disease. Proceedings of the National Academy of Sciences of the United States of America, 115(22), E5164–E5173. https://doi.org/10.1073/pnas.1718946115

Kim, N. S., & Chung, W. S. (2022). Astrocytes regulate neuronal network activity by mediating synapse remodeling. Neuroscience research, S0168-0102(22)00252-8. Advance online publication. https://doi.org/10.1016/j.neures.2022.09.007

Kim, Y., Ho, S. O., Gassman, N. R., Korlann, Y., Landorf, E. V., Collart, F. R., & Weiss, S. (2008). Efficient site-specific labeling of proteins via cysteines. Bioconjugate chemistry, 19(3), 786–791. https://doi.org/10.1021/bc7002499

Klegeris, A., Giasson, B. I., Zhang, H., Maguire, J., Pelech, S., & McGeer, P. L. (2006). Alpha-synuclein and its disease-causing mutants induce ICAM-1 and IL-6 in human astrocytes and astrocytoma cells. FASEB journal : official publication of the Federation of American Societies for Experimental Biology, 20(12), 2000–2008. https://doi.org/10.1096/fj.06-6183com

Koch, C., & Engele, J. (2020). Functions of the CXCL12 Receptor ACKR3/CXCR7-What Has Been Perceived and What Has Been Overlooked. Molecular pharmacology, 98(5), 577–585. https://doi.org/10.1124/molpharm.120.000056

Koeppen, J., Nguyen, A. Q., Nikolakopoulou, A. M., Garcia, M., Hanna, S., Woodruff, S., Figueroa, Z., Obenaus, A., & Ethell, I. M. (2018). Functional Consequences of Synapse Remodeling Following Astrocyte-Specific Regulation of Ephrin-B1 in the Adult Hippocampus. The Journal of neuroscience : the official journal of the Society for Neuroscience, 38(25), 5710–5726. https://doi.org/10.1523/JNEUROSCI.3618-17.2018

Koeppen, J., Nguyen, A. Q., Nikolakopoulou, A. M., Garcia, M., Hanna, S., Woodruff, S., Figueroa, Z., Obenaus, A., & Ethell, I. M. (2018). Functional Consequences of Synapse Remodeling Following Astrocyte-Specific Regulation of Ephrin-B1 in the Adult Hippocampus. The Journal of neuroscience : the official journal of the Society for Neuroscience, 38(25), 5710–5726.

Koistinaho, M., Lin, S., Wu, X., Esterman, M., Koger, D., Hanson, J., Higgs, R., Liu, F., Malkani, S., Bales, K. R., & Paul, S. M. (2004). Apolipoprotein E promotes astrocyte colocalization and degradation of deposited amyloid-beta peptides. Nature medicine, 10(7), 719–726. https://doi.org/10.1038/nm1058

Konishi, H., Koizumi, S., & Kiyama, H. (2022). Phagocytic astrocytes: Emerging from the shadows of microglia. Glia, 70(6), 1009–1026. https://doi.org/10.1002/glia.24145

Konishi, H., Okamoto, T., Hara, Y., Komine, O., Tamada, H., Maeda, M., Osako, F., Kobayashi, M., Nishiyama, A., Kataoka, Y., Takai, T., Udagawa, N., Jung, S., Ozato, K., Tamura, T., Tsuda, M., Yamanaka, K., Ogi, T., Sato, K., & Kiyama, H. (2020). Astrocytic phagocytosis is a compensatory mechanism for microglial dysfunction. The EMBO journal, 39(22), e104464. https://doi.org/10.15252/embj.2020104464

Krieger, J., Sforza, E., Apprill, M., Lampert, E., Weitzenblum, E., & Ratomaharo, J. (1989). Pulmonary hypertension, hypoxemia, and hypercapnia in obstructive sleep apnea patients. Chest, 96(4), 729–737. https://doi.org/10.1378/chest.96.4.729

Kumamaru, H., Saiwai, H., Kobayakawa, K., Kubota, K., van Rooijen, N., Inoue, K., Iwamoto, Y., & Okada, S. (2012). Liposomal clodronate selectively eliminates microglia from primary astrocyte cultures. Journal of neuroinflammation, 9, 116. https://doi.org/10.1186/1742-2094-9-116

Law, A. L., Ling, Q., Hajjar, K. A., Futter, C. E., Greenwood, J., Adamson, P., Wavre-Shapton, S. T., Moss, S. E., & Hayes, M. J. (2009). Annexin A2 regulates phagocytosis of photoreceptor outer segments in the mouse retina. Molecular biology of the cell, 20(17), 3896–3904. https://doi.org/10.1091/mbc.e08-12-1204

Lawand, N. B., Saadé, N. E., El-Agnaf, O. M., & Safieh-Garabedian, B. (2015). Targeting α-synuclein as a therapeutic strategy for Parkinson's disease. Expert opinion on therapeutic targets, 19(10), 1351–1360. https://doi.org/10.1517/14728222.2015.1062877

Lee, H. J., Patel, S., & Lee, S. J. (2005). Intravesicular localization and exocytosis of alpha-synuclein and its aggregates. The Journal of neuroscience : the official journal of the Society for Neuroscience, 25(25), 6016–6024. https://doi.org/10.1523/JNEUROSCI.0692-05.2005

Lee, H. J., Suk, J. E., Bae, E. J., & Lee, S. J. (2008). Clearance and deposition of extracellular alpha-synuclein aggregates in microglia. Biochemical and biophysical research communications, 372(3), 423–428. https://doi.org/10.1016/j.bbrc.2008.05.045

Lee, J. H., Han, J. H., Kim, H., Park, S. M., Joe, E. H., & Jou, I. (2019). Parkinson's disease-associated LRRK2-G2019S mutant acts through regulation of SERCA activity to control ER stress in astrocytes. Acta neuropathologica communications, 7(1), 68. https://doi.org/10.1186/s40478-019-0716-4

Lee, J. H., Kim, J. Y., Noh, S., Lee, H., Lee, S. Y., Mun, J. Y., Park, H., & Chung, W. S. (2021). Astrocytes phagocytose adult hippocampal synapses for circuit homeostasis. Nature, 590(7847), 612–617. https://doi.org/10.1038/s41586-020-03060-3

Lee, S. J., Desplats, P., Sigurdson, C., Tsigelny, I., & Masliah, E. (2010). Cell-to-cell transmission of non-prion protein aggregates. Nature reviews. Neurology, 6(12), 702–706. https://doi.org/10.1038/nrneurol.2010.145

Lee, S. J., Jeon, H., & Kandror, K. V. (2008). Alpha-synuclein is localized in a subpopulation of rat brain synaptic vesicles. Acta neurobiologiae experimentalis, 68(4), 509–515.

Lemke G. (2013). Biology of the TAM receptors. Cold Spring Harbor perspectives in biology, 5(11), a009076. https://doi.org/10.1101/cshperspect.a009076

Levoye, A., Balabanian, K., Baleux, F., Bachelerie, F., & Lagane, B. (2009). CXCR7 heterodimerizes with CXCR4 and regulates CXCL12-mediated G protein signaling. Blood, 113(24), 6085–6093. https://doi.org/10.1182/blood-2008-12-196618

Levy, O. A., Malagelada, C., & Greene, L. A. (2009). Cell death pathways in Parkinson's disease: proximal triggers, distal effectors, and final steps. Apoptosis : an international journal on programmed cell death, 14(4), 478–500. https://doi.org/10.1007/s10495-008-0309-3

Li, T., Chiou, B., Gilman, C. K., Luo, R., Koshi, T., Yu, D., Oak, H. C., Giera, S., Johnson-Venkatesh, E., Muthukumar, A. K., Stevens, B., Umemori, H., & Piao, X. (2020). A splicing isoform of GPR56 mediates microglial synaptic refinement via phosphatidylserine binding. The EMBO journal, 39(16), e104136. https://doi.org/10.15252/embj.2019104136

Li, T., Yu, D., Oak, H. C., Zhu, B., Wang, L., Jiang, X., Molday, R. S., Kriegstein, A., & Piao, X. (2021). Phospholipid-flippase chaperone CDC50A is required for synapse maintenance by regulating phosphatidylserine exposure. The EMBO journal, 40(21), e107915. https://doi.org/10.15252/embj.2021107915

Lian, H., Litvinchuk, A., Chiang, A. C., Aithmitti, N., Jankowsky, J. L., & Zheng, H. (2016). Astrocyte-Microglia Cross Talk through Complement Activation Modulates Amyloid Pathology in Mouse Models of Alzheimer's Disease. The Journal of neuroscience : the official journal of the Society for Neuroscience, 36(2), 577–589. https://doi.org/10.1523/JNEUROSCI.2117-15.2016

Liddelow, S. A., Guttenplan, K. A., Clarke, L. E., Bennett, F. C., Bohlen, C. J., Schirmer, L., Bennett, M. L., Münch, A. E., Chung, W. S., Peterson, T. C., Wilton, D. K., Frouin, A., Napier, B. A., Panicker, N., Kumar, M., Buckwalter, M. S., Rowitch, D. H., Dawson, V. L., Dawson, T. M., Stevens, B., … Barres, B. A. (2017). Neurotoxic reactive astrocytes are induced by activated microglia. Nature, 541(7638), 481–487. https://doi.org/10.1038/nature21029

Lindström, V., Gustafsson, G., Sanders, L. H., Howlett, E. H., Sigvardson, J., Kasrayan, A., Ingelsson, M., Bergström, J., & Erlandsson, A. (2017). Extensive uptake of α-synuclein oligomers in astrocytes results in sustained intracellular deposits and mitochondrial damage. Molecular and cellular neurosciences, 82, 143–156. https://doi.org/10.1016/j.mcn.2017.04.009

Liu, C. C., Hu, J., Zhao, N., Wang, J., Wang, N., Cirrito, J. R., Kanekiyo, T., Holtzman, D. M., & Bu, G. (2017). Astrocytic LRP1 Mediates Brain Aβ Clearance and Impacts Amyloid Deposition. The Journal of neuroscience : the official journal of the Society for Neuroscience, 37(15), 4023–4031. https://doi.org/10.1523/JNEUROSCI.3442-16.2017

Liu, Y., Carson-Walter, E., & Walter, K. A. (2014). Chemokine receptor CXCR7 is a functional receptor for CXCL12 in brain endothelial cells. PloS one, 9(8), e103938. https://doi.org/10.1371/journal.pone.0103938

Liu, Z., Xu, E., Zhao, H. T., Cole, T., & West, A. B. (2020). LRRK2 and Rab10 coordinate macropinocytosis to mediate immunological responses in phagocytes. The EMBO journal, 39(20), e104862. https://doi.org/10.15252/embj.2020104862

Lööv, C., Mitchell, C. H., Simonsson, M., & Erlandsson, A. (2015). Slow degradation in phagocytic astrocytes can be enhanced by lysosomal acidification. Glia, 63(11), 1997–2009. https://doi.org/10.1002/glia.22873

Loria, F., Vargas, J. Y., Bousset, L., Syan, S., Salles, A., Melki, R., & Zurzolo, C. (2017). α-Synuclein transfer between neurons and astrocytes indicates that astrocytes play a role in degradation rather than in spreading. Acta neuropathologica, 134(5), 789–808. https://doi.org/10.1007/s00401-017-1746-2

Lovatt, D., Sonnewald, U., Waagepetersen, H. S., Schousboe, A., He, W., Lin, J. H., Han, X., Takano, T., Wang, S., Sim, F. J., Goldman, S. A., & Nedergaard, M. (2007). The transcriptome and metabolic gene signature of protoplasmic astrocytes in the adult murine cortex. The Journal of neuroscience : the official journal of the Society for Neuroscience, 27(45), 12255–12266. https://doi.org/10.1523/JNEUROSCI.3404-07.2007

Lucas, C. V., Reaven, E. P., Bensch, K. G., & Eng, L. F. (1980). Immunoperoxidase staining of glial fibrillary acidic (GFA) protein polymerized in vitro: an ultramicroscopic study. Neurochemical research, 5(11), 1199–1209. https://doi.org/10.1007/BF00964899

Luk, K. C., Kehm, V., Carroll, J., Zhang, B., O'Brien, P., Trojanowski, J. Q., & Lee, V. M. (2012). Pathological α-synuclein transmission initiates Parkinson-like neurodegeneration in nontransgenic mice. Science (New York, N.Y.), 338(6109), 949–953. https://doi.org/10.1126/science.1227157

Määttä, T. A., Rettel, M., Sridharan, S., Helm, D., Kurzawa, N., Stein, F., & Savitski, M. M. (2020). Aggregation and disaggregation features of the human proteome. Molecular systems biology, 16(10), e9500. https://doi.org/10.15252/msb.20209500

Magnus, T., Chan, A., Linker, R. A., Toyka, K. V., & Gold, R. (2002). Astrocytes are less efficient in the removal of apoptotic lymphocytes than microglia cells: implications for the role of glial cells in the inflamed central nervous system. Journal of neuropathology and experimental neurology, 61(9), 760–766. https://doi.org/10.1093/jnen/61.9.760

Mahul-Mellier, A. L., Burtscher, J., Maharjan, N., Weerens, L., Croisier, M., Kuttler, F., Leleu, M., Knott, G. W., & Lashuel, H. A. (2020). The process of Lewy body formation, rather than simply α-synuclein fibrillization, is one of the major drivers of neurodegeneration. Proceedings of the National Academy of Sciences of the United States of America, 117(9), 4971–4982. https://doi.org/10.1073/pnas.1913904117

Männistö, P. T., & García-Horsman, J. A. (2017). Mechanism of Action of Prolyl Oligopeptidase (PREP) in Degenerative Brain Diseases: Has Peptidase Activity Only a Modulatory Role on the Interactions of PREP with Proteins?. Frontiers in aging neuroscience, 9, 27. https://doi.org/10.3389/fnagi.2017.00027

Manzoni, C., Mamais, A., Dihanich, S., Abeti, R., Soutar, M. P. M., Plun-Favreau, H., Giunti, P., Tooze, S. A., Bandopadhyay, R., & Lewis, P. A. (2013a). Inhibition of LRRK2 kinase activity stimulates macroautophagy. Biochimica et biophysica acta, 1833(12), 2900–2910. https://doi.org/10.1016/j.bbamcr.2013.07.020

Manzoni, C., Mamais, A., Dihanich, S., McGoldrick, P., Devine, M. J., Zerle, J., Kara, E., Taanman, J. W., Healy, D. G., Marti-Masso, J. F., Schapira, A. H., Plun-Favreau, H., Tooze, S., Hardy, J., Bandopadhyay, R., & Lewis, P. A. (2013b). Pathogenic Parkinson's disease mutations across the functional domains of LRRK2 alter the autophagic/lysosomal response to starvation. Biochemical and biophysical research communications, 441(4), 862–866. https://doi.org/10.1016/j.bbrc.2013.10.159

Manzoni, C., Mamais, A., Roosen, D. A., Dihanich, S., Soutar, M. P., Plun-Favreau, H., Bandopadhyay, R., Hardy, J., Tooze, S. A., Cookson, M. R., & Lewis, P. A. (2016). mTOR independent regulation of macroautophagy by Leucine Rich Repeat Kinase 2 via Beclin-1. Scientific reports, 6, 35106. https://doi.org/10.1038/srep35106

Maruyama, T., Otagiri, M., & Takadate, A. (1990). Characterization of drug binding sites on alpha 1-acid glycoprotein. Chemical & pharmaceutical bulletin, 38(6), 1688–1691. https://doi.org/10.1248/cpb.38.1688

Massano, J., & Bhatia, K. P. (2012). Clinical approach to Parkinson's disease: features, diagnosis, and principles of management. Cold Spring Harbor perspectives in medicine, 2(6), a008870. https://doi.org/10.1101/cshperspect.a008870

McMahan U. J. (1967). Fine structure of synapses in the dorsal nucleus of the lateral geniculate body of normal and blinded rats. Zeitschrift fur Zellforschung und mikroskopische Anatomie (Vienna, Austria : 1948), 76(1), 116–146. https://doi.org/10.1007/BF00337036

Medina, M., & Avila, J. (2014). The role of extracellular Tau in the spreading of neurofibrillary pathology. Frontiers in cellular neuroscience, 8, 113. https://doi.org/10.3389/fncel.2014.00113

Middeldorp, J., & Hol, E. M. (2011). GFAP in health and disease. Progress in neurobiology, 93(3), 421–443. https://doi.org/10.1016/j.pneurobio.2011.01.005

Miklossy, J., Arai, T., Guo, J. P., Klegeris, A., Yu, S., McGeer, E. G., & McGeer, P. L. (2006). LRRK2 expression in normal and pathologic human brain and in human cell lines. Journal of neuropathology and experimental neurology, 65(10), 953–963. https://doi.org/10.1097/01.jnen.0000235121.98052.54

Mioka, T., Fujimura-Kamada, K., Mizugaki, N., Kishimoto, T., Sano, T., Nunome, H., Williams, D. E., Andersen, R. J., & Tanaka, K. (2018). Phospholipid flippases and Sfk1p, a novel regulator of phospholipid asymmetry, contribute to low permeability of the plasma membrane. Molecular biology of the cell, 29(10), 1203–1218. https://doi.org/10.1091/mbc.E17-04-0217

Miyata, T., Kawaguchi, A., Okano, H., & Ogawa, M. (2001). Asymmetric inheritance of radial glial fibers by cortical neurons. Neuron, 31(5), 727–741. https://doi.org/10.1016/s0896-6273(01)00420-2

Mochizuki, H., Choong, C. J., & Masliah, E. (2018). A refined concept: α-synuclein dysregulation disease. Neurochemistry international, 119, 84–96. https://doi.org/10.1016/j.neuint.2017.12.011

Moreau, K., Ghislat, G., Hochfeld, W., Renna, M., Zavodszky, E., Runwal, G., Puri, C., Lee, S., Siddiqi, F., Menzies, F. M., Ravikumar, B., & Rubinsztein, D. C. (2015). Transcriptional regulation of Annexin A2 promotes starvation-induced autophagy. Nature communications, 6, 8045. https://doi.org/10.1038/ncomms9045

Morizawa, Y. M., Hirayama, Y., Ohno, N., Shibata, S., Shigetomi, E., Sui, Y., Nabekura, J., Sato, K., Okajima, F., Takebayashi, H., Okano, H., & Koizumi, S. (2017). Reactive astrocytes function as phagocytes after brain ischemia via ABCA1-mediated pathway. Nature communications, 8(1), 28. https://doi.org/10.1038/s41467-017-00037-1

Morozova, K., Sridhar, S., Zolla, V., Clement, C. C., Scharf, B., Verzani, Z., Diaz, A., Larocca, J. N., Hajjar, K. A., Cuervo, A. M., & Santambrogio, L. (2015). Annexin A2 promotes phagophore assembly by enhancing Atg16L^{+} vesicle biogenesis and homotypic fusion. Nature communications, 6, 5856. https://doi.org/10.1038/ncomms6856

Mozrzymas, J., Szczęsny, T., & Rakus, D. (2011). The effect of glycogen phosphorolysis on basal glutaminergic transmission. Biochemical and biophysical research communications, 404(2), 652–655. https://doi.org/10.1016/j.bbrc.2010.12.033

Mugnaini, E., & Walberg, F. (1967). An experimental electron microscopical study on the mode of termination of cerebellar corticovestibular fibres in the cat lateral vestibular nucleus (Deiters' nucleus). Experimental brain research, 4(3), 212–236. https://doi.org/10.1007/BF00248023

Nalls, M. A., McLean, C. Y., Rick, J., Eberly, S., Hutten, S. J., Gwinn, K., Sutherland, M., Martinez, M., Heutink, P., Williams, N. M., Hardy, J., Gasser, T., Brice, A., Price, T. R., Nicolas, A., Keller, M. F., Molony, C., Gibbs, J. R., Chen-Plotkin, A., Suh, E., … Parkinson's Disease Biomarkers Program and Parkinson's Progression Marker Initiative investigators (2015). Diagnosis of Parkinson's disease on the basis of clinical and genetic classification: a population-based modelling study. The Lancet. Neurology, 14(10), 1002–1009. https://doi.org/10.1016/S1474-4422(15)00178-7

Nayak, D., Roth, T. L., & McGavern, D. B. (2014). Microglia development and function. Annual review of immunology, 32, 367–402. https://doi.org/10.1146/annurev-immunol-032713-120240

Negro, S., Stazi, M., Marchioretto, M., Tebaldi, T., Rodella, U., Duregotti, E., Gerke, V., Quattrone, A., Montecucco, C., Rigoni, M., & Viero, G. (2018). Hydrogen peroxide is a neuronal alarmin that triggers specific RNAs, local translation of Annexin A2, and cytoskeletal remodeling in Schwann cells. RNA (New York, N.Y.), 24(7), 915–925. https://doi.org/10.1261/rna.064816.117

Noctor, S. C., Flint, A. C., Weissman, T. A., Dammerman, R. S., & Kriegstein, A. R. (2001). Neurons derived from radial glial cells establish radial units in neocortex. Nature, 409(6821), 714–720. https://doi.org/10.1038/35055553

Norenberg M. D. (1979). Distribution of glutamine synthetase in the rat central nervous system. The journal of histochemistry and cytochemistry : official journal of the Histochemistry Society, 27(3), 756–762. https://doi.org/10.1177/27.3.39099

Noyce, A. J., Bestwick, J. P., Silveira-Moriyama, L., Hawkes, C. H., Giovannoni, G., Lees, A. J., & Schrag, A. (2012). Meta-analysis of early nonmotor features and risk factors for Parkinson disease. Annals of neurology, 72(6), 893–901. https://doi.org/10.1002/ana.23687

Nwaobi, S. E., Cuddapah, V. A., Patterson, K. C., Randolph, A. C., & Olsen, M. L. (2016). The role of glial-specific Kir4.1 in normal and pathological states of the CNS. Acta neuropathologica, 132(1), 1–21. https://doi.org/10.1007/s00401-016-1553-1

Obara, M., Szeliga, M., & Albrecht, J. (2008). Regulation of pH in the mammalian central nervous system under normal and pathological conditions: facts and hypotheses. Neurochemistry international, 52(6), 905–919. https://doi.org/10.1016/j.neuint.2007.10.015

Oberheim, N. A., Takano, T., Han, X., He, W., Lin, J. H., Wang, F., Xu, Q., Wyatt, J. D., Pilcher, W., Ojemann, J. G., Ransom, B. R., Goldman, S. A., & Nedergaard, M. (2009). Uniquely hominid features of adult human astrocytes. The Journal of neuroscience : the official journal of the Society for Neuroscience, 29(10), 3276–3287. https://doi.org/10.1523/JNEUROSCI.4707-08.2009

Odemis, V., Moepps, B., Gierschik, P., & Engele, J. (2002). Interleukin-6 and cAMP induce stromal cell-derived factor-1 chemotaxis in astroglia by up-regulating CXCR4 cell surface expression. Implications for brain inflammation. The Journal of biological chemistry, 277(42), 39801–39808. https://doi.org/10.1074/jbc.M200472200

Paisán-Ruíz, C., Jain, S., Evans, E. W., Gilks, W. P., Simón, J., van der Brug, M., López de Munain, A., Aparicio, S., Gil, A. M., Khan, N., Johnson, J., Martinez, J. R., Nicholl, D., Martí Carrera, I., Pena, A. S., de Silva, R., Lees, A., Martí-Massó, J. F., Pérez-Tur, J., Wood, N. W., … Singleton, A. B. (2004). Cloning of the gene containing mutations that cause PARK8-linked Parkinson's disease. Neuron, 44(4), 595–600. https://doi.org/10.1016/j.neuron.2004.10.023

Paisán-Ruiz, C., Lewis, P. A., & Singleton, A. B. (2013). LRRK2: cause, risk, and mechanism. Journal of Parkinson's disease, 3(2), 85–103. https://doi.org/10.3233/JPD-130192

Pan, J., Ma, N., Yu, B., Zhang, W., & Wan, J. (2020). Transcriptomic profiling of microglia and astrocytes throughout aging. Journa

Panatier, A., Arizono, M., & Nägerl, U. V. (2014). Dissecting tripartite synapses with STED microscopy. Philosophical transactions of the Royal Society of London. Series B, Biological sciences, 369(1654), 20130597. https://doi.org/10.1098/rstb.2013.0597

Paolicelli, R. C., Bolasco, G., Pagani, F., Maggi, L., Scianni, M., Panzanelli, P., Giustetto, M., Ferreira, T. A., Guiducci, E., Dumas, L., Ragozzino, D., & Gross, C. T. (2011). Synaptic pruning by microglia is necessary for normal brain development. Science (New York, N.Y.), 333(6048), 1456–1458. https://doi.org/10.1126/science.1202529

Paolicelli, R. C., Jawaid, A., Henstridge, C. M., Valeri, A., Merlini, M., Robinson, J. L., Lee, E. B., Rose, J., Appel, S., Lee, V. M., Trojanowski, J. Q., Spires-Jones, T., Schulz, P. E., & Rajendran, L. (2017). TDP-43 Depletion in Microglia Promotes Amyloid Clearance but Also Induces Synapse Loss. Neuron, 95(2), 297–308.e6. https://doi.org/10.1016/j.neuron.2017.05.037

Park, J., Choi, Y., Jung, E., Lee, S. H., Sohn, J. W., & Chung, W. S. (2021). Microglial MERTK eliminates phosphatidylserine-displaying inhibitory post-synapses. The EMBO journal, 40(15), e107121.
https://doi.org/10.15252/embj.2020107121https://doi.org/10.1523/JNEUROSCI.3618-17.2018

Pelvig, D. P., Pakkenberg, H., Stark, A. K., & Pakkenberg, B. (2008). Neocortical glial cell numbers in human brains. Neurobiology of aging, 29(11), 1754–1762. https://doi.org/10.1016/j.neurobiolaging.2007.04.013

Penzes, P., Cahill, M. E., Jones, K. A., VanLeeuwen, J. E., & Woolfrey, K. M. (2011). Dendritic spine pathology in neuropsychiatric disorders. Nature neuroscience, 14(3), 285–293. https://doi.org/10.1038/nn.2741

Perea, G., Navarrete, M., & Araque, A. (2009). Tripartite synapses: astrocytes process and control synaptic information. Trends in neurosciences, 32(8), 421–431. https://doi.org/10.1016/j.tins.2009.05.001

Pérez, M., Avila, J., & Hernández, F. (2019). Propagation of Tau via Extracellular Vesicles. Frontiers in neuroscience, 13, 698. https://doi.org/10.3389/fnins.2019.00698

Phillips, M. C. L., Murtagh, D. K. J., Gilbertson, L. J., Asztely, F. J. S., & Lynch, C. D. P. (2018). Low-fat versus ketogenic diet in Parkinson's disease: A pilot randomized controlled trial. Movement disorders : official journal of the Movement Disorder Society, 33(8), 1306–1314. https://doi.org/10.1002/mds.27390

Pieri, M., Albo, F., Gaetti, C., Spalloni, A., Bengtson, C. P., Longone, P., Cavalcanti, S., & Zona, C. (2003). Altered excitability of motor neurons in a transgenic mouse model of familial amyotrophic lateral sclerosis. Neuroscience letters, 351(3), 153–156. https://doi.org/10.1016/j.neulet.2003.07.010

Pirttimaki, T., Parri, H. R., & Crunelli, V. (2013). Astrocytic GABA transporter GAT-1 dysfunction in experimental absence seizures. The Journal of physiology, 591(4), 823–833. https://doi.org/10.1113/jphysiol.2012.242016

Pivato, M., De Franceschi, G., Tosatto, L., Frare, E., Kumar, D., Aioanei, D., Brucale, M., Tessari, I., Bisaglia, M., Samori, B., de Laureto, P. P., & Bubacco, L. (2012). Covalent α-synuclein dimers: chemico-physical and aggregation properties. PloS one, 7(12), e50027. https://doi.org/10.1371/journal.pone.0050027

Poewe, W., Seppi, K., Tanner, C. M., Halliday, G. M., Brundin, P., Volkmann, J., Schrag, A. E., & Lang, A. E. (2017). Parkinson disease. Nature reviews. Disease primers, 3, 17013. https://doi.org/10.1038/nrdp.2017.13

Polymeropoulos, M. H., Higgins, J. J., Golbe, L. I., Johnson, W. G., Ide, S. E., Di Iorio, G., Sanges, G., Stenroos, E. S., Pho, L. T., Schaffer, A. A., Lazzarini, A. M., Nussbaum, R. L., & Duvoisin, R. C. (1996). Mapping of a gene for Parkinson's disease to chromosome 4q21-q23. Science (New York, N.Y.), 274(5290), 1197–1199. https://doi.org/10.1126/science.274.5290.1197

Polymeropoulos, M. H., Lavedan, C., Leroy, E., Ide, S. E., Dehejia, A., Dutra, A., Pike, B., Root, H., Rubenstein, J., Boyer, R., Stenroos, E. S., Chandrasekharappa, S., Athanassiadou, A., Papapetropoulos, T., Johnson, W. G., Lazzarini, A. M., Duvoisin, R. C., Di Iorio, G., Golbe, L. I., & Nussbaum, R. L. (1997). Mutation in the alpha-synuclein gene identified in families with Parkinson's disease. Science (New York, N.Y.), 276(5321), 2045–2047. https://doi.org/10.1126/science.276.5321.2045

Pontejo, S. M., & Murphy, P. M. (2021). Chemokines act as phosphatidylserine-bound "find-me" signals in apoptotic cell clearance. PLoS biology, 19(5), e3001259. https://doi.org/10.1371/journal.pbio.3001259

Pringsheim, T., Jette, N., Frolkis, A., & Steeves, T. D. (2014). The prevalence of Parkinson's disease: a systematic review and meta-analysis. Movement disorders: official journal of the Movement Disorder Society, 29(13), 1583–1590. https://doi.org/10.1002/mds.25945

Puchert, M., Pelkner, F., Stein, G., Angelov, D. N., Boltze, J., Wagner, D. C., Odoardi, F., Flügel, A., Streit, W. J., & Engele, J. (2017). Astrocytic expression of the CXCL12 receptor, CXCR7/ACKR3 is

a hallmark of the diseased, but not developing CNS. Molecular and cellular neurosciences, 85, 105–118. https://doi.org/10.1016/j.mcn.2017.09.001

Purice, M. D., Speese, S. D., & Logan, M. A. (2016). Delayed glial clearance of degenerating axons in aged Drosophila is due to reduced PI3K/Draper activity. Nature communications, 7, 12871. https://doi.org/10.1038/ncomms12871l of neuroinflammation, 17(1), 97. https://doi.org/10.1186/s12974-020-01774-9

Ramirez, A., Heimbach, A., Gründemann, J., Stiller, B., Hampshire, D., Cid, L. P., Goebel, I., Mubaidin, A. F., Wriekat, A. L., Roeper, J., Al-Din, A., Hillmer, A. M., Karsak, M., Liss, B., Woods, C. G., Behrens, M. I., & Kubisch, C. (2006). Hereditary parkinsonism with dementia is caused by mutations in ATP13A2, encoding a lysosomal type 5 P-type ATPase. Nature genetics, 38(10), 1184–1191. https://doi.org/10.1038/ng1884

Ramos-Gonzalez, P., Mato, S., Chara, J. C., Verkhratsky, A., Matute, C., & Cavaliere, F. (2021). Astrocytic atrophy as a pathological feature of Parkinson's disease with LRRK2 mutation. NPJ Parkinson's disease, 7(1), 31. https://doi.org/10.1038/s41531-021-00175-w

Reemst, K., Noctor, S. C., Lucassen, P. J., & Hol, E. M. (2016). The Indispensable Roles of Microglia and Astrocytes during Brain Development. Frontiers in human neuroscience, 10, 566. https://doi.org/10.3389/fnhum.2016.00566

Renner, M., & Melki, R. (2014). Protein aggregation and prionopathies. Pathologie-biologie, 62(3), 162–168. https://doi.org/10.1016/j.patbio.2014.01.003

Repetto, G., del Peso, A., & Zurita, J. L. (2008). Neutral red uptake assay for the estimation of cell viability/cytotoxicity. Nature protocols, 3(7), 1125–1131. https://doi.org/10.1038/nprot.2008.75

Reyniers, L., Del Giudice, M. G., Civiero, L., Belluzzi, E., Lobbestael, E., Beilina, A., Arrigoni, G., Derua, R., Waelkens, E., Li, Y., Crosio, C., Iaccarino, C., Cookson, M. R., Baekelandt, V., Greggio, E., & Taymans, J. M. (2014). Differential protein-protein interactions of LRRK1 and LRRK2 indicate roles in distinct cellular signaling pathways. Journal of neurochemistry, 131(2), 239–250. https://doi.org/10.1111/jnc.12798

Roosen, D. A., & Cookson, M. R. (2016). LRRK2 at the interface of autophagosomes, endosomes and lysosomes. Molecular neurodegeneration, 11(1), 73. https://doi.org/10.1186/s13024-016-0140-1

Ross, C. A., & Poirier, M. A. (2004). Protein aggregation and neurodegenerative disease. Nature medicine, 10 Suppl, S10–S17. https://doi.org/10.1038/nm1066

Rostami, J., Fotaki, G., Sirois, J., Mzezewa, R., Bergström, J., Essand, M., Healy, L., & Erlandsson, A. (2020). Astrocytes have the capacity to act as antigen-presenting cells in the Parkinson's disease brain. Journal of neuroinflammation, 17(1), 119. https://doi.org/10.1186/s12974-020-01776-7

Rostami, J., Holmqvist, S., Lindström, V., Sigvardson, J., Westermark, G. T., Ingelsson, M., Bergström, J., Roybon, L., & Erlandsson, A. (2017). Human Astrocytes Transfer Aggregated Alpha-Synuclein via Tunneling Nanotubes. The Journal of neuroscience : the official journal of the Society for Neuroscience, 37(49), 11835–11853. https://doi.org/10.1523/JNEUROSCI.0983-17.2017

Rostami, J., Mothes, T., Kolahdouzan, M., Eriksson, O., Moslem, M., Bergström, J., Ingelsson, M., O'Callaghan, P., Healy, L. M., Falk, A., & Erlandsson, A. (2021). Crosstalk between astrocytes and microglia results in increased degradation of α-synuclein and amyloid-β aggregates. Journal of neuroinflammation, 18(1), 124. https://doi.org/10.1186/s12974-021-02158-3

Ruggiero, L., Connor, M. P., Chen, J., Langen, R., & Finnemann, S. C. (2012). Diurnal, localized exposure of phosphatidylserine by rod outer segment tips in wild-type but not Itgb5-/- or Mfge8-/- mouse retina. Proceedings of the National Academy of Sciences of the United States of America, 109(21), 8145–8148. https://doi.org/10.1073/pnas.1121101109

Russo, I., Berti, G., Plotegher, N., Bernardo, G., Filograna, R., Bubacco, L., & Greggio, E. (2015). Leucine-rich repeat kinase 2 positively regulates inflammation and down-regulates NF-κB p50 signaling in cultured microglia cells. Journal of neuroinflammation, 12, 230. https://doi.org/10.1186/s12974-015-0449-7

Rustom, A., Saffrich, R., Markovic, I., Walther, P., & Gerdes, H. H. (2004). Nanotubular highways for intercellular organelle transport. Science (New York, N.Y.), 303(5660), 1007–1010. https://doi.org/10.1126/science.1093133

Sacino, A. N., Brooks, M. M., Chakrabarty, P., Saha, K., Khoshbouei, H., Golde, T. E., & Giasson, B. I. (2017). Proteolysis of α-synuclein fibrils in the lysosomal pathway limits induction of inclusion pathology. Journal of neurochemistry, 140(4), 662–678. https://doi.org/10.1111/jnc.13743

Sakai J. (2020). Core Concept: How synaptic pruning shapes neural wiring during development and, possibly, in disease. Proceedings of the National Academy of Sciences of the United States of America, 117(28), 16096–16099. https://doi.org/10.1073/pnas.2010281117

Salazar, N., Carlson, J. C., Huang, K., Zheng, Y., Oderup, C., Gross, J., Jang, A. D., Burke, T. M., Lewén, S., Scholz, A., Huang, S., Nease, L., Kosek, J., Mittelbronn, M., Butcher, E. C., Tu, H., & Zabel, B. A. (2018). A Chimeric Antibody against ACKR3/CXCR7 in Combination with TMZ Activates Immune Responses and Extends Survival in Mouse GBM Models. Molecular therapy : the journal of the American Society of Gene Therapy, 26(5), 1354–1365. https://doi.org/10.1016/j.ymthe.2018.02.030

Salmon, C. K., Syed, T. A., Kacerovsky, J. B., Alivodej, N., Schober, A. L., Pratte, M. T., ... & Murai, K. K. (2021). Organizing Principles of Astrocytic Nanoarchitecture in the Mouse Cerebral Cortex. bioRxiv.

Sánchez-Alcañiz, J. A., Haege, S., Mueller, W., Pla, R., Mackay, F., Schulz, S., López-Bendito, G., Stumm, R., & Marín, O. (2011). Cxcr7 controls neuronal migration by regulating chemokine responsiveness. Neuron, 69(1), 77–90. https://doi.org/10.1016/j.neuron.2010.12.006

Schafer, D. P., Lehrman, E. K., Kautzman, A. G., Koyama, R., Mardinly, A. R., Yamasaki, R., Ransohoff, R. M., Greenberg, M. E., Barres, B. A., & Stevens, B. (2012). Microglia sculpt postnatal neural circuits in an activity and complement-dependent manner. Neuron, 74(4), 691–705. https://doi.org/10.1016/j.neuron.2012.03.026

Schapansky, J., Khasnavis, S., DeAndrade, M. P., Nardozzi, J. D., Falkson, S. R., Boyd, J. D., Sanderson, J. B., Bartels, T., Melrose, H. L., & LaVoie, M. J. (2018). Familial knockin mutation of LRRK2 causes lysosomal dysfunction and accumulation of endogenous insoluble α-synuclein in neurons. Neurobiology of disease, 111, 26–35. https://doi.org/10.1016/j.nbd.2017.12.005

Scheff, S. W., Neltner, J. H., & Nelson, P. T. (2014). Is synaptic loss a unique hallmark of Alzheimer's disease?. Biochemical pharmacology, 88(4), 517–528. https://doi.org/10.1016/j.bcp.2013.12.028

Schönemeier, B., Kolodziej, A., Schulz, S., Jacobs, S., Hoellt, V., & Stumm, R. (2008). Regional and cellular localization of the CXCl12/SDF-1 chemokine receptor CXCR7 in the developing and adult rat brain. The Journal of comparative neurology, 510(2), 207–220. https://doi.org/10.1002/cne.21780

Schrag, A., & Schott, J. M. (2006). Epidemiological, clinical, and genetic characteristics of early-onset parkinsonism. The Lancet. Neurology, 5(4), 355–363. https://doi.org/10.1016/S1474-4422(06)70411-2

Scott-Hewitt, N., Perrucci, F., Morini, R., Erreni, M., Mahoney, M., Witkowska, A., Carey, A., Faggiani, E., Schuetz, L. T., Mason, S., Tamborini, M., Bizzotto, M., Passoni, L., Filipello, F., Jahn, R., Stevens, B., & Matteoli, M. (2020). Local externalization of phosphatidylserine mediates developmental synaptic pruning by microglia. The EMBO journal, 39(16), e105380. https://doi.org/10.15252/embj.2020105380

Seifert, G., Henneberger, C., & Steinhäuser, C. (2018). Diversity of astrocyte potassium channels: An update. Brain research bulletin, 136, 26–36. https://doi.org/10.1016/j.brainresbull.2016.12.002

Selkrig, J., Stanifer, M., Mateus, A., Mitosch, K., Barrio-Hernandez, I., Rettel, M., Kim, H., Voogdt, C. G. P., Walch, P., Kee, C., Kurzawa, N., Stein, F., Potel, C., Jarzab, A., Kuster, B., Bartenschlager, R., Boulant, S., Beltrao, P., Typas, A., & Savitski, M. M. (2021). SARS-CoV-2 infection remodels the host protein thermal stability landscape. Molecular systems biology, 17(2), e10188. https://doi.org/10.15252/msb.202010188

Shankar, G. M., Bloodgood, B. L., Townsend, M., Walsh, D. M., Selkoe, D. J., & Sabatini, B. L. (2007). Natural oligomers of the Alzheimer amyloid-beta protein induce reversible synapse loss by modulating an NMDA-type glutamate receptor-dependent signaling pathway. The Journal of neuroscience : the official journal of the Society for Neuroscience, 27(11), 2866–2875. https://doi.org/10.1523/JNEUROSCI.4970-06.2007

Sharma, S., Bandopadhyay, R., Lashley, T., Renton, A. E., Kingsbury, A. E., Kumaran, R., Kallis, C., Vilariño-Güell, C., O'Sullivan, S. S., Lees, A. J., Revesz, T., Wood, N. W., & Holton, J. L. (2011). LRRK2 expression in idiopathic and G2019S positive Parkinson's disease subjects: a morphological and quantitative study. Neuropathology and applied neurobiology, 37(7), 777–790. https://doi.org/10.1111/j.1365-2990.2011.01187.

Shi, X., Luo, L., Wang, J., Shen, H., Li, Y., Mamtilahun, M., Liu, C., Shi, R., Lee, J. H., Tian, H., Zhang, Z., Wang, Y., Chung, W. S., Tang, Y., & Yang, G. Y. (2021). Stroke subtype-dependent synapse elimination by reactive gliosis in mice. Nature communications, 12(1), 6943. https://doi.org/10.1038/s41467-021-27248-x

Shih, A. Y., Johnson, D. A., Wong, G., Kraft, A. D., Jiang, L., Erb, H., Johnson, J. A., & Murphy, T. H. (2003). Coordinate regulation of glutathione biosynthesis and release by Nrf2-expressing glia potently protects neurons from oxidative stress. The Journal of neuroscience : the official journal of the Society for Neuroscience, 23(8), 3394–3406. https://doi.org/10.1523/JNEUROSCI.23-08-03394.2003

Shimojo, H., Ohtsuka, T., & Kageyama, R. (2011). Dynamic expression of notch signaling genes in neural stem/progenitor cells. Frontiers in neuroscience, 5, 78. https://doi.org/10.3389/fnins.2011.00078

Sian-Hulsmann, J., Monoranu, C., Strobel, S., & Riederer, P. (2015). Lewy Bodies: A Spectator or Salient Killer?. CNS & neurological disorders drug targets, 14(7), 947–955. https://doi.org/10.2174/1871527314666150317225659

Sickmann, H. M., Walls, A. B., Schousboe, A., Bouman, S. D., & Waagepetersen, H. S. (2009). Functional significance of brain glycogen in sustaining glutamatergic neurotransmission. Journal of neurochemistry, 109 Suppl 1, 80–86. https://doi.org/10.1111/j.1471-4159.2009.05915.x

Siddiqui, A., Chinta, S. J., Mallajosyula, J. K., Rajagopolan, S., Hanson, I., Rane, A., Melov, S., & Andersen, J. K. (2012). Selective binding of nuclear alpha-synuclein to the PGC1alpha promoter under conditions of oxidative stress may contribute to losses in mitochondrial function: implications for Parkinson's disease. Free radical biology & medicine, 53(4), 993–1003. https://doi.org/10.1016/j.freeradbiomed.2012.05.024

Simard, M., & Nedergaard, M. (2004). The neurobiology of glia in the context of water and ion homeostasis. Neuroscience, 129(4), 877–896. https://doi.org/10.1016/j.neuroscience.2004.09.053

Singleton, A. B., Farrer, M., Johnson, J., Singleton, A., Hague, S., Kachergus, J., Hulihan, M., Peuralinna, T., Dutra, A., Nussbaum, R., Lincoln, S., Crawley, A., Hanson, M., Maraganore, D., Adler, C., Cookson, M. R., Muenter, M., Baptista, M., Miller, D., Blancato, J., … Gwinn-Hardy, K. (2003). alpha-Synuclein locus triplication causes Parkinson's disease. Science (New York, N.Y.), 302(5646), 841. https://doi.org/10.1126/science.1090278

Singleton, A., & Hardy, J. (2016). The Evolution of Genetics: Alzheimer's and Parkinson's Diseases. Neuron, 90(6), 1154–1163. https://doi.org/10.1016/j.neuron.2016.05.040

Sipe, G. O., Lowery, R. L., Tremblay, M. È., Kelly, E. A., Lamantia, C. E., & Majewska, A. K. (2016). Microglial P2Y12 is necessary for synaptic plasticity in mouse visual cortex. Nature communications, 7, 10905. https://doi.org/10.1038/ncomms10905

Smit, M. J., Schlecht-Louf, G., Neves, M., van den Bor, J., Penela, P., Siderius, M., Bachelerie, F., & Mayor, F., Jr (2021). The CXCL12/CXCR4/ACKR3 Axis in the Tumor Microenvironment: Signaling, Crosstalk, and Therapeutic Targeting. Annual review of pharmacology and toxicology, 61, 541–563. https://doi.org/10.1146/annurev-pharmtox-010919-023340

Sofroniew, M. V., & Vinters, H. V. (2010). Astrocytes: biology and pathology. Acta neuropathologica, 119(1), 7–35. https://doi.org/10.1007/s00401-009-0619-8

Söllvander, S., Nikitidou, E., Brolin, R., Söderberg, L., Sehlin, D., Lannfelt, L., & Erlandsson, A. (2016). Accumulation of amyloid-β by astrocytes result in enlarged endosomes and microvesicle-induced apoptosis of neurons. Molecular neurodegeneration, 11(1), 38. https://doi.org/10.1186/s13024-016-0098-z

Soto, C., & Pritzkow, S. (2018). Protein misfolding, aggregation, and conformational strains in neurodegenerative diseases. Nature neuroscience, 21(10), 1332–1340. https://doi.org/10.1038/s41593-018-0235-9

Stanhope, B. A., Jaggard, J. B., Gratton, M., Brown, E. B., & Keene, A. C. (2020). Sleep Regulates Glial Plasticity and Expression of the Engulfment Receptor Draper Following Neural Injury. Current biology : CB, 30(6), 1092–1101.e3. https://doi.org/10.1016/j.cub.2020.02.057

Stephan, A. H., Madison, D. V., Mateos, J. M., Fraser, D. A., Lovelett, E. A., Coutellier, L., Kim, L., Tsai, H. H., Huang, E. J., Rowitch, D. H., Berns, D. S., Tenner, A. J., Shamloo, M., & Barres, B. A. (2013). A dramatic increase of C1q protein in the CNS during normal aging. The Journal of neuroscience : the official journal of the Society for Neuroscience, 33(33), 13460–13474. https://doi.org/10.1523/JNEUROSCI.1333-13.2013

Stevens, B., Allen, N. J., Vazquez, L. E., Howell, G. R., Christopherson, K. S., Nouri, N., Micheva, K. D., Mehalow, A. K., Huberman, A. D., Stafford, B., Sher, A., Litke, A. M., Lambris, J. D., Smith, S. J., John, S. W., & Barres, B. A. (2007). The classical complement cascade mediates CNS synapse elimination. Cell, 131(6), 1164–1178. https://doi.org/10.1016/j.cell.2007.10.036

Stoker, T. B., & Barker, R. A. (2020). Recent developments in the treatment of Parkinson's Disease. F1000Research, 9, F1000 Faculty Rev-862. https://doi.org/10.12688/f1000research.25634.1

Streubel-Gallasch, L., Giusti, V., Sandre, M., Tessari, I., Plotegher, N., Giusto, E., Masato, A., Iovino, L., Battisti, I., Arrigoni, G., Shimshek, D., Greggio, E., Tremblay, M. E., Bubacco, L., Erlandsson, A., & Civiero, L. (2021). Parkinson's Disease-Associated LRRK2 Interferes with Astrocyte-Mediated Alpha-Synuclein Clearance. Molecular neurobiology, 58(7), 3119–3140. https://doi.org/10.1007/s12035-021-02327-8

Stukes, S., Coelho, C., Rivera, J., Jedlicka, A. E., Hajjar, K. A., & Casadevall, A. (2016). The Membrane Phospholipid Binding Protein Annexin A2 Promotes Phagocytosis and Nonlytic Exocytosis of Cryptococcus neoformans and Impacts Survival in Fungal Infection. Journal of immunology (Baltimore, Md. : 1950), 197(4), 1252–1261. https://doi.org/10.4049/jimmunol.1501855

Suh, S. W., Bergher, J. P., Anderson, C. M., Treadway, J. L., Fosgerau, K., & Swanson, R. A. (2007). Astrocyte glycogen sustains neuronal activity during hypoglycemia: studies with the glycogen phosphorylase inhibitor CP-316,819 ([R-R*,S*]-5-chloro-N-[2-hydroxy-3-(methoxymethylamino)-3-oxo-1-(phenylmethyl)propyl]-1H-indole-2-carboxamide). The Journal of pharmacology and experimental therapeutics, 321(1), 45–50. https://doi.org/10.1124/jpet.106.115550

Suzuki, A., Stern, S. A., Bozdagi, O., Huntley, G. W., Walker, R. H., Magistretti, P. J., & Alberini, C. M. (2011). Astrocyte-neuron lactate transport is required for long-term memory formation. Cell, 144(5), 810–823. https://doi.org/10.1016/j.cell.2011.02.018

Tamgüney, G., & Korczyn, A. D. (2018). A critical review of the prion hypothesis of human synucleinopathies. Cell and tissue research, 373(1), 213–220. https://doi.org/10.1007/s00441-017-2712-y

Tansey, M. G., & Goldberg, M. S. (2010). Neuroinflammation in Parkinson's disease: its role in neuronal death and implications for therapeutic intervention. Neurobiology of disease, 37(3), 510–518. https://doi.org/10.1016/j.nbd.2009.11.004

Tong, Y., Giaime, E., Yamaguchi, H., Ichimura, T., Liu, Y., Si, H., Cai, H., Bonventre, J. V., & Shen, J. (2012). Loss of leucine-rich repeat kinase 2 causes age-dependent bi-phasic alterations of the

autophagy pathway. Molecular neurodegeneration, 7, 2. https://doi.org/10.1186/1750-1326-7-2

Torres-Platas, S. G., Hercher, C., Davoli, M. A., Maussion, G., Labonté, B., Turecki, G., & Mechawar, N. (2011). Astrocytic hypertrophy in anterior cingulate white matter of depressed suicides. Neuropsychopharmacology : official publication of the American College of Neuropsychopharmacology, 36(13), 2650–2658. https://doi.org/10.1038/npp.2011.154

Trachtenberg, J. T., Chen, B. E., Knott, G. W., Feng, G., Sanes, J. R., Welker, E., & Svoboda, K. (2002). Long-term in vivo imaging of experience-dependent synaptic plasticity in adult cortex. Nature, 420(6917), 788–794. https://doi.org/10.1038/nature01273

Tremblay, M. E., Cookson, M. R., & Civiero, L. (2019). Glial phagocytic clearance in Parkinson's disease. Molecular neurodegeneration, 14(1), 16. https://doi.org/10.1186/s13024-019-0314-8

Tremblay, M. È., Lowery, R. L., & Majewska, A. K. (2010). Microglial interactions with synapses are modulated by visual experience. PLoS biology, 8(11), e1000527. https://doi.org/10.1371/journal.pbio.1000527

Tsigelny, I. F., Sharikov, Y., Wrasidlo, W., Gonzalez, T., Desplats, P. A., Crews, L., Spencer, B., & Masliah, E. (2012). Role of α-synuclein penetration into the membrane in the mechanisms of oligomer pore formation. The FEBS journal, 279(6), 1000–1013. https://doi.org/10.1111/j.1742-4658.2012.08489.x

Uchihara, T., & Giasson, B. I. (2016). Propagation of alpha-synuclein pathology: hypotheses, discoveries, and yet unresolved questions from experimental and human brain studies. Acta neuropathologica, 131(1), 49–73. https://doi.org/10.1007/s00401-015-1485-1

Vaikath, N., Sudhakaran, I., Abdi, I., Gupta, V., Majbour, N., Ghanem, S., Abdesselem, H., Vekrellis, K., & El-Agnaf, O. (2022). Structural and Biophysical Characterization of Stable Alpha-Synuclein Oligomers. International journal of molecular sciences, 23(23), 14630. https://doi.org/10.3390/ijms232314630

Vainchtein, I. D., Chin, G., Cho, F. S., Kelley, K. W., Miller, J. G., Chien, E. C., Liddelow, S. A., Nguyen, P. T., Nakao-Inoue, H., Dorman, L. C., Akil, O., Joshita, S., Barres, B. A., Paz, J. T., Molofsky, A. B., & Molofsky, A. V. (2018). Astrocyte-derived interleukin-33 promotes microglial synapse engulfment and neural circuit development. Science (New York, N.Y.), 359(6381), 1269–1273. https://doi.org/10.1126/science.aal3589

Van Den Eeden, S. K., Tanner, C. M., Bernstein, A. L., Fross, R. D., Leimpeter, A., Bloch, D. A., & Nelson, L. M. (2003). Incidence of Parkinson's disease: variation by age, gender, and race/ethnicity. American journal of epidemiology, 157(11), 1015–1022. https://doi.org/10.1093/aje/kwg068

van der Vorst, E. P. C., Peters, L. J. F., Müller, M., Gencer, S., Yan, Y., Weber, C., & Döring, Y. (2019). G-Protein Coupled Receptor Targeting on Myeloid Cells in Atherosclerosis. Frontiers in pharmacology, 10, 531. https://doi.org/10.3389/fphar.2019.00531

Vargas, K. J., Makani, S., Davis, T., Westphal, C. H., Castillo, P. E., & Chandra, S. S. (2014). Synucleins regulate the kinetics of synaptic vesicle endocytosis. The Journal of neuroscience :

the official journal of the Society for Neuroscience, 34(28), 9364–9376. https://doi.org/10.1523/JNEUROSCI.4787-13.2014

Varyukhina, S., Lamazière, A., Delaunay, J. L., de Wreede, A., & Ayala-Sanmartin, J. (2022). The Ca2+- and phospholipid-binding protein Annexin A2 is able to increase and decrease plasma membrane order. Biochimica et biophysica acta. Biomembranes, 1864(1), 183810. https://doi.org/10.1016/j.bbamem.2021.183810

Vasile, F., Dossi, E., & Rouach, N. (2017). Human astrocytes: structure and functions in the healthy brain. Brain structure & function, 222(5), 2017–2029. https://doi.org/10.1007/s00429-017-1383-5

Vasile, F., Dossi, E., & Rouach, N. (2017). Human astrocytes: structure and functions in the healthy brain. Brain structure & function, 222(5), 2017–2029. https://doi.org/10.1007/s00429-017-1383-5

Ventura, R., & Harris, K. M. (1999). Three-dimensional relationships between hippocampal synapses and astrocytes. The Journal of neuroscience : the official journal of the Society for Neuroscience, 19(16), 6897–6906. https://doi.org/10.1523/JNEUROSCI.19-16-06897.1999

Vicente-Gutierrez, C., Bonora, N., Bobo-Jimenez, V., Jimenez-Blasco, D., Lopez-Fabuel, I., Fernandez, E., Josephine, C., Bonvento, G., Enriquez, J. A., Almeida, A., & Bolaños, J. P. (2019). Astrocytic mitochondrial ROS modulate brain metabolism and mouse behaviour. Nature metabolism, 1(2), 201–211. https://doi.org/10.1038/s42255-018-0031-6

Volpicelli-Daley, L. A., Luk, K. C., Patel, T. P., Tanik, S. A., Riddle, D. M., Stieber, A., Meaney, D. F., Trojanowski, J. Q., & Lee, V. M. (2011). Exogenous α-synuclein fibrils induce Lewy body pathology leading to synaptic dysfunction and neuron death. Neuron, 72(1), 57–71. https://doi.org/10.1016/j.neuron.2011.08.033

Wakabayashi, K., Hayashi, S., Yoshimoto, M., Kudo, H., & Takahashi, H. (2000). NACP/alpha-synuclein-positive filamentous inclusions in astrocytes and oligodendrocytes of Parkinson's disease brains. Acta neuropathologica, 99(1), 14–20. https://doi.org/10.1007/pl00007400

Wakabayashi, K., Hayashi, S., Yoshimoto, M., Kudo, H., & Takahashi, H. (2000). NACP/alpha-synuclein-positive filamentous inclusions in astrocytes and oligodendrocytes of Parkinson's disease brains. Acta neuropathologica, 99(1), 14–20. https://doi.org/10.1007/pl00007400

Wakida, E. K., Talib, Z. M., Akena, D., Okello, E. S., Kinengyere, A., Mindra, A., & Obua, C. (2018). Barriers and facilitators to the integration of mental health services into primary health care: a systematic review. Systematic reviews, 7(1), 211. https://doi.org/10.1186/s13643-018-0882-7

Walch, P., Selkrig, J., Knodler, L. A., Rettel, M., Stein, F., Fernandez, K., Viéitez, C., Potel, C. M., Scholzen, K., Geyer, M., Rottner, K., Steele-Mortimer, O., Savitski, M. M., Holden, D. W., & Typas, A. (2021). Global mapping of Salmonella enterica-host protein-protein interactions during infection. Cell host & microbe, 29(8), 1316–1332.e12. https://doi.org/10.1016/j.chom.2021.06.004

Wallings, R., Manzoni, C., & Bandopadhyay, R. (2015). Cellular processes associated with LRRK2 function and dysfunction. The FEBS journal, 282(15), 2806–2826. https://doi.org/10.1111/febs.13305

Walls, A. B., Heimbürger, C. M., Bouman, S. D., Schousboe, A., & Waagepetersen, H. S. (2009). Robust glycogen shunt activity in astrocytes: Effects of glutamatergic and adrenergic agents. Neuroscience, 158(1), 284–292. https://doi.org/10.1016/j.neuroscience.2008.09.058

Walter, J., Bolognin, S., Antony, P. M. A., Nickels, S. L., Poovathingal, S. K., Salamanca, L., Magni, S., Perfeito, R., Hoel, F., Qing, X., Jarazo, J., Arias-Fuenzalida, J., Ignac, T., Monzel, A. S., Gonzalez-Cano, L., Pereira de Almeida, L., Skupin, A., Tronstad, K. J., & Schwamborn, J. C. (2019). Neural Stem Cells of Parkinson's Disease Patients Exhibit Aberrant Mitochondrial Morphology and Functionality. Stem cell reports, 12(5), 878–889. https://doi.org/10.1016/j.stemcr.2019.03.004

Wang, P., & Ye, Y. (2021). Filamentous recombinant human Tau activates primary astrocytes via an integrin receptor complex. Nature communications, 12(1), 95. https://doi.org/10.1038/s41467-020-20322-w

Wang, Y., Balaji, V., Kaniyappan, S., Krüger, L., Irsen, S., Tepper, K., Chandupatla, R., Maetzler, W., Schneider, A., Mandelkow, E., & Mandelkow, E. M. (2017). The release and trans-synaptic transmission of Tau via exosomes. Molecular neurodegeneration, 12(1), 5. https://doi.org/10.1186/s13024-016-0143-y

Wiesel, T. N., & Hubel, D. H. (1963). Effects of visual deprivation on morphology and physiology of cells in the cats lateral geniculate body. Journal of neurophysiology, 26, 978–993. Https://doi.org/10.1152/jn.1963.26.6.978

Wilhelmsson, U., Bushong, E. A., Price, D. L., Smarr, B. L., Phung, V., Terada, M., Ellisman, M. H., & Pekny, M. (2006). Redefining the concept of reactive astrocytes as cells that remain within their unique domains upon reaction to injury. Proceedings of the National Academy of Sciences of the United States of America, 103(46), 17513–17518. https://doi.org/10.1073/pnas.0602841103

Wishart, T. M., Parson, S. H., & Gillingwater, T. H. (2006). Synaptic vulnerability in neurodegenerative disease. Journal of neuropathology and experimental neurology, 65(8), 733–739. https://doi.org/10.1097/01.jnen.0000228202.35163.c4

Wójtowicz, A. M., Dvorzhak, A., Semtner, M., & Grantyn, R. (2013). Reduced tonic inhibition in striatal output neurons from Huntington mice due to loss of astrocytic GABA release through GAT-3. Frontiers in neural circuits, 7, 188. https://doi.org/10.3389/fncir.2013.00188

Wolff, J. R., & Missler, M. (1993). Synaptic remodelling and elimination as integral processes of synaptogenesis. APMIS. Supplementum, 40, 9–23.

Wu, T., Hu, E., Xu, S., Chen, M., Guo, P., Dai, Z., Feng, T., Zhou, L., Tang, W., Zhan, L., Fu, X., Liu, S., Bo, X., & Yu, G. (2021). clusterProfiler 4.0: A universal enrichment tool for interpreting omics data. Innovation (Cambridge (Mass.)), 2(3), 100141. https://doi.org/10.1016/j.xinn.2021.100141

Xing, W., Liu, J., Cheng, S., Vogel, P., Mohan, S., & Brommage, R. (2013). Targeted disruption of leucine-rich repeat kinase 1 but not leucine-rich repeat kinase 2 in mice causes severe osteopetrosis. Journal of bone and mineral research : the official journal of the American Society for Bone and Mineral Research, 28(9), 1962–1974. https://doi.org/10.1002/jbmr.1935

Yang, J., Yang, H., Liu, Y., Li, X., Qin, L., Lou, H., Duan, S., & Wang, H. (2016). Astrocytes contribute to synapse elimination via type 2 inositol 1,4,5-trisphosphate receptor-dependent release of ATP. eLife, 5, e15043. https://doi.org/10.7554/eLife.15043

Yim, W. W., Yamamoto, H., & Mizushima, N. (2022). Annexins A1 and A2 are recruited to larger lysosomal injuries independently of ESCRTs to promote repair. FEBS letters, 596(8), 991–1003. https://doi.org/10.1002/1873-3468.14329

Yim, W. W., Yamamoto, H., & Mizushima, N. (2022). Annexins A1 and A2 are recruited to larger lysosomal injuries independently of ESCRTs to promote repair. FEBS letters, 596(8), 991–1003. https://doi.org/10.1002/1873-3468.14329

Yu, G., Wang, L. G., Han, Y., & He, Q. Y. (2012). clusterProfiler: an R package for comparing biological themes among gene clusters. Omics : a journal of integrative biology, 16(5), 284–287. https://doi.org/10.1089/omi.2011.0118

Yun, S. P., Kam, T. I., Panicker, N., Kim, S., Oh, Y., Park, J. S., Kwon, S. H., Park, Y. J., Karuppagounder, S. S., Park, H., Kim, S., Oh, N., Kim, N. A., Lee, S., Brahmachari, S., Mao, X., Lee, J. H., Kumar, M., An, D., Kang, S. U., … Ko, H. S. (2018). Block of A1 astrocyte conversion by microglia is neuroprotective in models of Parkinson's disease. Nature medicine, 24(7), 931–938. https://doi.org/10.1038/s41591-018-0051-5

Zabel, B. A., Wang, Y., Lewén, S., Berahovich, R. D., Penfold, M. E., Zhang, P., Powers, J., Summers, B. C., Miao, Z., Zhao, B., Jalili, A., Janowska-Wieczorek, A., Jaen, J. C., & Schall, T. J. (2009). Elucidation of CXCR7-mediated signaling events and inhibition of CXCR4-mediated tumor cell transendothelial migration by CXCR7 ligands. Journal of immunology (Baltimore, Md. : 1950), 183(5), 3204–3211. https://doi.org/10.4049/jimmunol.0900269

Zhang, C., Zhou, T., Chen, Z., Yan, M., Li, B., Lv, H., Wang, C., Xiang, S., Shi, L., Zhu, Y., & Ai, D. (2020). Coupling of Integrin α5 to Annexin A2 by Flow Drives Endothelial Activation. Circulation research, 127(8), 1074–1090. https://doi.org/10.1161/CIRCRESAHA.120.316857

Zhang, H. T., Zeng, Q., Wu, B., Lu, J., Tong, K. L., Lin, J., Liu, Q. Y., Xu, L., Yang, J., Liu, X., Liu, W., Zhang, Y. F., Lian, Q., Liu, L., & Gao, X. (2021). TRIM21-regulated Annexin A2 plasma membrane trafficking facilitates osteosarcoma cell differentiation through the TFEB-mediated autophagy. Cell death & disease, 12(1), 21. https://doi.org/10.1038/s41419-020-03364-2

Zhang, H., Su, Y. J., Zhou, W. W., Wang, S. W., Xu, P. X., Yu, X. L., & Liu, R. T. (2014). Activated scavenger receptor A promotes glial internalization of aβ. PloS one, 9(4), e94197. https://doi.org/10.1371/journal.pone.0094197

Zhang, Y., Sloan, S. A., Clarke, L. E., Caneda, C., Plaza, C. A., Blumenthal, P. D., Vogel, H., Steinberg, G. K., Edwards, M. S., Li, G., Duncan, J. A., 3rd, Cheshier, S. H., Shuer, L. M., Chang, E. F., Grant, G. A., Gephart, M. G., & Barres, B. A. (2016). Purification and Characterization of Progenitor and Mature Human Astrocytes Reveals Transcriptional and Functional Differences with Mouse. Neuron, 89(1), 37–53. https://doi.org/10.1016/j.neuron.2015.11.013

Zoidl, G., & Dermietzel, R. (2002). On the search for the electrical synapse: a glimpse at the future. Cell and tissue research, 310(2), 137–142. https://doi.org/10.1007/s00441-002-0632-x